Stable Segment Formation Control of Multi-Robot System

Wan Jie

A THESIS SUBMITTED

FOR THE DEGREE OF DOCTOR OF PHILOSOPHY

DEPARTMENT OF MECHANICAL ENGINEERING

NATIONAL UNIVERSITY OF SINGAPORE

2011

Statement of Originality

I hereby certify that the content of this thesis is the result of work done by me and has not been submitted for a higher degree to any other University or Institution.

.....	.....
Date	Wan Jie

Acknowledgments

First and foremost, I would like to express my warmest and sincere appreciation to my supervisor, Dr. Peter Chen Chao Yu, for his invaluable guidance, insightful comments, strong encouragements and personal concerns both academically and otherwise throughout the course of the research. I benefit a lot from his comments and critiques.

I gratefully acknowledge the financial support provided by the National University of Singapore through Research Scholarship that makes it possible for me to study for academic purpose.

Thanks are also given to my friends and technicians in Mechatronics and Control Lab for their constant support. They have provided me with helpful comments, great friendship and a warm community during the past several years in NUS.

Finally, my deepest thanks go to my parents and my family for their encouragements, moral supports and loves.

Abstract

The aim of this dissertation is to investigate the formation control of multiple mobile robots based on the *queue* and *artificial potential trench* method. In general, this thesis addresses the following topics: (1) comparative analysis of two nonlinear feedback controls and study of an improved robust control for mobile robots; (2) real implementation of multi-robot system formation control; (3) extracting explicit control laws and analyzing the associated stability problems based on the framework of queue and artificial potential trench method; (4) zoning potentials for maintaining robot-to-robot distances; (5) stability analysis on attracting robots to the nearest points on the segment and collision avoidance methods; (6) input-to-state stability of formation control of multi-robot systems.

A detailed analysis of the qualitative characteristics of two nonlinear feedback controls of mobile robots is presented. The robustness of a tracking control is investigated. Based on the research results, an improved control is proposed. In addition to robustness, the improved method produces faster response. Real implementation of formation control is conducted on a multi-robot system. The triangle and square pattern formations of MRKIT robots are successfully demonstrated.

Based on the framework of *queue* and *artificial potential trench* for multi-robot formation, we aim to extract explicit multi-robot formation control laws and provide stability analysis for a group of robots assigned to the same segment. A refined definition of artificial potential trench, which allows the potential function to be nonsmooth, is defined and various ways to construct admissible potential trench functions have been proposed. Stability of formation control is investigated through a solid mathematical nonsmooth analysis.

We investigate the stability of formation control for multi-robot systems operating as a coordinated chain. In this study, a group of robots are organized in leader-follower pairs with constraints of maximum and minimum separations imposed on a robot with respect to its leader and new stable controls are synthesized. The introduction of the concept of zoning scheme, together with the associated zoning potentials, enables a robot to maintain a certain separation from its leader while forming a formation. Computer simulation has been conducted to demonstrate the effectiveness of this approach.

We investigate a generic formation control, which attracts a team of robots to the nearest points on the same segment while taking into account obstacle avoidance. A novel obstacle avoidance method, based on the new concept of apparent obstacles, is proposed to cope with concave obstacles and multiple moving obstacles. Comparison between apparent obstacle avoidance method and other alternative solutions is discussed. An elaborated algorithm dedicated to seeking the nearest point on a segment with the presence of obstacles is presented. Local minima are discussed and the corresponding simple solutions are provided. Theoretical analysis and computer simulation have been

performed to show the effectiveness of this framework.

The input-to-state stability of the formation control of multi-robot systems using artificial potential trench method and queue formation method is investigated. It is shown that the closed-loop system of each robot is input-to-state stable in relation to its leader's initial formation error. Furthermore, queue formation is robust with respect to structural changes and intermittent breakdown of communication link.

Table of Contents

List of Figures

List of Tables

Chapter 1

Introduction

1.1 Background

During the past few decades, we have witnessed increasing research and development in the area of Autonomous Multi-robot System (AMRS) or Autonomous Multi-Vehicle System (AMVS). An autonomous multi-robot (or multi-vehicle) system usually comprises a group of (often homogenous) unmanned robots (or vehicles); each has a certain degree of mobility and autonomy. Before we can have a formal discussion, we first need to define the terms ”autonomous” or ”multi-robot system”. It is difficult to use precise words to explain these terms because each of them may involve a great variety of technologies and disciplines, which are getting much more sophisticated nowadays. Nevertheless we would try to present rough definitions. The multi-robot/multi-vehicle systems under consideration here refer to all types of unmanned autonomous mobile robot/vehicle components, which include (but not limited to) ground robot/vehicle, underwater robot/vehicle, and flying robot/vehicle. These machines are organized in ei-

ther homogeneous or heterogeneous forms and operate in a cooperative way. In order to make the definition more precise, we would like to point out the essential components of the autonomous multi-robot system. There are three key attributes that are inherent in these systems: *locomotion*, *perception*, and *autonomy*.

Locomotion means that each robot has certain on-board mechanism to voluntarily perform motions in its environment. The nature of locomotion mechanism is usually properly designed to adapt to the intended surrounding environments. For instance, a robot which moves on ground has a different locomotion mechanism from that of these which are intended to perform underwater tasks. Even for ground robots, the design of locomotion mechanisms to explore a tough terrain is usually different from that of robots deployed in a jungle. Therefore, there are numerous solutions for various kinds of robots and the selection of a proper method of locomotion plays an important role in robot design. An introduction to common locomotion mechanisms on mobile robots can be found in the book written by R. Siegwart and I. R. Nourbakhsh [78].

Perception is one of the most important capabilities for an autonomous robot to actively acquire information from the surrounding environment and its internal states. A great variety of kinds of sensors are normally integrated into autonomous robots. Readings from these sensors provide the necessary knowledge of the outside environment like ambient temperature, humidity, etc.; they also supply data of internal states, such as tire pressure and battery voltage. Detailed information of common sensors used in mobile robots can be found in the book authored by H. R. Everett [23].

In simple words, autonomy is the attribute, which enables the system to adapt to the out-

side environment with minimum human instructions while controlling its own internal states. As indicated by the word ”adapt”, autonomous systems, often possess flexible capabilities such as perception, learning, computation, and decision-making. On the other hand, autonomous robots are often required to operate in unconstructed environments. In these situations, the capabilities of navigation and planning are vital to robust mobility and performance. Moreover, with autonomy it means the whole robot team can complete assigned tasks in a coordinated, cooperative and even negotiated way. In other words, autonomy operates in the context of the whole team and it is not limited to an individual robot. Normally research on team-level autonomy attracts interest than that on an individual robot.

The above definitions help to draw distinct lines between autonomous multi-robot systems and other terms such as ”autonomous mobile robots” and ”multi-agent system”. Obviously autonomous mobile robots can be the atomic components of autonomous multi-robot systems and the components of autonomous multi-vehicle systems are not limited to mobile robots in the ordinary sense. Unmanned flying vehicles and underwater vehicles may also be utilized as basic components. Although autonomous multi-robot or multi-vehicle systems can be viewed as multi-agent system from the software perspective, autonomous multi-vehicle systems are inevitably linked to a certain hardware platform which features competence of sensing and locomotion. Moveover, many of the multi-agent systems usually are not autonomous multi-vehicle system. Multi-agent systems is a much broader term than autonomous multi-robot or multi-vehicle systems. Discussion on definitions of ”agent”, ”agent-based system”, and ”multi-agent

system" can be found in the reference book [37].

There is a great variety of motivations to research and develop multi-robot systems or multi-vehicle systems. One of the obvious reasons for such growing interests is the potentials of this type of robotic systems to perform a variety of tasks in environments inaccessible or too dangerous to humans. While a single autonomous robot may be very useful in performing a given robotic task, multiple robots that can accomplish various tasks cooperatively may offer even greater advantages. This is due to the increased and synergistic effectiveness in certain applications. One of such examples is the "target search and detection" job in a large area of coverage. The procedure can be carried out in this manner: distribute a group of mobile robots over the area to be searched; program the robots to do the searching individually and collaboratively with all other robots. As a result of the cooperative works, the searching tasks and targets location can accomplished in much shorter time.

In some applications like object transport and manipulation, it is difficult if not impossible for a single autonomous robot to complete an assigned task by itself. But a group of robots operating in a cooperative way can carry or push objects. They even demonstrate promising potentials and advantages in handling complex missions. Other benefits that multi-robot systems have over single-robot systems include a large range of task domains, greater efficiency with inherent parallelism, improved system performance, fault tolerance, comparatively lower cost, and ease of development [58]. In addition, a team of multiple robots has better survivability, enhanced reliability guaranteed by its inherent redundancy and cooperation mechanism in the battle or other adverse environments

where damages or losses are inevitable. This is one of the most important and overriding advantages of multi-robot system over single robots.

Research interests in unmanned autonomous vehicles have been growing significantly in recent years, especially with the advent of highly publicized events such as DARPA's Grand Challenge [89]. Most of the autonomous multi-vehicle systems have been employed in military applications [89].These systems are usually intended for missions that are either too difficult or too dangerous for humans to accomplish alone. Areas of application include reconnaissance/surveillance, target observation/acquisition, mine clearing and using the vehicles as communications hubs/relays. For example, the U.S. Navy has been doing extensive research on using Autonomous Underwater Vehicles (AUVs) for mine hunting, maritime reconnaissance, underwater mapping, tracking of submarines and even as communication and navigation aids mainly through the use of networks of small Unmanned Undersea Vehicles (UUVs) [94]. However, the potential widespread adoptions of multi-robot technology beyond the aforementioned military applications should never be underestimated. For instance, the use of UUVs is being commercialized to support offshore oil field and pipeline route surveys [94].

A single autonomous robot is a complicated system requiring the integration of many technologies; a multi-robot system is even more complicated, because of the added coordination and collaboration duties among the robots. Dealing with such complications requires many technologies across many engineering disciplines. Some comprehensive surveys exist, such as [1], and those which have more specific focus or perspective, such as [19] for vision and [35] for robot-soccer, are also available.

Formation control is one of the focuses of multi-robot system research. The formation control problem is described as the coordination of a group of moving robots while maintaining the formation of a certain shape. This aspect of navigation is important in applications such as search and rescue operations, landmine clearing, and remote terrain and space exploration. Developments in this area are often derived from biological examples such as flying formations of migratory birds flying in the air and schools of fish swimming in the ocean. Some centralized formation coordination approaches are described in [22, 44] and [46]. Due to the centralized approach to the problem, these methods are less robust to withstand failures, less scalable to larger systems and more costly in terms of computational needs. On the other hand, feasible decentralized approaches include the Leader-Follower method [11], the Control Lyapunov Function approach [67] and Motor Schemas [2]. In the leader-follower approach, individual vehicles would basically take reference from a ”leader” vehicle and keep to a predetermined distance and orientation as they travel along the planned path. However, problems may arise when the team of vehicles is large and direct communication with the ”leader” vehicle is not possible. Thus, an alternative approach is to take reference from one or two neighboring vehicles [3]. On the other hand, the Control Lyapunov Function (CLF) approach uses CLFs to solve the coordination problem; it changes the motion control problem into a ”stabilization problem for one single system” [67]. Finally, the motor schema method is a behavior-based approach to formation control. Each motor schema (or behavior) generates a vector representing a desired direction and distance of travel. These vectors are later integrated to give a resultant action that will be communicated to the actuators for execution.

1.2 Motivations

In this dissertation, differential mobile robot with built-in locomotion mechanism and certain capabilities of sensing nearby surroundings and communicating with other robots or host (such as a human operator or high-level supervisor like PC machine) is considered. The specific type of two-wheel differential mobile robot or commonly referred to as Wheeled Mobile Robot (WMR) illustrated in Figure 1.1(a), is considered in this work. This kind of mobile robot has a left wheel and a right wheel which are controlled and driven independently. There is no mechanical or electrical couplings between the wheels. Various ways exist for driving the wheels. The most common way is to use electric motors, such as step motor and brushless DC motor. We use the term ”multi-robot system” to refer to a group of mobile robots which are organized in certain way; they are capable of operating in a coordinated and cooperated manner to accomplish certain tasks. The foregoing statement, which describes the working of an autonomous multi-robot system, implies a fundamental prerequisite: each member (robot) within the system must be able to communicate with other members directly or indirectly. The wireless technology is an ideal tool to build the communication components in mobile robots; it is also the best network communication link for multi-robot systems. Wireless communication technology are inherent with many advantages including functionality, mobility, small physical size, reliability, commercial availability, affordability and low power consumption. Figure 1.1(b) depicts a robot community consisting of three differential mobile robots each with an integrated wireless communication device. Robot community can be established by the robots' on-board wireless communication mod-

ules. The wireless signal of each module can cover a certain area. The reception areas generated by the respective robots would inadvertently overlap one another to some extent such that any robot can reach at least one other member of the community via wireless communication.

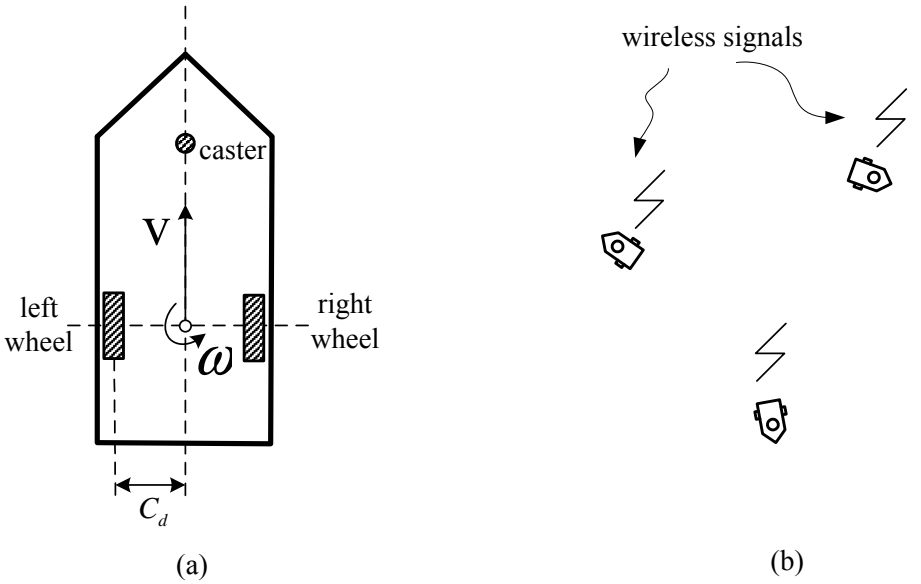

Figure 1.1: A differential mobile robot and a robot community consisting of multiple robots: (a) representation of a single mobile robot; (b) a robot community with three mobile robots which are connected to each other via wireless communication.

It is reasonable to assume that each mobile robot has certain essential but limited abilities of perception and communication. For instance, a commercial mobile robot named MRKIT shown in Figures 1.2 - 1.4, can be regarded as a prototype of the generic mobile robot model, which is depicted in Figure 1.1(a). MRKIT is developed for experiments on multi-robot systems. Top view of one of the MRKIT mobile robots used for multi-robot formation implementation is shown in Figure 1.2. Its on-board wireless Radio Frequency (RF) module can be seen on the top right side of this robot from this figure. There is also another counterpart of RF module on the workstation side. Figure 1.3

depicts the RF module on the workstation side which can be connected to a PC via Universal Serial Bus (USB) interface. Because of its on-board RF module, each robot can directly talk to its neighbors which fall within its wireless coverage range. A robot may also indirectly reach those robots located outside its wireless broadcast coverage with assistance from its neighbors. The RF device on the workstation side, however, provides possible bi-directional communication paths between the host (e.g., a high-level supervisor or human commander) and robots. Global information such as the task to be performed can be transmitted to each robot by the host. The infrared sensors located on MRKIT emit a ray of infrared light to detect nearby objects. Although such localized sensory capability of nearby environment is not global, it is crucial not only to the single robot but also to the whole group of robots. Any robot in the group must have such access to the knowledge of nearby environment to determine its next-step of action and to avoid possible collisions with obstacles or other robots. Next to the RF device shown in Figure 1.2 is a 32-bit Micro Computer Unit (MCU), which provides the basic computation capabilities, low level programmable logic control, and implementation of algorithms through firmware development. The on-board MCU can control all other electronic modules of the robots including sensors, RF module, locomotion actuators and other components. The codes for the MCU can be programmed and flashed when necessary and this flexibility greatly facilitates implementation.

Figure 1.4 shows bottom view of a MRKIT mobile robot. On the bottom of the robot, the white ball-shape parts are castors. Also from this picture, it can be observed that the two wheels are symmetrically located on two sides of the robot. Each wheel is controlled and

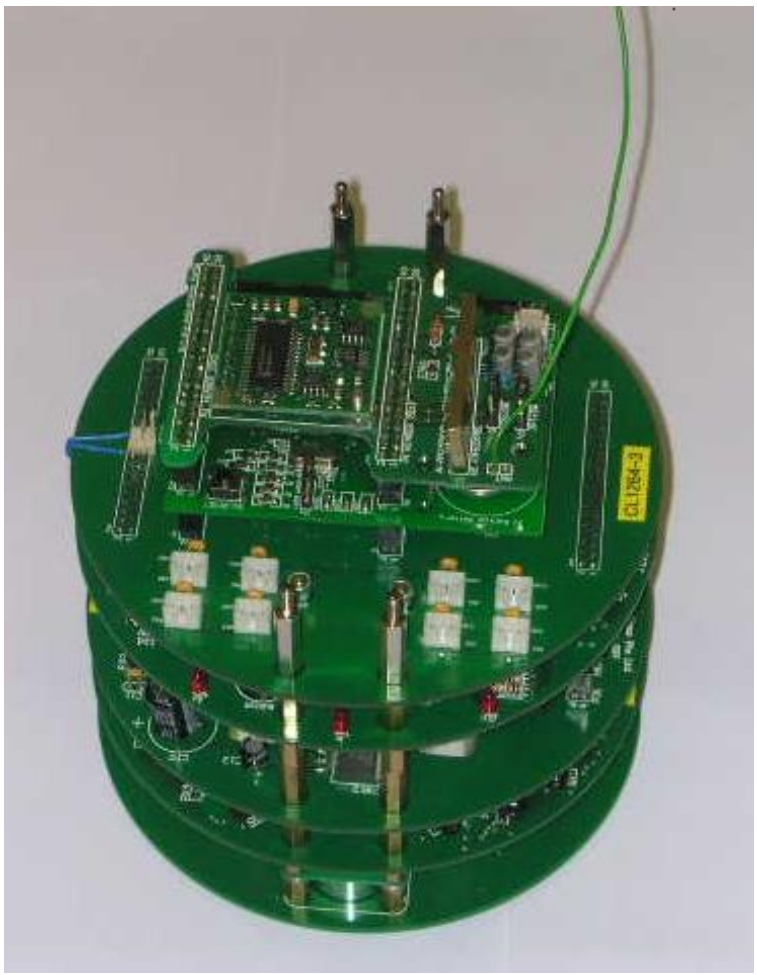

Figure 1.2: Top view of MRKIT mobile robot.

driven by two independent step motors which constitute the robot's actuators. These are hidden behind the lowest Printed Circuit Board (PCB) in Figure 1.4. The power to drive the two step motors are supplied by a rechargeable battery, which is hidden behind the lowest PCB mounted close to the motors. Current will flow from the battery to the step motors under the control of MCU and peripheral circuitry such as H-bridge MOSFETs or transistors to render mobility for the robot. The rotational motions of the step motors will then be translated into mobility for the robot. H-bridge MOSFETs or transistors can drive the motor to rotate in clockwise or counterclockwise directions.

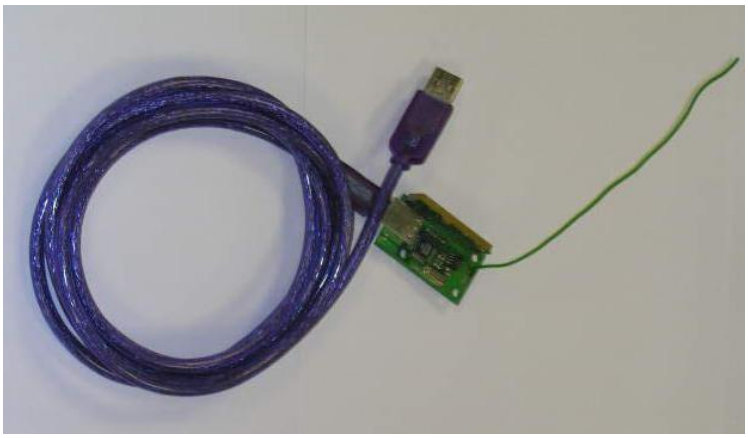

Figure 1.3: USB interface RF module on the workstation side.

Formation control of multi-robot systems involves a series of topics to be investigated and several of the key issues of formation control have been addressed by this thesis. To illustrate the generic scenario of formation control of a group of mobile robots, Figure 1.5 is depicted to highlight the fundamental tasks involved. As it is typical for most of the multi-robot formation control, a group of mobile robots are initially randomly scattered within a certain area. In Figure 1.5, initially all robots are stationed within the area surrounded by dash lines. Usually all the robots are identical and we refer to such a group of robots as homogeneous. Before the formation starts to shape, each robot has very limited information about its surroundings. At the very beginning, it needs to talk to its neighbors to get acquainted with the whole group of robots so as to establish the robot community, namely the whole group of robots with certain social characteristics. The social characteristics may include the following: which neighboring robots are within its directly communication coverage range and who else are within the community but cannot be reached directly. Sometimes, it is convenient for a robot to identify and form certain relationship with others. For instance, a robot may follow or lead another robot during the formation process. This initialization stage before the formation starts is

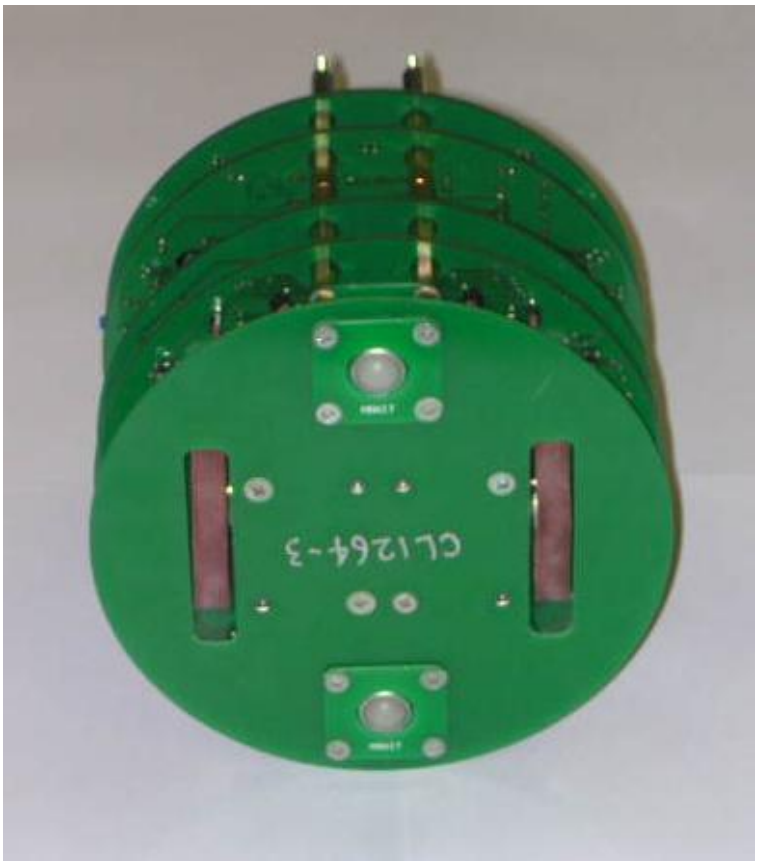

Figure 1.4: Bottom view of MRKIT mobile robot.

important. After this stage, the group of robots is organized in certain manner rather than a mere band of robots.

Specifications on the desired geometric pattern may be transmitted to each robot by the host. The robot community then has to figure out how to perform the task. Although the simplest way is to do it through human interventions, autonomous intelligent methods with minimum human interventions and resources are always preferred. In order to form the desired geometric pattern, the group of robots has to be distributed to occupy certain positions and ensure that each robot will be allocated with respect to the others in a harmonious way. Now, the key issue is the subdivision of the whole geometric pattern into several smaller representations, which can be executed by a single robot or

a couple of robots. With such representations, the robot community can be divided into several subgroups. Within each subgroup, an individual robot can manage to play its dedicated role. The interactions between an individual robot and others must be taken into account. There are two fundamental requirements for successful implementation. The first is collision avoidance with other robots for safety reasons. The second is to keep proper distances with respect to its immediate neighbors and to maintain constant wireless communication with the rest of the robot community. Broken communication may prevent the robot community from carrying out the assigned missions successfully.

As soon as the robot community figures out how to accomplish the desired pattern, it is ready to perform the assigned tasks such as patrol and surveillance. For certainty, the same fundamental requirements mentioned above also have to be complied. Sometimes, the robot community needs to perform multi-tasking functions with a certain geometric pattern while pursuing a moving target as depicted in Figure 1.5. It has to keep the pattern as much as possible when it is approaching the target. In real implementations, especially in an unconstructed dynamic environment, obstacles are of much concern because they may obstruct one or more robots to form the desired pattern or to approach the target. Such interruptions may finally ruin the robot community. As illustrated in Figure 1.5, obstacles are real threats as they cause one or more robots to stray away from the rest and disrupt the wireless communication among the rest of the robot community. Obstacles, especially moving obstacles, are menaces to any robot because they may lead to collisions and damage the robots involved.

There are two basic steps to achieve successful obstacles avoidance.: first detect and

identify the obstacles; second, share the acquired information among the robot community. In addition, the dedicated obstacle avoidance algorithms or schemes must be able to rule out possible collisions. The algorithms must also be capable of directing the affected robots to maintain their relative distances with the other robots. The ultimate goal is this, when a robot confronts an obstacle, the dedicated algorithms must be able to assist the affected robot to move pass the obstruction without collisions while maintaining real-time communication relationship with at least one robot of the robot community. In the process of avoiding the obstacle, the original geometric pattern may be disturbed temporarily. Stability issues of formation control may arise when synthesizing a comprehensive controller for the whole robot community and individual robots to deal with target tracking, separation managing, collision avoidance and other functions.

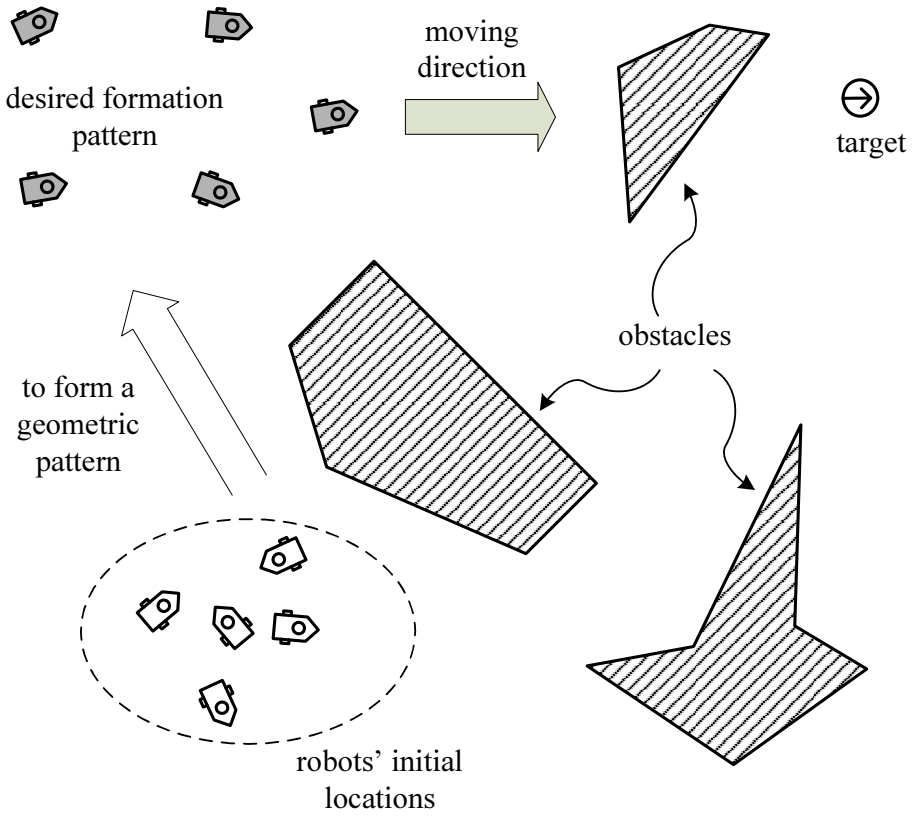

Figure 1.5: A generic scenario of multi-robot system formation control.

1.3 Objectives

Driving a single mobile robot to track a moving target represents a basic endeavor before the multi-robot formation control is ready to be addressed. It is a well-known fact that a differential mobile robot depicted in Figure 1.1(a) has non-integrable kinematic constraints. Due to these constraints, nonlinear feedback control based on the kinetic model is commonly used. A great number of nonlinear feedback control methods have been proposed [43][20]. Suitable nonlinear feedback controls can be constructed using Lyapunov functions. This is a typical engineering comprehensive practise to solve the problem of controller design and at the same time to guarantee the associated stability. Based on this simple observation and beginning with Lyapunov functions, we investigate the nonlinear controller design problem. Our discussion goes beyond the usual stability issues and includes the robustness for a given controller as a major concern. The ultimate purpose of this part of work is to figure out a robust nonlinear control which can be implemented by MRKIT robots (presented in Figures 1.2 - 1.4) driven by step motors. One of the objectives of this thesis is to apply the robust nonlinear feedback control in a multi-robot system consisting of several MRKIT robots for formation control. To this end, the whole implementation which involves a vision system, firmware, hardware and integration with other subsystems is to be developed and multi-robot formation control will be performed based on it. Three-robot triangle formation and four-robot square formation are conducted as experimental examples to verify the proposed robust control and formation control in the absence of obstacles.

For a geometric pattern to be formed by a multi-robot system, there are several methods

to break it down into low-level components to be executed by several robots or and individual robot. Among these methods, one solution (also known as ”queue and artificial potential trench scheme”) proposed by Ge and Hua [29] in 2005 is to conveniently subdivide the whole geometric shapes into a series of smooth curves. Several robots of the whole robot community are then distributed or allocated to one of the smooth curves according to certain algorithm. Consequently, the whole robot community is divided into several subgroups and each of them shares the same segment. In this way, an individual robot only needs to focus on tracking along the assigned curve while keeping proper distances to its neighbors, which are also assigned to the same curve. In other words, any robot in the formation can decide its motion depending upon its local environment variables, such as its distances to nearby neighbors. This method can greatly simplify the complexity especially when the size of robot community is a concern (for instance the multi-robot system has up to 20 robots) and the geometric pattern is complicated.

The main portion of the work reported in this thesis focuses on extending the original idea ”queue and artificial potential trench scheme” by Ge and Hua [29]. Although this scheme is essentially a behavior based control for multiple robots to provide the needed flexibilities and scalability, it is only partially done. Despite extensive simulations that have been done, a rigorous framework which is built on solid theoretical grounds has to be completed and it presents the core of the work of this dissertation.

More often than not, initially robots are scattered far away from the assigned curve, and therefore they have to move close to the curve first. Even robots which are at their desired positions along the curve and the geometric pattern is perfectly formed, some

disturbances due to unexpected circumstances such as obstacles may cause the robots to drift away from the curve. There is an effective way to drive a mobile robot moving towards a given curve or to correct the position error with respect to the curve during formation control. This simple and elegant method entails the artificial creation of a potential field where the curve becomes its bottom. A potential field, with mathematical simplicities for analytic study and computation efficiency, can attract the robots to fall into its bottom, namely the assigned curves. The commonly used potential fields are ideally supposed to be differentiable. In other words, the potential fields are smooth. However, sometimes the potential fields may fail to be differentiable at somewhere on its domain. Inevitably we have no other options but to investigate the nonsmooth cases and the associated problems such as whether the robots can be successfully driven to the curve and what conditions or constraints have to be applied to these potential fields. One of the objectives of this work is to introduce a new framework to accommodate the nonsmooth potentials and to complete the associated stability issues for the multi-robot system and single robots.

For the robots assigned to the same segment, it is convenient to deploy them along the curve (of the segment) and then turn on a cascade form. It is natural to let them be organized such that a robot can takes the robot ahead as its ”leader” and it becomes a ”follower” to this robot ahead. We refer to such a relationship as leader-follower pair. This notion is very handy for formation control. As mentioned in the previous section, separations among robots are to be regulated during formation control. To maintain a desired distance between a robot and its leader, a zoning scheme and associated zoning

potentials are introduced in our work. The basic idea is to attract the follower towards to its leader if it gets too far away from the leader. If it gets too close to the leader, it has to be pushed away. Basically an attracting zoning and a repulsive zoning together make the separation between a leader and a follower to fall within certain reasonable range. However, a simple zoning scheme may fail in formation control as it only guarantees collision avoidance between the leader and follower. The collision between a robot and another one which is not its leader or follower still may happen. To prevent possible collisions among the robots on the same segment, an improved collision avoidance method based on zoning potentials has to be developed. In this thesis, we have proposed a hierarchical collision avoidance method to serve this purpose.

To attract robots to a segment, the conventional method is to assign a goal point for each robot to pursue. A mechanism must exist to generate goal points, and usually these goal points are specified *a priori*. In order to attract robots to segments without *a priori* goal points, we have to think of a new solution. The concept of direction of attraction is proposed and it can let the robot decide how to approach the segment and hence no goal points are necessary. Now with the concept of attraction and zoning potential, we are ready to come up with explicit control laws to complete formation control for a multi-robot system. The related stability or attractiveness is to be studied. The aim is to generalize a novel framework, which can analyze and grantee the stability of multi-robot formation based on synergy of the notion of artificial potential trench, direction of attraction and zoning potentials.

To avoid using pre-determined goal points, we may also think of driving any robot to its

nearest point on the segment. However, there are theoretical difficulties even though the idea seems simple. Obviously for a single robot, there may be more than one nearest points on the segment giving rise to a series of questions such as which nearest point to follow. In contrast to the pre-determined goal points which can ensure the continuous motion of goal points on the segment, attracting robot to its nearest point may cause the motion of the nearest points to be discontinuous. Theoretical barriers arise as stability theories usually require smooth functions. To solve these challenges entirely, we have done a mathematical framework on the properties of nearest point. Based on the results we are able to complete the stability analysis.

In real world applications, obstacles have to be handled carefully for feasible formation control. Obstacles may have a great variety of shapes. Generally speaking, in terms of the shapes, there are two main categories of obstacles: convex and concave. Convex obstacles are more manageable in that they can make the analysis greatly simplified. However concave shape obstacles are more likely to be encountered and therefore present greater challenges especially for potential fields. It is common that the attractive force trying to pull a robot to the segment may be cancelled out by a repulsive force due to the existence of obstacles. If this happens, the robot will be trapped in somewhere off the segment and fail to meet the formation requirements. Moreover, obstacles may occupy some portions of the segment. If the robots are instructed to approach their nearest points on the segment, then dedicated nearest points seeking algorithms have to take into account the presence of obstacles. To cope with the generic formation control scenario as shown in Figure 1.5, a complete framework must consider the following items:

- (i) there are multiple obstacles which may affect the formation and these obstacles can be static or dynamic, convex or concave;
- (ii) each robot approaches its nearest point on the segment and some portions of the segment may be occupied by obstacles and thus are not available for the robot to dwell on;
- (iii) each robot in the same segment must maintain a reasonable distance with respect to its leader or follower;
- (iv) no robots will experience collisions with either other robots or obstacles under whatever conditions;
- (v) no robots will be trapped during formation control and they are able to recover from such adverse situations in the event of occurrence.

This is one of the most important tasks of this thesis. For any effective formation control, it is worthwhile to study the formation error propagation behavior during the formation process. At the end of this dissertation, some theoretical analysis on the formation input-to-state stability will be reported.

1.4 Organization of the Thesis

The thesis is organized as follows: **Chapter 1** introduces the background of the multi-robot systems and the generic problem of multi-robot formation control. Motivations of

the research work on formation control of this thesis is stated and the main objectives are outlined and summarized.

Chapter 2 reviews several available approaches to formation control. The associated control stability and performance such as scalability and flexibility are surveyed. The advantages and disadvantages are also briefly reviewed.

Chapter 3 presents the technical basics and formulations of the research problems, which will be addressed in this thesis. The commonly used models of mobile robots are reviewed. Fundamentals of nonsmooth analysis, which is the key mathematical tool for stability study in this thesis are also covered.

Chapter 4 addresses a detailed analysis of the qualitative characteristics of two continuous nonlinear feedback controls of differential mobile robots. It also touches on the application of an improved robust feedback control on multi-robot formation control implementation.

For the study on mobile robot tracking control, the main contents include: (i) the evolution of heading; (ii) trajectory characteristics; (iii) robustness of one of the two nonlinear feedback controls; (iv) an improved controller design and its performance. More details of the improved control law are revealed and the benefits of facilitating real implementation are discussed.

The multi-robot formation control experiments are based on the concept of the queue and artificial potential trench scheme, which is the main topic of this thesis. First, a real-time vision system, which is used to detect robots' positions and headings, is de-

veloped and its performance is evaluated. Analysis shows that the noise level in the measurement of position and orientation is relatively lower than resolution of the vision system. Therefore, the measurement can be used for the experiment. Based on the novel robust nonlinear feedback control law which is proposed in the this chapter, a 3-robot triangle formation and a 4-robot square formation experiments on multi-robot system are conducted.

Chapter 5 investigates the nonlinear tracking control based on the concept of artificial potential trench. The original idea is briefly reviewed and some refined key concepts such as admissible potential trench function are defined. It moves on to deal with the stability of controlling a team of mobile robots to track goal points on segments. Various ways of constructing potential trench functions are proposed. The response is revealed using available results on Lienard's Equation. Based on the results, we synthesize a control law that stabilizes a team of robots on a given formation without considering specific requirement on the distance between any two robots. We verify its effectiveness through simulations.

Chapter 6 deals with the a novel zoning scheme with emphasis on managing separations among a team of robots during formation. In the proposed zoning scheme, zoning potentials include attracting potentials and repulsive potentials, which can provide collision avoidance and prevention of communication linkage breakdown. It is a novel framework, which can analyze the stability of multi-robot formation based on the notion of artificial potential trench. While the notion of artificial potential trench provides scalability in multi-robot formation, the controls presented in this chapter ensure that such

scalable formations are stable even under the constraints of separation coordination. Apart from separation management which relies on zoning potentials, a new method is introduced to remove the pre-determined goal points by assigning a direction for robots to approach. This procedure is incorporated into the formation controller design. Computer simulations are carried out to verify the effectiveness of this approach.

Chapter 7 aims to investigate a generic formation control, which attracts a team of coordinated robots to their own nearest points on the assigned segment. Meanwhile, the robots are capable of avoiding collisions with multiple static or moving obstacles in a dynamic environment. A mathematical framework is developed beforehand to analyze the characteristics of motions of the nearest points on the segment. Although the nearest points may undergo a discontinuity as revealed by the analysis, such transitions of the nearest points are well handled by nonsmooth analysis. A novel method of obstacle avoidance is based on the new concept of apparent obstacle scheme. Together with the associated local minima recovery scheme, the method is proposed to cope with concave obstacles and multiple moving obstacles. Comparison between apparent obstacle avoidance method and other alternative solutions is summarized. A detailed algorithm to seek the nearest point on a segment in the presence of obstacles is presented. The special cases of local minima and the corresponding simple solutions are discussed in detail.

Chapter 8 deals with the stability of the formation control of multiple robots based on artificial potential trench method and queue formation method. It is shown that the closed-loop system of each robot is input-to-state stable to its leader's initial forma-

tion error and each queue formation is globally uniformly asymptotically stable. Furthermore, queue formation is robust with respect to structural changes and intermittent breakdown of communication link.

Chapter 9 summarizes the contributions of this thesis and outlines the directions for future research.

Chapter 2

Literature Review

Cooperative control for multi-agent systems can be categorized as either formation control problems with applications to mobile robots, unmanned air vehicles (UAVs), autonomous underwater vehicles (AUVs), satellites, aircraft, spacecraft, and automated highway systems, or nonformation cooperative control problems such as task assignment, payload transport, role assignment, air traffic control, timing, and search. The cooperative control of multi-agent systems poses significant theoretical and practical challenges. For cooperative control strategies to be effective, numerous issues must be addressed, including the definition and management of shared information among a group of agents to facilitate the coordination of these agents. In cooperative control problems, shared information may take the form of common objectives, common control algorithms, relative position information, or a world map. Information necessary for cooperation may be shared in a variety of ways.

For cooperative control strategies to be effective, a team of agents must be able to re-

spond to unanticipated situations or change in the environments that are sensed as a co-operative task is carried out. As the environment changes, the agents on the team must be in agreement as to what changes took place. A direct consequence of the assumption that shared information is a necessary condition for coordination is that cooperation requires that the group of agents reach consensus on the coordination data. In other words, the instantiation of the coordination data on each agent must asymptotically approach a sufficiently common value. Convergence to a common value is called the consensus or agreement problem in the literature.

2.1 Formation Control Methods

Formation control is an important issue in coordinated control for a group of unmanned autonomous vehicles/robots. In many applications, a group of autonomous vehicles are required to follow a predefined trajectory while maintaining a desired spatial pattern. Moving in formation has many advantages over conventional systems, for example, it can reduce the system cost, increase the robustness and efficiency of the system while providing redundancy, reconfiguration ability and structure flexibility for the system. Formation control has broad applications, for example, security patrols, search and rescue in hazardous environments. In military missions, a group of autonomous vehicles are required to keep in a specified formation for area coverage and reconnaissance; in small satellite clustering, formation helps to reduce the fuel consumption for propulsion and expand their sensing capabilities. In automated highway system (AHS), the throughput of the transportation network can be greatly increased if vehicles can form

platoons at a desired velocity while keeping a specified distance between vehicles. Research on formation control also helps people to better understand some biological social behaviors, such as swarm of insects and flocking of birds.

In formation control for a group of coordinated robots, different control topologies can be adopted depending on the specific scenarios. There may exists one or more leaders in the group while other robots follow one or more leaders in a specified way. Each robot has onboard sensing and computation ability. In some application scenarios, robots can have limited communication ability. But generally speaking, not all the global information is available for each robot.

A centralized controller usually is not assumed to exist. The design of the controller for each robot has to be based on the local information. If no leader is designated, then all robots must coordinate with each other by relying on some global consensus for a common goal achievement. There are many issues need to be considered when designing a distributed controller for mobile robot formation, such as the stability of the formation, controllability of different formation patterns, safety and uncertainties in formations. Many control approaches have been proposed to solve the problems in formation control, for example, leader-follower strategy [25], virtual structure approach [55][22] and behavior-based method [4] [85] [97], passivity-based decomposition approach [52]. In this chapter, we will cover the main issues in formation control and give a review on current technologies in formation control.

2.1.1 Behavior-Based Approach

Behavior-based approach is one of the most widely used methods for formation control. It is well-known that formation behaviors in nature such as schooling and flocking benefit the animals in a variety of ways. Sensors are combined by animals via grouping to maximize the chance of detecting predators or to more efficiently forage for food [90]. Studies of flocking and schooling in [76] reveal that these behaviors emerge as a combination of a desire to stay in the group and yet simultaneously keep a separation distance from other members of the group.

A pioneering work [73] provides important results based on the behavioral simulation of flocks of birds and schools of fish and a simple egocentric behavioral model for flocking which is instantiated in each member of the simulated group of birds. In this work, the behavior includes inter-agent collision avoidance, velocity matching and flock centering and successfully generates an overall group behavior while individual agent only sense their local environment and close neighbors. Improvements to this approach have been made in [87], where more realistic simulated fish schooling by accurately modelling the animals' muscle and behavioral systems are developed. Moreover [9] developed a system for realistically animating herds of one-legged agents using dynamical models of robot motion.

In contrast to the afore-mentioned work [9][73][76][87][90] which are focused on the generation of visually realistic flocks and herds for large numbers of simulated animals, behaviors for a small group (up to four) of mobile robots are studied in [4] [85], where

each robot has a basic motor schema, which can generates a vector representing the desired behavior response to sensory inputs. The motor schemas include move-to-goal, avoid-static-obstacle, avoid-robot and maintain-formation. The control action of each robot is represented by a vector weighted average of the control for each motor schema behavior. Three zones (ballistic zone, controlled zone, and dead zone) are predefined to compute the magnitude of the vector. In [97], the Genetic Algorithm is used to decide the control weights and choose the appropriate behavior for formation maintains and obstacle avoidance. In [65], the behavior-based formation control is modelled as a non-linear dynamic system for trajectory generation and obstacle avoidance. In [21], the robot's behavior is based on a subsumption architecture. The primary behavior explored in this work is a group formation behaviors based on social potential fields [71]. In this paper, the social potential fields method is extended and evaluated in the presence of agent failure and imperfect sensory input. In general, behavior-based approach typically lacks rigorous analysis and therefore this weakness imposes limit on its applications.

2.1.2 Potential Field Approach

The method of artificial potential fields [40], usually combined with behavior-based approach, has been applied to formation control. This method is also widely utilized in motion planning of mobile robots [50], ranging from obstacle avoidance [47][68][41], to robot navigation [42][74][75][93][92], and global path planning [91][88][33]. In this method, the control is synthesized based on a linear relationship involving the gradient of a potential field [34].

In [27], potential functions were used for a target tracking problem by considering both the instantaneous position and velocity of the target in a dynamic environment. When applied to the problem of formation control, however, the conventional potential field method yields deficient solutions because of lacking scalability of the prescribed formation as the robots are to be attracted to predetermined points that define the formation. The notion of queues and artificial potential trenches was introduced in [29] to provide the needed scalability. Since in practical applications, a formation taking certain geometric pattern shapes can be conveniently subdivided into a series of smooth line segments, each of these line segments are referred to as *queue*. Some of the key concepts such as *queue* and *segment* are adopted from the original work [29] as follows:

Definition 2.1.1 *A queue Q_j is defined as $Q_j = (S_j, X_j, C_j, \varepsilon_j(n))$, where S_j is a set of points defined by some smooth function $f : R^3 \rightarrow R^3$, $X_j \subseteq S_j$ is a set consisting of one or two formation vertices, C_j is the percentage of n robots that belong to Q_j, and $\varepsilon_j(n)$ defines the set of points within a certain distance of f.* □

Definition 2.1.2 *A segment S is a curve defined by some smooth (i.e., at least twice-differentiable) function in R^3 that passes through one or two formation vertices.* □

According to [29], a vertex is the terminal node of segments and is represented by its position relative to the coordinate frame of the target. In this approach, the definition of a formation is usually specified by a higher level decision maker, such as a human user. An example of queues, segments and the formation vertices from [29] is shown in Figure 2.1, where six robots are randomly scattered around three segments. These

robots are required to form some geometric pattern by allocating them to the segments at the desired locations. The idea is that, instead of being attracted to a predetermined point, each robot is to be attracted to the bottom of the "valley" artificially created by a so-called potential trench, and once there, move along the trench to distribute themselves along the trench in order to form a formation by maintaining the desired separation in relation to other robots. In Figure 2.1, each robot is supposed to be attracted to the corresponding location (denoted by shaded robot) on the assigned segment via artificial potential trench. Generally speaking, artificial potentials are inherent with local minima issues (which may cause the robots stuck) and this thesis will address such issues in detail.

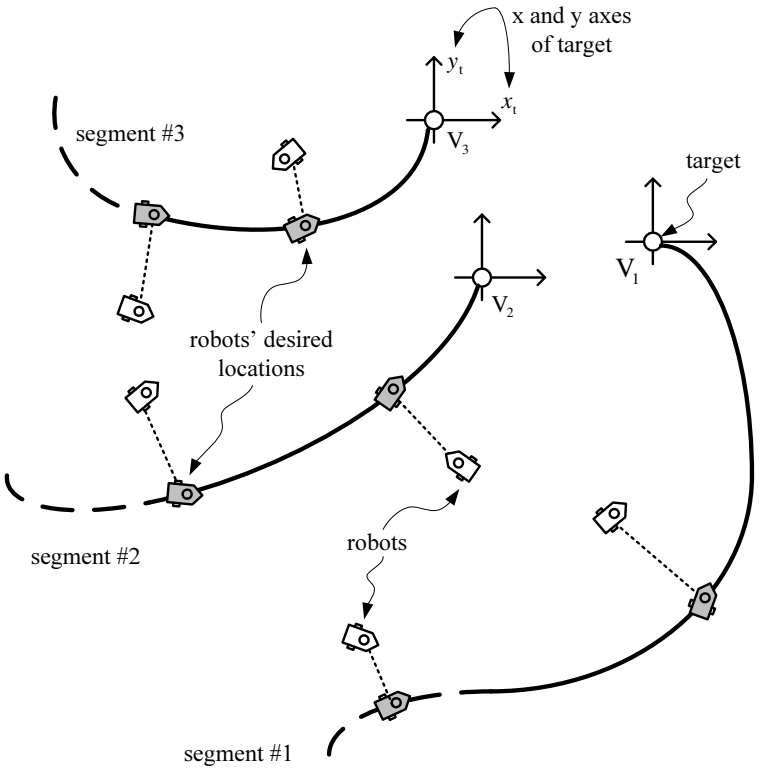

Figure 2.1: Examples of queues, segments and formation vertices(circles), where x_t and y_t are the axes of the coordinates frame of the target centered at V_1. Open queues are drawn with solid and dashed lines, indicating that they extend indefinitely from the vertex.

2.1.3 Leader-Follower Approach

Based on the assumption that only local sensor-based information is available for each robot, another approach using leader-follower pairing [84] is also widely adopted in formation control. The notion of leader-follower pairing can be illustrated in Figure 2.2. Two typical leader-follower pairing are depicted in this figure with the Figure 2.2(a) and Figure 2.2(b) denoting a cascade pattern and a parallel pattern respectively. Take the Figure 2.2(a) for instance, agent 2 and 3 depicted in circles are followers while agent 1 is the leader. Specially agent 1 and 2 form a leader-follower pair and so it is for agent 2 and 3.

In [84], two types of feedback controllers for maintaining formations of multiple mobile robots are proposed. One is the $l-\psi$ controller, which is illustrated by Figure 2.3 and the other one is the $l-l$ controller, of which the corresponding scenario is depicted in Figure 2.4. In the $l-\psi$ controller, the objective is to maintain a desired length l_{12}^d and a desired relative angle ψ_{12}^d between the leader and the follower. By using input/output feedback linearizaiton, a controller can be designed so that l_{12}^d and ψ_{12}^d can exponentially convergence to the desired values.

Figure 2.4 illustrates the $l-l$ controller considering the relative position of three mobile robots, where one robot is supposed to follow the other two robots. The objective is to maintain the desired lengths l_d^{13} and l_d^{23} between the follower and its two leaders. A controller is also designed by using input/output feedback linearization in [84]. The application of leader-follower approach can be found in [81]. Although leader-follower

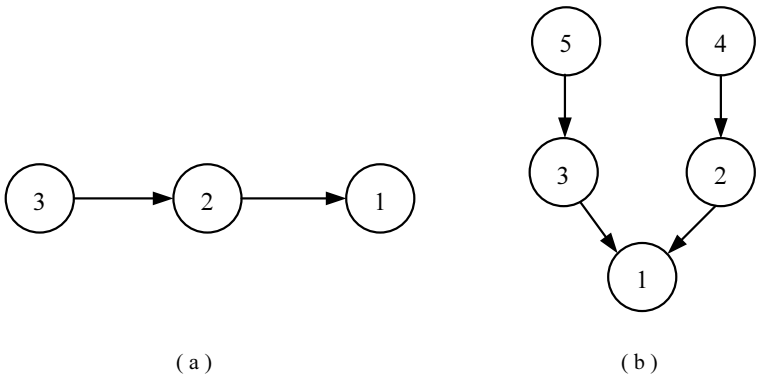

Figure 2.2: Leaders and followers in formation.

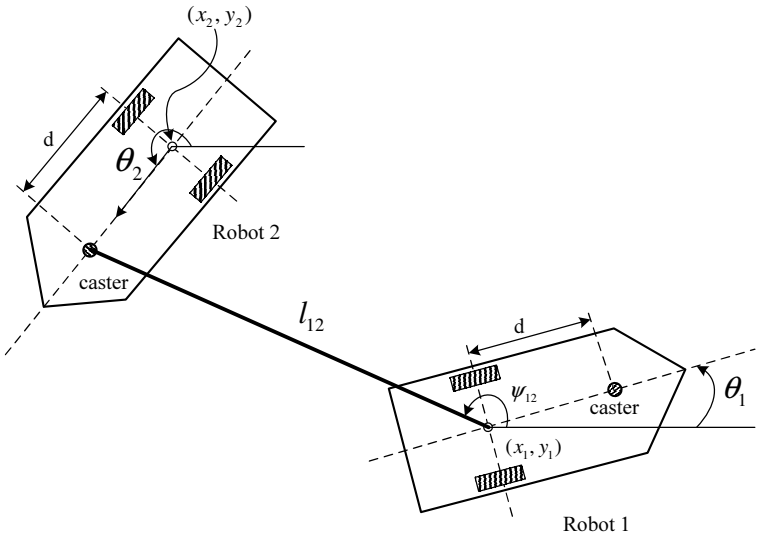

Figure 2.3: Notation for $l - \psi$ control.

approach is an important concept in formation, the controller methods introduced in [84] obviously lacks a framework to represent complicated geometric patterns and is not scalable to a team of robots with a great number of members.

2.1.4 Generalized Coordinates Approach

In [80], a control methodology based on generalized coordinates was presented. The generalized coordinates characterize the vehicles location (L), orientation (O) and its shape (S) with respect to a formation reference point in the formation. The trajectories

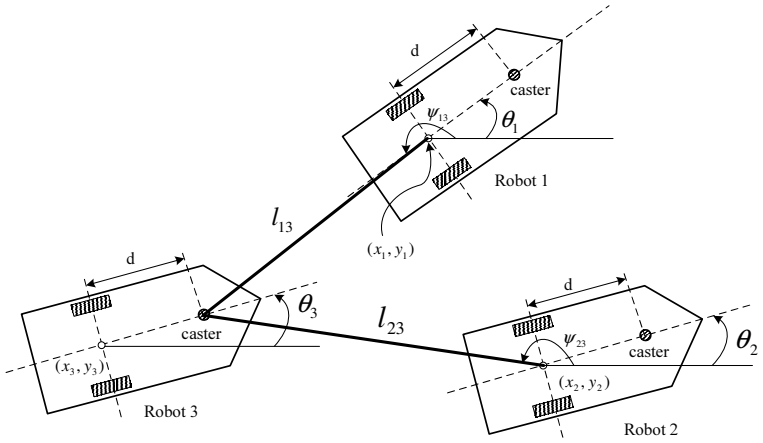

Figure 2.4: Notation for $l-l$ control.

of the formation group can be specified in terms of L, O and S coordinates. Formation control laws have been developed for asymptotic tracking of trajectories while maintaining a desired formation geometry. A similar idea was presented in [99], [95], where the shape of the formation is expressed in shape coordinates. In this approach, the robots are modelled as controlled Lagrangian systems on Jacobi shape space to allow a block-structured control of position, orientation and shape of the formation. Feedback control derived from Lyapunov functions leads the controlled dynamics to converge to the invariant set where the desired shape is achieved. Normally this kind of approach is useful for a small group of robots. However, it is hard to extend to large-scale multi-robot applications. Besides, the frameworks with collision prevention and obstacle avoidance are not clearly formulated and addressed.

2.1.5 Virtual Structure Method

The concept of virtual structure was first introduced in [55]. The virtual structure approach is usually used in spacecraft or small satellite formation flying control [22]. Con-

trol methods are developed to force a group of robots to behave in a rigid formation. In virtual structure approach, the controller is derived in three steps. First, the desired dynamics of the virtual structure is defined. Second, the desired motion of the virtual structure is translated into desired motions for each agent. Finally, individual tracking controllers for each agent are derived for agent tracking. In [54], the virtual structure method is combined with leader-following method and behavioral approach to formation control of multiple spacecraft interferometer in deep space. A similar idea in [17] was applied for spacecraft formation flying control. It should be noted that virtual structure method is similar to the 'node-to-robot' scheme and therefore is usually employed only in those applications where strict adherence of each robot to specific points is required.

2.1.6 Model Predictive Control (MPC) Method

Model Predictive Control (MPC), namely Receding Horizon Control (RHC), has been one of the well-established and probably the most popular forms of optimized process control and has been widely applied in many industries such as oil and chemical engineering. MPC is an optimal control strategy. The current control action is calculated by solving a constrained finite horizon open-loop optimal control problem at each sampling instant such that the current state of the system is used to compute the optimal input and state trajectories. The solution of the optimization problem turns out to be an optimal control sequence and according to the MPC strategy, only the first control action in the sequence is applied to the system.

A thorough survey of nonlinear MPC stability theory is given by Mayne et al in [62]. The generalized formulation and conditions for stability stated in [62] [61] are used as a guide for the formulation here. Recently MPC has been receiving more attention from researchers on formation control. There are several appealing aspects of MPC for the coordination of multiple vehicles to stabilize a formation. The advantages include inherent consideration of state, input and output constraints and its capabilities in dealing with Multiple Input, Multiple Output (MIMO) systems, etc. Moreover, as an optimization based method, it allows the cost functions and constraints in the optimal control problem to be potentially changed on-the-fly to accommodate new formations and limitations, such as inter-vehicle and obstacle collision avoidance [64]. In [96], MPC is utilized as a local control law to meet with the overall formation performance under imperfect inter-vehicle communication. The error in inter-vehicle communication is modelled as white noise. In [12], the problems associated with formation keeping of mobile robots is studied and control solutions to maintain a formation of robots as well as implementing a system to localize robots in an indoor environment is developed. In this work, several control strategies including an explicit MPC controller, made possible by the very low sampling rate of the system, are implemented.

Despite MPC's theoretical elegance and prominent advantages, it is facing challenges even from the very beginning because of its inherent tremendous demands on computational capabilities. The difficulties may aggregate and thus make the situation even worse with enhanced complexities when dealing multi-robot formation control in unstructured dynamic environments. As far as the high sampling rate of the robotic system

is concerned, online computation of the optimal control actions is not currently feasible [12], considering the current computational power of todays CPUs.

2.2 Stability Analysis Approaches for Formation Control

2.2.1 Lyapunov Function

In [69], the multi-agent coordination problem is studied in the framework of control Lyapunov functions. The main assumption is that each individual robot has a control Lyapunov function. Then, sufficient conditions for the existence of a control Lyapunov function for the formation of robots are derived. This function is a weighted sum of individual control Lyapunov function of each robot. Further investigation on the properties of the control Lyapunov function to maintain formation stability is applied by parameterized formation approach.

In [72], the stability of a decentralized virtual structure based spacecraft formation flying is studied using a Lyapunov function. In this paper, asymptotic stability is shown for each spacecraft's dynamic with respect to the corresponding desired states. In [54], a framework for coordinated and distributed control of multiple autonomous vehicle using artificial potentials and virtual leaders is proposed. Closed-loop stability is proved by constructing a Lyapunov function based on the system's kinetic energy and artificial potential energy. Asymptotic stability is achieved by integrating the dissipative control terms in the controller.

2.2.2 Nonsmooth Analysis

It is well-known that classical theorems for ordinary differential equations require vector fields to be at least Lipschitz continuous, of which the definition is given as follows.

Definition 2.2.1 *For a differential equation*

$$\dot{x} = f(x,t), x(t_0) = x_0,$$

where $f : R^n \times R \to R^n$ *is piecewise continuous in* t. f *is sLipschitz if the following inequality holds*

$$||f(t,x) - f(t,y)|| \leq L||x-y||,$$

where L is a positive constant. □

However, nonsmooth dynamics such as Coulomb friction, contact interactions existing in the nature feature discontinuous control inputs and thus cannot be addressed by classical stability theory. These observations make it essential to develop rigorous analysis and deal with the associated issues such as the existence of equilibria, stability and qualitative dynamics. Moreover, variable structure systems in control engineering where control inputs usually are discontinuous is another motivation for developing a formal tools dedicated to the analysis of differential equations with discontinuous right-hand sides.

There are many literatures such as [13] on nonsmooth analysis. As far as the generalized Lyapunov analysis is concerned, Lyapunov stability theory of nonsmooth systems was developed in [70][77],with which the stability properties of nonsmooth dynamic system

can be calculated and determined. In [83], the stability properties of a system of multiple mobile agents with double integrator dynamics are investigated by using nonsmooth analysis. Owing to nonsmooth analysis, control discontinuities arising from dynamic control interconnection topology and switching control law which are allowed to vary with time are handled at no expense of system stabilities.

2.2.3 Graph Theory

Graph theory is the branch of mathematics on graphs, mathematical structures used to model pairwise relations between objects from a certain collection. It plays an important role in the stability analysis of the formations as it caters for a natural presentation of the interconnection of coordinated robots for information exchange. An example where the formation pattern is represented as ”graph formation” is provided in Figure 2.5 with each circle denoting an agent in the formation. There are several appealing characteristics of graph theory which motivate the application research for multi-robot formation control. First, characterization of the topology of a graph can be used which greatly facilitates the stability analysis of robot formations. Second, it can also be employed to determine an appropriate controller for a specific formation pattern or even decide if such a controller can exist. There are rich literatures on graph theory [31], [32], [82]. An undirected graph G consists of a vertex set $V(G)$ and an edge set $E(G)$, where an edge is denoted as a pair of distinct vertices of G. In [24], the directed graph is used to represent a formation of agents while the dynamics of the agents are represented by linear time-invariant systems. By analyzing the eigenvalues of the graph Laplacian matrix,

a Nyquist criterion is developed to determine the effect of the communication topology on formation stability. In [49], the connection between the spectral graph theory and the control problem in vehicle formations is further investigated. The vehicles exchange information according to a pre-specified undirected communication graph. A statespace approach was developed to stabilize the formation. It is proved that a linear stabilizing feedback law always exists provided that the communication graph is connected. The rate of convergence to formation is governed by the size of the smallest positive eigenvalue of the Laplacian of the communication graph. Some research has been focused on how the characteristics of the interconnection graph will change when the formation is changed from one pattern to another. In [18], under the framework of leader-following approach, the number of possible control graphs is derived, depending how the following pattern for each local controller is chosen. This result is used to search for the possible transient control graph when the formation is changing. In [60], the geometric formations of multiple vehicles are studied under cyclic pursuit control law. The stability of the equilibrium formations of unicycle robots is related to the graph characteristic of the patterns. In [56], based on the analysis of the directed graph from the interconnection of individual robots, the feasibility of achieving a desired pattern is investigated. Generally speaking, despite convenience of stability analysis for graph-based formation control, the complexity of theory is a barrier for widely application of this method and there is still much fundamental work to be done in this research area.

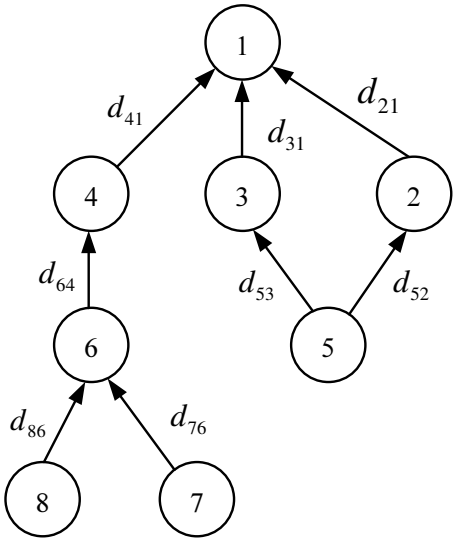

Figure 2.5: An example of graph formation.

2.3 Summary

In the chapter, we reviewed several available approaches to multi-robot formation control together with the performance such as scalability, flexibility. The associated control stability and analysis methodologies are also surveyed.

Chapter 3

Formulation of Research Problems

In this chapter, formulations of the significant research problems of this dissertation and the fundamentals of nonsmooth analysis are to be addressed. Previously in Chapter 1, a typical scenario of multi-robot formation control is shown in Figure 1.5 and an informal discussion on topics of multiple robotic system formation control is presented. In this chapter, more technical details including fundamentals of the relevant key concepts and notions (such as the modelling of differential mobile robots) and the statements of research problems to be investigated is covered.

3.1 Modelling of Differential Mobile Robots

3.1.1 Dynamics Model

We consider Hilare-type mobile robots with two rear wheels and a front caster. Figure 3.1 illustrates one such robot with its inertial coordinates frame. The two rear wheels of

the robot are controlled independently by motors. The center of the wheels is denoted by (x_i, y_i), the center of mass of the robot is denoted by (x_{hi}, y_{hi}), and the distance between (x_i, y_i) and (x_{hi}, y_{hi}) denoted by L_i. It is assumed that the wheels of the robot do not slide, so that the velocity of (x_i, y_i) is orthogonal to the axis of the wheels. Without

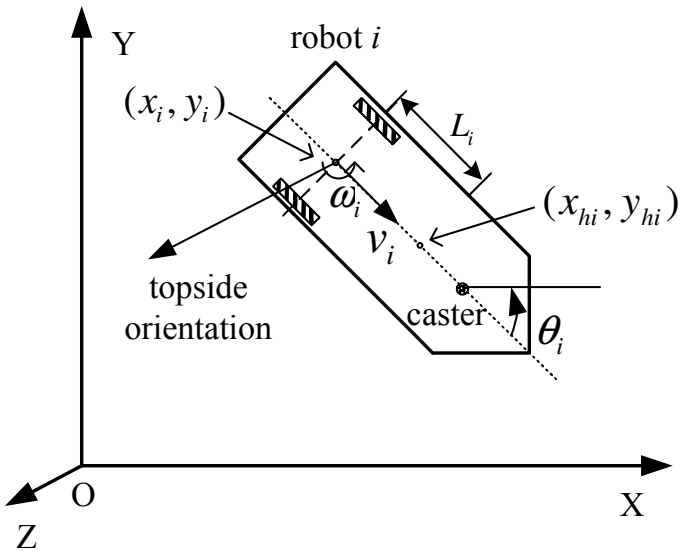

Figure 3.1: A wheeled mobile robot.

considering the rolling friction forces or torques produced by the casters, the dynamics of a robot is described by the following equations of motion:

$$\begin{cases} \dot{x}_i &= v_i \cos\theta_i, \\ \dot{y}_i &= v_i \sin\theta_i, \\ \dot{\theta}_i &= \omega_i, \\ \dot{v}_i &= F_i/m_i, \\ \dot{\omega}_i &= \tau_i/J_i, \end{cases}$$

where, with respect to the inertial coordinates frame with its origin at O, $[x_i, y_i]^T \in R^2$ is the position vector of a robot i, θ_i is the orientation, v_i is the translational velocity,

ω_i is the angular velocity, F_i is the force input, m_i is the mass, τ_i is the torque input and J_i is the moment of inertia. Define vectors $\vec{q}_i = [x_i, y_i, \theta_i, v_i, \omega_i]^T$ and $\vec{\mu}_i = [F_i, \tau_i]^T$, which represents the physical inputs to the actuators. To facilitate analysis, the above nonholonomic system can be feedback linearized by some diffeomorphic coordinate transformation $\vec{\Xi}_i = T_1(\vec{q}_i)$ with $\vec{\Xi}_i = [\xi_{1i}, \xi_{2i}, ..., \xi_{5i}]^T$ and state feedback $\vec{\mu}_i = T_2(\vec{q}_i, \vec{u}_i)$. Define a new position vector as

$$\begin{aligned} x_{hi} &= x_i + L_i \cos(\theta_i), \\ y_{hi} &= y_i + L_i \sin(\theta_i). \end{aligned}$$

Differentiating (x_{hi}, y_{hi}) with respect to time twice yields,

$$\begin{bmatrix} \ddot{x}_{hi} \\ \ddot{y}_{hi} \end{bmatrix} = \begin{bmatrix} -v_i\omega_i \sin(\theta_i) - L_i\omega_i^2 \cos(\theta_i) \\ v_i\omega_i \cos(\theta_i) - L_i\omega_i^2 \sin(\theta_i) \end{bmatrix} + \begin{bmatrix} \frac{1}{m_i}\cos(\theta_i) & -\frac{L_i}{J_i}\sin(\theta_i) \\ \frac{1}{m_i}\sin(\theta_i) & \frac{L_i}{J_i}\cos(\theta_i) \end{bmatrix} \begin{bmatrix} F_i \\ \tau_i \end{bmatrix}$$

Let $T_1(\vec{q}_i) : \vec{q}_i \rightarrow \vec{\Xi}_i$ as

$$\begin{cases} \xi_{1i} &= x_i + L_i\cos(\theta_i), \\ \xi_{2i} &= y_i + L_i\sin(\theta_i), \\ \xi_{3i} &= v_i\cos(\theta_i) - L_i\omega_i\sin(\theta_i) = \dot{\xi}_{1i}, \\ \xi_{4i} &= v_i\sin(\theta_i) + L_i\omega_i\cos(\theta_i) = \dot{\xi}_{2i}, \\ \xi_{5i} &= \theta_i. \end{cases}$$

It is known that the map T_1 is a diffeomorphism with its inverse given by

$$\vec{q}_i = T_1^{-1}(\vec{\Xi}_i) = \begin{bmatrix} \xi_{1i} - L_i\cos(\xi_{5i}) \\ \xi_{2i} - L_i\sin(\xi_{5i}) \\ \xi_{5i} \\ \xi_{3i}\cos(\xi_{5i}) + \xi_{4i}\sin(\xi_{5i}) \\ -\frac{1}{L_i}\xi_{3i}\sin(\xi_{5i}) + \frac{1}{L_i}\xi_{4i}\cos(\xi_{5i}) \end{bmatrix}$$

Let the state feedback $T_2(\vec{q}_i) : \vec{\mu}_i \rightarrow \vec{u}_i$ be as

$$\begin{aligned} \vec{\mu}_i &= \begin{bmatrix} \frac{1}{m_i}\cos(\theta_i) & -\frac{L_i}{J_i}\sin(\theta_i) \\ \frac{1}{m_i}\sin(\theta_i) & \frac{L_i}{J_i}\cos(\theta_i) \end{bmatrix}^{-1} \times \\ &\quad \begin{bmatrix} \vec{u}_i - \begin{bmatrix} -v_i\omega_i\sin(\theta_i) - L_i\omega_i^2\cos(\theta_i) \\ v_i\omega_i\cos(\theta_i) - L_i\omega_i^2\sin(\theta_i) \end{bmatrix} \end{bmatrix}. \end{aligned}$$

which gives

$$\begin{bmatrix} \dot{\xi}_{1i} \\ \dot{\xi}_{2i} \end{bmatrix} = \begin{bmatrix} \xi_{3i} \\ \xi_{4i} \end{bmatrix}, \tag{3.1}$$

$$\begin{bmatrix} \dot{\xi}_{3i} \\ \dot{\xi}_{4i} \end{bmatrix} = \vec{u}_i, \tag{3.2}$$

$$\dot{\xi}_{5i} = -\frac{1}{L_i}\xi_{3i}\sin(\xi_{5i}) + \frac{1}{L_i}\xi_{4i}\cos(\xi_{5i}). \tag{3.3}$$

Note that Equation (3.3) represents the *internal dynamics* (see page 517 of the monograph [39]) of the transformed systems. Its zero dynamics can be obtained by setting $\xi_{1i} = \xi_{2i} = \xi_{3i} = \xi_{4i} = 0$, yielding $\dot{\xi}_{5i} = 0$, which is stable. The stability issues of the internal dynamics are addressed in [98], which shows that the internal motion is asymptotically sable when the reference point is to move forward, and unstable when it moves backward. Defining the vector $\vec{r}_i = [x_{hi}, y_{hi}]^T$ and noting that $x_{hi} = \xi_{1i}$ and $y_{hi} = \xi_{2i}$, from Equations (3.1) and (3.2), we have

$$\ddot{\vec{r}}_i = \vec{u}_i, \tag{3.4}$$

which is a two-dimensional double integrator and $\vec{u}_i$ is the control input for this linearized model.

3.1.2 Kinematic Model

Usually the motion of WMR can be depicted by kinematic models. Define the posture variable as $p_i = [x_i, y_i, \theta_i]^T$, then the kinematics of a WMR is given by

$$\begin{aligned} \dot{p}_i &= \begin{bmatrix} \cos(\theta_i) & 0 \\ \sin(\theta_i) & 0 \\ 0 & 1 \end{bmatrix} \begin{bmatrix} v_i \\ \omega_i \end{bmatrix} \\ &= S(p_i) \begin{bmatrix} v_i \\ \omega_i \end{bmatrix}. \end{aligned} \tag{3.5}$$

As shown in Equation (3.5), the posture of a WMR is a time-varying nonlinear system with three outputs and two inputs.

3.2 Point Tracking Control of Mobile Robots

3.2.1 Comparative Study of Two Nonlinear Feedback Controls

It is well-known that usually WMRs are characterized by non-integrable kinematic constraints, namely the nonholonomic constraints. The consequence is that these constraints rule out the possibility of direct application of standard control theories, such as linear control theory. Furthermore, as pointed out in a landmark paper [8], nonholonomic systems cannot be stabilized by continuously differentiable, time-invariant, state feedback controls. To deal with the challenges arising in nonhonomic system control, a great

number of approaches have been proposed and some selections of the vast amount of published literature are reflected in the survey paper [43] and the book [20] and in Chapters (7-9) of the book [15]. Several controls from experiment perspectives are examined and implemented in [59].

Central to the WMR motion control are the tracking control problems. Normally there are two categories of tracking control: *posture tracking* and *point tracking*. The former aims to achieving stably tracking a moving reference posture (i.e., position and orientation) while the latter only concerns about position tracking. Nonlinear feedback control strategies [16, 30, 38, 63, 86] are often preferred in dealing with tracking control problem to compensate disturbances and uncertainties although open-loop controls are also workable [66, 48, 10, 7].

We consider the *point tracking* problem for a wheeled mobile robot that is depicted in the world frame OXY as shown in Figure 3.2. In this scenario, a wheeled mobile robot is supposed to track a series of goal points denoted by q_g along a smooth curve, which is usually referred as a ”segment” in the sequel. Referring to this figure, intuitively we refer to notations r and ϕ as ”distance to target” and ”misalignment angle” respectively. As far as tracking control is concerned, an effective control should be able to drive the robot approaching the desired goal point. In other words, the distance to target r has to be reduced as small as possible by manipulating with the velocities of left wheel and right wheel.

In order to take advantages of kinematic model described by Equation (3.5) for the wheeled mobile robot, it is convenient to transform it into another type of kinematic

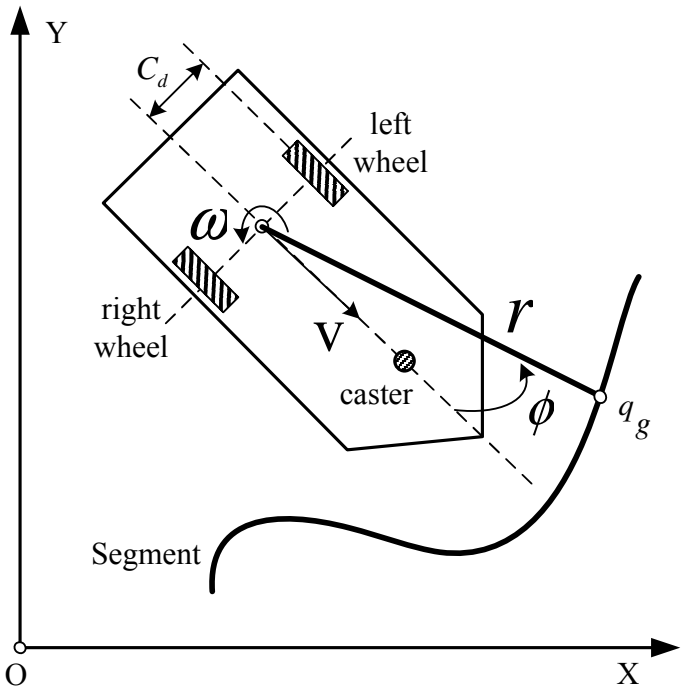

Figure 3.2: Illustration of a wheeled mobile robot and its goal point q_g, which may be moving on a segment (smooth curve) in the world frame.

model in a polar coordinates as shown in Figure 3.3. In this figure, a differential mobile robot, together with the associated notations, is illustrated in a polar coordinates $O'X'Y'$. It should be noted that deliberately we assign the origin to be the goal point (on a segment that is not depicted in this figure) for the robot to track. Namely the origin of the polar frame $O'X'Y'$ in Figure 3.3 denotes the aforementioned goal point q_g (for the robot to track) in Figure 3.2. The separation between point (x,y) and center of each wheel is represented by C_d, which is a fixed constant parameter for a given model of real robot. The heading of the robot is θ while its translational velocity and angular velocity are denoted by v and ω respectively. Note that throughout this chapter, both ϕ and θ are defined in the domain $(-\pi,\pi]$.

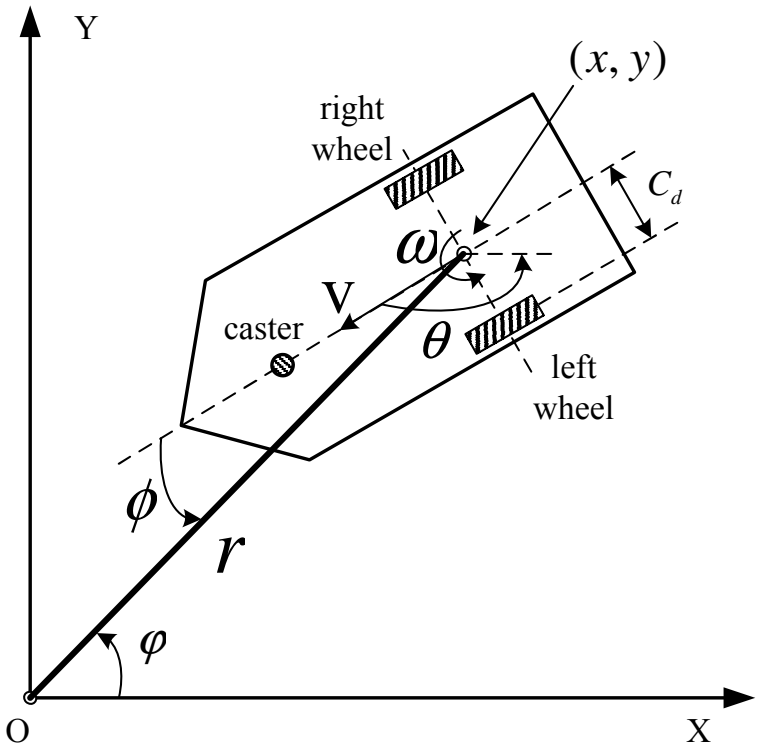

Figure 3.3: Representation of a wheeled mobile robot in the polar coordinates frame $O'X'Y'$ with the origin being its goal point.

Referring to Figure 3.3, the motion of a differential mobile robot can be described by

$$\begin{aligned} \dot{x} &= v\cos(\theta), \\ \dot{y} &= v\sin(\theta), \\ \dot{\theta} &= \omega. \end{aligned} \tag{3.6}$$

To link this model with the notations in polar coordinates, we can calculate r and ϕ as

$$r = \sqrt{x^2 + y^2},$$

$$\phi = \pi + \theta - \varphi,$$

respectively.

A kinematic model of a differential mobile robot in the polar coordinates can be derived as follows:

$$\begin{bmatrix} \dot{\theta} \\ \dot{r} \\ \dot{\phi} \end{bmatrix} = \begin{bmatrix} 0 & 1 \\ -\cos(\phi) & 0 \\ \frac{1}{r}sin(\phi) & 1 \end{bmatrix} \begin{bmatrix} v \\ \omega \end{bmatrix}. \tag{3.7}$$

Detailed derivation of Equation (3.7) can be found in [53] and is omitted for brevity. This model is similar to the ones used in Chapter 3 of [78]. From this model, specifically we have the relationship between $\dot{r}$, $\dot{\phi}$ and v, ω as

$$\begin{bmatrix} \dot{r} \\ \dot{\phi} \end{bmatrix} = \begin{bmatrix} -\cos(\phi) & 0 \\ \frac{1}{r}\sin(\phi) & 1 \end{bmatrix} \begin{bmatrix} v \\ \omega \end{bmatrix}. \tag{3.8}$$

Two similar continuous nonlinear feedback controls were proposed by [36] and [53] respectively. In [36], a simple feedback control taking on the following form:

$$\begin{aligned} v &= K_1 r, \\ \omega &= -K_1 \sin(\phi) - K_2 \phi, \end{aligned} \tag{3.9}$$

together with some analytic results is presented. A similar control law is first proposed

in [53] and it is represented as follows:

$$\begin{aligned} v &= K_1 r\cos(\phi), \\ \omega &= -K_1\sin(\phi)\cos(\phi) - K_2\phi. \end{aligned} \tag{3.10}$$

Up to date, the essentially common features of these two nonlinear feedback controls are rarely addressed by researchers. In this thesis, we investigate the evolutions of robot's heading for each control. From this starting point, we are led to the special characteristics of the trajectory's uniqueness with respect to gain ratio and features of trajectory curvature. It is shown that the gain ratio plays a vitally important role in the motion of mobile robot. To synthesize these fruitful results and to facilitate real applications, we generalize the concept of "critical gain ratio" for the first time.

To sum up, a comparative study for these two nonlinear feedback controls, represented by Equations (3.10) and (3.9) respectively, is to be performed and the main tasks of this study include:

- (i) for the system described by Equation (3.8), study the Lyapunov stability problem that can lead to a generic form of nonlinear controls and then show that it can be simplified into the control represented by Equations (3.10) and (3.9);
- (ii) derive analytic expressions of robot's heading $\theta(t)$ and misalignment angle $\phi(t)$ by solving the corresponding differential equations;
- (iii) based on results obtained from (ii), calculate the overall turning of robot's

heading defined as $H_c = |\theta(\infty) - \theta(0)|$, namely the evolution of robot's heading;

- (iv) extract trajectory's characteristics with respect to gain ratio defined as $\lambda = \frac{K_1}{K_2}$;
- (v) investigate characteristics of trajectory curvature defined as $\mathscr{K}(t) = \frac{|\omega(t)|}{|v(t)|}$.

3.2.2 Formulation of the Robustness Problem

For the specific nonlinear control law described by Equation (3.10), which is stated in previous subsection, there exists a fundamental challenge beneath this control law although the stability issue seems to be affirmatively guaranteed by Lyapunov stability theorem. To look into this challenge, we can substitute Equation (3.10) in to Equation (3.8) and obtain

$$\begin{bmatrix} \dot{r} \\ \dot{\phi} \end{bmatrix} = \begin{bmatrix} -K_1 r\big(\cos(\phi)\big)^2 \\ -K_2\phi + \big(K_1\sin(\phi)\cos(\phi) - K_1\sin(\phi)\cos(\phi)\big) \end{bmatrix}, \tag{3.11}$$

where $-K_2\phi + \big(K_1\sin(\phi)\cos(\phi) - K_1\sin(\phi)\cos(\phi)\big)$ can be simplified as $-K_2\phi$. Usually a Lyapunov function candidate is chosen as $V = \frac{1}{2}r^2 + \frac{1}{2}\phi^2$. Accordingly, with Equation (3.11), the derivative of V can be calculated as follows:

$$\begin{aligned} \dot{V} &= \begin{bmatrix} r & \phi \end{bmatrix} \begin{bmatrix} \dot{r} \\ \dot{\phi} \end{bmatrix} \\ &= -K_1 r^2\big(\cos(\phi)\big)^2 - K_2\phi^2 \\ &\leq 0. \end{aligned} \tag{3.12}$$

Evidently, the technique of term cancellation, namely $\big(K_1 \sin(\phi)\cos(\phi) - K_1 \sin(\phi)\cos(\phi)\big)$, is the key to obtain the simplified result represented by Equation (3.12), which leads to invoking Lyapunov stability theorem. One may be interested in the following question: what if the gain K_1 in v and ω does not match? Consider an alternative to the control law in Equation (3.10) as follows:

$$\begin{aligned} v &= K_1 \cdot r\cos(\phi), \\ \omega &= -K_3 \sin(\phi)\cos(\phi) - K_2\phi, \end{aligned} \tag{3.13}$$

where K_3 is not necessarily equal to K_1. Then it is equivalent to say: "will the closed-loop system be stable if an alternative control represented in Equation (3.13) rather than the one in Equation (3.10) is applied to the system?".

In the real world, there are numerous factors contributing to such kind of "gain mismatching". Take the digital control for example, truncation error of numerical calculation of triangle functions of ϕ is unavoidable. Moreover, in terms of real outputs of physical actuator, this "mismatching gain" phenomenon may happen from time to time. To explain it, let v_L, v_R denote the tangent velocities of each wheel about the centers of rotation.

$$\begin{aligned} v &= \frac{v_L + v_R}{2}, \\ \omega &= \frac{v_R - v_L}{2C_d}, \end{aligned} \tag{3.14}$$

where C_d is the displacement from the point (x,y) to each wheel. We can establish the relationship between the vector $[v \;\; \omega]^T$ and $[v_L \;\; v_R]^T$ as follows:

$$\begin{bmatrix} v \\ \omega \end{bmatrix} = \frac{1}{2} \begin{bmatrix} 1 & 1 \\ \frac{1}{C_d} & \frac{1}{C_d} \end{bmatrix} \begin{bmatrix} v_L \\ v_R \end{bmatrix}, \tag{3.15}$$

$$\begin{bmatrix} v_L \\ v_R \end{bmatrix} = \begin{bmatrix} 1 & C_d \\ 1 & -C_d \end{bmatrix} \begin{bmatrix} v \\ \omega \end{bmatrix}. \tag{3.16}$$

The ideal control law Equation (3.10) is based on the assumption that the following equations

$$\begin{aligned} v_L &= K_1 r\cos(\phi) - C_d\big(K_1\sin(\phi)\cos(\phi) + K_2\phi\big), \\ v_R &= K_1 r\cos(\phi) + C_d\big(K_1\sin(\phi)\cos(\phi) + K_2\phi\big), \end{aligned}$$

strictly hold for each moment during the operation. However, in the real world, this turns out to be unrealistic. Apart from external disturbances, there are many factors that can ruin the perfect diagnosing shown in aforementioned context. For instance, each motor have different electro-mechanical characteristics. And each motor has its own nonlinearities(e.g. saturation) and so on. So in dynamic scenarios, we only have the real velocities $v_L^{'}$ and $v_R^{'}$ instead of the ideal counterparts v_L and v_R. In other words, we need to evaluate the real-world relationships represented by $v_L^{'} \neq v_L$ and $v_R^{'} \neq v_R$ and their

effects on stability. Readily it flows that

$$\begin{aligned} v^{'} &= (v_L^{'} + v_R^{'})/2, \\ \omega^{'} &= (v_R^{'} - v_L^{'})/(2C_d). \end{aligned} \tag{3.17}$$

To simplify the analysis, we consider the mismatching of ω with respect to v, which is the case with control in Equation (3.13). Substituting Equation (3.13) into Equation (2) in the first part of this chapter, we obtain

$$\begin{aligned} \begin{bmatrix} \dot{r} \\ \dot{\phi} \end{bmatrix} &= \begin{bmatrix} -\cos(\phi) & 0 \\ \frac{1}{r}\sin(\phi) & 1 \end{bmatrix} \begin{bmatrix} K_1 r\cos(\phi) \\ -K_3\sin(\phi)\cos(\phi) - K_2\phi \end{bmatrix} \\ &= \begin{bmatrix} -K_1(\cos(\phi))^2 r \\ -K_2\phi - (\frac{K_3 - K1}{2})\sin(2\phi) \end{bmatrix}. \end{aligned} \tag{3.18}$$

Through studying the stability of the closed-loop system described by Equation (3.18), we are able to investigate the robustness of the alternative control law given in Equation (3.13).

The ultimate goal of this part of robustness analysis is to obtain an improved robust control on the basis of Equation (3.10) and then try to implement it on MRKIT robots on multi-robot formation control.

3.3 Implementation of Multi-Robot Formation Control

Based on the results obtained in the foregoing mentioned robustness analysis, the improved nonlinear feedback control given by Equation (3.13), rather than the original control described by Equation (3.10) is to be applied to multi-robot formation control. The specific MRKIT mobile robots shown in Figures 1.2 - 1.4) in Chapter 1, are instructed to form certain geometric pattern. In order to perform experiments on formation control, a complete set-up including hardware platform and software application program has been implemented. To provide real-time position and heading information of robots, a GPS system is simulated by a vision system comprising vision frame grabber, CCD color camera with lens, a working station, and wireless communication modules. Details of implementation will be discussed in the following chapter. To verify the robust improved feedback control and to demonstrate multi-robot formation control, two experiments of formation control implementation on multi-robot system are to be implemented. One experiment is to form 3-robot triangle formation while the other is a 4-robot square formation. Each robot will follow an assigned virtual robot, which can be viewed as a moving point. Figure 3.4 shows the scenario of these two experiments.

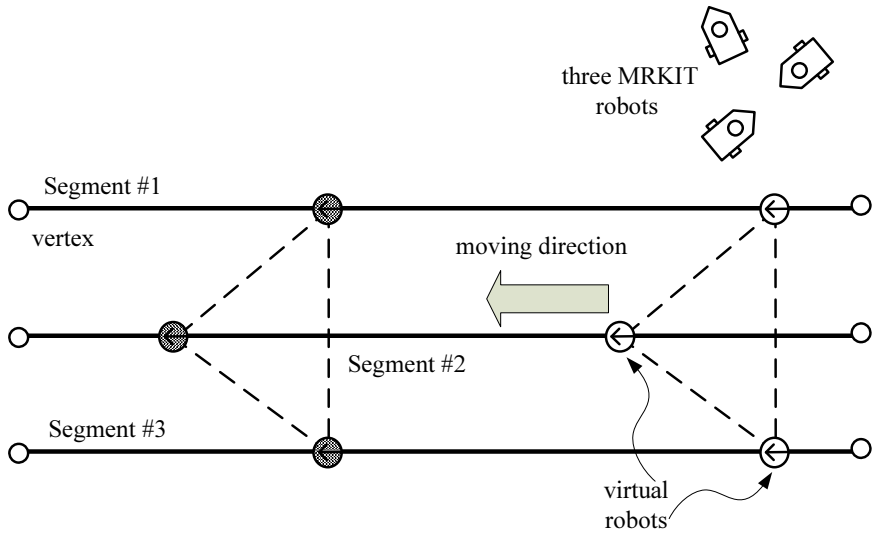

(a) Triangle formation of three robots

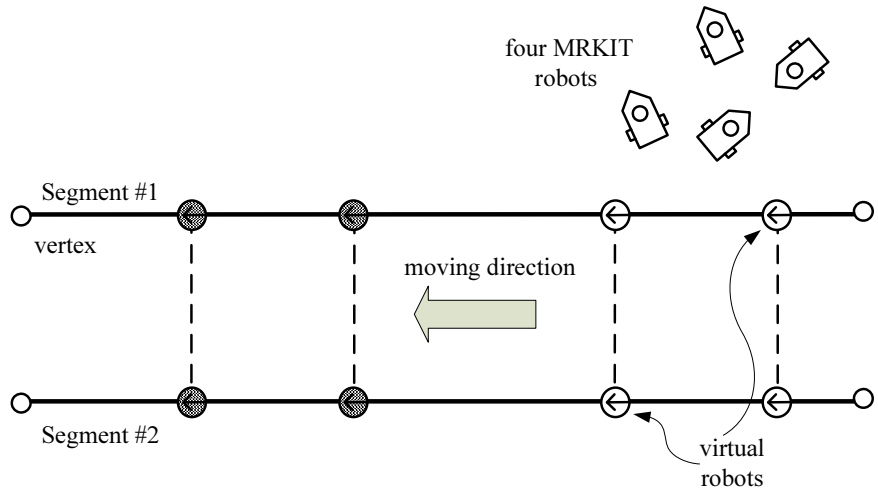

(b) Square formation of four robots

Figure 3.4: Illustration of segments, virtual robots and three-robot triangle formation and four-robot square formation.

3.4 Problem Formulation of Segment Formation Control

3.4.1 Mathematical Preliminaries

As far as stability of control system is concerned, Lyapunov stability theory is one of the most powerful analysis tools. The well known notion of stability in the sense of Lyapunov together with the main Lyapunov's Stability Theorem is summarized as follows.

Definition 3.4.1 *(Stability in the sense of Lyapunov) Consider the autonomous system* $\dot{x} = f(x)$, *where* $f : D \to R^n$. *Suppose that* $x_e \in D$ *is an equilibrium point, i.e.,* $f(x_e) = 0$. *The equilibrium point* x_e *is said to be stable if, for each* $\varepsilon > 0$, *there exists* $\delta = \delta(\varepsilon)$ *such that* $\|x(0)\| < \delta \Longrightarrow \|x(t)\| < \varepsilon, \forall\ t \geq 0$, *and asymptotically stable if it is stable and* δ *can be chosen such that* $\|x(0)\| < \delta \Longrightarrow \lim_{t\to\infty} x(t) = 0$, *and it is said to be globally asymptotically stable if* x_e *is stable and every initial state* $x(0)$ *results in* $\|x(t)\| \to 0$ *as* $t \ \to \infty$. □

Lyapunov's Stability Theorem [39]: The equilibrium point x_e is stable if there exists a continuously differentiable function $V : D \subset R^n \to R$ such that $V(0) = 0$, $V(x) > 0$ in $D - \{0\}$ and $\dot{V}(x) \leq 0$ in D. Moreover, the point $x_e = 0$ is asymptotically stable if $\dot{V}(x) < 0$ in $D - \{0\}$.

However, in order to invoke Lyapunov theorem, the corresponding Lyapunov function candidate must be continuously differentiable. Hence, it rules out some application cases with nonsmooth dynamics, such as Coulomb friction, variable structure systems

of which control inputs can be discontinuous, or contact interactions. For instance, the function $V = |x|$ where $x \in R$ fails to be differentiable at $x = 0$. In order to analyze such systems with discontinuities, some results from nonsmooth analysis will be utilized in this thesis when dealing with stability issues of formation control. To facilitate presentation, it is necessary to state some fundamentals of nonsmooth analysis.

Definition 3.4.2 *(Strict Differentiability) A map F is said to admit a strict derivative at x, denoted by $D_sF(x)$, if for each v, the following holds,*

$$\lim_{\substack{y \to x \\ t \downarrow 0}} \sup \frac{F(y+tv) - F(y)}{t} =< D_sF(x), v >,$$

and the convergence is uniform for v in compact sets. □

Definition 3.4.3 *(Filipov Solutions [77]) Consider the following differential equation*

$$\dot{x} = f(x,t), \tag{3.19}$$

where $f : R^n \times R \to R^n$ is discontinuous, measurable and locally bounded. A vector function $x(\cdot)$ is called a solution of (3.19) on $[t_0,t_1]$ if $x(\cdot)$ is absolutely continuous on $[t_0,t_1]$ and for almost all $t \in [t_0,t_1]$

$$\dot{x} \in K[f](x,t) \tag{3.20}$$

where

$$K[f](x,t) \equiv \bigcap_{\delta>0} \bigcap_{\mu N=0} \overline{co} f(B(x,\delta - N,t)) \tag{3.21}$$

and $\bigcap_{\mu N=0}$ denotes the intersection over all sets N of Lebesgue measure zero. □

To overcome the limitations of conventional derivative that is not defined at disconti-

nuities, F. H. Clarke introduced the generalized directional derivative and generalized gradient.

Definition 3.4.4 *(The Generalized Directional Derivative [13]) Let $f : R^n \times R \rightarrow R$ be locally Lipschitz at x and let v be any vector in a real Banach space X. The generalized directional derivative of f at x in the direction v, denoted f^o, is defined as follows:*

$$f^o(x;v) \equiv \lim_{\substack{y \rightarrow x \\ t \downarrow 0}} \sup \frac{f(y+tv) - f(y)}{t}, \tag{3.22}$$

where y is a vector in X and t is a positive scalar. □

Evidently, the generalized directional derivative greatly relaxes the constraints imposed on strict differentiability.

Definition 3.4.5 *(Clarke's Generalized Gradient [13]) Let $f : R^n \times R \rightarrow R$ be locally Lipschitz at x and let v be any vector in a real Banach space X. The generalized gradient of f at a given point x, denoted by $\partial f(x)$, is the subset of X^* given by*

$$\partial f(x) \equiv \{\zeta \in X^* : f^o(x;v) \geq < \zeta, v >, \forall v \in X\} \tag{3.23}$$

□

In the finite-dimensional case, the generalized gradient is a very useful property as shown in the following theorem.

Generalized Gradient Formula [14]: Let $x \in R^n$ and let $f : R^n \rightarrow R$ be locally Lipschitz near given point x. Let Ω be any subset of zero measure in R^n, and let Ω_f be the set of

points in R^n at which f fails to be differentiable. Then

$$\partial f(x) \equiv co\{lim\nabla f(x_i) : x_i \to x, x_i \notin \Omega, x_i \notin \Omega_f\} \tag{3.24}$$

Definition 3.4.6 *(Regular Function [13]) A function $f : R^n \to R$ is said to be regular at x provided that,*

(1) for all v, the usual one-sided directional derivative $f^{'}(x;v)$ exists.

(2) for all v, $f^{'}(x;v) = f^{o}(x;v)$.

□

Chain Rule Theorem [77]: Let $x(\cdot)$ be a Filipov solution to $\dot{x} = f(x,t)$ on an interval containing t and $V : R^n \times R \to R$ be a Lipschitz and regular function. Then $V = V(x(t),t)$ is absolutely continuous, $(d/dt)V(x(t),t)$ exists almost everywhere, and

$$\frac{d}{dt}V(x(t),t) \in^{a.e.} \dot{\tilde{V}}(x,t),$$

where

$$\dot{\tilde{V}}(x,t) \equiv \bigcap_{\xi \in \partial V(x(t),t)} \xi^T \begin{pmatrix} K[f](x(t),t) \\ \\ 1 \end{pmatrix},$$

and "a.e." is the abbreviation of "almost everywhere".

Now we present the nonsmooth version of Lyapunov's and LaSalle's Theorems. *Nonsmooth Version of Lyapunov's Theorem:* If a real-valued map $V : R^n \to R$ is definite

positive and for $x : R \rightarrow R^n$, $V(x(t))$ is absolutely continuous on $[t_0, \infty)$ with

$$\frac{d}{dt}[V(x(t))] < -\varepsilon < 0 \text{ a.e. on } \{t | x(t) \neq 0\},$$

then $x(t)$ converges to 0 in finite time.

Nonsmooth Version of LaSalle's Theorem [77]: Let Ω be a compact subset of R^n such that every Filipov solution to the autonomous systems $\dot{x} = f(x)$, $x(0) = x(t_0)$ starting in Ω is unique and remains in Ω for all $t \geq t_0$. Let $V : \Omega \rightarrow R$ be a time-independent regular function such that $v \leq 0$ for all $v \in \dot{\tilde{V}}$ (if $\dot{\tilde{V}}$ is the empty set then this is trivially satisfied). Define $S = \{x \in \Omega | 0 \in \dot{\tilde{V}}\}$. Then every trajectory in Ω converges to the largest invariant set, M, in the closure of S.

3.4.2 Segment Formation Control with Nonsmooth Artificial Potential Trenches

In the artificial potential trenches method introduced in [29], formations are defined using "queues" or "segments" instead of nodes or vertices, and potential trenches are designed to guide the robots into the formation rather than the exactly predetermined points in the formation. Before proceeding with the problem description, we make the following assumptions throughout the dissertation.

Assumption 3.4.1 *The whole team follows a leader (either virtual or real). The position $\vec{r}_0$, the velocity $\vec{v}_0$ and the topside orientation of the leader are known.*

Assumption 3.4.2 *Each robot is able to localize itself, and can estimate its global position $\vec{r}_i$, velocity $\vec{v}_i$ and orientation.*

At the initial stage of formation the randomly scattered robots have to determine to which segment they belong. As the robots can localize themselves in terms of global position and they can broadcast their position information among each other, it is possible for the robots to arrive at a decision of their segment status. The detailed decision making algorithms was described in [29].

The notion of artificial potential trench is illustrated in Figure 3.5). In this approach, for each instantaneous position $\vec{r}_i$ of a robot, there is a unique known goal point $q_{i,g}$ (stationary or in motion) with its position indicated by $\vec{r}_{i,g}$ on the segment for the robot to track. For each pair $(\vec{r}_i, \vec{r}_{i,g})$, we can construct a scalar function $\Phi(d_{i,g})$, where $d_{i,g} = \|\vec{d}_{i,g}\| = \|\vec{r}_{i,g} - \vec{r}_i\|$ represents the distance from the current position of robot r_i to its goal point on the segment. Intuitively, $\Phi(\cdot)$ forms a trench along the segment, and is referred to as the *potential trench function*. The motivation for creating such an artificial potential trench is to attract robots to the segment. The corresponding attractive force generated by artificial potential trench is calculated as

$$\vec{F}_{i,att} = \left(\nabla_x \Phi(x)|_{(d_{i,g})}\right) \hat{d}_{i,g}, \tag{3.25}$$

where $\hat{d}_{i,g} = \vec{d}_{i,g}/d_{i,g}$ is the unit vector pointing from instantaneous position of r_i to the nearest point $q_{i,g}$.

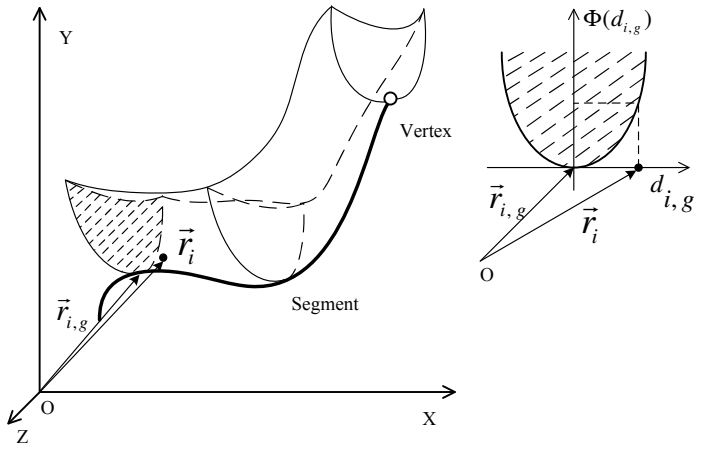

Figure 3.5: Illustration of an artificial potential trench on a segment.

Similar to the conventional smooth potential functions use in [6, 50, 27], many nonsmooth potential functions (including the previous example $V = |x|$, where $x \in R$) can be used to attract a robot to the desired goal point. With mathematical tools of nonsmooth analysis, it is possible to deal with the discontinuity of derivative, namely $\dot{V}$, and the generalized gradient of function $V = |x|$ can be expressed as follows:

$$\partial V(x) = \begin{cases} \{-1\} & x > 0 \\ \{+1\} & x < 0 \\ [-1,1] & x = 0 \end{cases}$$

In this thesis, the proposed artificial potential trench functions, which are limited to be smooth functions in the original work [29], are allowed to be nonsmooth to provide more flexibilities and design freedom. A refined formal definition of a potential trench function is given and then the artificial potential trench is synthesized in a controller design for the dynamics model given by Equation (3.4).

A group of mobile robots can form leader-follower pairs to facilitate formation control.

Similar to other papers [84, 81], two mobile robots r_i and r_{i-1} that share the same segment and are organized in leader-follower pairing are depicted in Figure 3.6. The vector $\vec{r}_i$ specifies the position of robot r_i, whose leader is robot r_{i-1}, with its position denoted by the vector $\vec{r}_{i-1}$. Similar to the the concept of virtual structure in [55, 17, 22], it is supposed that each robot has its own goal point on the segment. For instance, the goal point for robot r_i is $q_{i,g}$. A synthesized formation control will drive a group of robots with potential trench functions to approach the segment by tracking goal points on the segment.

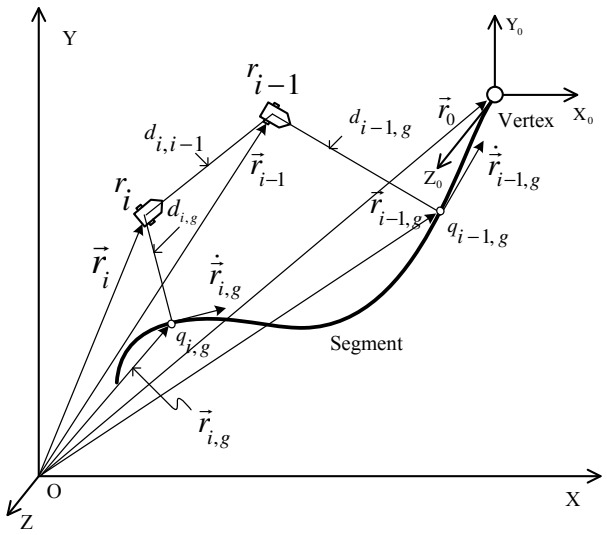

Figure 3.6: Representation of relevant variables for two robots together with the associated segment and vertex in the coordinates system.

To sum up, a framework of multi-robot formation control without considering obstacle avoidance is to be performed and the main tasks of this study include:

- (i) refine a formal definition of the potential trench function $\Phi(d_{i,g})$, which allows for discontinuity of its derivative such as the previously mentioned function $V(x) = |x|$, where $x \in R$;

- (ii) propose practical methods for constructing possible potential trench functions;
- (iii) based on mobile robot's dynamics model described by Equation (3.4), study the Lyapunov stability problem for a robot under the control of a potential trench function $\Phi(d_{i,g})$;
- (iv) for a group of mobile robots that are assigned to the same segment and organized in leader-follower pairs, study the associated stability problem if each robot is supposed to track its own goal point on the segment.

3.4.3 Zoning Potentials

As shown in Figure 1.1(b), each robot in the group can communicate with the rest via wireless signals. A wireless communication network among all members of the group is vital for them to accomplish certain tasks in a cooperative and coordinated way. Each robot can pass information such as its own location within the map to its neighbors. When obstacles are detected by one robot, information such as location and shape of obstacles should be shared as each robot has limited capabilities of sensing nearby surroundings. However the radio linkage among robots may be broken if they are separated too far away because robots' on-board wireless module can only cover a certain limited area. Therefore the separation among robots needs to be managed within reasonable range. Specifically if a group of mobile robots are organized in leader-follower pairs, separation between the leader and its follower must be controlled under an upper limit to prevent losing communication linkage.

On the other hand, to avoid collision among robots, the separation between any follower and its leader has to be greater than a certain threshold to prevent collision. Moreover, for robots that are not in leader-follower pairing, the separation between any one robot and another needs to be controlled. Hence, separation between any two robots must be sufficient to ensure that each robot can move in a collision-free path. To meet the requirements on separation management, a *zoning potential* is proposed. The basic idea of a zoning potential is that an attractive potential will be invoked whenever the separation is greater than certain threshold trying to reduce the separation and a repulsive potential will be applied whenever the separation is less than a threshold and will push the robot away from dangerous areas to prevent collisions.

Although it is a common practice to assign goal points to usher robots as it is in [55, 17, 22], such pre-determined goal points may not be necessary. Removing these goal point obviously can entitle the multi-robot systems to more autonomy and flexibilities. A convenient way is to attract the robots towards the assigned segment in a certain direction. Consequently, a similar artificial potential trench as illustrated in Figure 3.5 is also formed. In this way, the robot only needs to calculate how far it is away from the segment in this direction and then can generate a valley-shaped trench to stabilize on the segment. The benefits of removing goal points are obtained at the cost of introducing a direction to attract the robots towards segment. The effects of the assigned direction of attraction on robots also have to be addressed.

To completely solve all these challenges on separation management and removing pre-determined goal points, a framework involving synthesizing artificial potential trenches

and zoning potentials into formation controller design and the associated stability analysis will be the target of this portion of the research.

3.4.4 Segment Formation Control with Obstacle Avoidance

Another possible way to avoid using goal points is to drive any robot towards the nearest point on the segment. The basic idea is to let each mobile robot to autonomously find its nearest point on the segment, which also indicates the shortest path from the instantaneous position of robot to the assigned segment, and then move towards the nearest point with an artificial potential trench. Similar to the situations depicted in Figures 3.5 and 3.6, an artificial potential trench that features the shape of a "valley" with its bottom being the segment curve is presented in Figure 3.7. It should be noted that here the artificial potential trench attracts the robot towards its nearest point on the segment and hence there is no goal point at all in this scenario. In this figure, vector $\vec{r}_i$ denotes the instantaneous position of robot r_i while $q_{i,ns}$ stands for the nearest point on the segment to the robot. Similarly, $\vec{r}_{i,ns}$ is the vector representing the position of $q_{i,ns}$. The artificial potential trench can be calculated readily once the nearest point $q_{i,ns}$ is determined. The attractive force due to the potential trench $\Phi(d_{i,ns})$ can be calculated as

$$\vec{F}_{i,att} = \left(\nabla_x \Phi(x)|_{(d_{i,ns})}\right) \hat{d}_{i,ns}, \tag{3.26}$$

where $\hat{d}_{i,ns} = \vec{d}_{i,ns}/d_{i,ns}$ is the unit vector pointing from the instantaneous position of r_i

to the nearest point $q_{i,ns}$.

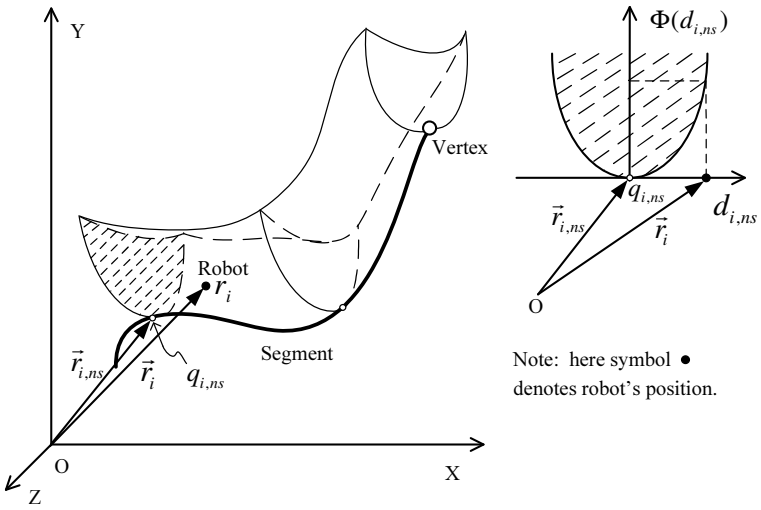

Figure 3.7: Cross section of a potential trench based on the shortest distance from a robot to the segment $d_{i,ns}$.

For this idea, there are three major challenges to be solved. First, there are theoretical difficulties even on the simple concept of ”nearest point”, as multiple nearest points on the segment may exist for a single robot. For these cases, in the original work [29] each robot is instructed to approach a specific nearest point which is closest to the target. In Figure 3.8, two mobile robots in leader-follower pairing are instructed to pursue their respective nearest points on the segment. The leader robot has a single nearest point, which is q_1, while the follower has two nearest points, namely q_1 and q_2. According to the simple control strategy in [29], the follower should approach q_1 rather than q_2 because q_1 is closer to the target. But q_1 happens to be the nearest point of the leader. Obviously, this control strategy lacks rigorous analysis and fails to handle complicated situations. Therefore a more sophisticated solution is needed. Usually robots with pre-determined goal points undergo a smooth motion. However, if a robot is instructed to approach one of nearest points on the segment, motion of the nearest point may be

discontinuous. Questions about how this will affect the robot's motion and trajectory and whether the whole group of robots can be stabilized on the segment need to be investigated.

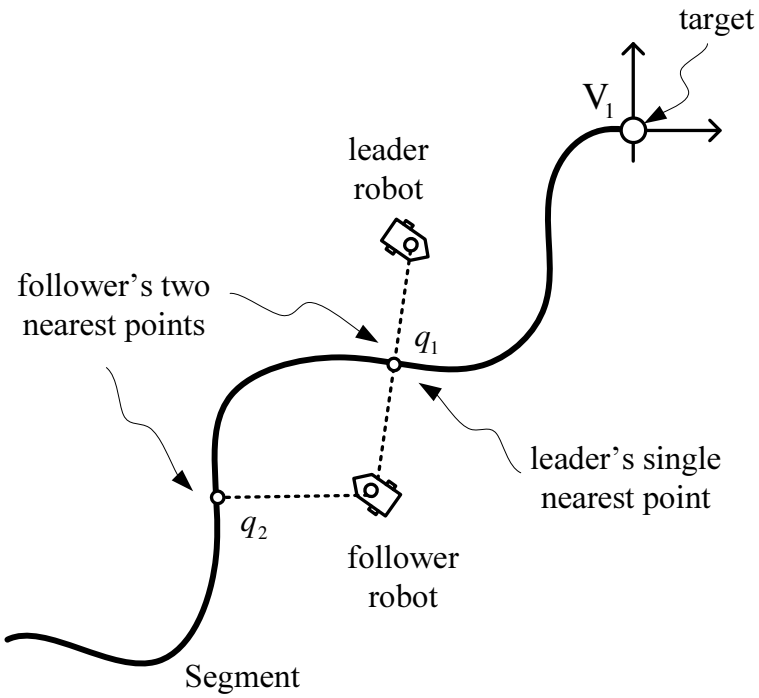

Figure 3.8: Two mobile robots and their nearest points on the segment.

Second, robots under the control of potentials are likely to be stuck at so-called *local minimum* locations where the attractive force cancels out the repulsive force. Usually repulsive potentials are utilized to avoid collisions. Without loss of generality, for robot r_i with the shortest distance to an obstacle is denoted by $d_{i,ob}$, the repulsive force generated by the repulsive potential U_{rep} can be calculated as

$$\vec{F}_{i,rep} = \left(-\nabla_x U(x)|_{(d_{i,ob})}\right) \hat{d}_{i,ob}, \tag{3.27}$$

where $\hat{d}_{i,ob} = \vec{d}_{i,ob}/d_{i,ob}$ is the unit vector pointing from the instantaneous position of r_i to the nearest point on the obstacle and the negative sign indicates that the direction

of the force is pushing the robot away from the obstacles. Local minimum may result when the sum of the repulsive forces and the attractive forces becomes zero, i.e.,

$$\vec{F}_{i,rep} + \vec{F}_{i,att} = 0.$$

The issue of local minimum leads to several problems [45, 26] including: (1) robots being trapped due to local minima; (2) no path between closely spaced obstacles; (3) goal nonreachable with obstacles nearby (GNRON). These problems are addressed in this thesis since the issue of local minimum is inherent in potential-based methods and frequently encountered. As far as approaching nearest points is concerned, the GNRON problem present practical challenges. Two examples of GNRON are illustrated in Figure 3.9. In Figure 3.9(a), a leader dwelling very close to the segment may cause its follower robot to be stuck because the repulsive force (to prevent collision) cancels out the attractive force generated by artificial potential trench.

Third, in the real world, the presence of obstacles must be considered for robot motion control and multi-robot formation control. Obstacles may give rise to local minimum issues. Take the simplified situation of a single obstacle for example; existence of the obstacle may prevent a robot from reaching the nearest point, and, in the worst case, the robot may get stuck somewhere off the segment. An obstacle which is close to the segment may cause local minimum even though it does not physically occupy the segment. This situation is depicted Figure 3.9(b), where the repulsive zone (dotted line) of the obstacle covers portion of the segment. In this case, the affected robot will be trapped somewhere off the segment and fail to reach the desired nearest point

q_3. Obstacles may also affect the segment as they may occupy certain portions of the segment. In turn, such obstacles will affect the robots and the availabilities of nearest points. Obstacles may be convex or concave shape. In this thesis obstacles with arbitrary shapes as shown in Figure 1.5 will be considered. An effective method is needed to handle obstacles of arbitrary shape and the presence of multiple obstacles.

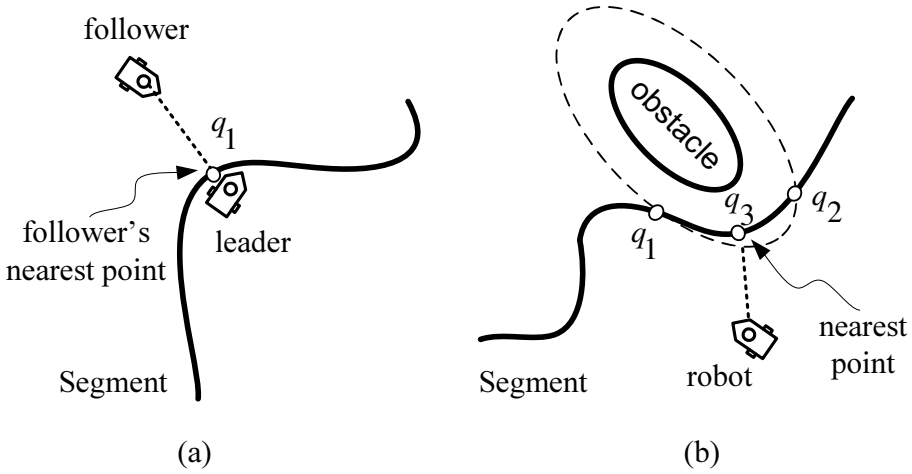

Figure 3.9: Two examples of local minima.

In summary, a framework of multi-robot formation control will be studied in the context of of the specifications below.

- (i) a group of robots must be able to approach the corresponding nearest points on the segment while the motion of these nearest points are subject to discontinuities;
- (ii) obstacles must be avoided and obstacles are allowed to be static or dynamic, convex or concave;
- (iii) separation between any leader and follower is maintained within a pre-defined range;
- (iv) no robots will collide with either another robot or an obstacle;

- (v) each robot will be able to approach its segment along a local-minima-free path.

3.5 Formation Control Input-to-State Stability

In [84], the concept of input-to-state stability based on leader-follower approach and graph formation is proposed. It can quantify error amplification during signal propagation in leader following formations. The input-to-state stability of formation is concerned as it not only guarantees stability but also it provides insights into robot-to-robot interactions in the formation. Therefore it is motivated to investigate some important properties of formation control based on queues and segments.

Consider the nonlinear system

$$\dot{x} = f(x,t) + g(x,t)d(t) \tag{3.28}$$

where $x \in D \subset R^n$ is the state, $d \in D_d \subset R^m$ is the disturbance, and $f(0,t) \equiv 0$.

The notion of input-to-state stability (ISS) is presented as follows:

Definition 3.5.1 *[79] The system (3.28) is said to be locally input-to-state stable (ISS) if there exist a class $\mathscr{KL}$ function β, a class $\mathscr{K}$ function χ, and positive constants k_1 and k_2 such that for any initial state $x(t_0)$ with $\|x(t_0)\| < k_1$ and any input $d(\cdot)$ with $\sup_{t \geq t_0} \|d(t)\| < k_2$, the solution $x(t)$ exists and satisfies*

$$\|x(t)\| \leq \beta(\|x(t_0)\|, t - t_0) + \chi\Big(\sup_{t_0 \leq \tau \leq t} \|d(\tau)\|\Big) \tag{3.29}$$

for all $t \geq t_0 \geq 0$. It is said to be input-to-state stable if $D = R^n$, $D_d = R^m$, and inequality

(3.29) is satisfied for any initial state $x(t_0)$ and any bounded input $d(t)$.

Similar to the work [84], the generic model of Linear-Time-Invariant (LTI) for each robot is adopted and finally the task to is to show that the formation control with queues and segments is input-to-state stable.

3.6 Summary

In this chapter, formulations of important research problems of this dissertation are discussed. The relevant key technical notions and fundamentals of nonsmooth analysis, which becomes the corner stone of stability analysis of this thesis are reviewed.

Chapter 4

A Robust Nonlinear Feedback Control and Implementation of Multi-Robot Formation Control

This chapter covers two topics. The first one begins with stability analysis on nonlinear feedback control for mobile robots and the associated comparative study of two similar feedback controls to derive an improved robust control. The other topic is mainly on the implementation of multi-robot formation and experiments based on the proposed robust control law.

4.1 Nonlinear Control and Lyapunov Stability

Motion control of mobile robots usually features nonlinear feedback control and numerous methods have been proposed in the past decades [16, 30, 38, 63, 86, 66, 48, 10, 7, 51]. Specifically two similar continuous nonlinear feedback controls, of which

the expressions are described in Equations (3.9) and (3.10), were proposed by [36] and [53] respectively. A review of Lyapunov stability for nonlinear feedback control based on kinetics model is motivated to reveal the inherent linkage between these two similar controls.

Now for system kinetics model described by Equation (3.8), we consider to derive a general form of control laws which can stabilize the robot in the sense of Lyapunov stability theorems. It requires that both r and ϕ tend to zero as time $t \to \infty$. A possible way is to choose control laws which lead to diagonalization of the matrix on the right-hand-side of Equation (3.8). To this end, we let v and ω being

$$\begin{bmatrix} v \\ \omega \end{bmatrix} = \begin{bmatrix} g_1(r,\phi) & 0 \\ 0 & g_2(r,\phi) \end{bmatrix} \begin{bmatrix} r \\ \phi \end{bmatrix} + \begin{bmatrix} 0 \\ -g_1(r,\phi)\sin(\phi) \end{bmatrix}, \tag{4.1}$$

where $g_1(r,\phi)$ and $g_2(r,\phi)$ are certain unexplicit functions to be determined. It is worthwhile to note that while time-invariant state feedback control laws based on certain $g_1(r,\phi)$ and $g_2(r,\phi)$ functions are feasible, there is still a special term $-g_1(r,\phi)\sin(\phi)$ left on the right-hand-side of Equation (4.1) according to Brockett's theorem [8].

Then by substituting the above equations into Equation (3.8), we can rewrite the Equa-

tion (3.8) into

$$\begin{bmatrix} \dot{r} \\ \dot{\phi} \end{bmatrix} = \begin{bmatrix} -\cos(\phi) & 0 \\ \frac{1}{r}\sin(\phi) & 1 \end{bmatrix} \begin{bmatrix} g_1(r,\phi) & 0 \\ 0 & g_2(r,\phi) \end{bmatrix} \begin{bmatrix} r \\ \phi \end{bmatrix} + \begin{bmatrix} 0 \\ -g_1(r,\phi)\sin(\phi) \end{bmatrix}. \tag{4.2}$$

A family of possible functions $g_1(r,\phi)$ and $g_2(r,\phi)$ can be chosen as follows:

$$\begin{aligned} g_1(r,\phi) &= K_1 r^n \phi^{2q} (\cos(\phi))^{2p+1}, \\ g_2(r,\phi) &= -K_2 \phi^{2s}, \end{aligned} \tag{4.3}$$

where $n = 0,1,2,\cdots$, $p = 0,1,2,\cdots$, $q = 0,1,2,\cdots$ and $s = 0,1,2,\cdots$.

Accordingly Equation (4.1) can be rewritten into the following form:

$$\begin{aligned} v &= K_1 r^{n+1} \phi^{2q} (\cos(\phi))^{2p+1}, \\ \omega &= -K_1 r^n \phi^{2q} \sin(\phi)(\cos(\phi))^{2p+1} - K_2 \phi^{2s+1}. \end{aligned} \tag{4.4}$$

Proposition 4.1.1 *The family of control laws given in Equation (4.4) asymptotically stabilizes a differential robot on its goal point.* □

Proof: See Appendix A.1. □

It should be noted that although the general control law represented in Equation (4.4) can theoretically asymptotically stabilize the robot at its goal point, the term ϕ^{2q} will greatly slow down the system response. Therefore for the sake of practical considerations, $q = 0$ is preferred. Let us focus on the control with simple structure.

Proposition 4.1.2 *Both Equations (3.10) and (3.9) can be derived from the general control law given in Equation (4.4).* □

Proof: See Appendix A.2. □

Obviously, either Equations (3.9) (3.10) is verified to be special cases of Equation (4.4). Apart from this observation, similarity of these two nonlinear feedback controls inspires a comparative research work on their effects on the system's behavior. Although some preliminary analysis results on the control law represented by Equation (3.9) are available in [36], a comparative study on these two control laws proves to be more informative.

4.2 Analysis on Robot's Motion Behavior

4.2.1 Evolution of Heading

As mentioned, one interesting thing is to learn the behavior of the robot's heading when under control in Equations (3.10) or (3.9). To avoid expression confusion, we use $\theta_1(t)$ and $\theta_2(t)$ to denote the heading of robot under control in Equations (3.9) and (3.10) respectively. Let us process $\theta_2(t)$, namely the case with control in Equation (3.10) first.

The resultant closed loop system equation is

$$\begin{aligned} \dot{r} &= -K_1 r(\cos(\phi))^2, \\ \dot{\phi} &= -K_2 \phi. \end{aligned} \tag{4.5}$$

Solving the differential equations in Equation (4.5) yields

$$\begin{aligned} r(t) &= r_0 e^{-K_1 \int_0^t \cos^2(\phi_0 e^{-K_2 s}) ds}, \\ \phi(t) &= \phi_0 e^{-K_2 t}. \end{aligned} \tag{4.6}$$

We define a variable $\lambda = K_1/K_2 \in [0, +\infty)$ and refer to it as "gain ratio" throughout this chapter. Since $\dot{\theta} = \omega = -K_2\phi - K_1 \sin(\phi)\cos(\phi)$, substituting results from Equation (4.6) into Equation (4.5) we can have

$$\theta_2(t) = \theta_0 + \left[\phi_0 e^{-K_2 t}\right]_0^t + \left[\lambda Si(2\phi_0 e^{-K_2 t})/2\right]_0^t,$$

where θ_0 denotes the initial heading of robot and $Si(x)$ is the Sine Integral function defined as $Si(x) = \int_0^x \frac{\sin(t)}{t} dt$. Readily we obtain the information of $\theta_2(t)$ when $t \to \infty$ as

$$\theta_2(\infty) = \theta_0 - \phi_0 - \lambda Si(2\phi_0)/2.$$

Similarly, we can derive the solutions of the closed-loop system equations under control

in Equation (3.9) as

$$\begin{aligned} r(t) &= r_0 e^{-K_1 \int_0^t \cos(\phi_0 e^{-K_2 s}) ds} \\ \phi(t) &= \phi_0 e^{-K_2 t}. \end{aligned} \tag{4.7}$$

Consequently, we can acquire heading $\theta_1(t)$ as

$$\theta_1(t) = \theta_0 + \left[\phi_0 e^{-K_2 t}\right]_0^t + \left[\lambda Si(\phi_0 e^{-K_2 t})\right]_0^t,$$

where θ_0 denotes the initial heading of robot. Accordingly, we have $\theta_1(\infty)$ as

$$\theta_1(\infty) = \theta_0 - \phi_0 - \lambda Si(\phi_0).$$

From the foregoing results, for any given initial conditions, both $\theta_1(\infty)$ and $\theta_2(\infty)$ are only relevant to gain ratio λ rather than the amplitudes of gain K_1 or K_2.

Let us define turning of heading H_c as

$$H_c = |\theta(\infty) - \theta_0|,$$

and specifically $H_{c1} = |\phi_0 + \lambda Si(\phi_0)|$ and $H_{c2} = |\phi_0 + \frac{\lambda}{2} Si(2\phi_0)|$ for the two cases with control in Equation (3.9) and (3.10) respectively. Obviously H_c is the total change of heading of the robot along the whole trajectory from the starting point to the target.

It is of interest to compare H_{c1} with H_{c2} and $\theta_1(\infty)$ with $\theta_2(\infty)$, because their expressions look similar for any given ϕ_0. Let $F(x) = Si(x) - Si(2x)/2$, the first time derivative of F

with respect to x yields

$$F'(x) = \frac{\sin(x)}{x} - \frac{\sin(2x)}{4x} = \frac{\sin(x)}{x} \cdot (1 - \frac{\cos(x)}{2}) > 0,$$

for $\forall x \in (-\pi, \pi)$. It means that $F(x)$ is monotonically increasing on the whole interval.

The graph of $Si(x) - Si(2x)/2$(i.e. $F(x)$), $Si(x)$ and $Si(2x)/2$ are depicted in Figure 4.1.

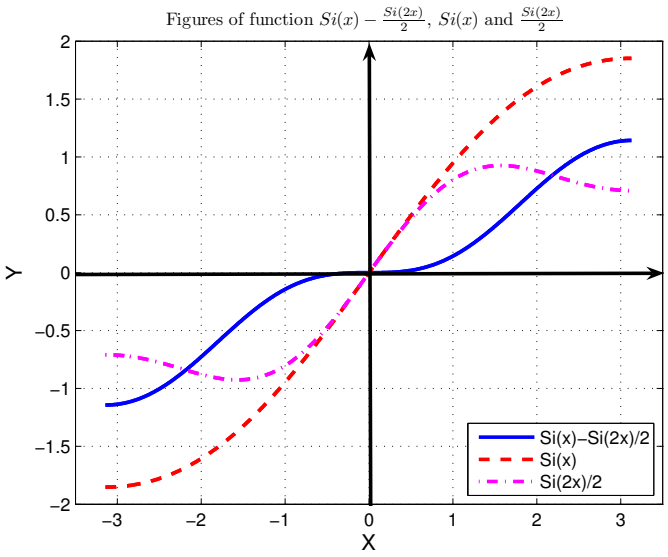

Figure 4.1: Figures of $F(x) = Si(x) - Si(2x)/2$, $Si(x)$ and $Si(2x)$ for $x \in (-\pi, \pi]$. The solid blue line is for the monotonically increasing function $F(x)$.

From this figure, it is clear that when $0 < \phi_0 \leq \pi$, we have $\theta_1(t) < \theta_2(t)$ (specifically $\theta_1(\infty) < \theta_2(\infty)$) while $\theta_1(t) > \theta_2(t)$ (specifically $\theta_1(\infty) > \theta_2(\infty)$) when $-\pi < \phi_0 < 0$. It is also noted from the figure that the bigger the initial ϕ_0, the more difference between $\theta_1(\infty)$ and $\theta_2(\infty)$ will be resulted.

In the terms of turning of heading H_c, we have the following conclusion:

$$H_{c1} - H_{c2} = \begin{cases} \lambda |Si(\phi_0) - \frac{Si(2\phi_0)}{2}| > 0 & \text{if } \phi_0 \neq 0 \\ 0 & \text{if } \phi_0 = 0. \end{cases}$$

In other words, when under control in Equation (3.9), the robot's heading will travel more than the counterpart under control in Equation (3.10) for any initial nonzero $\phi_0 \in (-\pi, \pi]$.

4.2.2 Unique Trajectory w.r.t. Gain Ratio λ

From the foregoing section, we can find that the headings $\theta_1(t)$ and $\theta_2(t)$ are actually a function of $\phi(t)$ and gain ratio λ in that they can be rewritten into the following forms:

$$\theta_1(t) = \theta_0 - \phi_0 + \phi(t) + \frac{\lambda}{2}\left[Si(2\phi(t)) - Si(2\phi_0)\right],$$

$$\theta_2(t) = \theta_0 - \phi_0 + \phi(t) + \lambda\left[Si(\phi(t)) - Si(\phi_0)\right].$$

And as mentioned, specially $\theta_1(\infty)$ and $\theta_2(\infty)$ are solely determined by λ for certain initial conditions. These observations release strong signals that there may be a unique relationship between the trajectory and λ. Hence we are inspired to find out the linkage between them. For the case with control in Equation (3.9), we have the following proposition:

Proposition 4.2.1 *If the differential mobile robot is under control in Equation (3.9), then its trajectory is solely determined by the gain ratio λ, where $\lambda \in (0, +\infty)$ for certain given initial conditions r_0 and ϕ_0.*

For the other case with control in Equation (3.10) we have a similar assertion given by the following proposition:

Proposition 4.2.2 *If the differential mobile robot is under control in Equation (3.10), then its trajectory is solely determined by the gain ratio λ, where $\lambda \in (0, +\infty)$ for certain given initial conditions r_0 and ϕ_0.*

For the sake of brevity, we only provide the proof for the latter case(see Appendix A.3) in this chapter and leave the proof for the former proposition that is relatively simpler to the readers.

As shown in Proposition 4.2.1 and 4.2.2, for any given initial conditions, the trajectory of the robot is unique as long as gain ratio λ is fixed. This conclusion is very useful in applications such as trajectory design, path planning, etc. For instance, we can determinate λ in accordance with the desired trajectory and then anticipate the magnitude of gain K_1 and K_2 according to the specifications on convergence rate of r and ϕ and technical specifications of the physical actuator.

4.2.3 Characteristics of Trajectory Curvature

Another appealing thing seems to be to comparatively investigate the curvature of the trajectories of mobile robots under the controls in Equations (3.10) and (3.9). It turns out that to directly analyze the exact curvature of the whole trajectory at an arbitrary moment is not easy because of the difficulties in expressing curvature in forms of elementary functions. However, to some extent we are able to extract some characteristics of the curvature.

The curvature of the trajectory generated by a mobile robot is $\mathscr{K}(t) = \frac{|\omega(t)|}{|v(t)|}$. The case

with control in Equation (3.9) is relatively simpler than the case with control in Equation (3.10). Let us deal with the former case first. We can write the curvature $\mathscr{K}_1$ as

$$\mathscr{K}_1(t) = \frac{|K_2\phi_0 e^{-K_2 t} + K_1 \sin(\phi_0 e^{-K_2 t})|}{K_1 r_0 e^{-K_1 \int_0^t \cos(\phi_0 e^{-K_2 s})ds}}.$$

The derivative of $\mathscr{K}_1$ when $\phi_0 \in (0,\pi]$ can be calculated as $d\mathscr{K}_1(t)/dt = \big[\omega^{'}(t)v(t) - \omega(t)v^{'}(t)\big]/v^2(t)$. Since the numerator determines the sign of $d\mathscr{K}_1(t)/dt$, we are able to judge the sign from it. Letting $d\mathscr{K}_1(t)/dt = Num_1/Den_1$ yields

$$\begin{aligned} Num_1 &= -[K_2^2\phi_0 + K_1K_2\phi_0\cos(\phi_0 e^{-K_2 t})] \\ &\quad e^{-K_2 t}K_1 r_0 e^{-K_1\int_0^t \cos(\phi_0 e^{-K_2 s})ds} + \\ &\quad K_1^2 r_0 e^{-K_1\int_0^t \cos(\phi_0 e^{-K_2 s})ds}[K_2\phi_0 e^{-K_2 t} \\ &\quad + K_1\sin(\phi_0 e^{-K_2 t})] \\ &= K_1 r_0 e^{-K_1\int_0^t \cos(\phi_0 e^{-K_2 s})ds}\big[-K_2^2\phi_0 e^{-K_2 t} \\ &\quad + K_1^2\sin(2\phi_0 e^{-K_2 t})/2\big]. \end{aligned}$$

Letting $A = \phi_0 e^{-K_2 t}$ and substituting $K_1 = \lambda K_2$, we will find that $\lambda^2\sin(2A)/2 - A$ where $A \in (0,\pi]$ has the same sign as that of $d\mathscr{K}_1(t)/dt$. Similarly we can conclude that in the case with $\phi_0 \in (-\pi, 0)$, $-\lambda^2\sin(2A)/2 + A$ has the same sign of $d\mathscr{K}_1(t)/dt$. In short,

we can generalize these two facts into an function $\mathscr{S}_1$ as

$$\mathscr{S}_1(A) = \begin{cases} \lambda^2 \sin(2A)/2 - A & \text{if } A \in (0, \pi], \\ -\lambda^2 \sin(2A)/2 + A & \text{if } A \in (-\pi, 0), \end{cases}$$

where $\lambda \in [0, +\infty)$. Then from this function $\mathscr{S}_1$, we can try to extract some useful information on curvature $\mathscr{K}_1(t)$. It of significance to find the invariant set of Ω_λ given by

$$\Omega_\lambda = \{\lambda \,|\, \mathscr{S}_1(A) < 0, \forall A \in (-\pi, 0) \cup (0, \pi]\}.$$

This invariant set Ω_λ turns out to be $\Omega_\lambda = [0, 1]$. The illustration of function $\mathscr{S}_1(A)$ with respect to a variety of λ is shown in Figure 4.2. From this figure, it is obvious that for these $\lambda \in \Omega_\lambda$, curvature $\mathscr{K}_1(t)$ is monotonically decreasing almost everywhere on time domain $t \in [0, +\infty)$ except at $t = +\infty$ for any nonzero ϕ_0.

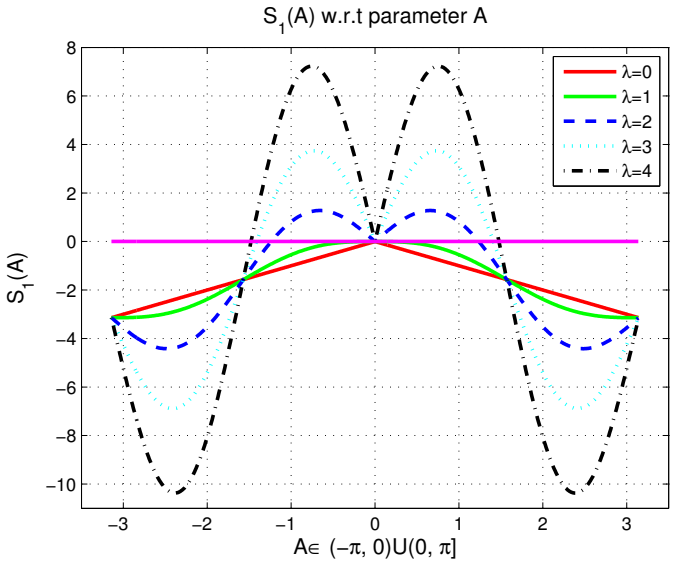

Figure 4.2: Illustration of $\mathscr{S}_1(A)$ w.r.t A for gain ratios $\lambda = 0, 1, 2, 3, 4$.

The special cases with nonzero initial condition ϕ_0 and $t \to \infty$ have to be handled with

care in that both the numerator and denominator of $\mathscr{K}_1(t)$ tend to zero as $t \to \infty$. It means that L′Hôspital's rule is applicable in such cases rather than the previously used general differentiation rule $d\mathscr{K}_1(t)/dt = \left[\omega^{'}(t)v(t) - \omega(t)v^{'}(t)\right]/v^2(t)$. Considering the special case $\phi_0 = 0$ we always have $\mathscr{K}_1(t) = 0$, the curvature $\mathscr{K}_1(t)$ at $t = \infty$ can calculated as

$$\mathscr{K}_1(\infty) = \begin{cases} 0 & \text{if } \lambda < 1 \text{ or } \phi_0 = 0, \\ \frac{2|\phi_0|}{r_0} & \text{if } \lambda = 1, \\ \infty & \text{if } \lambda > 1 \text{ and } \phi_0 \neq 0. \end{cases}$$

by invoking L′Hôspital's rule.

From the above expression, it is noted that for any nonzero ϕ_0, $\lambda = 1$ is "critical" in the sense that any value of λ below it will lead the curvature $\mathscr{K}_1(t)$ to be monotonically decreasing on time domain $t \in [0, +\infty)$. Moreover, the curvature of trajectory at the origin of the goal frame will be expected to be zero for any $\lambda < 1$ otherwise it will be infinity for any $\lambda > 1$. Thanks to this observation, we refer to $\lambda = K_1/K_2 = 1$ as the "critical gain ratio".

Now we move on to the more complicated case with control in Equation (3.10). The curvature $\mathscr{K}_2$ of the corresponding trajectory can be written as

$$\mathscr{K}_2(t) = \frac{|K_2\phi_0 e^{-K_2 t} + K_1 \sin(2\phi_0 e^{-K_2 t})/2|}{K_1 r_0 e^{-K_1 \int_0^t \cos^2(\phi_0 e^{-K_2 s})ds} |\cos(\phi_0 e^{-K_2 t})|}.$$

Letting $d\mathscr{K}_2(t)/dt = Num_2/Den_2$, for any $\phi_0 \in (0, \pi/2)$ then we can write the numera-

tor as

$$
\begin{aligned}
Num_2 &= -e^{-K_2t}[K_2^2\phi_0 - K_1K_2\phi_0\cos(2\phi_0e^{-K_2t})] \\
&\quad K_1r_0e^{-K_1\int_0^t\cos^2(\phi_0e^{-K_2s})ds}\cos(\phi_0e^{-K_2t}) - \\
&\quad [K_2\phi_0e^{-K_2t} + K_1\sin(2\phi_0e^{-K_2t})][K_2^2\phi_0^2\sin(\phi_0 \\
&\quad e^{-K_2t})e^{-2K_2t} - K1K_2\phi_0e^{-K_2t}\cos^3(\phi_0e^{-K_2t})] + \\
&\quad K_1K_2\phi_0e^{-K_2t}\sin(\phi_0e^{-K_2t})\sin(2\phi_0e^{-K_2t})/2 - \\
&\quad K_1^2\sin(2\phi_0e^{-K_2t})\cos^3(\phi_0e^{-K_2t})/2] \\
&= K_1r_0e^{-K_1\int_0^t\cos^2(\phi_0e^{-K_2s})ds}\big[-K_2^2\phi_0 \\
&\quad \cos(\phi_0e^{-K_2t})e^{-K_2t} - K_2^2\phi_0^2\sin(\phi_0e^{-K_2t}) \\
&\quad e^{-2K_2t} - K_2^2\phi_0^2\sin(\phi_0e^{-K_2t})e^{-2K_2t} + \\
&\quad K_1^2\sin(2\phi_0e^{-K_2t})\cos^3(\phi_0e^{-K_2t})/2\big].
\end{aligned}
$$

Letting $A = \phi_0e^{-K_2t}$ and $K_1 = \lambda K_2$ where $\lambda \in [0, +\infty)$, then the following expression

$$\lambda^2\sin(2A)\cos^3(A)/2 - A\cos(A) - A^2\sin(A),$$

where $A \in (0, \pi/2)$ has the same sign as that of $d\mathscr{K}_2(t)/dt$ for any $\phi_0 \in (0, \pi/2)$. Since $\mathscr{K}_2$ is an even function with respect to ϕ_0, we can conclude that

$$-\lambda^2\sin(2A)\cos^3(A)/2 + Acos(A) + A^2\sin(A),$$

where $A \in (-\pi/2, 0)$ has the same sign as that of $d\mathscr{K}_2(t)/dt$ for $\phi_0 \in (-\pi/2, 0)$. How-

ever, unfortunately we cannot simply extend the above results to the cases with $\phi_0 \in (-\pi, -\pi/2)$ and $\phi_0 \in (\pi/2, \pi]$ because the sign of the numerator undergoes a more sophisticated situation for these cases. One interesting thing is to find the approximate value of $\lambda^* = min\{\lambda_1, \lambda_2\}$, where λ_1 and λ_2 can be determined by the following equations

$$\lambda_1 = sup\{\lambda | A + \lambda \sin(2A)/2 < 0, \forall A \in (\pi/2, \pi]\},$$

$$\lambda_2 = sup\{\lambda | A + \lambda \sin(2A)/2 > 0, \forall A \in (-\pi, -\pi/2)\},$$

respectively. It turns out that when $\lambda^* \approx 4.6033$ a function $\mathscr{S}_2(A)$ shown in Figure 4.3 has the same sign of $d\mathscr{K}_2(t)/dt$. As to the special cases with $A = \pm\pi/2$ or equivalently $\phi(t) = \pm\pi/2$, we have curvature $\mathscr{K}_2 = \infty$. we can make the following conclusions: the sign of $d\mathscr{K}_2(t)/dt$ on time domain $(0, +\infty)$ can be determined from function $\mathscr{S}_2$ as

$$\mathscr{S}_2(A) = \begin{cases} Acos(A) + A^2 \sin(A) - \lambda^2 \sin(2A)\cos^3(A)/2 & \text{if } A \in (\pi/2, \pi], \text{and } \lambda < 4.6033, \\ -Acos(A) - A^2 \sin(A) + \lambda^2 \sin(2A)\cos^3(A)/2 & \text{if } A \in (0, \pi/2), \\ Acos(A) + A^2 \sin(A) - \lambda^2 \sin(2A)\cos^3(A)/2 & \text{if } A \in (-\pi/2, 0), \\ -Acos(A) - A^2 \sin(A) + \lambda^2 \sin(2A)\cos^3(A)/2 & \text{if } A \in (-\pi, -\pi/2), \text{and } \lambda < 4.6033, \end{cases}$$

for certain sets of λ as designated in the above equation. The cases with $\lambda \geq 4.6033$ when $A \in (\pi/2, \pi] \cup (-\pi, -\pi/2)$ are not considered here.

Referring to Figure 4.3, it is obvious that unlike the case with control in Equation (3.9), we cannot find the invariant set of λ on the domain either $\phi_0 \in (-\pi, 0)$ or $\phi_0 \in (0, \pi)$. Instead, we have the same invariant set $\Omega_\lambda = [0, 1]$ on domain $\phi_0 \in (-\pi/2, 0)$ or $(0, \pi/2)$.

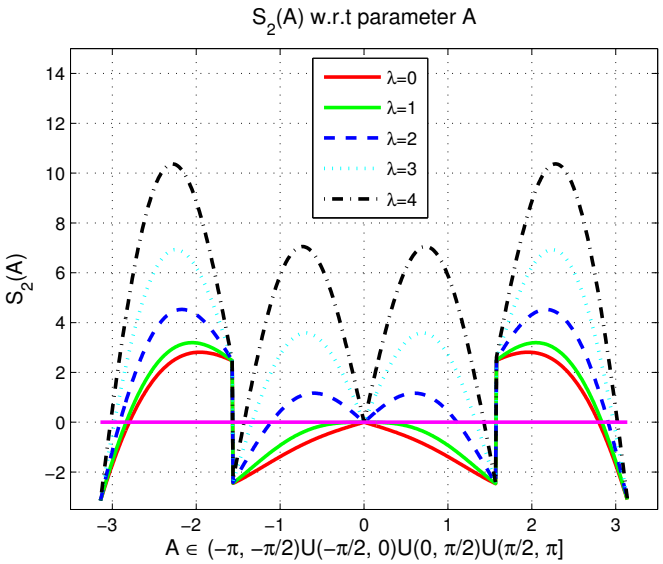

Figure 4.3: Illustration of $\mathscr{S}_2(A)$ w.r.t A for $\lambda = 0, 1, 2, 3, 4$.

Now it is time to investigate the all specials cases left, namely $\phi_0 = 0$ and $t \to \infty$ when $\phi_0 \neq 0$. Taking the special case $\mathscr{K}_2(t) = 0$ when $\phi_0 = 0$ into account, we can obtain the curvature of trajectory at origin of the goal frame as given by the following equation by invoking L′Hôspital's rule again:

$$\mathscr{K}_2(\infty) = \begin{cases} 0 & \text{if } \lambda < 1 \text{ or } \phi_0 = 0, \\ \frac{2|\phi_0|}{r_0} & \text{if } \lambda = 1, \\ \infty & \text{if } \lambda > 1 \text{ and } \phi_0 \neq 0. \end{cases}$$

Comparing $\mathscr{K}_2(\infty)$ with $\mathscr{K}_1(\infty)$ obtained in previous analysis, it is remarkable to find that $\mathscr{K}_2(\infty) = \mathscr{K}_1(\infty)$. In other words, the curvatures of trajectory at the origin of goal frame under controls in Equations (3.10) or (3.9) turn on the same characteristics.

Similar to the characteristics of trajectory curvature under control in Equation (3.9), there is a critical gain ratio $\lambda = 1$ for any $|\phi_0| < \pi/2$ in the sense that any value of λ beyond it will lead the curvature of trajectory at the origin of the goal frame be infinity

while below it zero curvature is expected. Again it is observed that for any $0 < |\phi_0| < \pi/2$ if we choose any gain ratio λ to be $0 < \lambda < 1$, the maximum curvature of the trajectory happens at the very beginning moment $t = 0$. In other words,

$$\mathscr{K}_2(0) = \frac{|\phi_0/\lambda + \sin(2\phi_0)/2|}{r_0 \cos(\phi_0)}, \text{ where } \lambda \in (0,1),$$

is the maximum value of trajectory curvature for these cases. Compared with $\mathscr{K}_1(0)$, we have $\mathscr{K}_2(0) \geq \mathscr{K}_1(0)$ and $\mathscr{K}_2(0) = \mathscr{K}_1(0)$ holds only if $\phi_0 = 0$ or $\phi_0 = \pi$. However different from scenarios with control in Equation (3.9), $\mathscr{K}_2$ tends to infinity at $\phi(t) = \pm\pi/2$.

4.3 Robustness Analysis

More than stability issues, robustness of nonlinear feedback control is worthwhile to study. Specifically in this chapter, robustness analysis for the nonlinear feedback control represented by Equation (3.10) is to be performed to achieve a improved robust control. Later on this robust control law will be applied to implementation of multiple robot formation control.

4.3.1 Stable Zone

We refer to the model in Equation (3.18) as the real closed-loop system model. Then our problem is to analyze the stability and robustness of this real-world model. We can

decompose this model into two subsystems as follows.

$$\begin{aligned} \dot{r} &= -K_1(\cos(\phi))^2 r, \\ \dot{\phi} &= -K_2\phi - \left(\frac{K_3 - K1}{2}\right)\sin(2\phi). \end{aligned}$$

Obviously except the special case with $\cos(\phi(t)) \equiv 0$, $r(t)$ is at least asymptotically convergent to zero. As to $\phi(t)$, the situation is more complicated.

Let $K_4 = (K_3 - K_1)/2$, then we have

$$\dot{\phi} = -K_2\phi - K_4\sin(2\phi) \tag{4.8}$$

As to the subsystem denoted by Equation (4.8), construct a Lyapunov candidate as $V = \frac{1}{2}\phi^2$. The derivative of V with respect to time is

$$\dot{V} = \phi\dot{\phi} = -K_2\phi^2 - K_4\phi\sin(2\phi). \tag{4.9}$$

As shown by the closed-loop system equation in Equation (3.18), this system is time-invariant. It means that LaSalle's theorem is applicable. Therefore we are motivated to find out the invariant set $\Sigma = \{(K_1, K_2, K_3) | \dot{V} < 0\}$. To this end we let $\dot{V} = 0$, then we have to make either $\phi = 0$ or $\phi = -K_4/K_2\sin(2\phi)$.

To find out the solution of $\phi = -K_4/K_2\sin(2\phi)$ for $\phi \in [0, \pi)$, we perform numerical calculation in Matlab environment. There are two scenarios: either $K_4/K_2 \geq 0$ or $K_4/K_2 < 0$. The illustration of different solutions when $K_4/K_2 > 0$ is shown in Figure

4.4 while the case with $K_4/K_2 < 0$ is shown in Figure 4.5. The calculation shows that:

- (i) if $K_4/K_2 \geq 0$ when $0 \leq K_4/K_2 < c_1$, equation $\phi = -K_4/K_2 \sin(2\phi)$ has only one solution, i.e., $\phi = 0$,
- (ii) if $K_4/K_2 < 0$ when $c_2 < K_4/K_2 < 0$, equation $\phi = -K_4/K_2 \sin(2\phi)$ has only one solution, i.e., $\phi = 0$,

where c_1 and c_2 are constants. The numerical calculations offer approximation values of c_1 and c_2 as $c_1 \approx 2.30$ and $c_2 \approx -0.50$.

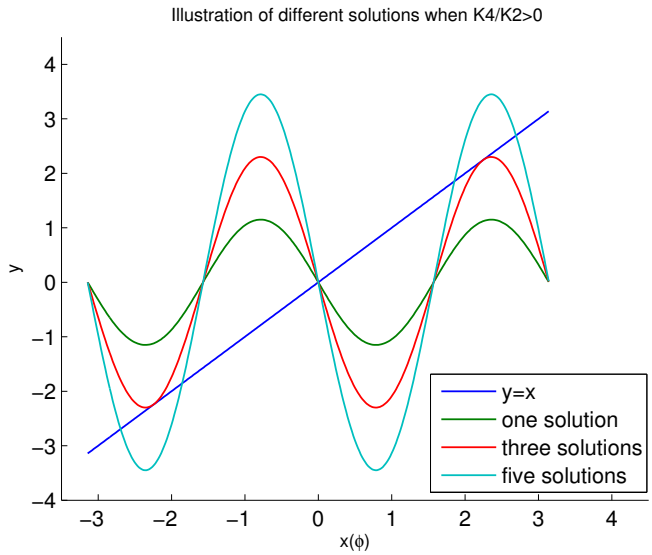

Figure 4.4: Illustration of different solutions with $K_4/K_2 > 0$.

To sum up, the ratio K_4/K_2 should be within the range (c_2, c_1) to make subsystem Equation (4.8) asymptotically stable. Or in other words, the relationship among K_1, K_2, K_3 to make subsystem Equation (4.8) stable is: $K_1 + 2c_2K_2 < K_3 < 2c_1K_2 + K_1$ ($K_2 > 0$) or $2c_1K_2 + K_1 < K_3 < K_1 + 2c_2K_2$ ($K_2 < 0$). Illustrations of the stable zone are shown in Figures 4.6 and 4.7 for the cases of $K_2 > 0$ and $K_2 < 0$ respectively. It is noted that in

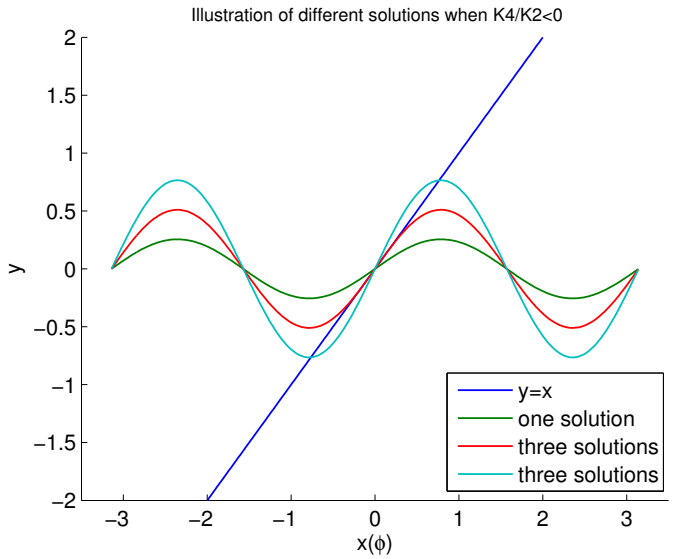

Figure 4.5: Illustration of different solutions with $K_4/K_2 < 0$.

these two scenarios, the stable zone forms a wedge shape and all the sets of $(K1, K2, K3)$ within the zone (not including the edge) will stabilize the system.

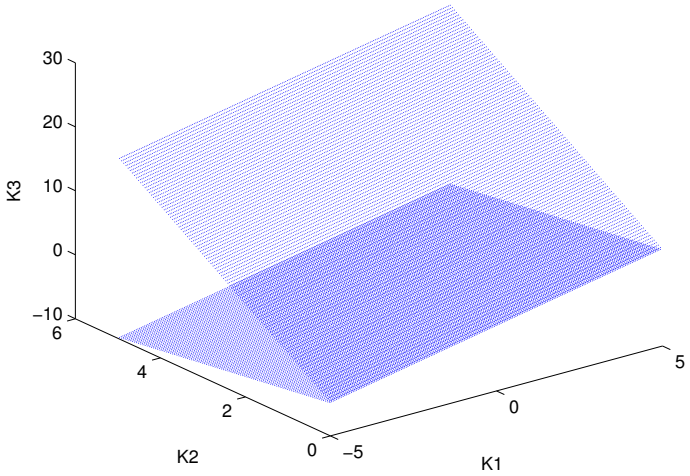

Figure 4.6: Illustration of stable zone with $K_2 > 0$.

In practise, K_2 is usually chosen to be positive. So we can further the above conclusions. Any positive K_4 will make the subsystem stable and actually expedite the converging rate of ϕ. In this case, the whole stable range of K_3 is $K_1 + 2c_2K_2 < K_3 < 2c_1K_2 + K_1$. The

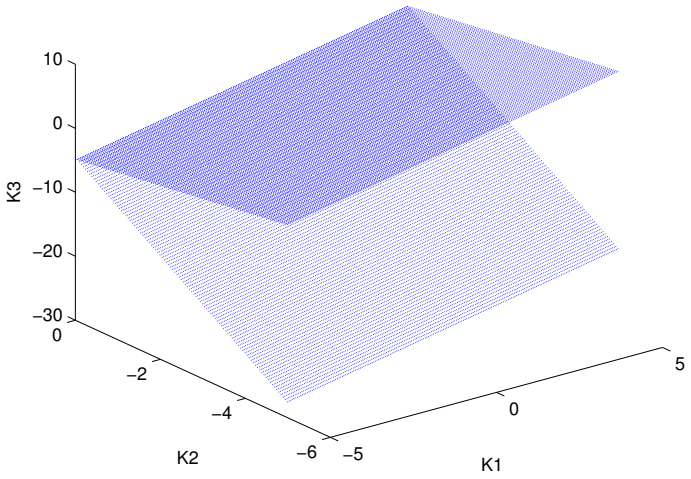

Figure 4.7: Illustration of stable zone with $K_2 < 0$.

stable zone is shown in Figure 4.8. The stable zone is the whole wedge and is separated by a plane with $K3 = K1$. The upper part of this wedge has the property of $K4 > 0$ while the lower part with $K4 < 0$. The difference of these two parts of the zone lies in that the sets of $(K1, K2, K3)$ in the upper part contributes to expediting system response while these sets in the lower parts will lag the system response when compared with the nominal sets of parameters in the plane $K3 = K1$.

4.3.2 Improvements and Control Design Guidelines

Proposition 4.3.1 *If $K_4 \geq 0$, namely, $K_3 - K_1 \geq 0$, $\phi(t)$ is exponentially convergent to zero for arbitrary initial ϕ_0.*

The proof is pretty straightforward and hence omitted here for brevity.

Proposition 4.3.2 *Sets of $(K1, K2, K3)$ in the upper part of the wedge in Figure 4.8 expedites the response of ϕ.*

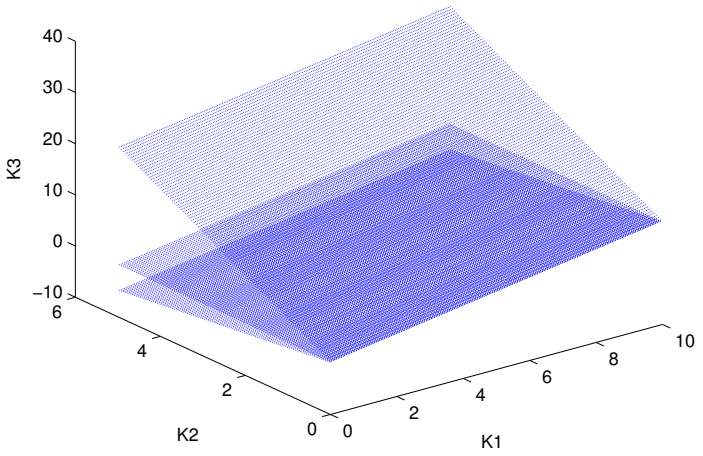

Figure 4.8: Illustration of stable zone with practical concerns in the case when $K_1 > 0$ and $K_2 > 0$. Note that the whole zone is separated by a plane $K3 = K1$, i.e., $K4 = 0$.

Proof: See Appendix A.4. □

According to Proposition A.4, we can deliberately choose $K_3 \geq K_1$ to make the system more robust. Obviously it is not a good strategy to choose $K_3 = K_1$ in terms of robustness. To improve it, specifically we can design real application control laws in light with the following guidelines.

(1) As revealed in Figure 4.8, K_2 should not be too close to zero as the bigger K_2, the wider zone between upper bound and lower bound.

(2) To maximize the stability zone for a given set of (K_1, K_2, K_3), it is desirable to choose $K_3 = K_1 + (c_1 + c_2)K_2$. In other words, (K_1, K_2, K_3) is within the plane in the middle of upper bound and lower bound as illustrated in Figure 4.8.

(3) To obtain comparatively large stability zone for a given set of (K_1, K_2, K_3) while keep the converging rate from being negatively affected, it is desirable to choose

$K_3 = K_1 + c_1 K_2$.

4.4 Numerical Examples

4.4.1 Typical Trajectories of Robots

To verify and illustrate the conclusions on the trajectory characteristics in the foregoing context, we design experiments on a mobile robot that starting from four different points $(1,0)$, $(0,1)$, $(-1,0)$, $(0,-1)$ on a $2D$ plane. The origin of the goal point frame is the target and at each starting point initial ϕ_0 is chosen to be $\pi/4$. For all the experiments, $K_1 = 1$ is fixed while $K_2 = K_1/\lambda$ is varied with respect to λ. To show the typical scenarios of trajectories based on different settings of λ, we take $\lambda = 0.2, 1, 5$ for each starting point. The case with control in Equation (3.9) is depicted in Figure 4.9 and the part of trajectories near the origin is highlighted in Figure 4.10 to show the characteristics of trajectory curvature near the goal point. Correspondingly, Figures 4.11 and 4.12 are dedicated to the case with control in Equation (3.10). To compare the trajectories under these two different control laws, we put all the two kinds of cases with $\lambda = 1$ and $\lambda = 5$ together into Figure 4.13. And it is highlighted in Figure 4.14 to show more details of the features of trajectories near target point.

From all these figures, all the trajectories show some common features. First, the lower the gain ratio λ, the shorter the distance the robot needs to approach the origin. Second, these trajectories with lower λ also exhibit less turning of heading. Third, specifically in the blow-ups i.e., Figures 4.10 and 4.12, the trajectories with gain ratio higher than

the critical gain ratio ($\lambda = 1$) is quite different from those with $\lambda \leq 1$. All the blue trajectories ($\lambda = 1$) in the blow-ups (referring to Figures 4.10 and 4.12) entry into another quadrant before reaching the target point. Moreover from Figure 4.13 and its blow-up in Figure 4.14, it is shown that under the same conditions, the robot under control in Equation (3.9) turns a bit more than the one under control in Equation (3.10). All of these observations are consistent with our theoretical analysis.

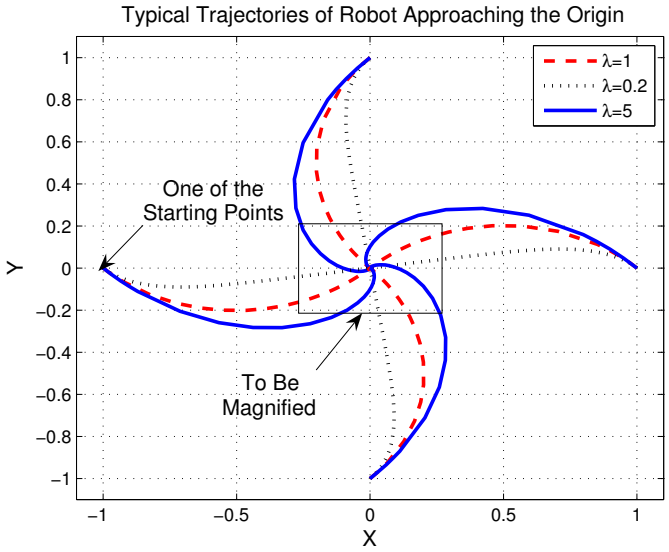

Figure 4.9: Trajectories of robot starting at four different points on x- and y- axis with initial $\phi_0 = \pi/4$ when applied with control law in Equation (3.9). The red color trajectory stands for the case with critical gain ratio ($\lambda = 1$), blue color for $\lambda = 0.2$ and black-color for $\lambda = 5$. Note that the portion within the rectangle is magnified in Figure 4.10.

4.4.2 Unique Trajectories of Robots w.r.t. λ

To verify the assertion that the trajectories of a differential mobile under controls in Equations (3.9) and (3.10) are invariant to the gain ratio λ, we design several experiments similar to those in previous section. For all the experiments in this section, initially the robot is located at four different points $(1,0)$, $(0,1)$, $(-1,0)$, $(0,-1)$ on a

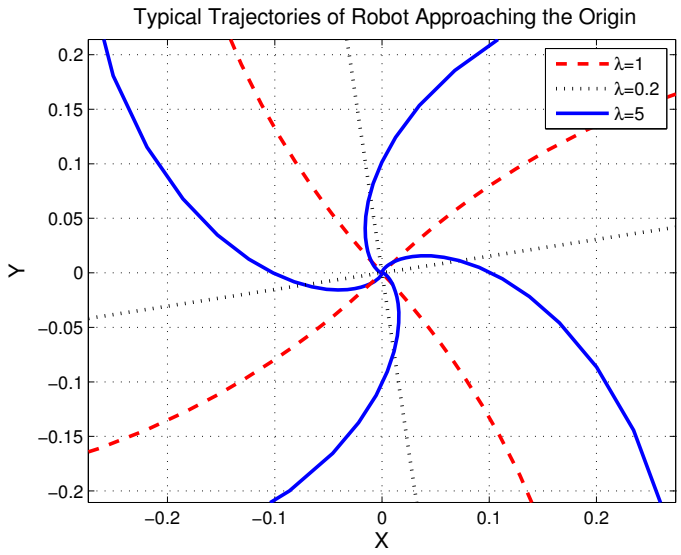

Figure 4.10: Highlights of the trajectories near the goal point (referring to Figure 4.9). Note that different from the red and black color trajectories, the blue one with $\lambda = 5$ entries into another quadrant.

$2D$ plane with initial ϕ_0 chosen to be $\pi/4$. The target for each trajectory is the the origin of the goal point frame.

For the cases with control in Equation (3.9), Figures 4.15, 4.16 and 4.17 show the unique trajectories generated by $K_1/K_2 = 1$, $K_1/K_2 = 5$, $K_1/K_2 = 0.2$ respectively. For the others with control in Equation (3.10), the unique trajectories corresponding to $K_1/K_2 = 1$, $K_1/K_2 = 5$, $K_1/K_2 = 0.2$ are depicted in Figures 4.18, 4.19 and 4.20 respectively. As shown by all these figures, it is clear that the trajectory of the robot solely depends on gain ratio λ.

4.4.3 Mismatching K_3 and K_1

A simulation in Matlab is designed to show two cases of mismatching K_3 and K_1. In case one, initial conditions are set to be $\phi_0 = 1$ rad and $r_0 = 1$ and in case two $\phi_0 = \pi$

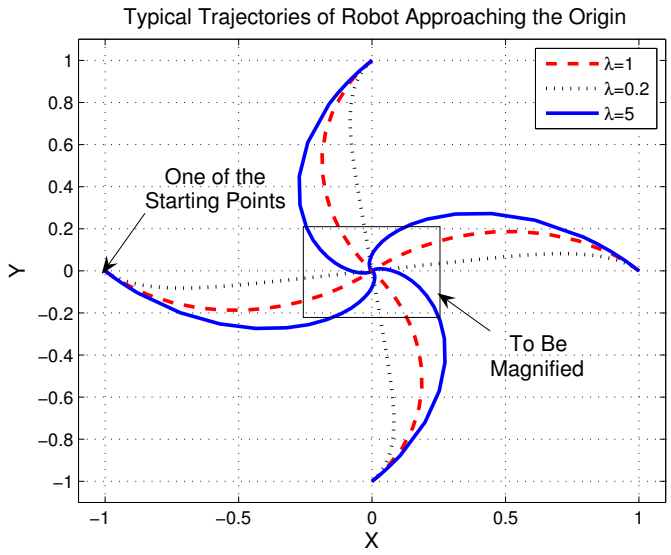

Figure 4.11: Trajectories of robot starting at four different points on x- and y- axis with initial $\phi_0 = \pi/4$ when applied with control law in Equation (3.10). The red color trajectory stands for the case with critical gain ratio ($\lambda = 1$), blue color for $\lambda = 0.2$ and black color for $\lambda = 5$. Note that the portion within the rectangle is magnified in Figure 4.12.

rad and $r_0 = 1$. The nominal gains are chosen as $K_1 = 20$ and $K2 = 1$. Suppose there is -6% deviation of K_3 with respect to K_1, i.e., $K_3 = 18.8$ in case one and a positive 24% deviation of K_3, i.e., $K_3 = 24.8$ in case two.

The simulation results of system response are depicted in Figure 4.21 with (a), (b) for case one and (c), (d) for case two. From this figure, it is obvious that in these two cases $\phi(t)$ fails to approach to zero due to -6% and 24% deviation of K_3 respectively.

4.4.4 Effects of K_3 on System Response

In this simulation we investigate the effects of mismatching K_3 on system response through simulation. Initial conditions are set to be $\phi_0 = 1$ rad and $r_0 = 1$ and gain $K_1 = 20$ and $K2 = 1$. We vary the value of K_3 with respect to K_1. Refer to the stable

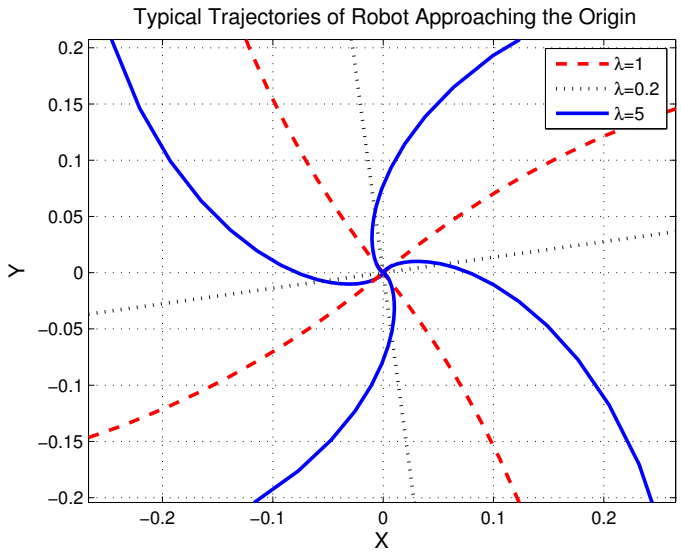

Figure 4.12: Highlights of the trajectories near the goal point (referring to Figure 4.11). Note that different from the red and black color trajectories, the blue one with $\lambda = 5$ entries into another quadrant.

zone illustrated in Figure 4.8, we deliberately choose several sets of $(K1, K2, K3)$ from upper part, separation plane ($K_1 = K_3$) and lower part respectively. According to design guidelines, in this experiment, we choose $K_3 = 22.30, 21.8$ from upper part and $K_3 = 20$ for the nominal case and $K_3 = 19.2$ from the lower part. The results are depicted in Figure 4.22. From this figure, it is noted that compared with $K_3 = 20$, a set in upper part of the wedge in Figure 4.8 contributes to expediting the system's response while a set in lower part of the wedge will negative affect the system's response. The most significant effects of mismatching K_3 is on the converging rate of term $\phi(t)$. Since they are all within the stable wedge, both $r(t)$ and $\phi(t)$ approach to zero as time $t \to 0$.

To compare the energy needed for each controller, we define a function J_n, which is describe by

$$J_n = \int_0^t \left(v^2(\tau) + \omega^2(\tau)\right) d\tau.$$

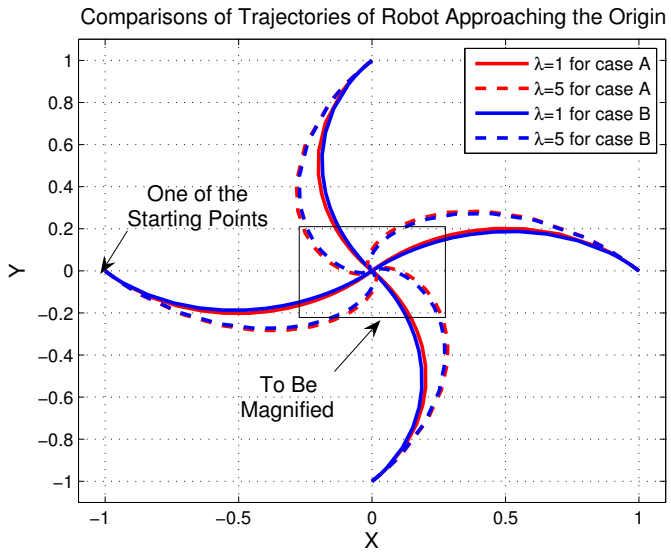

Figure 4.13: Comparison of the trajectories under two different control laws. The ”case A” (represented by red color lines) in the figure denotes the case with control in Equation (3.9) while ”case B” (represented by blue color lines) is for the case with control in Equation (3.10). The portion within the rectangle is magnified in Figure 4.14.

In this simulation, the integral of the norm squared of the actual velocity signals for each controller is shown in Table 4.1. From the figures shown in this table, the control laws recommended by design guidelines seem to be more efficient than the nominal case with $K_3 = K_1$ and the one with negative deviation ($K_3 = 19.2$). And there is not significant difference between the two recommended control laws, i.e.,$K_3 = 21.80$ and $K_3 = 22.30$ respectively.

Table 4.1: Comparison of the integral of the norm squared of the velocity input signals $\int_0^{30} \left(v^2(t) + \omega^2(t)\right) dt$.

$K_3 = 19.2$	$K_3 = 20$	$K_3 = 21.80$	$K_3 = 22.30$
331.8	129.8	69.78	63.87

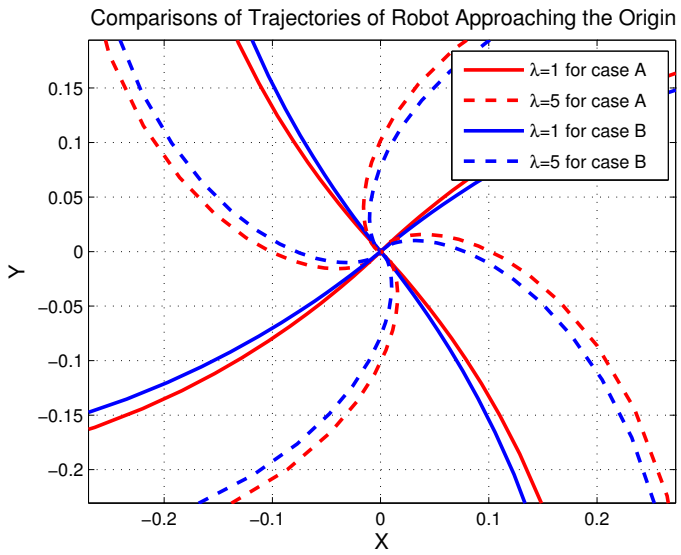

Figure 4.14: Highlights of the trajectories under two different control laws (referring to Figure 4.13). The ”case A” (represented by red color lines) in the figure denotes the case with control in Equation (3.9) while ”case B” (represented by blue color lines) is for the case with control in Equation (3.10). Note that the robot's heading in case A travels a bit more that in case B.

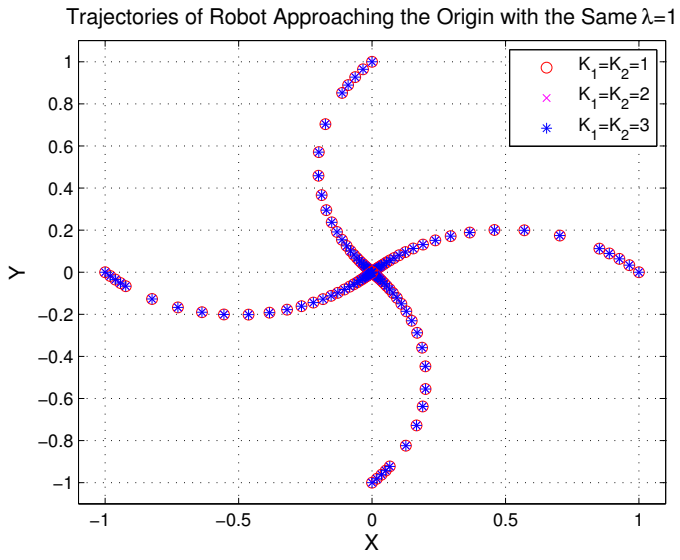

Figure 4.15: The same trajectory for different gain sets of (K_1, K_2) with control in Equation (3.9). For each gain set, the ratio $K_1/K_2 = 1$ is maintained to be the same.

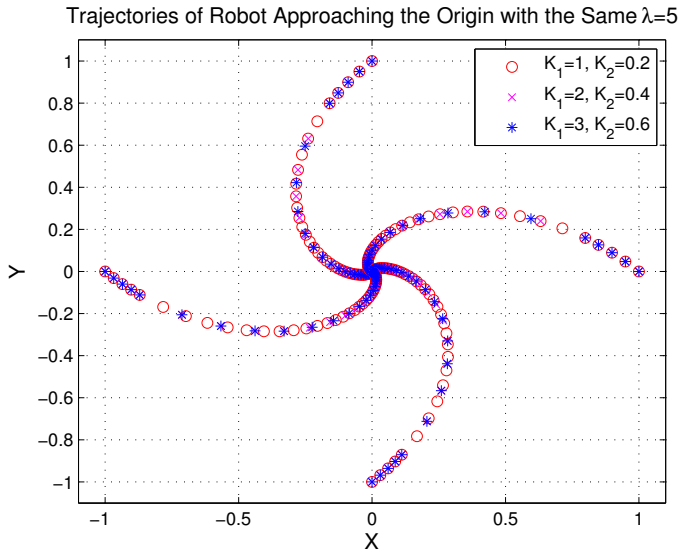

Figure 4.16: The same trajectory for different gain sets of (K_1, K_2) with control in Equation (3.9). For each gain set, the ratio $K_1/K_2 = 5$ is maintained to be the same.

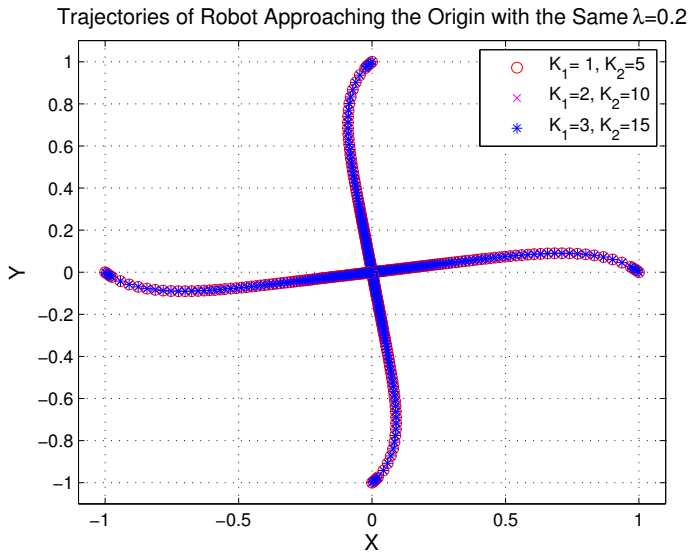

Figure 4.17: The same trajectory for different gain sets of (K_1, K_2) with control in Equation (3.9). For each gain set, the ratio $K_1/K_2 = 0.2$ is maintained to be the same.

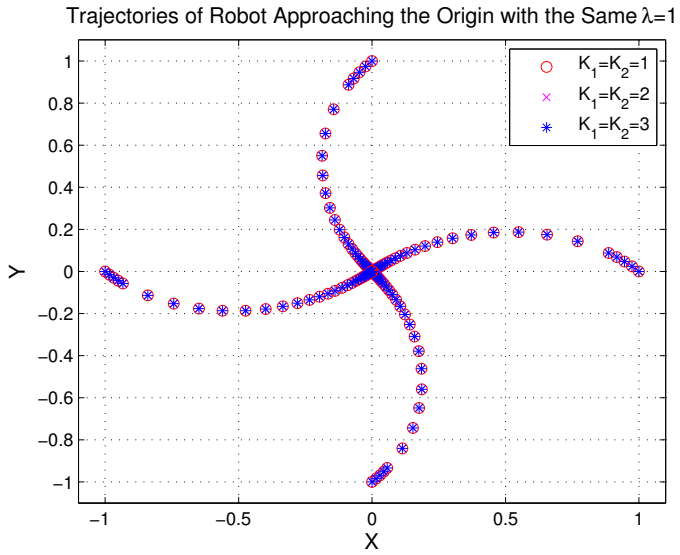

Figure 4.18: The same trajectory for different gain sets of (K_1, K_2) with control in Equation (3.10). For each gain set, the ratio $K_1/K_2 = 1$ is maintained to be the same.

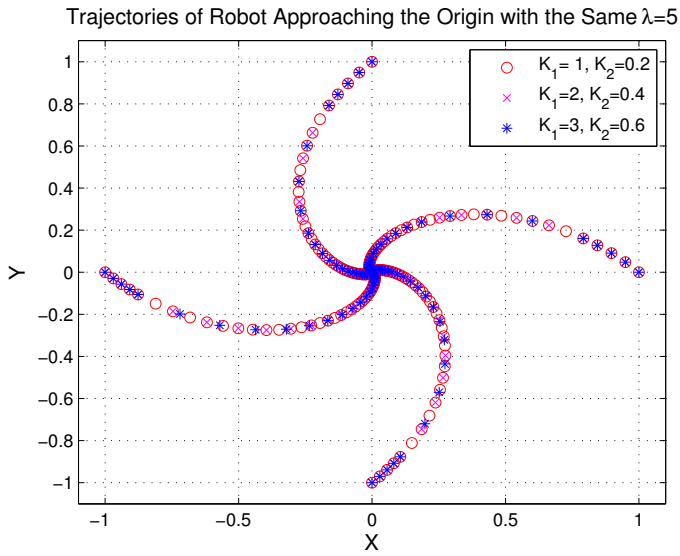

Figure 4.19: The same trajectory for different gain sets of (K_1, K_2) with control in Equation (3.10). For each gain set, the ratio $K_1/K_2 = 5$ is maintained to be the same.

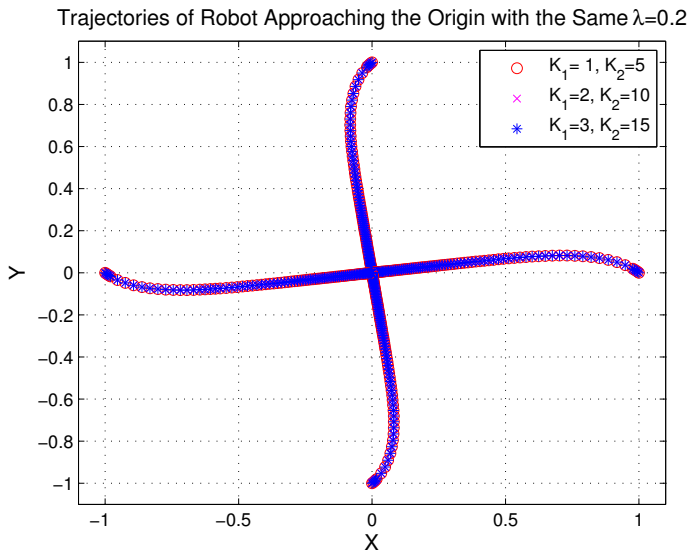

Figure 4.20: The same trajectory for different gain sets of (K_1, K_2) with control in Equation (3.10). For each gain set, the ratio $K_1/K_2 = 0.2$ is maintained to be the same.

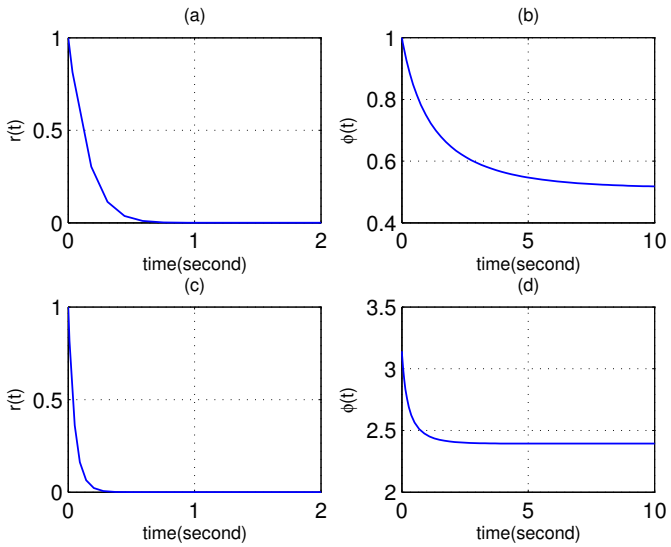

Figure 4.21: Illustration of mismatching K_3 and K_1. In (a) and (b) initial conditions are $\phi_0 = 1$ rad and $r_0 = 1$ and gain $K_1 = 20$, $K2 = 1$ and $K3 = 18.8$ (i.e., -6% deviation). And in (c) and (d) initial conditions are $\phi_0 = \pi$ rad and $r_0 = 1$ and gain $K_1 = 20$, $K2 = 1$ and $K3 = 24.8$ (i.e., 24% deviation).

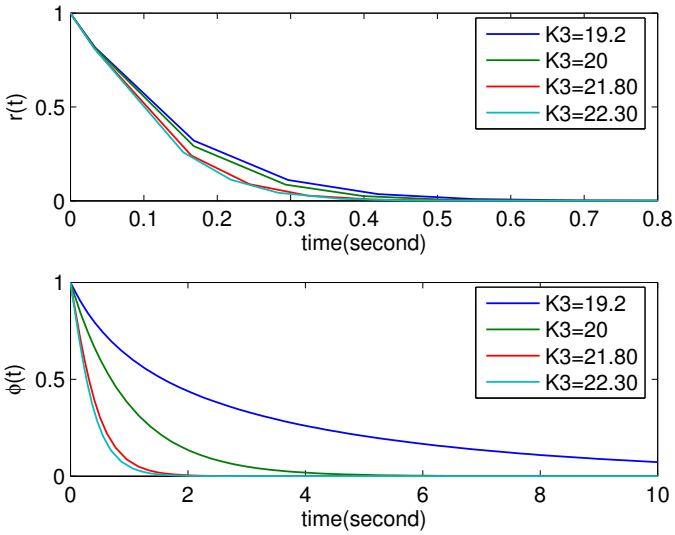

Figure 4.22: Illustration of the effects of mismatched K_3 on the system response. Initial conditions are $\phi_0 = 1$ rad. and $r_0 = 1$ and gain $K_1 = 20$, $K2 = 1$ and $K3 = 19.2, 20, 21.80, 22.30$ respectively.

4.5 Implementation

In previous sections of this chapter, a robust nonlinear feedback control has been proposed. Based on this robust control law, a real implementation of multi-robot formation control is to be presented.

4.5.1 Overview of the Implementation

A picture of the real implementation is presented by Figure 4.23. In this figure, a 4m by 2.8m wooden test bed offers the field for a group of mobile robots. The MRKIT mobile robots presented in Figure 4.23 with on-board infrared sensors and compass, which are used in the experiments consist of the main platform to verify algorithms. Each robot has two independently controlled wheels driven by stepper motors. A GPS system is simulated by a vision system comprising vision frame grabber, CCD color camera with lens, a working station, and wireless communication modules. Two web-cam are mounted on the ceiling and can be used for robot tracking or video recording and only one is showed in Figure 4.23. The key modules of this implementation are connected as shown by Figure 4.25.

4.5.2 Parameters of MRKIT Mobile Robots

Each wheel of MRKIT robot is driven independently with step motor being controlled by on-board micro-controller. The wheel velocity is controlled via PWM waveform and is determined by an internal time interval T in the micro-controller. The relationship

Figure 4.23: Picture of real robots, test bed(on the floor), CCD color camera with wide-angle lens and one web-cam(mounted on the ceiling).

between the velocity V of a wheel and T can be represented as

$$V = \frac{D\pi}{NP},$$

where $D = 54$ mm is the diameter of the wheel; $N = 400$ is the step of motor per revolution; P is the time (second) per step and $P = \frac{T \cdot 10^{-6}}{2.5}$. Finally we arrive at $V = \frac{1060.288}{T}$ m/s and T is a 16-bit integer, which can be set in micro-controller. Due to the finite length of T and physical limitations of motor, V has a minimum $V_{min} = 0.0162$ m/s and a maximum $V_{max} = 0.3$ m/s.

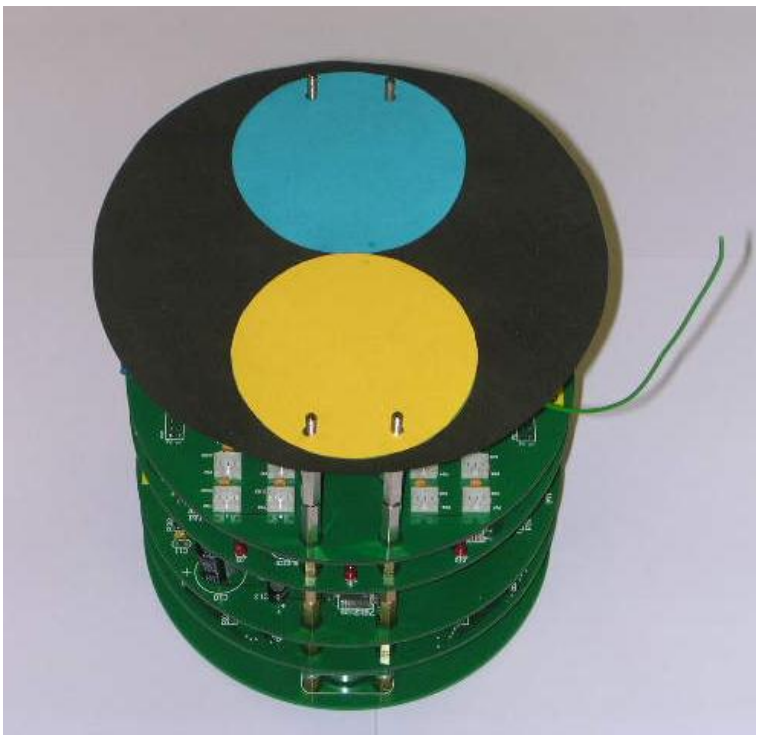

Figure 4.24: Picture of a MRKIT mobile robot with on-board color pads.

4.5.3 Vision System: Resolution and Noise Analysis

A vision system, comprising of CCD camera, lens, frame grabber and application program as shown in Figure 4.25, is developed for tracking the mobile robots and detecting their position/orientation. Its resolution is largely determined by the resolution of the CCD camera and the optical system. In the experiment, the CCD camera is mounted on a bracket fixed on the ceiling. Due to the limitation of ceiling height, the viewable area on the test bed is 1800mm by 2480mm. The CCD camera has a resolution of 576 by 768 pixels. Accordingly calculation results show that along the x-axis, the resolution is 3.229mm per pix while along the y-axis, 3.177mm per pix.

To identify the robot's position and orientation, a color pad is attached on the top of a robot as shown in Figure 4.24. Each color pad has two different color 65mm-diameter

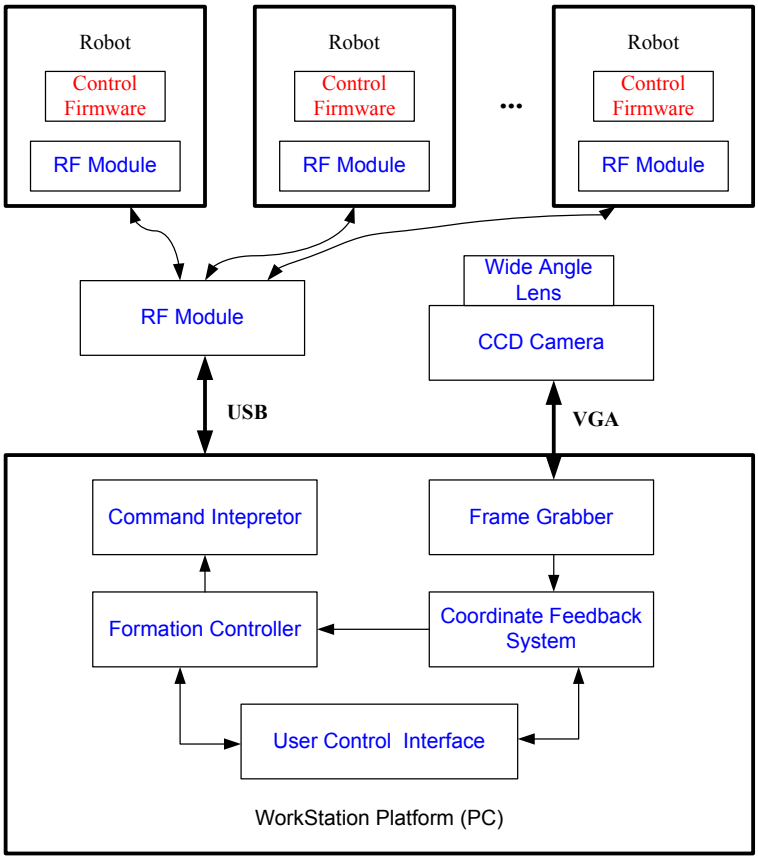

Figure 4.25: Illustration of connection of the whole implementation.

circles aligned in a line. One circle is painted blue and the other one yellow. The center of each circle can be determined using the image processing hardware and software, namely the frame grabber and the corresponding vision processing software running on working station. We can use coordinates of the centers of the two color circles to calculate the position of the robot's center and its orientation. Let (x_a, y_a) and (x_b, y_b) denote the measured coordinates of the center of yellow circle and blue circle respectively. Hence, the coordinates of the robot's center can be represented as $(\frac{x_a+x_b}{2}, \frac{y_a+y_b}{2})$. Meanwhile the orientation of the robot can be calculated as $\theta = \cos^{-1}(\frac{x_a-x_b}{\rho})$, where $\rho = \sqrt{(x_a-x_b)^2+(y_a-y_b)^2}$.

The measurement of the position of each color circle is a resultant of its real position

and the error signal together with noise. The position error is incurred by the hardware of the system. For instance, the field is not even and can end up with position error. Optical system is another source of error. The distortion of the lens on the margin of the viewable area is relatively salient and such distortion in fact affects the accuracy of the measurement. Roughly the measurement of position can be expressed in the following equation.

$$X_m = x_r + x_e + x_n,$$

where x_r is the real position; x_e is the system error and x_n the noise. Basic procedures of image processing are employed. Calibration of the optical system is performed to remove radial and tangential distortions, which are the major contributor of x_e. Effects of lighting on the test bed are evaluated. The R, G, and B components of each pixel on the color pad are determined through experiments. It is of interest and practically importance to know the noise level of the measured signal. For any static robot on the test bed, its real position and system error are always constant and contribute no variation to the mean value of X_m and its variance. From this observation, it helps to sample the measurement for a certain period and then use the spectrum analysis tools to obtain information on the noise. A convenient way is to use the FFT technique. It is well known that Microsoft Windows is not a real time operating system. For the purpose of FFT, it is required to evenly sample the data. To solve this conflict, a high resolution timer without accumulation error is in need. In this experiment, the multi-media timer is used. It is a high resolution timer with accuracy and resolution of 1 millisecond while the system resource used is relatively small. We set the sampling rate to be 500 Hz. A

period of 2 minutes is used to sample the data and for example, the error signal along x-axis is presented in Figure 4.26(figures of error signal along y-axis the associated orientation error signal are omitted for the sake of brevity). Then we apply the FFT technique and analyze its frequency components. It turns out that the noise signals on x, y and orientation all show on the feature of Gaussian noise. The analysis shows that $\delta_x = 0.142$ pix, $\delta_y = 0.154$ pix $\delta_\theta = 0.0122$ radius. Obviously, the noise level of position signal is relatively low compared with the vision system's resolution.

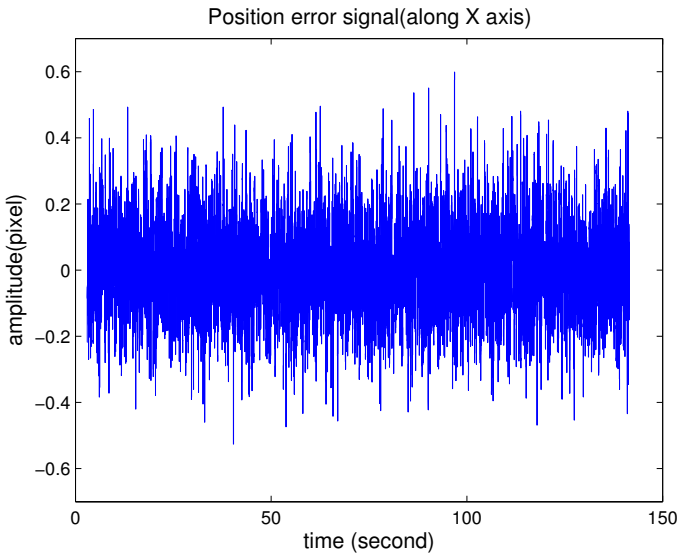

Figure 4.26: Position error signal along x-axis with sampling rate $f = 500$Hz.

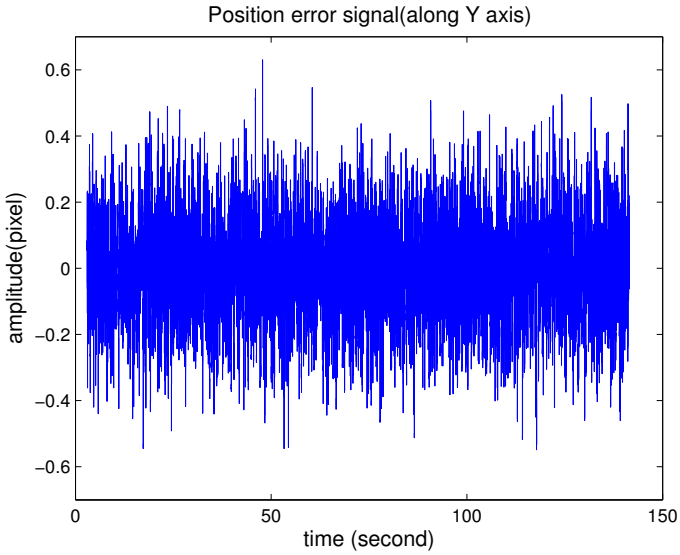

Figure 4.27: Position error signal along y-axis with sampling rate $f = 500$Hz.

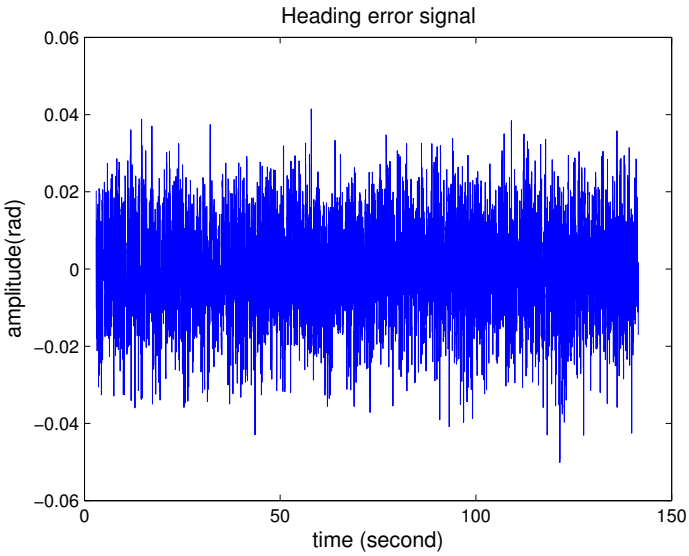

Figure 4.28: Angular error signal with sampling rate $f = 500$Hz.

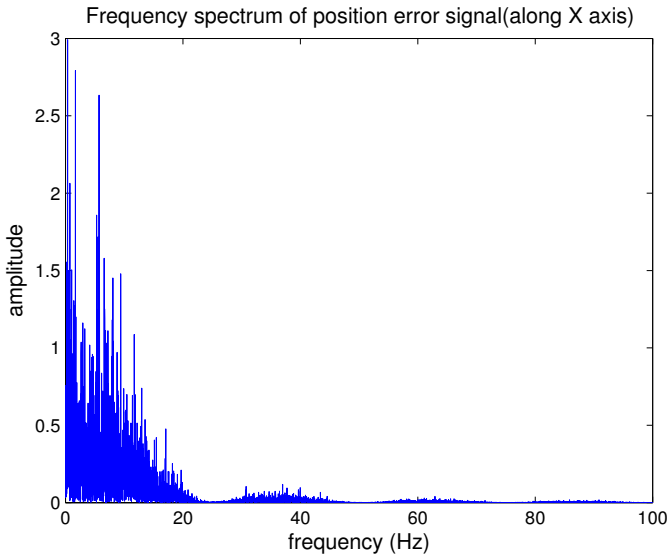

Figure 4.29: Spectrum analysis of position error signal along x-axis with FFT transformation.

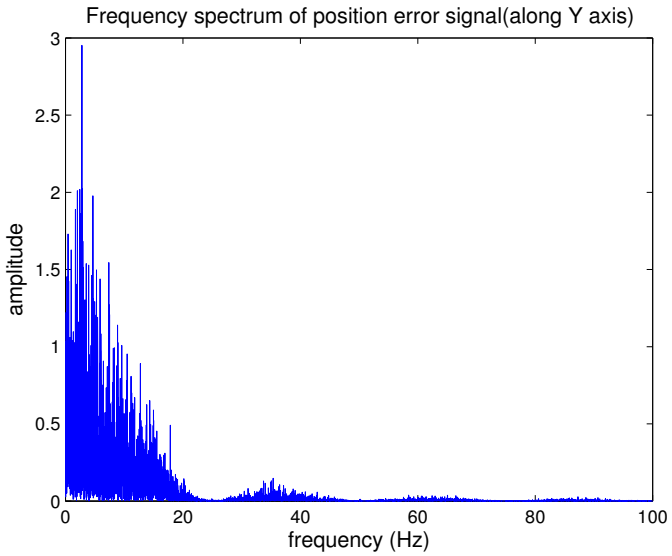

Figure 4.30: Spectrum analysis of position error signal along y-axis with FFT transformation.

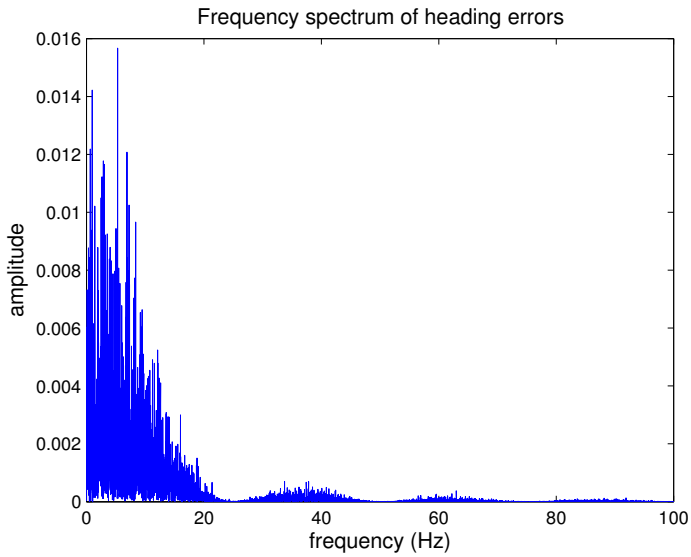

Figure 4.31: Spectrum analysis of angular error signal with FFT transformation.

4.6 Experimental Results

A scalable formation control scheme is introduced in [29]. The idea is that, instead of being attracted to a predetermined point, each robot is to be attracted to the corresponding segment, and once there, move along the segment to distribute themselves along the trench in order to form a formation by maintaining the desired position in relation to other robots. Aa shown in Figure 2.1, in this situation there are a series of segments and a team of robots are supposed to fall into the assigned segments. Usually a segment S is a curve defined by some smooth (i.e., at least twice-differentiable) function in R^3 that passes through one or two formation vertices. And a robot will arrive at the nearest point on the segment and then move along the curve of the segment.

A group of n robots may be arranged in a certain formation. Certain pertinent locations in a particular formation are defined as formation vertices. A detailed discussion on the determination of formation vertices can be found in [29]. For the purpose of the work reported in this thesis, it suffices to consider a formation vertex as a point in R^3.

4.6.1 Experiment-1: Triangle Formation of Three Robots

In this experiment, it is assumed that assignment mechanism of segment is known and initially all robots are static. Referring to Figure 3.4(a), three segments (straight lines) are assigned to three robots respectively. For the first 8 seconds, each robot will try to approach the nearest point on the segment and then three virtual points moving along segments are assigned to each robot. These three virtual points form a triangle pattern

and will stop at the vertices of segments. The velocity of virtual points are set to be 20 pix per second. During the process of formation, velocities and headings of each robot are depicted in Figures 4.32 - 4.35. Snapshots of video (taken by web-cam) at $t = 0, 4, 8, 12, 16, 20, 24$ seconds respectively are shown in Figure 4.36. The controller parameters are set to be $K_1 = 0.1$, $K_3 = 0.12$ and $K_2 = 1.0$. From these figures, it can be seen that all the robots are attracted to the segment for the first 8 seconds and later on form the triangular pattern while moving forward. The video fore this experiment is available online at $http://youtu.be/wEQ\_9HZUzhl$.

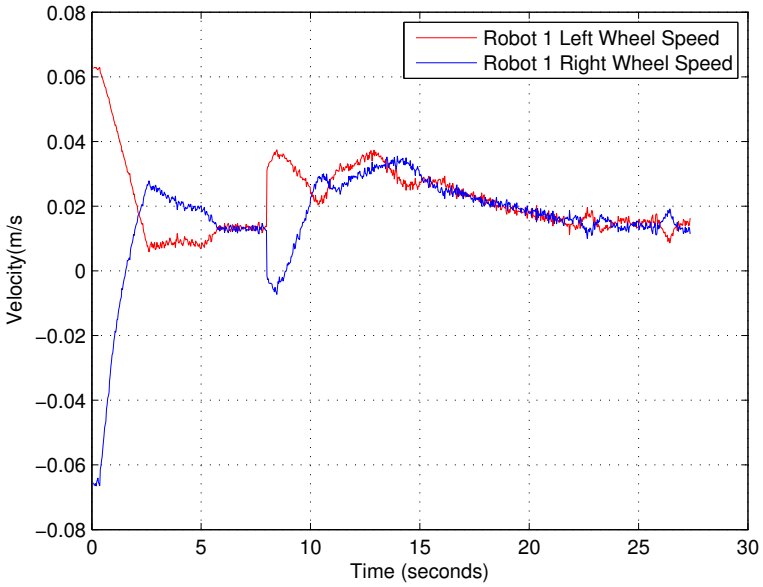

Figure 4.32: Velocity of robot 1 during 3-robot triangle formation control.

4.6.2 Experiment-2: Square Formation of Four Robots

In this experiment, four robots that are initially randomly scattered are required to form a square patter. Referring to Figure 3.4(b), two segments (straight lines) are assigned. For the first 3 seconds, each robot will try to approach the corresponding nearest point on the segment and then try to approach to four virtual points moving along seg-

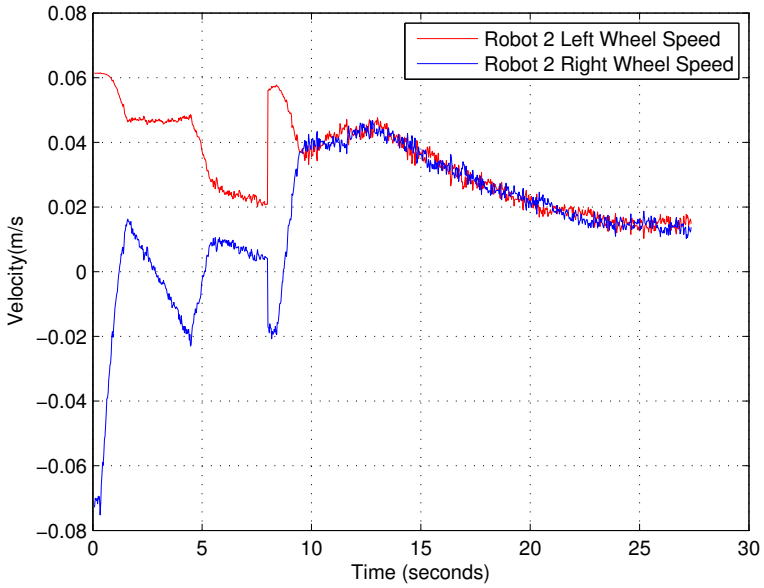

Figure 4.33: Velocity of robot 2 during 3-robot triangle formation control.

ments are assigned to each robot. These three virtual points form a triangle pattern and will stop at the vertices of segments. The velocity of virtual points are set to be 20 pix per second. During the process of formation, velocities and headings of each robot are depicted in Figures 4.37 - 4.41. Snapshots of video (taken by web-cam) at $t = 0, 4, 6, 8, 12, 16, 20$ seconds respectively are shown in Figure 4.42. The controller parameters are set to be $K_1 = 0.1$, $K_3 = 0.12$ and $K_2 = 1.0$. From these figures that all the robots are attracted to the segment for the first 3 seconds and later on form the square pattern while moving forward. The video fore this experiment is available online at $http://youtu.be/NJUSR6bvcTk$.

4.6.3 Discussions on Locomotion Limitations of MRKIT Robots

Each wheel of MRKIT utilizes an independent step motor for locomotion. There are two outstanding drawbacks that impede implementation. As indicated by Equation (3.10),

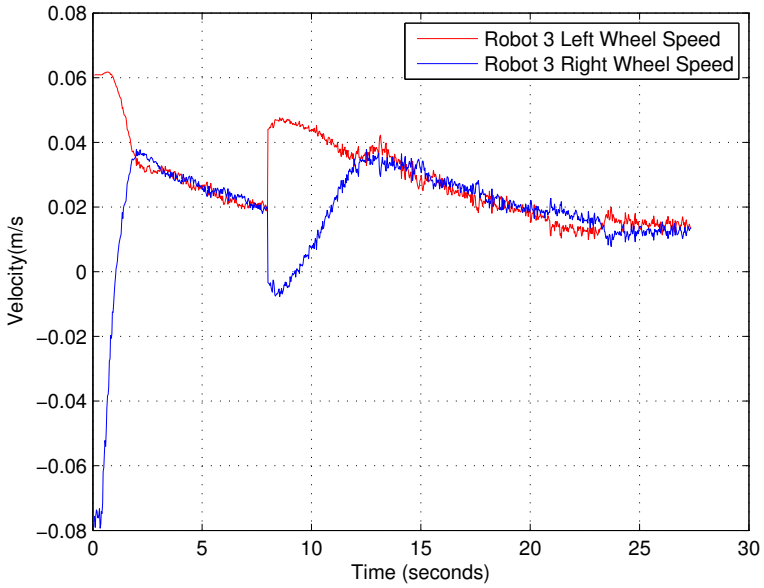

Figure 4.34: Velocity of robot 3 during 3-robot triangle formation control.

the desired velocity is proportional to the distance to goal point (namely, r). If a robot is initially placed far away from its goal point, the desired velocity will be relatively high. However, step motor usually is weak on its maximum starting speed and starting torque. If the gains K_1, K_2, and K_3 are set too high, a robot initially at standstill will immediately miss its step at the very beginning of formation control. The other shortcoming arises from the minimum speed of step motor. Due to the limitation of minimum speed, a wheeled mobile robot in fact cannot reach a fixed goal point. Instead it will stop moving once it is within a certain range with respect to its goal point, thus creating a dead-zone. To reduce the size of dead zone, higher gain is required and thus increases the risk of missing steps. Trade-off has to be done for real implementation. To overcome such downside of locomotion, other motors with high starting torque such as permanent magnet brushless DC motor is more suitable for real implementation.

Meanwhile it is worthwhile to note that step motors which drive MRKIT robots are

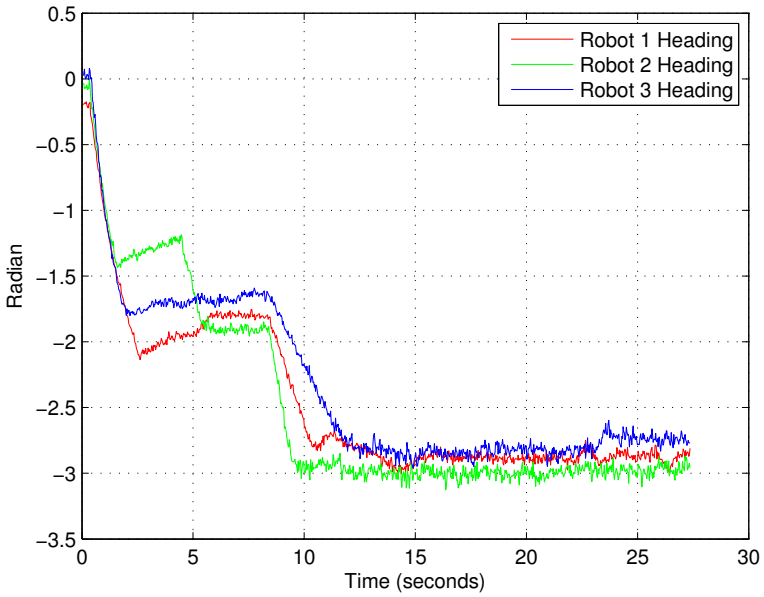

Figure 4.35: Headings of all robots during 3-robot triangle formation control.

highly undesirable for controllers based on dynamics model given by Equation (3.4). Because for this model it is the force inputs or torques inputs rather than velocity input that directly applied on the actuators and step motors is usually controlled through velocity inputs.

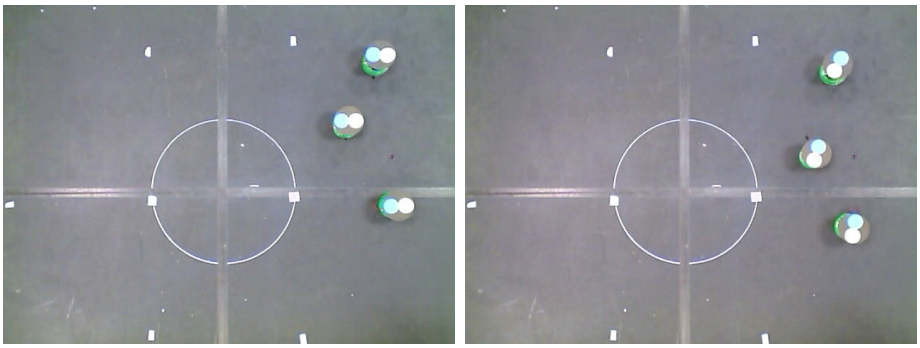

(a) t=0s (b) t=4s

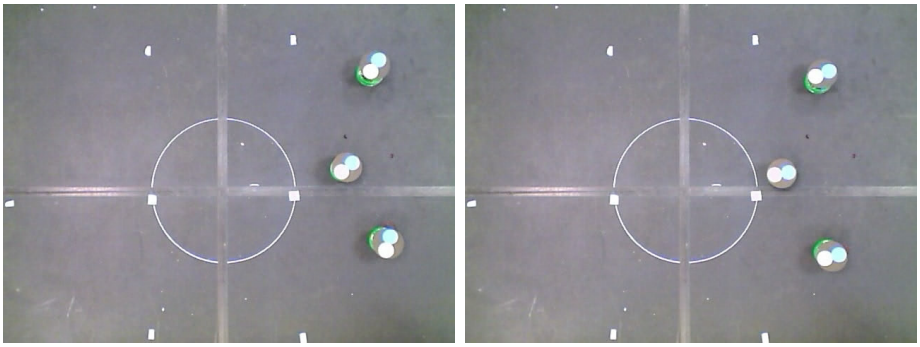

(c) t=8s (d) t=12s

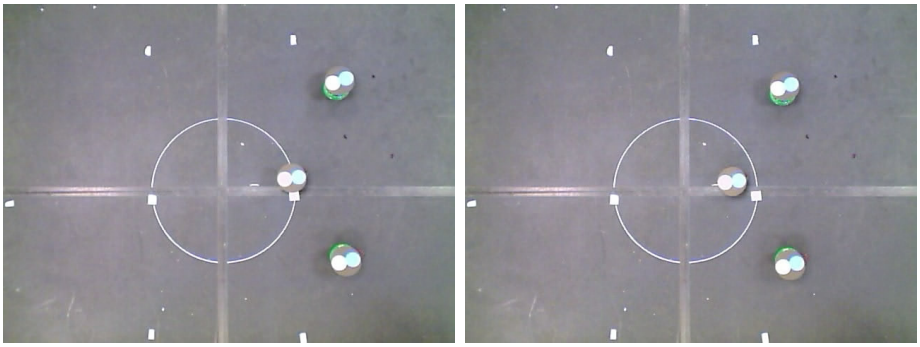

(e) t=16s (f) t=20s

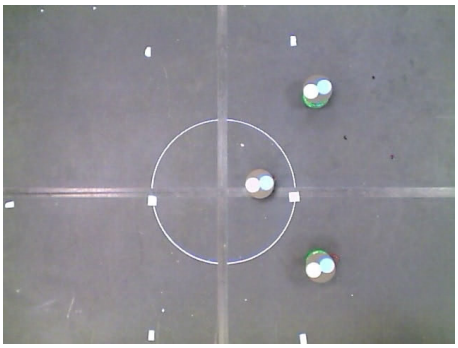

(g) t=24s

Figure 4.36: Snapshots of 3-robot motion under triangle-formation control.

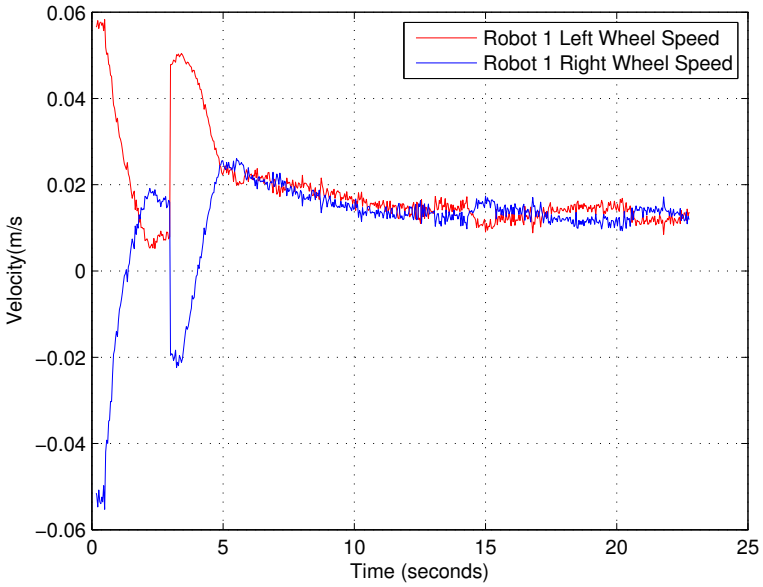

Figure 4.37: Velocity of robot 1 during 4-robot square formation control.

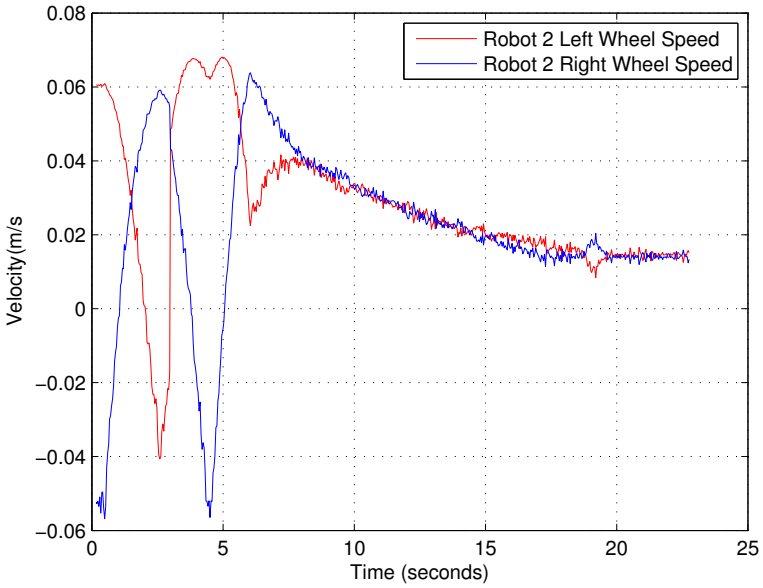

Figure 4.38: Velocity of robot 2 during 4-robot square formation control.

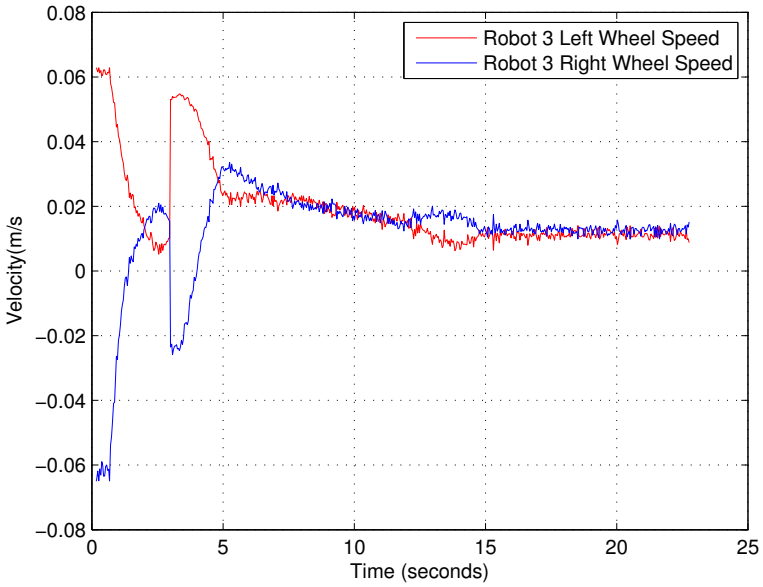

Figure 4.39: Velocity of robot 3 during 4-robot square formation control.

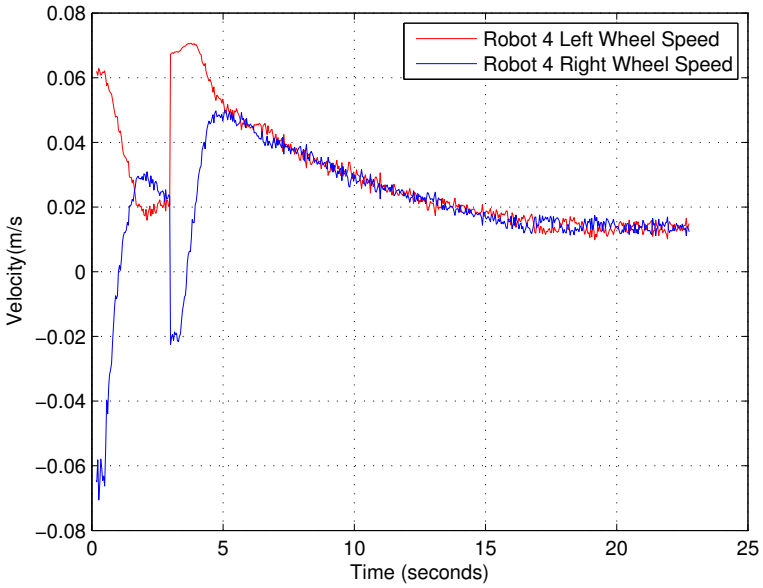

Figure 4.40: Velocity of robot 4 during 4-robot square formation control.

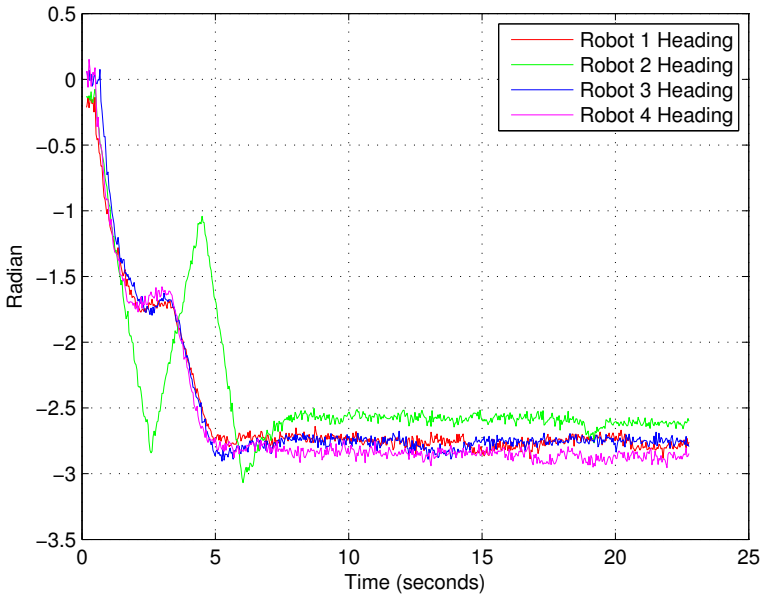

Figure 4.41: Headings of all robots during 4-robot square formation control.

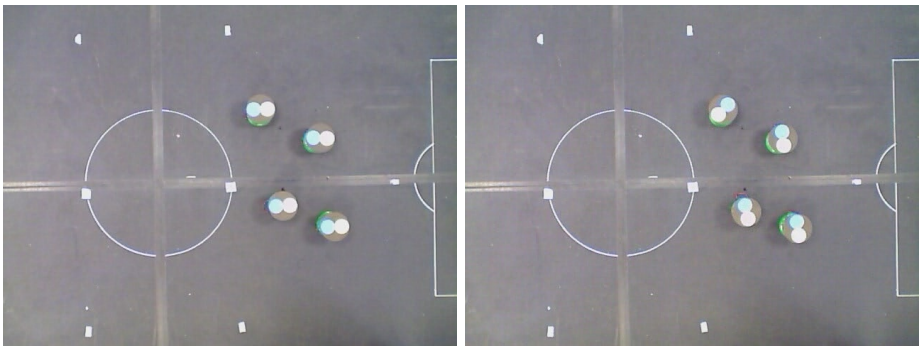

(a) t=0s (b) t=4s

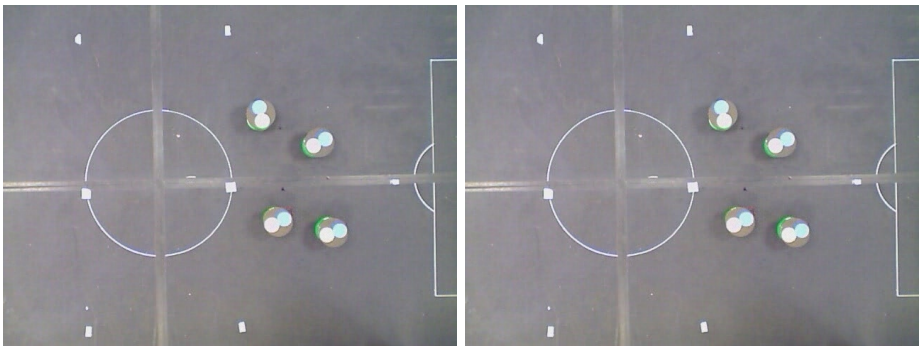

(c) t=6s (d) t=8s

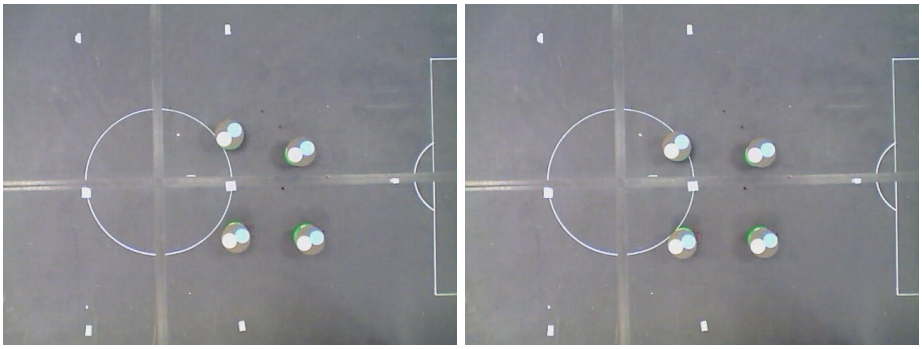

(e) t=12s (f) t=16s

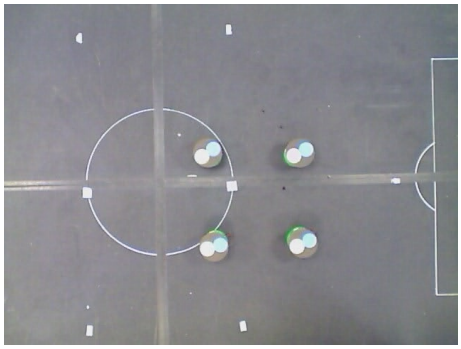

(g) t=20s

Figure 4.42: Snapshots of 4-robot motion under square-formation control.

4.7 Summary

In this chapter, we provided a detailed analysis of the qualitative characteristics of two continuous nonlinear feedback controls of differential mobile robots. It shows that the evolution of heading and trajectory characteristics of the robot are essentially similar when subject to these two similar controls. Such information can facilitate real implementation when the final heading or trajectory curvature are concerned and may inspire more attempts to seek for the essential linkages between proposed controllers and the corresponding trajectories in future research work.

Also we studied the robustness of a nonlinear feedback control based on kinematic model. It provides insight into the stability zone for a given set of controller gains and it is found that under certain circumstances the closed-looped system may fails in reaching the desired control objectives and performance. Thanks to the robustness analysis, we are able to improve the controller design by choosing proper controller gains K_3 when K_1 and K_2 are given. This remedy successfully overcomes the drawbacks of the common nonlinear control law discussed. More details of the improved control law are revealed and facilitate real implementation.

In the second part of this chapter, a real implementation of multi-robot formation control on the basis of the proposed robust nonlinear feedback control is presented. The analysis on the vision subsystem shows that the noise level in the measurement of position and orientation is acceptable compared with the system resolution. Two experiments on multi-robot formation control, namely a three-robot triangle formation and a four-robot

square formation, have been conducted successfully.

Chapter 5

Formation Stability Using Artificial Potential Trench Method

5.1 Motivations

To provide the needed scalability, the notion of artificial potential trenches [29] was introduced. The idea is that, instead of being attracted to a predetermined point, each robot is to be attracted to the bottom of the "valley" artificially created by a so-called potential trench (or simply, trench), and once there, it moves along the trench to distribute themselves along the trench in order to form a formation by maintaining the desired position in relation to other robots. The proposed artificial potential trench is illustrated in Figure 3.5.

Although extensive simulations have been performed in [29], explicit control laws and stability of the corresponding controlled multi-robot formation are not addressed in this paper. Our work aims to present multi-robot formation control laws with a solid stability

proof on the basis of potential trench, a novel method proposed in the paper. Moreover, as shown by Equation (33, 34) in previous work [29], the simulations are based on kinematics model of differential mobile robots, where the force imposed on a robot can determine its velocity directly. This is no problem with motion planning for a robot, but definitely it is not the natural way that robot should react to force. Normally when exposed to exogenous forces, the robot has one thing determinate, which is the acceleration, not the velocity, because velocity is the integral of acceleration on time domain plus the initial condition. Since we consider the potential trench and forces (generated by trench), it is natural to deal with the dynamics model of non-holonomic robots. To make the control laws and stability proof feasible, one way is to derive a feedback linearization model of the robot. That is the well-known double integrator of look-ahead control which is described by Equation (3.4).

Because the artificial potential trench $\Phi(d_{i,g})$ is a scalar function and it does not explicitly contain speed information of robot or goal point, the trench potential is a speed-nulling potential. Therefore it is neat and appealing as it only cares about the displacement of the robot's current position to its target. If we can show that a properly designed potential can stabilize a robot on its target point, then the problem of controlling a single robot during formation of certain pattern is to find a suitable trench potential. In this chapter, we investigate the stability of formation control based on the method of artificial potential trench and the results are from solid mathematical nonsmooth analysis. We impose constraints on artificial potential trench to synthesize a control law that stabilizes a team of robots on a given formation without considering specific requirements

on the distance between any two robots. Such constraints provide sufficient conditions for choosing proper potential functions and therefore facilitate the controller design.

5.2 Potential Trench Functions and Mobile Robot Tracking Control

5.2.1 Definition of Potential Trench Functions

Based on the knowledge of nonsmooth analysis stated in Chapter 3, a formal definition of a potential trench function is given as follows:

Definition 5.2.1 *A potential trench function is a real-valued map* $\Phi : R \to R$ *with following properties:*

(1) Φ *is globally Lipschitz and regular on the domain.*

(2) Φ *is positive definite, i.e.,* $\Phi(0) = 0$ *and* $\Phi(x) > 0$ *for* $\forall x \neq 0$.

(3) The Clarke's generalized gradient of Φ *at* $x = 0$ *contains zero, i.e.,* $0 \in \partial\Phi(0)$. □

Various types of functions can be constructed to be used as potential trench functions. Detailed techniques to construct such functions are to be discussed later. Three typical examples of potential trench function are highlighted in Examples 5.2.1, 5.2.2, and 5.2.3.

We consider the following scenario concerning the notion of forming a formation. Initially, a group of robots are assumed to be randomly scattered in an area, each within a pre-defined distance from at least one other robot. We assume that a formation which the

robots are to take up is known, and that a mechanism for assigning a robot to a particular segment exists. (Discussion on these two issues can be found in [29].) The set of robots that are assigned the same segment is referred to as a *team*. A robot is said to conform to a segment if it is located with certain tolerance on the segment. The individual teams in the group is then required to approach and conform to their respective segments, thus producing the overall formation.

5.2.2 A Single Robot Approaching and Conforming to a Segment

As shown in Figure 3.5, a robot r_i is at certain position $\vec{r}_i$ off the segment, the set of points representing certain geometric shapes. A segment may have either one or two vertices to denote the end point of the curve of segment. For instance, in this figure, the segment has one vertex. For each instantaneous position (i.e. current position) $\vec{r}_i$, there is a unique known goal point $q_{i,g}$ (stationary or in motion) with its position denoted by $\vec{r}_{i,g}$ on the segment for the robot to track. For each pair $(\vec{r}_i, \vec{r}_{i,g})$, we can construct a potential $\Phi(\cdot)$, which is a scalar function of $d_{i,g} = \|\vec{d}_{i,g}\| = \|\vec{r}_{i,g} - \vec{r}_i\|$, where $d_{i,g}$ denotes the distance from the current position of robot r_i to its goal point on the segment. As shown at the right upper corner of the Figure 3.5, the existence of $\Phi(\cdot)$ for each instantaneous position $\vec{r}_i$ contributes a roughly "U-shape" section with its bottom on the segment (note that just for illustration here, the real shape is dependent on definition of $\Phi(\cdot)$). If the robot r_i moves from one end point of the segment to another (e.g. vertex in Figure 3.5) with nonzero $\|\vec{d}_{i,g}\|$, finally there will be a valley-shape trench with its bottom being the segment curve due to Φ. Throughout this thesis, we refer to this valley-shape trench as

Artificial Potential Trench, or for simplicity, Potential Trench and refer to the associated $\Phi(\cdot)$ as Potential Trench Function. The motivation of potential trench is to attract robots in a team to the bottom of the trench, i.e., points on the segment.

However, it should be noted that there is a minor difference between the description of potential trench in this thesis and the one in the original work [29]. Instead of fixing the nearest point on the segment with respect to the robot as the goal point towards which the robot will approach the segment (which is the case in [29]), we allow the goal point to be any point on the segment subject only to proper choice of $\Phi(d_{i,g})$. This leads to a framework of formation control that admits a wider range of formation-forming behavior, as discussed subsequently.

Figure 3.6 illustrates the coordinates system for locating robots in a segment. The vector $\vec{r}_0$ defines the vertex, while $\vec{r}_i$ specifies the position of the i^{th} robot, whose leader is robot $i-1$, as indicated by the vector $\vec{r}_{i-1}$. Each robot has its own goal point on the segment. For instance, the goal point for robot i is $q_{i,g}$. We definite the displacement vector $\vec{d}_{i,g} = \vec{r}_{i,g} - \vec{r}_i$ with $d_{i,g}$ and $\hat{d}_{i,g}$ denoting its length and the corresponding unit vector in the direction of $\vec{d}_{i,g}$ respectively.

Proposition 5.2.1 *A robot r_i (whose goal point is specified by the twice-differentiable vector $\vec{r}_{i,g}$ on a segment) is globally asymptotically stable with respect to $\vec{r}_{i,g}$ under the control*

$$\vec{u}_i = \ddot{\vec{r}}_{i,g} + k_i \dot{\vec{d}}_{i,g} + \Phi'_{i,g} \hat{d}_{i,g}, \tag{5.1}$$

where $\Phi(d_{i,g})$ *is an admissible potential trench function,* $\dot{\vec{d}}_{i,g} = d(\vec{d}_{i,g})/dt$, $\Phi'_{i,g} = d(\Phi(d_{i,g}))/d(d_{i,g})$, $\hat{d}_{i,g} = \vec{d}_{i,g}/d_{i,g}$, *and* k_i *is a positive scalar.*

Proof: See Appendix A.5. □

Remark 5.2.1 *On the right-hand-side of Equation (5.1) given in Proposition 5.2.1, the first term* $\ddot{\vec{r}}_{i,g}$ *is the feed-forward control signal represented by the difference in acceleration between the robot and the corresponding goal point, and vanishes (i.e.,* $\ddot{\vec{r}}_{i,g} = 0$*) when the goal point is moving at constant speed; the second term* $k_i\dot{\vec{d}}_{i,g}$ *contains the difference in velocity between the robot and its goal point, and represents a damping effect on the dynamics of the robot controlled by* u_i*; and the third term is derived from the potential trench function* Φ*, the derivative with respect to* $d_{i,g}$.

5.2.3 Methods for Construction of Potential Trench Functions

To find out the admissible potential trench functions is key to the approach introduced above. To this end, we introduce a few lemmas and propositions as shown below:

Lemma 5.2.1 *For a real-valued map* $f : R \to R$ *and* $f(\cdot) \in L^\infty$ *space, define the function* $F : R \to R$ *as* $F(x) = \int_0^x f(s)ds$ *and denote the Clarke's generalized gradient of* F *at each point* x *as* $\partial F(x)$*, then*

(1) F *is Lipschitz continuous and regular;*

(2) $\partial F(x) = [f^-(x), f^+(x)]$*, where* $f^-(x)$ *and* $f^+(x)$ *denote the essential supremum and essential infimum of* f *at* x*, and especially at those points where* F *is strictly differentiable, generalized gradient reduces to* $\partial F(x) = \{f(x)\}$.

Proof: See Appendix A.6. □

Lemma 5.2.2 *Suppose a real-valued map $f : R \to R$ and $f(\cdot) \in L^\infty$ space. In addition, $f(x)$ satisfies $xf(x) > 0$ for all $x \notin \{0\} \cup \Omega_{\mu L=0}$, where $\Omega_{\mu L=0}$ denotes the union of all sets of Lebesgue measure zero. Then the function $F : R \to R$ defined by $F(x) = \int_0^x f(s)ds$ has the following properties:*

(1) F is positive definite;

(2) At the origin $x = 0$, $0 \in \partial F(0)$.

Proof: See Appendix A.7. □

Lemma 5.2.3 *If a convex function $F : R \to R$ is continuously differentiable and positive definite, then its derivative with respect to x, namely, $f(x) = d(F(x))/dx$ satisfies $f(0) = 0$.*

Proof: See Appendix A.8. □

For convex functions, there are a couple of desirable properties. The following Propositions 5.2.2 and 5.2.3 link convexity with Lipschitz condition and regularity which are relevant to this topic. Both propositions are from the monograph [13] by F. H. Clarke where detailed proofs are given.

Proposition 5.2.2 *Let a real-valued map $f : D \subset R^n \to R$ be convex and be bounded on a neighborhood of some point of U. Then, for and x in U, f is Lipschitz near x.*

Proposition 5.2.3 *Let a real-valued map $f : D \subset R^n \to R$ be Lipschitz near x.*

(1) If f is strictly differentiable at x, then f is regular at x.

(2) If f is convex, then f is regular at x.

From Propositions 5.2.2 and 5.2.3, we know that twice differentiable convex function $F(x)$ given in Lemma 5.2.3 is Lipschitz and regular.

In Lemma 5.2.2 and 5.2.3, we proposed two criteria for constructing proper potential trench function candidates. It is worthwhile to note that the former is essentially bounded while the latter may not. Both of them can be applied to smooth functions. However, the former is significantly helpful when dealing nonsmooth dynamics. Thanks to this capability, Lemma 5.2.2 can be used to deal with the limitations of physical systems, for instance, the input saturation of real actuators which is very common in control engineering.

Letting Φ be a continuously differentiable convex function seems desirable as it is entitled to a couple of desirable properties of convex function, which are very useful in functional analysis, not to mention that the above proof of stability will be greatly simplified. Due to the special properties of convex functions (for example, a local minimum of a convex function is a global minimum), the potential trench function candidate can be readily chosen. However, convexity requirement seems to be too strong and some relaxation is desirable. Basically, there are two reasons motivating this relaxation: firstly a great number of functions in the real world fail to be continuously differentiable (for instance, the absolute-value function is not differentiable at $x = 0$.); secondly, convexity condition excludes many qualified potential trench function candidates. As shown in

conditions of Lemma 5.2.2, a qualified potential trench function candidate does not need be continuously differentiable. Moreover, even for the continuously differentiable potential trench functions, them may not be convex. More details are revealed in Examples 5.2.1 - 5.2.3.

Example 5.2.1 *A commonly used potential function is given by [50]:* $\Phi(x) = \alpha\eta^m(x)/2$, *where* α *is a positive scaling factor,* $m = 1$ *or 2, and* $\eta(\cdot)$ *is a scalar function. If* $\alpha = 2$, $m = 1$, *and* $\eta(x) = |x|$, *then* $\Phi(x) = |x|$ *which corresponds to an absolute-value function. The function* $\Phi(x) = |x|$ *is differentiable almost everywhere with derivative(*$\phi(x) = \frac{d\Phi(x)}{dx}$*)* $\phi(x) = 1$ *for* $x > 0$ *and* $\phi(x) = -1$ *for* $x < 0$. *Although it is a convex function, Lemma 5.2.3 is not applicable here since it is not differentiable at* $x = 0$. *It is easy to show that* $\Phi(x) = |x|$ *is a qualified potential trench function candidate by invoking Lemma 5.2.2 and we can calculate its generalized gradient at* $x = 0$ *as* $\partial\Phi(0) = [-1, 1]$ *which contains the origin* $x = 0$.

Example 5.2.2 *In [29], the authors used the potential trench function largely taking the form* $\Phi(x) = \alpha(\sqrt{x^2 + a^2} - a)$, *where* α *is a positive scaling factor and a is a nonnegative constant. The special case of* $a = 0$ *is already addressed in Example 5.2.1. Without loss of generality, we assume that* $\alpha = 1$ *and* $a > 0$, *then the potential trench function is* $\Phi(x) = \sqrt{x^2 + a^2} - a$. *Its derivative can be calculate as* $\phi(x) = x/\sqrt{x^2 + a^2}$. *Since the derivative is monotonically increasing,* $\Phi(x) = \sqrt{x^2 + a^2} - a$ *is a convex function. Furthermore, we can obtain the second derivative as* $\phi'(x) = a^2/\sqrt{x^2 + a^2}$ *which is positive. This fact shows that* $\Phi(x) = \sqrt{x^2 + a^2} - a$ *is strictly convex. It is easy to verify that this potential trench function is positive definite. According to Lemma 5.2.3, it is a*

qualified potential trench function. Whereas Lemma 5.2.2 is also applicable as the first derivative $\phi(x) = x/\sqrt{x^2+a^2}$ *is bounded on the domain.*

Example 5.2.3 *Here we show simple examples of potential trench function candidate that are Lipschitz continuous but not convex. First we construct a function on domain* $(-\infty, +\infty)$ *as*

$$F_1(x) = \begin{cases} -x+1 & x \leq -1 \\ 2x^2 & -1 < x < 1 \\ x+1 & x \geq 1 \end{cases},$$

of which the derivative can be calculated as

$$f_1(x) = \begin{cases} -1 & x < -1 \\ 4x & -1 < x < 1 \\ 1 & x > 1 \end{cases}.$$

Obviously, function F_1 *is Lipschitz continuous and its derivative is bounded although the derivative is discontinuous at point* $x = 1$ *and* $x = -1$*. By Lemma 5.2.2,* F_1 *is a qualified potential trench function. But* F_1 *is not convex. Second, we can construct a smooth function that is continuously differentiable and Lipschitzian. Define a function* F_2 *on domain* $(-\infty, +\infty)$ *as*

$$F_2(x) = \begin{cases} 4\sqrt{-x}-3 & x \leq -1 \\ x^2 & -1 < x < 1 \\ 4\sqrt{x}-3 & x \geq 1 \end{cases},$$

of which the derivative can be calculated as

$$f_2(x) = \begin{cases} -\frac{2}{\sqrt{-x}} & x \leq -1 \\ 2x & -1 < x < 1 \\ \frac{2}{\sqrt{x}} & x \geq 1 \end{cases}.$$

It is easy to show that F_2 is a qualified potential trench function by Lemma 5.2.2. However it is not convex thus Lemma 5.2.3 is not applicable in this case. The figures of all the functions discussed in this example are illustrated in Figure 5.1.

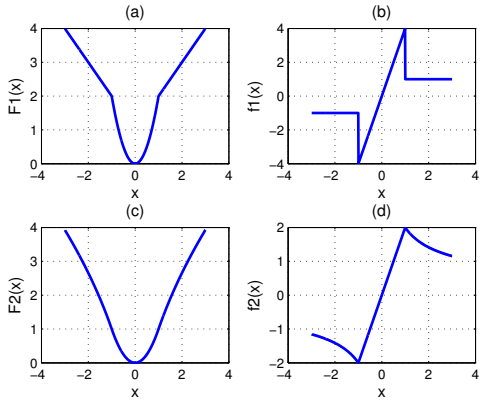

Figure 5.1: Figures of function $F_1(x)$, $f_1(x)$, $F_2(x)$ and $f_2(x)$.

In fact, there are other approaches to construct admissible potential trench functions. One convenient method is to leverage from available results on Lienard's Equation. The relevant notions and more examples of potential trench functions can be found in Appendix A.9.

5.3 A Generic Tracking Control

Now with the definition of potential trench function and associated results, we can move on to the generic tracking control problem of mobile robots in connection with artificial potential trench scheme. To this end, we propose a stable tracking control law as presented in the following theorem.

Theorem 5.3.1 *For twice-differentiable $\vec{r}_{i,g}$ and admissible potential trench function*

$\Phi(d_{i,g})$ together with $K_i(d_{i,g})$ of which $\partial K_i(d_{i,g})$ is positive for any nonzero $d_{i,g}$, a robot r_i is globally asymptotically stable on its goal point on the segment under the control

$$\vec{u}_i = \ddot{\vec{r}}_{i,g} + K'_{i,g}\dot{\vec{d}}_{i,g} + \Phi'_{i,g}\hat{d}_{i,g}, \tag{5.2}$$

where $\dot{\vec{d}}_{i,g}$ is the derivative of displacement vector $\vec{d}_{i,g} = \vec{r}_{i,g} - \vec{r}_i$ with respect to time, $\Phi'_{i,g} = d\big(\Phi(d_{i,g})\big)/d(d_{i,g})$, $K'_{i,g} = d\big(K(d_{i,g})\big)/d(d_{i,g})$ and $\hat{d}_{i,g} = \vec{d}_{i,g}/d_{i,g}$ is a unit vector.

Proof: See Appendix A.10. □

Remark 5.3.1 *Theorem 5.3.1 extends Proposition 5.2.1 to relax the constraints on the damping term $K'(d_{i,g})$. According to Theorem 5.3.1, $K'(d_{i,g})$ does not need to be smooth thus greatly facilitates the controller design. It should be noted that the options of $K'(d_{i,g})$ and $\Phi'_{i,g}$ can be independent without violating stability. It means that both $K'(d_{i,g})$ and $\Phi'_{i,g}$ are allowed to be discontinuous and can be designed independently on their own accord. With this observation and for the sake of focusing on the specific research problems to be addressed in the upcoming context, the nonsmooth potentials on $\Phi_{i,g}$ rather than the damping term will be emphasized.*

5.4 Stability Analysis of Multi-Robot Formation Control

The foregoing analysis concerning a single robot can be extended to multiple robots approaching a segment without considering the interaction between individual robots.

Consider the same control strategy as Equation (5.1) for each robot in the chain provided that each robot has its unique goal point on the segment. It is easy to assign goal points to the chain. For instance, once the leader has been assigned a known goal point, for any of the others the goal point of robot r_i can be set as a point at a fixed distance behind the current position of robot r_{i-1}.

Theorem 5.4.1 *Under the control given by Equation (5.1), a chain of N robots is asymptotically stable with respect to the given segment.*

Proof: See Appendix A.11. □

Considering the following special case of Proposition 5.3.1: static segment formation (i.e., when $\dot{\vec{r}}_{i,g} = 0$ and $\ddot{\vec{r}}_{i,g} = 0$). Readily we will arrive at the following conclusions:

A robot r_i can be globally asymptotically stabilized at a given fixed goal point on a segment by the potential trench-augmented control

$$\vec{u}_i = -k_i \dot{\vec{r}}_i + \Phi'_{i,g} \hat{d}_{i,g}, \tag{5.3}$$

where k_i is a positive scalar, $\Phi'_{i,g} = d(\Phi(d_{i,g}))/d(d_{i,g})$, and unit vector $\hat{d}_{i,g} = \vec{d}_{i,g}/d_{i,g}$.

5.5 Comparison with Alternative Potential Field Methods

A great variety of potential field methods have been developed in the past decades for mobile robots motion planning or navigation. The purposes of these methods normally

are to guide a robot to approach an assigned goal point or a moving target in a dynamic environment. Let q and q_{goal} denote the locations of a robot and its goal point respectively, then the most commonly used attractive potential function can be represented by the following form [6][50]:

$$U_{att}(q) = \frac{1}{2}\xi\rho^m(q, q_{goal}), \tag{5.4}$$

where ξ is a positive scalar, $\rho(q, q_{goal})$ is the distance between a robot q and goal q_{goal}, and m is constant usually to be either 1 or 2. For instance, if $m = 1$, the potential described by Equation (5.4) turns out to conic in shape and the corresponding attractive force will be a constant. On the other hand, if $m = 2$, the attractive potential takes the parabolic shape and its attractive force will be proportional to $\rho(q, q_{goal})$ as F_{att} is ruled by the following formula:

$$F_{att} = -\nabla U_{att}(q) = -\xi\rho(q, q_{goal}).$$

Conventional potential functions are designed to be smooth and thus they are differentiable every where in their domains. However, the artificial potential trench function defined in this chapter allows nonsmooth functions and thus provides more flexibilities and design freedom. Obviously the potential in Equation (5.4) is suitable attractive a robot to a static goal point. However, for a moving target in dynamic environments, such a potential is far from satisfying as it does not taking the velocity of the target into

account. Position error with respect to target is usually considered. For our case, we synthesize the artificial potential trench into a controller design given by Equation (5.1) and position error with respect to target is eradiated.

To overcome the drawbacks of conventional potentials in tracking moving targets, a new potential field function is proposed in [27]. The conventional potential field given by Equation (5.4) is based on only pure position information and therefore it is not suitable for dynamic environments. Modifications have been made on Equation (5.4) in [27] by taking into velocity information into account. Therefore a new potential field is constructed as follows [27]:

$$U_{att}(q,v) = \alpha_p ||q_{targ}(t) - q(t)||^m + \alpha_v ||v_{targ}(t) - v(t)||^n, \tag{5.5}$$

where $q(t)$, $q_targ(t)$ denote the positions of the robot and its target at time t, respectively; $v(t)$ and $v_{targ}(t)$ denote the velocities of the robot and the target at time t, respectively; $||q_{targ}(t) - q(t)||$ is the Euclidean distance between the robot and its target at time t; $||v_{targ}(t) - v(t)||$ is the magnitude of the relative velocity between the target and the robot at time t; α_p, α_p are scalar positive parameters; m, n are positive constants.

Obviously, Equation (5.5) combines the velocity information and position information into a new potential field function. With the introduction of the velocity term $||v_{targ}(t) - v(t)||$, a robot under this potential can approach a moving target. This is quite different from our method. First, only smooth functions are considered in Equation (5.5) while

artificial potential trench adopts nonsmooth potentials. Second, the velocity information is directly combined with the overall potential field function and inevitably it aggravates the complexity of control design and performance analysis. In our case, no explicit velocity information is applied in constructing the artificial potential trench function. Instead, we only synthesize velocity information into the controller design in Equation (5.1). Our method successfully separated the velocity based potentials and position based potentials. Therefore, it is entitled to more flexibilities. Third, even velocity potential is constructed in Equation (5.5), tracking position error may result if $\dot{v}_{targ} \neq 0$. However, no such concerns in our method as the acceleration of target has been taken into account in Equation (5.1) and therefore tracking position error in dynamic environment is eradicated.

5.6 Simulation

In this section, we use the double integrator dynamic model of the differential robot as described previously. For the sake of simplicity, all the constants in the model were set to unity. All the simulations were done using MATLAB.

The simulation was implemented to verify the effectiveness of Proposition 5.3.1 and Theorem 5.4.1. A team of fifteen robots (indexed from 1 to 15) are supposed to track moving goal points on a sinusoid curve on a $2D$ plane. The team goal is a moving object with motion equation $x = 42 + t$ and $y = sin(0.5(42 + t))$ ($t \geq 0$). Robot r_1 will track this team goal while the others will track their own goal points. The robot r_i is to

track goal point $q_{i,g}$ with motion equations $x = 45 - i + t$ and $y = sin(0.5(45 - i + t))$, where $2 \leq i \leq 15$. Obviously all the goal points are evenly distributed along x axis with constant separation between two adjunct points being 3. Initially all robots are randomly scattered within neighborhood of their own goal points and to avoid the unstable moving backward of reference point, all robots are initially placed behind the corresponding goal points. The position error along x axis for robot r_i is defined as $\Delta_{ix} = r_{ix} - q_{i,gx}$, where r_{ix} and $q_{i,gx}$ are the x coordinates of robot r_i and goal point $q_{i,g}$ respectively. In a similar way, the position error along y axis is defined. Together with initial velocities, the initial position errors are shown in Table 5.1.

Two kinds of potentials have been applied in this simulation. In the first case, we use potential $\Phi_1(x) = 10(\sqrt{x^2+1} - 1)$ and in the second case, $\Phi_2(x)$ set to be $3.535x^2 + 7.07|x|$ for $|x| \geq 1$ and $3.535x^2$ for $|x| < 1$. Consequently we have derivatives of Φ_1 and Φ_1 as: $\Phi_1'(x) = 10x/\sqrt{x^2+1}$ and $\Phi_2'(x) = sgn(x)\min\{7.07, 7.07|x|\}$ (for all x except $x = \pm 1$). Therefore at specific points $x = \pm 1$, we have $\partial\Phi_1(1) = 7.07 \in \partial\Phi_2(1)$ and $\Phi_1(-1) = -7.07 \in \partial\Phi_2(-1)$.

Initial positions of robots and goal points are depicted in Figure 5.2. Snapshots of positions of each robot and the corresponding goal points are shown in Figures 5.3-5.6 for the first case with potential Φ_1 and Figures 5.9-5.12 for the second case with Φ_2. The trajectories of robot r_1 and the last robot r_{15} are highlighted in Figures 5.7-5.8 for the first case and Figures 5.13-5.14 for the second case. To compare the convergence behavior of position error ($\Delta = \sqrt{\Delta_x^2 + \Delta_y^2}$) in the presence of two different potentials, we especially choose the case of robot r_5 and highlight them in Figure 5.15. It can be

concluded from these simulation results that both Φ_1 and Φ_2 can stabilize the whole team when tracking moving goal points.

Table 5.1: Initial Position Errors and Velocities along x- and y- axis

robot	position error Δ_{x0}	position error Δ_{y0}	velocity V_{x0}	velocity V_{y0}
r_1	-1.9003	0.3772	0.0153	0.4055
r_2	-0.4623	-1.7419	0.7468	0.0931
r_3	-1.2137	-1.6676	0.4451	-0.1102
r_4	-0.9720	0.3589	0.9318	0.3891
r_5	-1.7826	-1.5746	0.4660	0.2426
r_6	-1.5242	1.7684	0.4186	0.5896
r_7	-0.9129	0.5885	0.8462	0.9137
r_8	-0.0370	-1.2527	0.5252	0.0452
r_9	-1.6428	1.9606	0.2026	0.7603
r_{10}	-0.8894	1.4444	0.6721	-0.6541
r_{11}	-1.2309	1.1889	0.8381	0.9595
r_{12}	-1.5839	1.2051	0.0196	-0.4571
r_{13}	-1.8436	-0.4152	0.6813	-0.4953
r_{14}	-1.4764	0.9112	0.3795	0.7515
r_{15}	-0.3525	1.2047	0.8318	0.4746

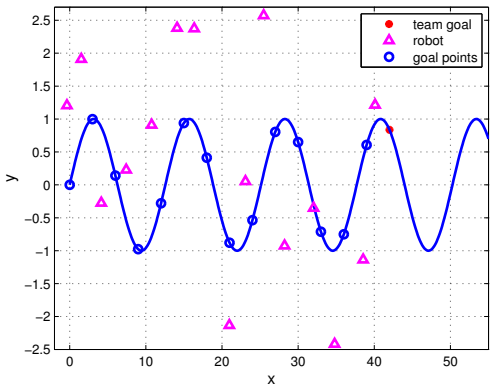

Figure 5.2: Snapshot of trajectories of robots and their goal points at $t = 0$ (i.e. initial conditions).

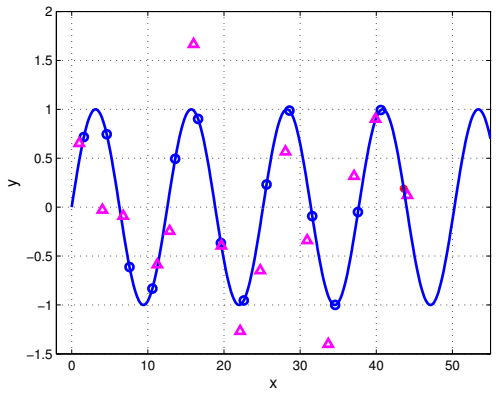

Figure 5.3: Snapshot of trajectories of robots and their goal points at $t = 1.6s$ under potential Φ_1.

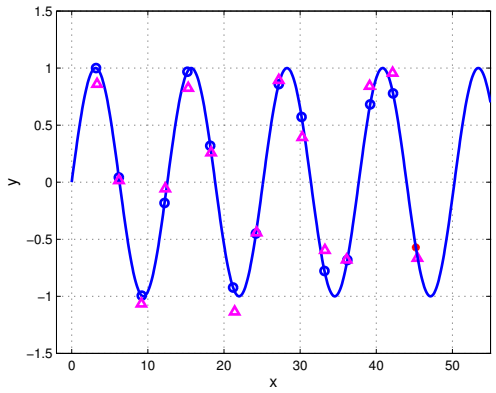

Figure 5.4: Snapshot of trajectories of robots and their goal points at $t = 3.2s$ under potential Φ_1.

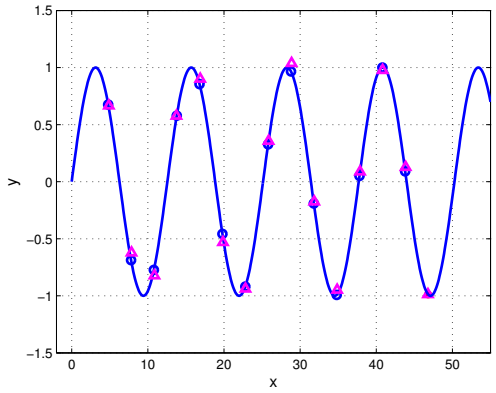

Figure 5.5: Snapshot of trajectories of robots and their goal points at $t = 4.8s$ under potential Φ_1.

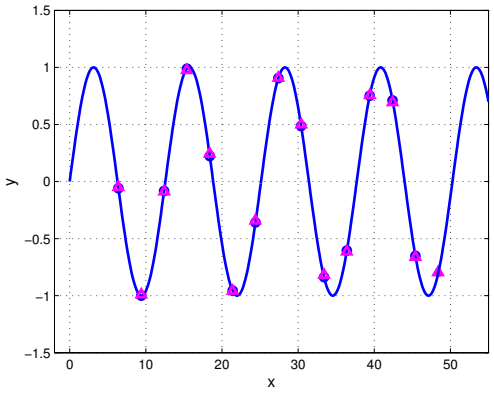

Figure 5.6: Snapshot of trajectories of robots and their goal points at $t = 6.4s$ under potential Φ_1.

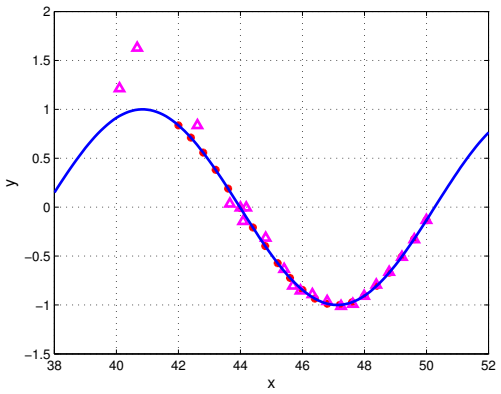

Figure 5.7: Trajectories of robot r_1 ($0 \leq t \leq 8s$) under potential Φ_1.

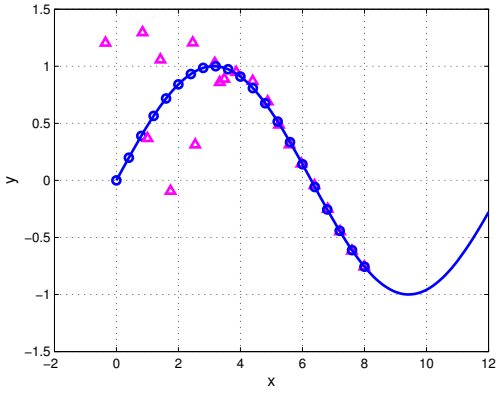

Figure 5.8: Trajectories of robot r_{15} ($0 \leq t \leq 8s$) under potential Φ_1.

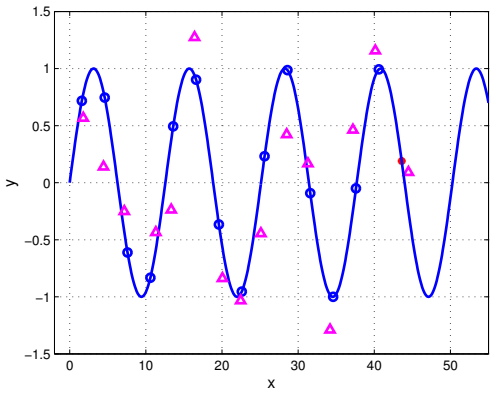

Figure 5.9: Snapshot of trajectories of robots and their goal points at $t = 1.6s$ under potential Φ_2.

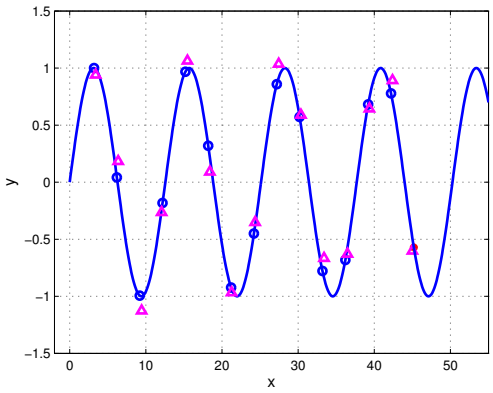

Figure 5.10: Snapshot of trajectories of robots and their goal points at $t = 3.2s$ under potential Φ_2.

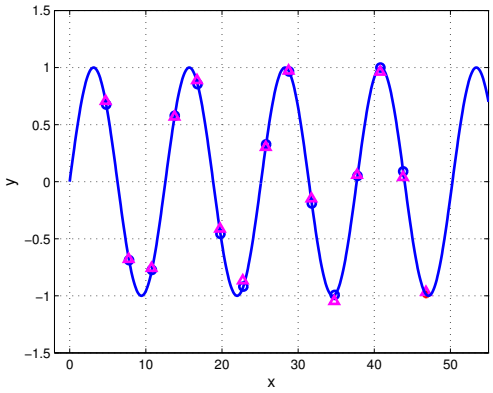

Figure 5.11: Snapshot of trajectories of robots and their goal points at $t = 4.8s$ under potential Φ_2.

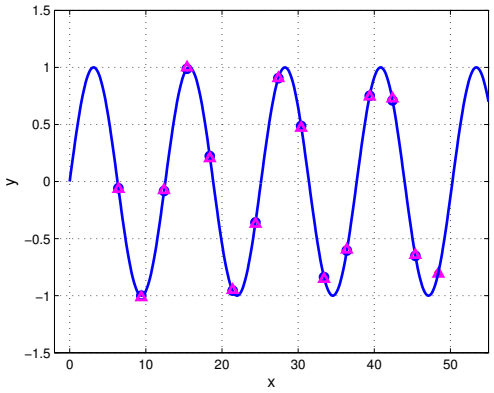

Figure 5.12: Snapshot of trajectories of robots and their goal points at $t = 6.4s$ under potential Φ_2.

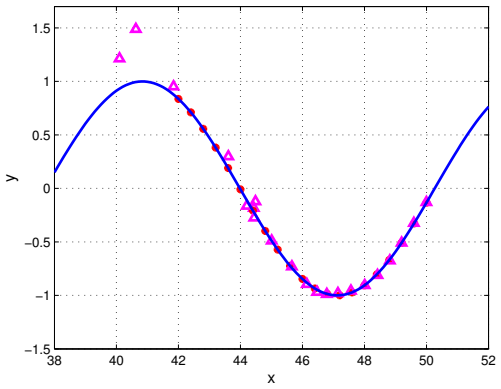

Figure 5.13: Trajectories of robot r_1 ($0 \leq t \leq 8s$) under potential Φ_2.

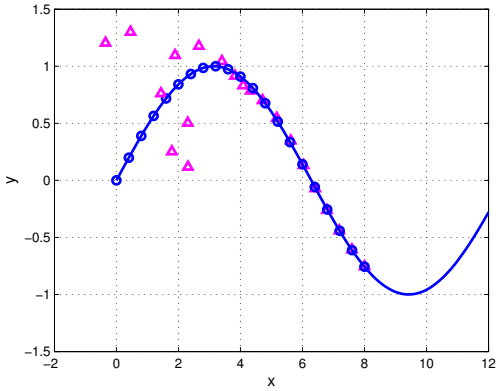

Figure 5.14: Trajectories of robot r_{15} ($0 \leq t \leq 8s$) under potential Φ_2.

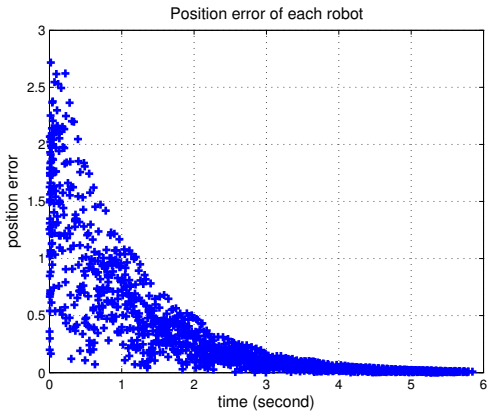

Figure 5.15: Comparison of position errors of robot r_5 under two different potentials.

5.7 Conclusions

In this chapter, we investigate nonlinear tracking control when dealing with the stability of controlling a mobile robot in connection with the method of artificial potential trench. Various ways to construct potential trench functions have been proposed. The response is revealed using available results on Lienard's Equation. Based on these results, we synthesize a control law that stabilizes a team of robots on a given formation without considering specific requirement on the distance between any two robots and verify its effectiveness through simulation.

Chapter 6

Zoning Scheme

6.1 Motivations

In Chapter 5, a simple scenario for multi-robot formation control with artificial potential trenches is addressed without considering robot to robot separations. However in practical applications, separations among robots is one of the key factors in formation control. Referring to Figure 1.1(b), each robot can communicate with the rest within the group via wireless signals and therefore a wireless communication network for the group is set up to accomplish certain tasks in a cooperative and coordinated way. Important information such as each robot's own location within the map or the obstacles detected during formation including location and obstacles' shapes should be shared among the group as each robot has limited capabilities of sensing nearby surroundings. To prevent possible breakdown of radio linkage among robots because they are separated too far away, the separations among robots need to be managed within reasonable range. Specifically, if a group of mobile robots are organized in leader-follower pairs, separation between

the leader and its follower must be controlled under an upper limit to prevent losing communication linkage.

On the other hand, for the sake of collision avoidance among robots, the separation between any follower and leader has to be greater than a lower limit to prevent collisions. Moreover, even those robots which are not in leader-follower pairing the separation between any robot and the others, which may not be its direct follower or leader, also has to be under control. Hence, separations among any two robots must be sufficient to ensure that each robot can move in a collision-free path. To meet the requirements on separation management, a *zoning potential* will be proposed. The basic idea of zoning potential is that an attractive potential will be invoked once the separation is greater than certain threshold trying to reduce the separation and a repulsive potential will be applied once the separation is less than a threshold and will push the robot away from dangerous areas to prevent collisions.

Although it is popular to assign goal points to usher robots as it is in [55, 17, 22], such pre-determined goal points may not be necessary. To get rid of these goal points, a convenient way is to attract the robots towards the assigned segment in certain direction. Consequently, a similar artificial potential trench as illustrated in Figure 3.5 is also formed. In this way, the robot only needs to calculate how far it is away from the segment in this direction and then can generate a valley-shaped trench to get the robot stabilized on the segment. The benefits of removing goal points are obtained at the sacrifice of introducing a direction to attract the robots towards segment. The effects of the assigned direction of attraction on robots also have to be addressed.

Therefore this chapter focuses on separation management and removing pre-determined goal points as well. A framework involving synthesizing artificial potential trench and zoning potentials into formation controller design and the associated stability analysis is to be developed.

6.2 Statements of Zoning Potentials

We consider the following scenario concerning the notion of forming a formation. Initially, a group of robots are assumed to be randomly scattered in an area, each within a pre-defined distance from at least one other robot. We assume that a formation which the robots are to take up is known, and that a mechanism for assigning a robot to a particular segment exists. (Discussion on these two issues can be found in [29].) The set of robots that are assigned the same segment is referred to as a *team*. A robot is said to conform to a segment if it is located with certain tolerance on the segment. The individual teams in the group is then required to approach and conform to their respective segments, thus producing the overall formation.

We investigate the process of a team approaching and then conforming to a given segment. This process can be divided into two phases: organization and coordination. During organization, the robots in a team are organized into leader-follower pairs. During coordination, the robots in leader-follower pairs approach and conform to their assigned segment while keeping within certain distance to each other.

6.2.1 Organization

In the sequel, it is assumed that initially any robot in a team is within the communication coverage of at least one other robot. A team is assigned a team goal, which can be a target to be tracked or a formation vertex. The robot located nearest to the team goal will be regarded as the *team leader* and indexed as r_1. The robot closest to r_1 will become the follower (indexed as r_2) of r_1. If there are more than one such candidate, then the robot (among all the candidates) nearest to the segment in terms of perpendicular distance will become the follower of r_1. If neither of these criteria results in a unique follower assignment, then a follower can be chosen by r_1 randomly or by some arbitration protocol executed by the candidates. The above procedure is applied in assigning a follower to r_2, and so repeated until the leader-follower pairs are identified and the robots in the team are indexed from r_1 to r_n. We note that the team leader r_1 itself is also a follower to the team goal. A team in which such leader-follower pairing for all robots has been established is referred to as a *chain*.

Remark 6.2.1 *In the adverse cases where team-wide communication link is not available, a chain may still be set up through some recovery mechanism. The simplest solution may be to have the robot that has lost communication reporting to the human operator for instructions. Another possible solution may be to have the robot, with its collision avoidance mechanism activated, approach the segment and move along it at maximum speed towards the team goal until it is able to establish communication with another robot in order to join the chain.*

6.2.2 Coordination

The objective in coordination is to control the chain to move towards and then conform to its segment, with the requirement that the distance between a leader and its follower be no greater than some limit $\bar{\rho}$ and no smaller than some clearance $\underline{\rho}$. To meet this requirement, the immediate area surrounding a robot is divided into five zones, as illustrated in Figure 6.1. For a follower located at the center of the concentric circles, the radius $\bar{\rho}$ represents the maximum allowable separation between itself and its leader. This limit can be used to define the coverage area of the wireless communication system installed on both robots. The radius $\underline{\rho}$ represents the minimum allowable separation between the two robots. This can be used to represent the safe distance set in a collision avoidance algorithm for both robots.

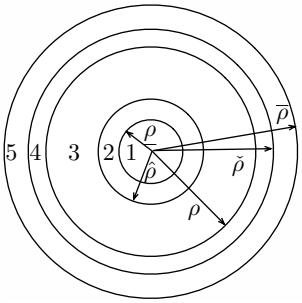

Figure 6.1: Zones of interaction of a robot located at the center of the concentric circles.

The rings labelled as 2 and 4 are essential zones for coordination. If a follower detects its leader to be in zone 4, then the follower must reduce the separation between itself and the leader. On the other hand, if a robot r_i detects another robot to be in its zone 2, then r_i must attempt to increase the separation between itself and that other robot. It is desirable that the speed at which the robot maneuvers such changes in separation is

inversely proportional to the distance between the other robot and the outer perimeter (for attraction) and the inner perimeter (for repulsion) of the respective zones. Thus, in actual implementation, limiting the maximum separation to some $\check{\rho} \leq \bar{\rho}$ reduces the risk of breaking the leader-follower contact because the maximal speed is expected to come into effect before the separation reach $\check{\rho}$. Similarly, limiting the minimum separation to some $\hat{\rho} \geq \underline{\rho}$ reduces the risk of collision. The leader-follower pairing is maintained wherever the leader is found to be in zone 3 of the follower. Zone 1 (i.e., the disk) is the region around a robot that other robots are prohibited to enter so as to avoid collision. We refer to zone 3 as the *neutral zone*. A chain in which the distance between a leader and its follower is no greater than $\bar{\rho}$ and no smaller than $\underline{\rho}$ is referred to as a *coordinated chain*.

This zoning scheme allows flexibility in implementation of formation control to deal with various situations. For instance, zone 5 represents a margin on the permissible separation between a leader and its follower. This margin provide a buffer zone in which a follower can may be useful in reducing the probability of losing the communication link between the leader and its follower due to the occurrence of unexpected events. Similarly, and the size of zones 2 and 3 can be suitably set to accommodate different densities of robot population in the segment. This requirement on separation has practical implications, specifically in collision avoidance among the robots and in maintaining a wireless communication network within the multi-robot system.

6.3 Direction of Attraction

As implied in the original approach of forming a formation based on the notion of artificial potential trench [29], each robot is assigned *a priori* a goal point (which could be simply defined as the nearest point on the segment with respect to the position of the robot). Such pre-fixing of the goal points restricts the motion of the robots when approaching the segment. We relax this restriction by introducing the concept of direction of approach, which enables the robots to approach and stabilize on the segment (while forming a formation) without the need to pre-define relevant goal points.

We consider the situation that, for a given robot, a direction has been specified for a potential trench to attract the robot to approach a segment. We refer to this direction as the *direction of attraction*, and denote its unit vector by $\vec{y}_a$. To form a (local) Cartesian coordinates system, the other direction (with its unit vector denoted by $\vec{x}_a$) is defined the usual way. Given the current position of a robot, if the line starting from this initial position and following $\vec{y}_a$ intersects the segment, we refer to the intersection point as the (instantaneous) point of attraction on the segment. This is illustrated in Figure 6.2.

For a segment with a finite length, it is possible that, given a direction of attraction, an instantaneous point of attraction may not exist when the robot is at a certain position. This is the case for robot 2 as illustrated in Figure 6.2. We say that a direction of attraction is *proper* if it meets the condition that an instantaneous point of attraction exists for the entire motion trajectory of the robot during its approach to the segment. This condition can be expressed in terms of a requirement on the projected length of

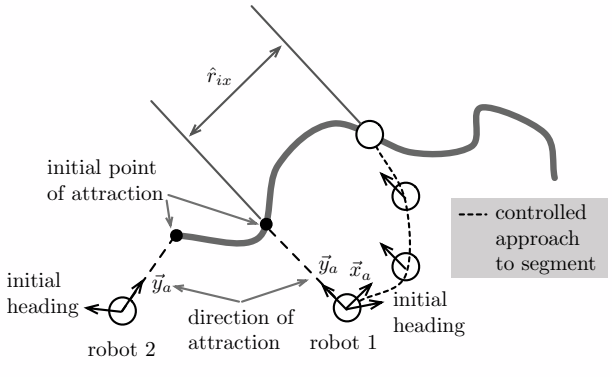

Figure 6.2: Direction of attraction and controlled approach.

the segment on the x_a-axis. Suppose that the robot has an initial speed v_0 and an initial heading at an angle of θ with respect to $\vec{x}_a$ at the time $t = 0$. If we apply the feedback control $\vec{u}_{ix} = -k_i\dot{\vec{r}}_{ix}$ (where k_i is a constant gain) to damp out the motion of the robot along the x_a-axis, then the dynamics of the robot along the x_a-axis can be expressed as $\ddot{\vec{r}}_{ix} + k_i\dot{\vec{r}}_{ix} = 0$, with the initial condition that $\dot{\vec{r}}_{ix}|_{t=t_0} = v_0(\cos\theta)\vec{x}_a$; that is, $\dot{r}_{ix} = v_0(\cos\theta)e^{-k_i t}$. The maximum distance that a robot may travel along the x_a-axis, denoted by $\hat{r}_{ix}$, is $\hat{r}_{ix} = \int_0^\infty \dot{r}_{ix}dt = v_0\cos\theta/k_i$, which depends on the chosen direction of attraction. To ensure that an instantaneous point of attraction exists whenever $\dot{r}_{ix} \neq 0$, it suffices to ensure that the projected length of the segment in the direction of $\dot{\vec{r}}_{ix}$ is greater than or equal to $\hat{r}_{ix}$.

6.4 A Coordinated Chain Stabilizing on a Segment

To control a team (in approaching and stabilizing on a given segment) as a coordinated chain, we augment the control as stated in Equation (5.1) with another potential function solely for the purpose of keeping two robots within a range of each other. The idea is

that, as a chain approaches the segment, a robot in the chain should normally stay within the neutral zone of its follower. Action must be taken by the follower to enforce this zoning requirement if the leader happens to enter either zone 2 or zone 4 of the follower.

A *zoning potential* is introduced specifically for this purpose. This potential is realized by a function Ψ, which takes on either of two forms, depending on the location of a robot in the zoning scheme of another. A repulsive potential $\hat{\Psi}$ comes into effect when a robot finds its leader in its zone 2, while an attractive potential $\check{\Psi}$ is in effect when a robot finds its leader in its zone 4. Specifically, we can choose

$$\check{\Psi}(d_{i,i-1}) = \begin{cases} \beta/(2\delta_a^m) & \text{if } \rho < d_{i,i-1} < \check{\rho}, \\ c_1/2 & \text{if } \underline{\rho} < d_{i,i-1} \leq \rho, \\ 0 & \text{elsewhere,} \end{cases}$$

$$\hat{\Psi}(d_{i,i-1}) = \begin{cases} \alpha/(2\delta_r^m) & \text{if } \underline{\rho} < d_{i,i-1} < \hat{\rho}, \\ c_2/2 & \text{if } \hat{\rho} \leq d_{i,i-1} < \check{\rho}, \\ 0 & \text{elsewhere,} \end{cases}$$

where $\delta_a = \check{\rho} - d_{i,i-1}$, $\delta_r = d_{i,i-1} - \underline{\rho}$, m (a constant) is either 1 or 2, $c_1 = \beta/(\check{\rho} - \rho)^m$, and $c_2 = \alpha/(\hat{\rho} - \underline{\rho})^m$. Therefore the function for the overall zoning potential, i.e., $\Psi(d_{i,i-1}) = \hat{\Psi}(d_{i,i-1}) + \check{\Psi}(d_{i,i-1})$, is absolutely continuous in the range $\underline{\rho} < d_{i,i-1} < \check{\rho}$. Moreover $\Psi(d_{i,i-1})$ is locally Lipschitz continuous and regular in the same range.

The repulsive potential specified above only ensures no collision between a robot and its leader. To avoid collision between any two robots r_i and r_j in a team (where $j \neq i-1$),

the repulsive potentials on r_i is invoked whenever any robot r_m (with $m < i$) enters zone 2 of r_i. Specifically, the potential

$$\Phi_{i,p}(d_{i,p}) + \Psi_{i,i-1}(d_{i,i-1}) + \sum_j \hat{\Psi}_{i,j}(d_{i,j})$$

is applied on robot r_i, where $j < i-1$. For the case of $j = i-1$, $\hat{\Psi}_{i,i-1}(d_{i,i-1})$ is already included in $\Psi_{i,i-1}(d_{i,i-1})$.

Thus, throughout the process of approaching a segment as a coordinated chain, each robot is subject to the influence of the potential trench function, and possibly additional zoning potentials (attractive or repulsive) depending on the location of a robot with respect to all other robots before it, in terms of the order of the leader-follower pairing.

Since these potentials are superimposed on each robot, a robot may experience the situation where the influence of these potentials exactly cancels out each other, resulting in the robot being trapped in zone 2 or zone 4 of another robot and unable to move towards the neural zone. We refer to a point in the motion trajectory of a robot where such cancellation occurs as a *local minimum*.

We next clarify some notations before presenting the synthesis of a control that enables a team to approach a segment as a coordinated chain. Rewrite the vectors $\vec{r}_i$ and $\vec{u}_i$ in the inertial coordinates frame as follows: $\vec{r}_i = r_{ix}\vec{j} + r_{iy}\vec{k}$, and $\vec{u}_i = u_{ix}\vec{j} + u_{iy}\vec{k}$, where $\vec{j}$ and $\vec{k}$ are the unit vector along *OX* and *OY* directions (as indicated in Figure 6.3) respectively. From the robot dynamics model (described in Chapter 3) we have $\ddot{r}_{ix} = u_{ix}$ and $\ddot{r}_{iy} = u_{iy}$. Similarly, we can rewrite the vectors $\vec{r}_{i,i-1}$ and $\vec{r}_{i,p}$ as: $\vec{r}_{i,i-1} = r_{(i-1)x}\vec{j} + r_{(i-1)y}\vec{k}$ and

$\vec{r}_{i,p} = r_{px}\vec{j} + r_{py}\vec{k}$, and so representing the vectors $\vec{d}_{i,i-1}$ and $\vec{d}_{i,p}$ as: $\vec{d}_{i,i-1} = \vec{r}_{i-1} - \vec{r}_i = (r_{(i-1)x} - r_{ix})\vec{j} + (r_{(i-1)y} - r_{iy})\vec{k}$ and $\vec{d}_{i,p} = \vec{r}_{i,p} - \vec{r}_i = (r_{px} - r_{ix})\vec{j} + (r_{py} - r_{iy})\vec{k}$, respectively, with $d_{i,i-1} \equiv \|\vec{d}_{i,i-1}\| = \left((r_{(i-1)x} - r_{ix})^2 + (r_{(i-1)y} - r_{iy})^2\right)^{\frac{1}{2}}$ and $d_{i,p} \equiv \|\vec{d}_{i,p}\| = \left((r_{px} - r_{ix})^2 + (r_{py} - r_{iy})^2\right)^{\frac{1}{2}}$. The direction of attraction is along $\vec{d}_{i,p}$ and $\vec{d}_{i-1,p}$ for robot r_i and r_{i-1} respectively. Figure 6.3 illustrates the relevant vectors and angles discussed above.

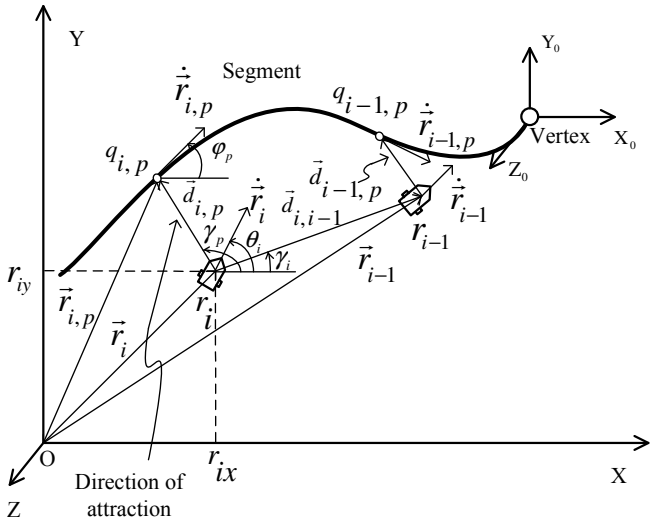

Figure 6.3: Illustration of relevant angles and vectors.

Given admissible Φ and Ψ, along with the conditions that the chain leader r_1 reaches $\dot{\vec{r}}_{1,g} = 0$ after a finite time T_1^*, and that the ratio $\lambda_i = \|\dot{\vec{r}}_{i,p}\|/\|\dot{\vec{r}}_i\| = (\dot{r}_{px}^2 + \dot{r}_{py}^2)^{\frac{1}{2}}/(\dot{r}_{ix}^2 + \dot{r}_{iy}^2)^{\frac{1}{2}}$ (where $\|\dot{\vec{r}}_i\| \neq 0$) is bounded, we have the following theorem.

Theorem 6.4.1 *Consider the following control*

$$\vec{u}_i = \zeta\vec{j} + \xi\vec{k}, \tag{6.1}$$

with

$$\begin{aligned}\zeta &= -k_i\dot{r}_{ix} + \Phi'_{i,p}\cos\gamma_p + \Psi'_{i,i-1}\cos\gamma_i + \delta_1 + \hat{\sigma}_c,\\ \xi &= -k_i\dot{r}_{iy} + \Phi'_{i,p}\sin\gamma_p + \Psi'_{i,i-1}\sin\gamma_i + \delta_2 + \hat{\sigma}_s,\end{aligned}$$

where $[\cdot]'_{(\cdot)} = d\left([\cdot](d_{(\cdot)})\right)/d(d_{(\cdot)})$, γ_p, γ_i *and* $\gamma_{i,j}$ *are the orientations of vectors* $\vec{d}_{i,p}$, $\vec{d}_{i,i-1}$ *and* $\vec{d}_{i,j}$ *respectively,* $\hat{\sigma}_c = \sum_j \hat{\Psi}'_{i,j}\cos\gamma_{i,j}$, $\hat{\sigma}_s = \sum_j \hat{\Psi}'_{i,j}\sin\gamma_{i,j}$, *and* $1 \le j \le i-2$. *The terms* δ_1 *and* δ_2 *are defined as follows:* $\delta_1 = \Phi'_{i,p}\lambda_i\cos\phi$ *if* $\|\dot{\vec{r}}_i\| \neq 0$, *and* $\delta_1 = 0$, *if* $\|\dot{\vec{r}}_i\| = 0$; $\delta_2 = \Phi'_{i,p}\lambda_i\sin\phi$ *if* $\|\dot{\vec{r}}_i\| \neq 0$ *and* $\delta_2 = 0$ *if* $\|\dot{\vec{r}}_i\| = 0$, *with* $\phi = \theta_i - (\gamma_p - \varphi_p) - \pi$, *and* θ_i *and* φ_p *being the orientations of vectors* $\dot{\vec{r}}_i$ *and* $\dot{\vec{r}}_{i,p}$ *respectively.*

In the absence of local minima in the trajectories of the robots, a coordinated chain can be stabilized within arbitrary small deviation from the segment by applying Equation (5.1) on the chain leader and Equation (6.1) on all other robots in the chain.

Proof: See Appendix A.12. □

Remark 6.4.1 *With reference to Equation (6.1), at a local minimum we have*

$$\Phi'_{i,p}(\cos\gamma_p + \lambda_i\cos\phi) + \Psi'_{i,i-1}\cos\gamma_i + \textstyle\sum_j \hat{\Psi}'_{i,j}\cos\gamma_{i,j} = 0$$

and

$$\Phi'_{i,p}(\sin\gamma_p + \lambda_i\sin\phi) + \Psi'_{i,i-1}\sin\gamma_i + \textstyle\sum_j \hat{\Psi}'_{i,j}\sin\gamma_{i,j} = 0.$$

One way to recover from such a situation is to immediately (but temporarily) disable the potential trench (by setting $\Phi'_{i,p} = 0$*) and reactivate it once the robot has escaped from the local minimum.*

We note that the introduction of either the attractive zone (i.e., zone 4) or the repulsive zone (zone 2) does not alter the equilibrium points of the dynamics of robot. In essence, robots in these two zones will experience a force (in addition to the potential trench) whose magnitude decreases rapidly with increasing inward separation from the outer edge of zone 4 or outward separation from the perimeter of zone 1. If initially a follower is in zone 2, 3, or 4 of its leader, it will stabilize on the segment within zone 3 (i.e., the neutral zone) of its leader by the control given in Equation (6.1). In actual implementation, it is practical to require that, for the cases of $\check{\rho} \leq d_{i,i-1} \leq \overline{\rho}$ and $0 < d_{i,i-1} \leq \underline{\rho}$, the follower is to approach to, or separate from, its leader at full acceleration.

6.5 Simulation

A computer simulation (using MATLAB) has been conducted to demonstrate the effectiveness of the proposed formation and zoning control of a coordinated chain. A group of ten robots, indexed from 1 to 10, were initially randomly placed on a plane with non-zero velocity. The robots were organized in leader-follower pairs. Only the goal point, fixed at $(70, 70)$, of the first robot was specified. Table 6.1 shows the initial (randomly selected) positions and velocities of each robot, while Table 7.1 lists the radii of the zoning scheme. The segment consists of a straight line connecting $(-5, -5)$ and $(100, 100)$. For those robots below the segment such as r_2 and r_3, the direction of attraction was set at 135° with respect to the X-axis, while for those robots above the segment such as r_1 and r_4, the direction of attraction was set at -45°. Consequently, we have either $\lambda_i = \|\dot{\vec{r}}_{i,p}\|/\|\dot{\vec{r}}_i\| = |\cos(\theta_i - \pi/4)|$ or $\lambda_i = \|\dot{\vec{r}}_{i,p}\|/\|\dot{\vec{r}}_i\| = |\cos(\theta_i + \pi/4)|$, which is bounded.

The repulsive zoning potential $\hat{\Psi}(d_{i,i-1})$ was set to be $5/(d_{i,i-1}-1)^2$ for $1 < d_{i,i-1} < 4$, $5/9$ for $4 \leq d_{i,i-1} < 13$, and 0 elsewhere, while the attractive zoning potential $\check{\Psi}(d_{i,i-1})$ was set to be $5/(13-d_{i,i-1})^2$ for $10 < d_{i,i-1} < 13$, $5/9$ for $1 < d_{i,i-1} \leq 10$, and 0 elsewhere. The potential trench function was set as $\Phi(d_{i,p}) = 10\left(d_{i,p}^2+1\right)^{\frac{1}{2}} - 10$. Figure 7.16 shows the segment and the initial positions of the ten robots.

Table 6.1: Initial positions and velocities of robots

robot	initial position	velocity V_{x0}	velocity V_{y0}
r_1	(26.0026, 29.7094)	0.0153	0.0056
r_2	(27.8260, 19.8633)	0.7468	0.4189
r_3	(25.4281, 16.7758)	0.4451	-0.1422
r_4	(14.8357, 21.3381)	0.9318	-0.3908
r_5	(14.2419, 15.1141)	0.4660	-0.6207
r_6	(13.7641, 8.8730)	0.4186	-0.6131
r_7	(12.3089, 4.2053)	0.8462	0.3644
r_8	(9.7197, 1.0574)	0.5252	-0.3945
r_9	(1.5191, 3.0657)	0.2026	0.0833
r_{10}	(0.7206, -1.0582)	0.6721	-0.6983

Table 6.2: Radii of zoning scheme.

$\underline{\rho}$	$\hat{\rho}$	ρ	$\check{\rho}$	$\bar{\rho}$
1	4	10	13	30

Figure 6.5 illustrates the closed-loop system of an individual robot. The simulation was run at a sampling rate of $T_s = 0.01$ second for a period of 300 seconds. For robots r_2 to r_{10}, the positions of their leaders were sampled every 0.01 second. The trajectories of all robots were recorded every 0.01 second.

Figure 7.18 shows the positions of the ten robots at the end of simulations, while Figure 7.19 shows the distance between a robot and its leader. It can be seen from these

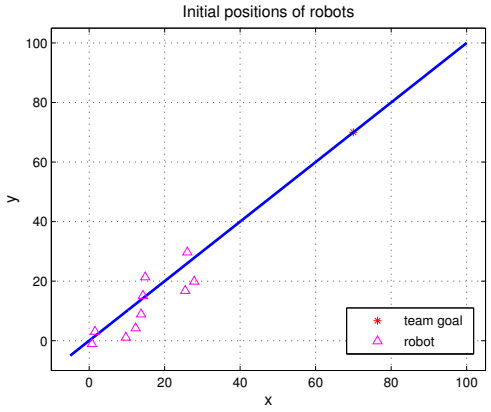

Figure 6.4: The segment, goal point and initial positions of 10 robots.

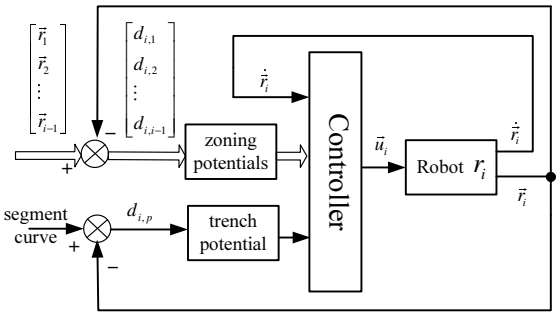

Figure 6.5: Structure of MATLAB simulation.

two figures that, although initially a robot may fall in zone 2 or 4 of its leader, it was eventually steered by the zoning potential and the potential trench to enter and reside in the neutral zone, leading to the final result that the robots approached and stabilized on the segment as a coordinated chain with the team leader r_1 asymptotically reaching the specified goal point.

To demonstrate the flexibilities of the zoning scheme, we modified the zoning parameters to be as shown in Table 6.3. Consequently, $\hat{\Psi}(d_{i,i-1})$ was modified to be $5/(d_{i,i-1}-1.5)^2$ for $1.5 < d_{i,i-1} < 4.5$, $5/9$ for $4.5 \leq d_{i,i-1} < 12$, and 0 elsewhere, and $\check{\Psi}(d_{i,i-1})$ was set to be $5/(12-d_{i,i-1})^2$ for $9 < d_{i,i-1} < 12$, $5/9$ for $1.5 < d_{i,i-1} \leq 9$, and 0 else-

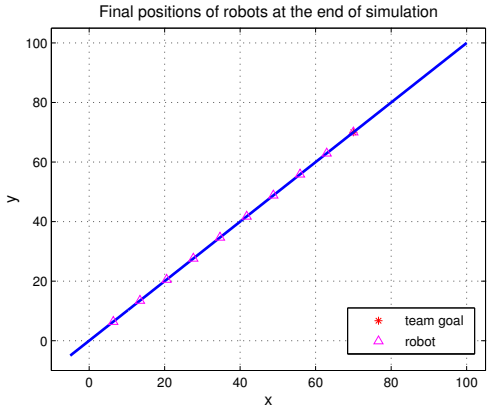

Figure 6.6: Positions of robots at the end of simulation ($t = 300$ seconds).

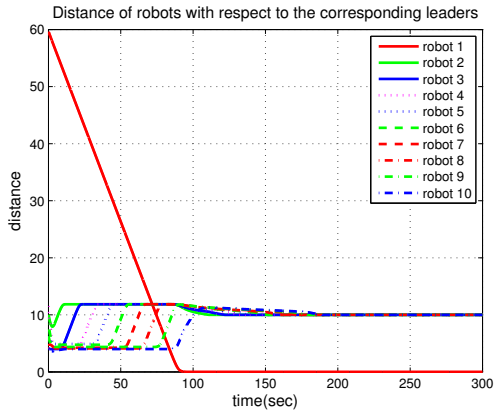

Figure 6.7: Distance between each robot and its leader.

where. All other conditions remained the same. Figure 7.20 shows the positions of the ten robots at the end of simulations, while Figure 7.22 shows the distance between a robot and its leader. The same convergent behavior of the ten robots is observed in this case.

Table 6.3: Modified radius of zoning scheme.

$\underline{\rho}$	$\hat{\rho}$	ρ	$\check{\rho}$	$\bar{\rho}$
1.5	4.5	9	12	30

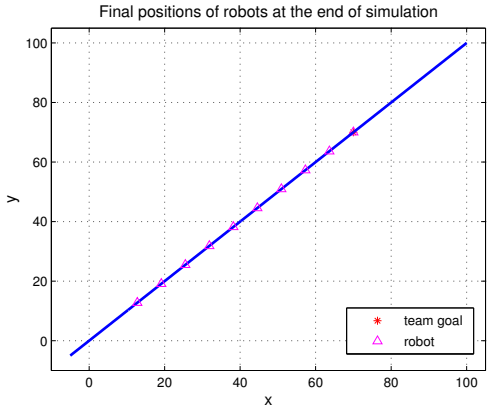

Figure 6.8: Positions of robots at the end of simulation ($t = 300$ seconds) with modified zoning parameter values.

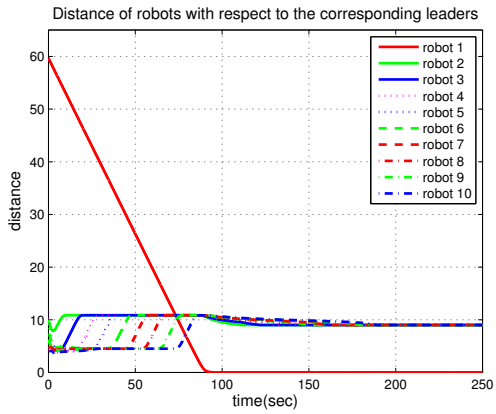

Figure 6.9: Distance between each robot and its leader for the case of modified zoning parameter values.

6.6 Conclusions

The analysis reported in this chapter provides a novel framework in which the stability of multi-robot formation based on the notion of artificial potential trench can be analyzed. By introducing a zoning scheme and the associated zoning potentials it is ensured in theory that a robot can maintain a certain separation from its direct leader and follower without collisions with others in the team while forming a formation. This

requirement on separation has significant practical implications, specifically in collision avoidance among the robots and in maintaining a wireless communication network within the group.

The concept of direction of attraction proposed in this chapter make it possible for a robot to approach the segment without a pre-assigned goal point. Another significance of this new idea is that a team of robots can approach the segment in a coordinated manner without the help of other methods such as virtual structure or virtual leaders. Directions of attraction for each robot can be varied if necessary to enhance the flexibilities or for the purpose of overcoming possible local minima. While the notion of artificial potential trench provides scalability in multi-robot formation, the synthesized controls, which is based on a complete nonsmooth analysis in this chapter guarantee that such scalable formations are stable even under the constraint of coordination. Simulation in a workspace without obstacles shows the effectiveness and flexibilities of the new controls.

Chapter 7

Attracting Robots to Nearest Points on Segments and A Novel Obstacle Avoidance Scheme

7.1 Introduction

To remove pre-determined goal points, a new method based on the concept of direction of attraction is proposed at Chapter 6. Actually, another intuitive and straightforward idea is to drive any robot towards the nearest point on the segment. Letting the robot itself autonomously find the nearest point on the segment, and then be attracted to follow the shortest path from the instantaneous position of robot to the assigned segment by artificial potential trench is the core of this idea. To this end, similar to the situations depicted in Figures 3.5 and 3.6, an artificial potential trench that also features the shape of a ”valley” with its bottom being the segment curve is presented in Figure 3.7. Obviously in this figure, the artificial potential trench attracts the robot towards the nearest

point on the segment and therefore there is no goal point at all in this scenario.

The commonly used ”leader-follower” concept is also adopted in this chapter during formation control. Figure 7.1 shows the coordinates system and relevant vectors for one of such scenarios with two robots r_i and r_{i-1}. Among them r_{i-1} is the leader and r_i is the follower. For each instantaneous position $\vec{r}_i$ and $\vec{r}_{i-1}$ of robot r_i and r_{i-1}, we suppose that there are uniquely known nearest points $q_{i,ns}$ and $q_{i-1,ns}$ respectively which are either stationary or in motion. Their positions are indicated by $\vec{r}_{i,ns}$ and $\vec{r}_{i-1,ns}$ on the segment for the robots to track. To distribute the robots along a segment and controlling $\vec{d}_{i,ns}$, $\vec{d}_{i-1,ns}$ and $\vec{d}_{i,i-1}$ will be the main goal of formation control, where $\vec{d}_{i,i-1}$ denotes the distance between r_{i-1} and r_i given by $\vec{d}_{i,i-1} = \vec{r}_{i-1} - \vec{r}_i$.

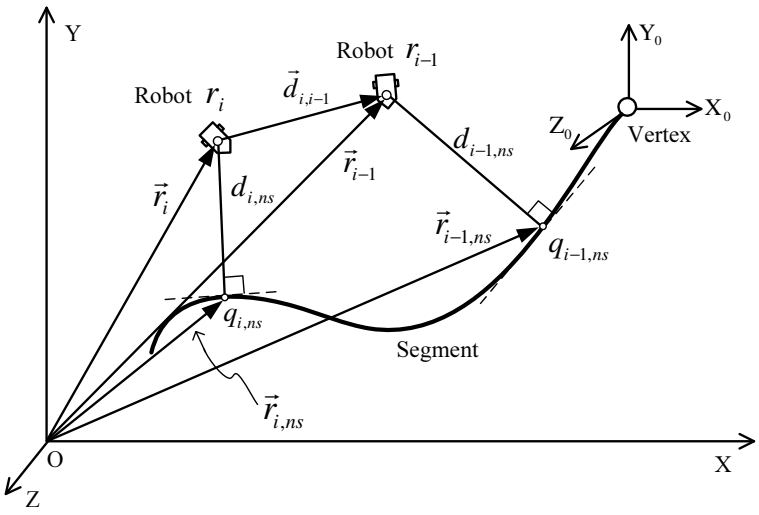

Figure 7.1: Coordinates system for a leader-follower pair r_{i-1} and r_i.

Consider a given segment S and a coordinated chain consisting of n robots, indexed from r_1 to r_n, with the following characteristics:

(i) The team leader is r_1.

(ii) All leader-follower pairings are known.

(iii) The team goal-point which may be stationary or moving is known and is assigned to be the goal point of r_1.

(iv) For robots r_i with $i = 1, \ldots, n$, the individual shape of each one is known.

(v) For each robot, the zoning radii are known.

(vi) For each obstacle, the boundary of its shape is known.

Determine a control that enables the coordinated chain to approach and attracts to the corresponding nearest points on a given segment.

7.2 Mathematical Framework

7.2.1 Shortest Distance from a Robot to the Segment

To attract a robot to the nearest point on a given segment is always of significant implications when utilizing artificial potentials. As pointed out by the original work [29], the nearest point on the segment to a robot is chosen to be the robot's goal point. The distance from a robot's instantaneous location, which is usually simplified as a single point as it is in this dissertation, to the corresponding nearest point on the segment stands for the shortest distance from robot to the segment.

In this sequel, we consider the segment and robot's trajectory defined in confined space. The segment is defined as a curve $y_s = f(x)$, where $x \in [a_s, b_s]$ while the robot's tra-

jectory is given as $y_t = g(x)$, where $x \in [a_t, b_t]$. And each segment has two vertices according to [29]. Usually $f = f(x)$ is smooth, and $g = g(x)$ is not necessarily smooth. It seems reasonable to assume that g is locally Lipschitz on the domain. As illustrated in Figure 7.2, for a point $\big(x, g(x)\big)$ on the robot's trajectory, there is a nearest point q_{ns} on the segment.

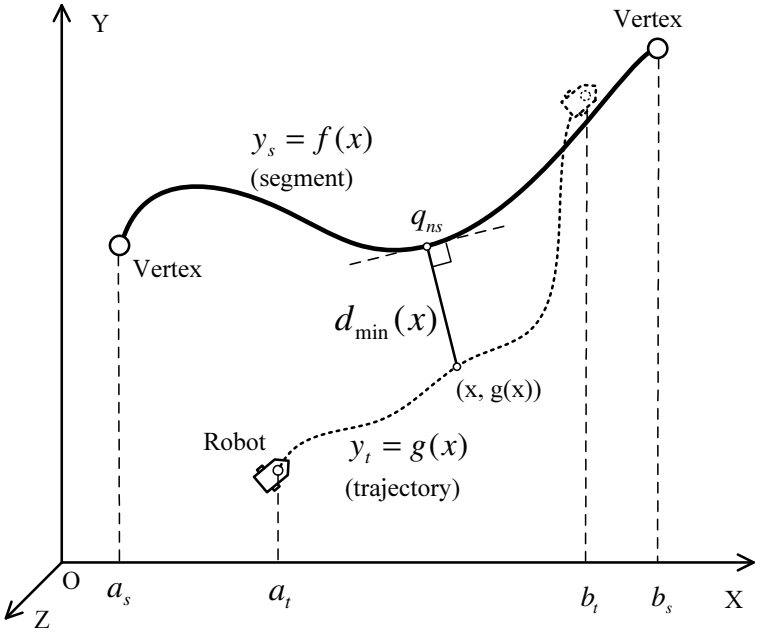

Figure 7.2: Illustration of the shortest distance of a point $(x, g(x))$ on robot's trajectory (i.e., the curve $y_t = g(x)$ depicted by dot line) to a given segment (i.e., the curve $y_s = f(x)$ depicted by solid line).

For the location $\big(x, g(x)\big)$ on trajectory, we can determine the nearest points on the segment by

$$d_{min}(x) = \min_{x_s \in [a_s, b_s]} \left\{ \sqrt{(x - x_s)^2 + \big(g(x) - f(x_s)\big)^2} \right\}. \tag{7.1}$$

As indicated by Equation (7.1), there may exist multiple nearest points although $d_{min}(x)$

is uniquely determined. Based on definition of $d_{min}(x)$, a set of all of those points denoted by q_{ns} which meets the following condition:

$$q_{ns} = \arg d_{min}(x) = \arg \min_{x_s \in [a_s, b_s]} \left\{ \sqrt{(x - x_s)^2 + \big(g(x) - f(x_s)\big)^2} \right\}, \tag{7.2}$$

is the nearest points on the segment to a given location $\big(x, g(x)\big)$ along the trajectory. The trivial case of a single nearest point is simple and easy for controller design. However, the multiplicity of nearest point greatly aggravates the mathematical complexity. To deal with multiple nearest points, the original work [29] "conceptually" proposed to choose the special one, which is nearest to the origin among all these points q_{ns}, to be the goal point for the robot to track without addressing the technical details. In the sequel, we will continue to explore other aspects, such as control law, stability related to this issue. Before discussing how to deal with multiple nearest points, it is necessary to derive some essential mathematical characteristics of the nearest points and the shortest distance $d_{min}(x)$.

Since $g(\cdot)$ is locally Lipschitz, we have

$$\frac{|g(x + \Delta x) - g(x)|}{|\Delta x|} \leq L,$$

or equivalently, $-L|\Delta x| \leq g(x + \Delta x) - g(x) \leq L|\Delta x|$, where L is a positive constant.

Letting $g(x+\Delta x) = g(x) + \Delta g(x)$, we have $-L|\Delta x| \leq \Delta g(x) \leq L|\Delta x|$. Thus,

$$\begin{aligned}\big(g(x+\Delta x) - f(x_s)\big)^2 &= \big(g(x) + \Delta g(x) - f(x_s)\big)^2 \\ &= \big(g(x) - f(x_s)\big)^2 + 2\Delta g(x)(g(x) - f(x_s)) + \big(\Delta g(x)\big)^2.\end{aligned}$$

7.2.2 Continuity of $d_{min}(\cdot)$

Proposition 7.2.1 *The function $d_{min}(\cdot)$ is continuous.* □

Proof: See Appendix A.13. □

7.2.3 Locally Lipschitz of $d_{min}(\cdot)$

In proceeding context, we already showed that $d_{min}(x)$ is continuous on the domain. It is natural to ask: Suppose that g is not smooth but locally Lipschitz, what conclusion can be drawn for the function d_{min}? Is it differentiable everywhere or just locally Lipschitz? The answers to these questions are provided by the following proposition.

Proposition 7.2.2 *$d_{min}(\cdot)$ is locally Lipschitz.* □

Proof: See Appendix A.14. □

Now, return to the questions posed at the beginning of this subsection. The foregoing analysis shows that d_{min} is indeed Lipshitz and may fail to be differentiable at certain points. In other words, d_{min} may not be continuously differentiable everywhere. Never-

theless, the fact that d_{min} is locally Lipchitz, as revealed by Proposition 7.2.2, is sufficient for a complete mathematical analysis.

Remark 7.2.1 *The trajectory of a robot depends on its locomotion mechanism and the control strategies applied on it. Sometimes, the trajectories are smooth and more often they are not. For example, nonsmooth trajectories for a differential mobile robot are usually expected. For real world mechanisms, the robot's velocity is bounded and so is its derivative with respect to time. To put it another way, the acceleration available to a robot is bounded. Therefore it does make sense to assume that g is locally Lipschitz rather than a smooth curve.*

7.2.4 Motion of the Nearest Points and Presence of Transit Points

In the previous section, it is pointed out that d_{min} is continuous and locally Lipschitz indicating d_{min} is likely to be continuously differentiable. Obviously, if Equation (7.2) always guarantees a uniquely determined point q_{ns}, the motion of nearest points is definitely continuous along the segment. In other words, the trajectory of near points is either the whole segment, or merely a portion of it which is continuous. However, the scenario may be quite different when uniqueness of q_{ns} is not asserted.

Due to the presence of multiple nearest points, motion of the nearest point may be discontinued along the segment. Here is an illustration for this phenomenon. Referring to Figure 7.3 for example, there are two possible trajectories I and II for a robot and both trajectories go through the same location, denoted by point P, where the following

relationship $||PN_1|| = ||PN_2||$ is met. It means that there are two nearest points (i.e., N_1 and N_2 respectively on the segment) dedicated to location P. For trajectory II, it is possible that motion of its nearest points is continuous near N_1 on the segment. But the situation is quite different for trajectory I because after P, the robot will be attracted by certain point near N_2 rather than N_1, thus for trajectory I, the motion of nearest points undergoes a "jump" from N_1 to N_2.

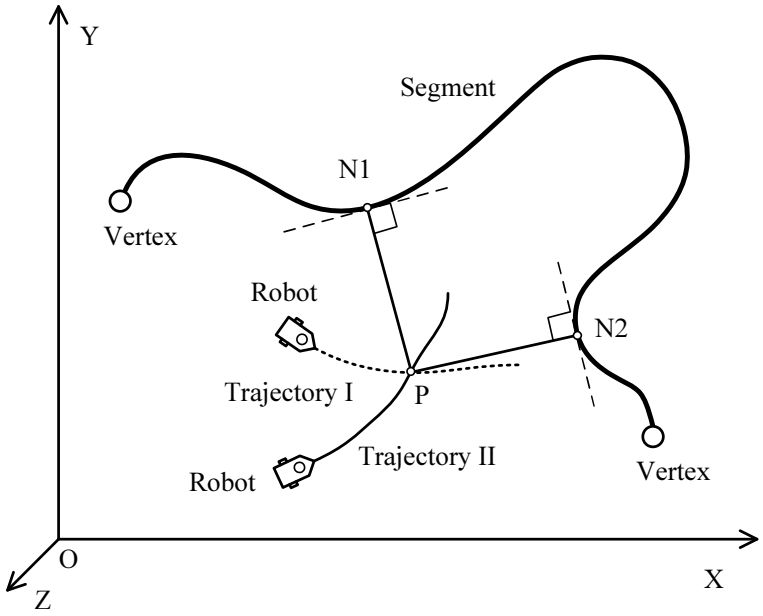

Figure 7.3: Illustration of transition of the nearest points on the segment (dot line for Trajectory I and solid line for Trajectory II).

We refer to nonadjacent points N_1 and N_2 as *transit points* as for certain location of a given trajectory at these points continuity of trajectory of nearest points is broken. Take the illustration presented in Figure 7.3 for example. The trajectory I at location P undergoes such a transition of nearest points. Furthermore a formal definition of transit point is summarized as follows:

Definition 7.2.1 *For a curve $y_s = f(x)$, where $x \in [a_s, b_s]$ and a point P on the robot's trajectory given by $y_t = g(x)$, where $x \in [a_t, b_t]$, two points N_1 and N_2 on the segment*

are referred as transit points if the following three constraints are met.

(i) The following equation holds at location P (with coordinates (x_p, y_p)) of the robot's trajectory:

$$\{N_1, N_2\} = \arg d_{min}(x)\big|_{x=x_p} = \arg \min_{x_s \in [a_s, b_s]} \left\{ \sqrt{(x_p - x_s)^2 + \big(y_p - f(x_s)\big)^2} \right\}.$$

(ii) There exist two open balls $B_1(N_1, r)$ and $B_2(N_2, r)$ centered at N_1 and N_2 respectively with radius r such that

$$B_1(N_1, r) \bigcap B_2(N_2, r) = \emptyset.$$

(iii) The trajectory of nearest point on the segment is discontinuous at N_1 or N_2. □

It is worthwhile to point out that as indicated in Figure 7.3, even Equation (7.1) has multiple solutions, the motion of nearest points may still be continuous such as the case for trajectory II. This observation implies that multiple nearest points may not necessarily be transit points. However transits points always indicate the existence of multiple nearest points. This fact is summarized in the following proposition.

Proposition 7.2.3 *Transit points only exist where q_{ns} is not unique.* □

Proof: See Appendix A.15. □

Proposition 7.2.3 can be useful when searching for transit points. A robot can check if there exist multiple nearest points and then determine if a transit is necessary. However this proposition fails to determine which multiple nearest points lead to transit point. Neither can this proposition tell under what conditions a set of multiple nearest point has

a ”transition”. Largely speaking, this question is related to the robot’s motion and even its decision on which nearest point to pursue when multiple nearest points available. For the robot illustrated in Figure 7.3, robot following trajectory II moves into the area formed by N_1PN_2 and there is no transition. On the other hand, trajectory I ushers the robot to undergo a transit of nearest points (from N_1 to N_2). Nevertheless, it should be noted that there is a special scenario where the trajectory cannot determine the transit of nearest points. Suppose that a robot passes by location P with exactly zero velocity, then whether the robot has to transit nearest point depends on nothing with its trajectory (obviously we do not know its trajectory after location P at this moment). The robot must make a decision and it is free to choose N_1 or N_2 to be its nearest point to which it will approach. Based on this observation, it is reasonable to make the following assumption.

Assumption 7.2.1 *The nearest point for a certain location of robot is uniquely determined by the robot even in the presence of multiple nearest points.*

In other words, the above assumption points out that the robot is entitled to choosing one of the multiple nearest point to approach for all the time. The issue of determining which nearest point to track will be addressed later on especially when a robot’s leader already stabilizes on the segment in association with zoning scheme. Mathematically transit points pronounce the discontinuity of the motion of nearest points whereas physically them give rise to ”sudden change” of attraction force which is pointed from location of a robot to its nearest point when artificial potentials are applied. Since normally potential functions are single-valued, ”sudden change” of attractive force is expressed in the sense

of abrupt change of its direction rather than its amplitude. As far as stability of control law is concerned, we need to evaluate the influence of such discontinuities and look into a formal framework of a complete analysis. This is the main interest of the following section.

7.3 Asymptotic Stability of Attracting a Robot to a Nearest Point on the Segment

In order to attract a robot to a nearest point on the segment by employing artificial potential trench method, we have to check the control law presented in previous chapter and make necessary modifications. Now we set the goal point to be a nearest point on the segment and apply the following control law for a robot r_i:

$$\vec{u}_i = \ddot{\vec{r}}_{i,ns} + k_i \dot{\vec{d}}_{i,ns} + \Phi'_{i,ns} \hat{d}_{i,ns}, \tag{7.3}$$

where $\hat{d}_{i,ns}$ is a unit vector pointing from robot's instantaneous location r_i to the nearest point $q_{i,ns}$ on segment. Note here we already made the assumption that the nearest point for a certain location of robot is uniquely determined by the robot despite of presences of multiple nearest points. Therefore the symbol $q_{i,ns}$ in Equation (7.3) is no longer a set of multiple possible nearest points but a uniquely determined point instead at any

time. Consequently $\hat{d}_{i,ns}$ is also unique. However, it is not the case for $\dot{\vec{d}}_{i,ns}$, which is time derivative.

As pointed out in proceeding sections, although $d_{i,ns}$ is continuous it may fail to be differentiable at some points. It is not surprise that we encounter nonsmooth issues again. The good news is that we already show that $d_{i,ns}$ is locally Lipschitz as long as the trajectory is locally Lipschitz. Thanks to Rademacher's Theorem (which is stated below), $d_{i,ns}$ is almost everywhere differentiable (everywhere except on a set of Lebegue measure 0)

Theorem 7.3.1 *(Rademacher's Theorem): A continuous map $f : I \longrightarrow R$, where I is an interval in R, is almost everywhere differentiable.*

In other words, owing to nonsmooth analysis, we can discard all of those points where $d_{i,ns}$ fails to be differentiable. This observation is key for a complete stability analysis of closed-loop system. Finally asymptoti stability of attracting a robot to a nearest point on the segment is equivalent to prove the stability problem which is described by the following differential equation:

$$\ddot{\vec{d}}_{i,ns} = -k_i \dot{\vec{d}}_{i,ns} - \Phi'_{i,ns} \hat{d}_{i,ns}.$$

If $\dot{\vec{d}}_{i,ns} = \dot{d}_{i,ns} = 0$ proves to be asymptotical stable at the origin, then it is clear that the robot will be stabilized on the segment. For the sake of completeness, the detailed procedures are shown below.

Theorem 7.3.2 *A robot r_i (whose goal point is specified by the twice-differentiable vector $\vec{r}_{i,ns}$ on a segment) is globally asymptotically stable with respect to $\vec{r}_{i,ns}$ under the control*

$$\vec{u}_i = \ddot{\vec{r}}_{i,ns} + k_i \dot{\vec{d}}_{i,ns} + \Phi'_{i,ns} \hat{d}_{i,ns}, \tag{7.4}$$

where $\Phi(d_{i,ns})$ is an admissible potential trench function, $\dot{\vec{d}}_{i,ns} = d(\vec{d}_{i,ns})/dt$, $\Phi'_{i,ns} = d(\Phi(d_{i,ns}))/d(d_{i,ns})$, $\hat{d}_{i,ns} = \vec{d}_{i,ns}/d_{i,ns}$, and k_i is a positive scalar.

Proof: See Appendix A.16. □

7.4 A Novel Obstacle Avoidance Method

In the real world, the presence of obstacles has to be taken into account for feasible robot motion control and multi-robot formation control. For a robot trying to approach a segment, a real obstacle or another robot in its way to the nearest points along the assigned segment can be regarded as an ”obstacle”. In other words, in this thesis meaning of the term ”obstacle” is inclusive of real obstacles or robots and therefore may vary from robot to robot and from time to time depending on relative separations from a specific robot to the others in a dynamic environment. Sometimes in order to avoid excessive complexity and facilitate analysis, the obstacles under consideration are assumed to be with convex shapes [27], like the ones used in analysis and simulations in previous chapter. In contrast to this restrictive assumption, non-convex shape obstacles are to be handled with a novel method in this chapter. Before proceeding, it makes sense

to assume that the shape of any obstacle is known or is at least able to be detected by robots' on-board sensors or instruments such as laser distance meter or supersonic sonar through team-wide coordination. In the upcoming context within this section, a more detailed discussion on this prerequisite will be addressed.

7.4.1 Obstacles and Convex Hull

We refer to the outer boundary of any obstacle with arbitrary shapes as Ω_{ob}, which can be regarded as a set of points forming a closed contour. Readily we can represent Ω_{ob} as

$$\Omega_{ob} = \{\big(x, \Omega_{ob}(x)\big) \mid \forall\, q_{ob} \in \Omega\}, \tag{7.5}$$

where q_{ob} can be any point on the obstacle and it is contained by Ω, the area encircled by obstacle's boundary. For the sake of expression simplicity and as far as collision avoidance requirement is concerned, it is sufficient and convenient to use Ω_{ob} to denote an obstacle. Generally speaking, Ω_{ob} may be a convex set such as obstacles with cylinder shape or a non-convex set like crescent-shape obstacles. Figure 7.4 shows a type of non-convex obstacle(in solid line) comprising of polygons. Crevices exist as the boundary is not convex. Moreover, there exist other types of non-convex shape obstacles. In contrast to Figure 7.4 where crevices are outside of obstacle, Figure 7.5 illustrates another example of obstacle(in solid line) with an internal cavity surrounded by the obstacle itself.

One of the dominating threats of non-convex shape obstacles to a robot controlled under

artificial potentials is that it may cause the robot stuck in crevices or cavities of the obstacles. Several solutions have been proposed to cope with such kind of local minima in preceding research work, such as the Instant Goal (IG) Method [28], Virtual Obstacle Method [57]. In this chapter, however, we are going to deal with this issue from a novel perspective. For any obstacle Ω_{ob}, we define the corresponding convex closure as

$$\Omega_{ob}^{'} = \overline{co}\{\Omega_{ob}\} = \overline{co}\{\big(x, \Omega_{ob}(x)\big) \mid \forall\, q_{ob} \in \Omega\}. \tag{7.6}$$

In this way, obstacles with non-convex shape can be transformed into "virtual obstacles" with convex boundaries. Figures 7.4 and 7.5 show two examples of non-convex shape obstacles Ω_{ob} and the corresponding convex hulls $\Omega_{ob}^{'}$. Specifically in Figure 7.4, convex hull of the obstacle turns out to be a convex polygon. Readily it flows that $\Omega_{ob}^{'} = \Omega_{ob}$ for convex shape obstacles and $\Omega_{ob}^{'} \subset \Omega_{ob}$ for non-convex shape counterparts. To distinguish the actual obstacles boundary Ω_{ob} from its convex hull $\Omega_{ob}^{'}$, we refer to the terms $\Omega_{ob}^{'}$ as "apparent obstacles" in this thesis.

Remark 7.4.1 *The aforementioned prerequisite on knowledge of obstacles' boundaries can be met when such information is available or able to be acquired. For instance the shape of a robot, which may be viewed as an obstacle by another one during formation, is usually known beforehand. Such information of obstacle sometimes may be able to be acquired through off-line surveillance or identification. However in real implementation especially for unconstructed environments, this prerequisite seems to be a little*

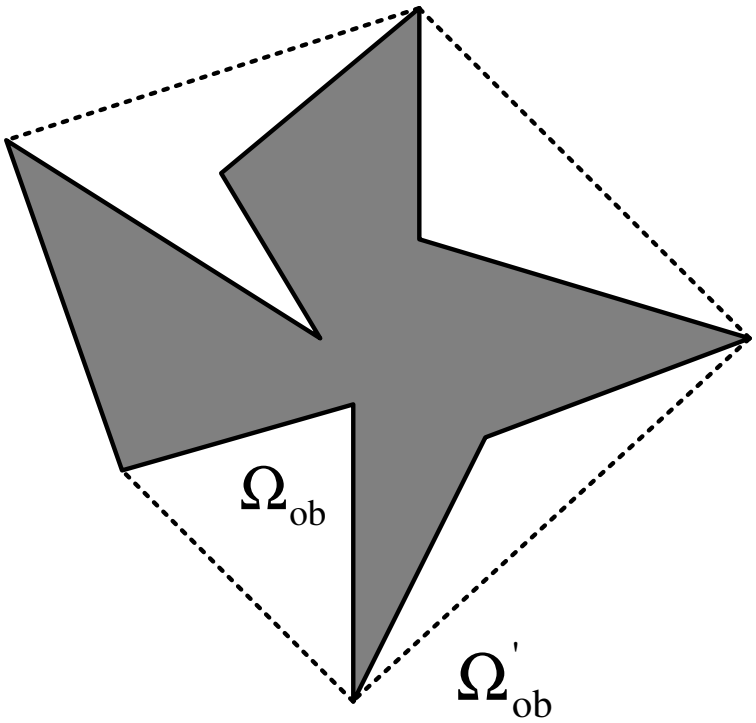

Figure 7.4: A non-convex obstacle Ω_{ob} and its convex hull Ω'_{ob}. Note here the obstacle is represented by shaded area while its boundary Ω_{ob} is in solid lines. The corresponding Ω'_{ob} is depicted in dot lines, of which a minor portion on the left side of this figure overlaps on the boundary.

bit restrictive. One example is illustrated in Figure 7.6, where two static concave obstacles, which are very close to each other, are in the robot's way to the segment. If all boundary information for each obstacle is available, a combined apparent obstacle can be calculated readily. However in this situation, not all boundary information are necessarily needed for collision avoidance. Sometimes, incomplete information of obstacle boundary under certain constraints may be sufficient for constructing or approximating the convex hull. For instance, if boundary information of all these portions of obstacles in Figure 7.6 below the curve P_1P_2 (depicted in a dot line) is known, it suffices for obstacle avoidance purpose. The question here would rather be when and how to make such a decision and under what conditions we can get approximately the same perfor-

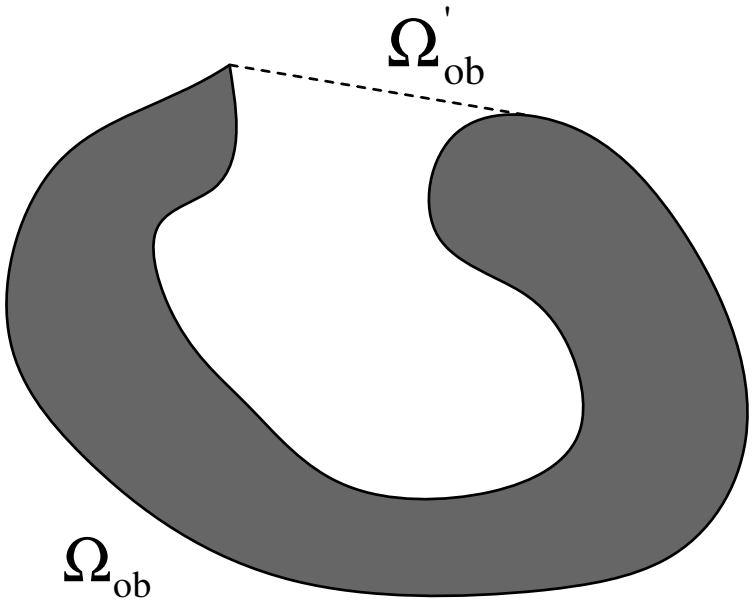

Figure 7.5: Another non-convex obstacle Ω_{ob} and its convex hull Ω'_{ob}. Note here the obstacle is represented by shaded area while its boundary Ω_{ob} is in solid lines. The corresponding Ω'_{ob} is depicted in dot lines, of which a major portion overlaps on the boundary.

mance based on only partial obstacles' boundary information. Meanwhile in practical implementations, each robot only has limited obstacle detection capability. Therefore an intelligent sensor network based on information flow of multiple robots team-work is critical to for apparent obstacle scheme. If no global information for each obstacle is ready or available, then a solution has to figure out. We leave this study to further work.

7.4.2 Combined Convex Hull

Furthermore, it is worthwhile to note that a robot may fall into "crevices" or "cavities" formed by multiple obstacles even though they may not physically contact with each other. For instance if two obstacles are located too close to form deep "crevices" or

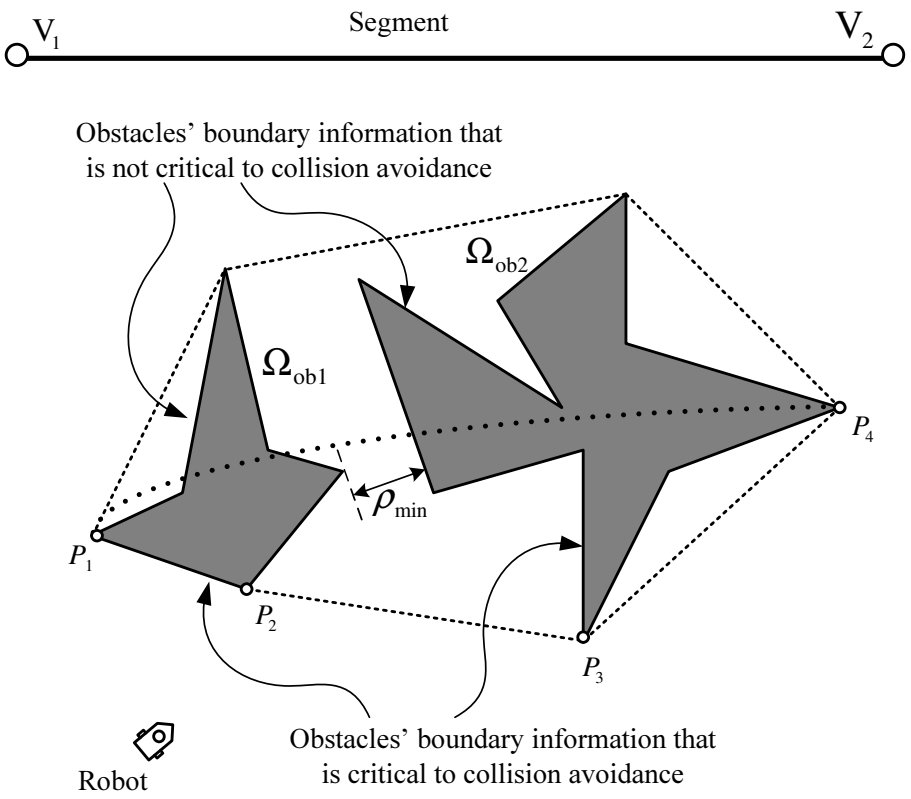

Figure 7.6: Partial obstacles' boundary information may be sufficient for collision avoidance.

"cavities" such that there is insufficient separation between them to allow a robot to pass through safely. Such a scenario is illustrated in Figure 7.7, where the minimum separation of two obstacles (Ω_{ob1} and Ω_{ob2}), represented by ρ_{min} is less than the required minimum clearance $\rho_{clearance}$ for a given robot. Although the obstacles Ω_{ob1} and Ω_{ob2} in Figure 7.7 are of non-convex shapes, it is worthwhile to point out that even two convex shape obstacles may also contribute to the same phenomena as illustrated in Figure 7.8 where both obstacles Ω_{ob1} and Ω_{ob2} are with convex shapes.

To avoid problematic local minima issues in such situations, the combined convex hull of multiple obstacles rather than individual ones are calculated as follows:

$$\Omega'_{combo} = \overline{co}\left\{\Omega_{ob1} \bigcup \Omega_{ob2} \bigcup \cdots \Omega_{obi} \bigcup \cdots \Omega_{obn}\right\}. \tag{7.7}$$

Note that for each of all these obstacles there exists at least one minimum separation such that

$$\rho_{min}^{i,j} < \rho_{clearance}, \tag{7.8}$$

where $i \neq j$. In other words, for any robot there must exist at least another one to which the separation is less than the required clearance $\rho_{clearance}$. Similarly, to distinguish the actual obstacles boundary from the corresponding combined convex hulls, we refer to terms $\Omega_{combo}^{'}$ as "apparent obstacles". By transforming a single non-convex obstacle or a specific group of obstacles into convex "apparent obstacles", all the obstacles seen by a robot are convex. Owing to this observation, the aforementioned obstacle-avoidance method is thereafter referred to as "apparent obstacle scheme" in this thesis.

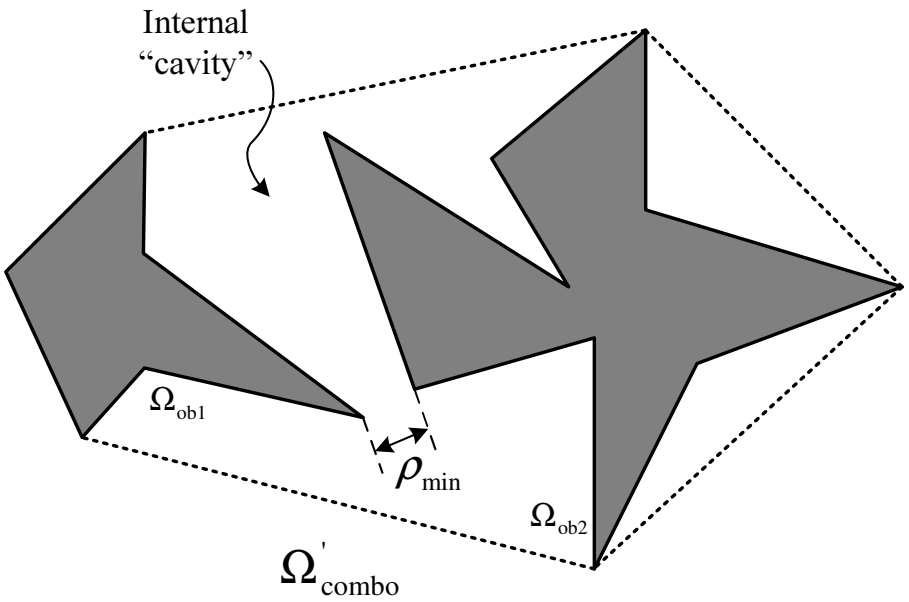

Figure 7.7: Illustration of a combined convex hull $\Omega_{combo}^{'}$ resulting from two obstacles Ω_{ob1} and Ω_{ob2} between which the separation is too narrow for a robot to pass through safely (here dot lines for $\Omega_{combo}^{'}$ and shaded area for obstacles Ω_{ob1} and Ω_{ob2} with solid lines for their boundaries). Note that there is a "cavity" between obstacles Ω_{ob1} and Ω_{ob2} threatening a nearby robot to fall into local minima.

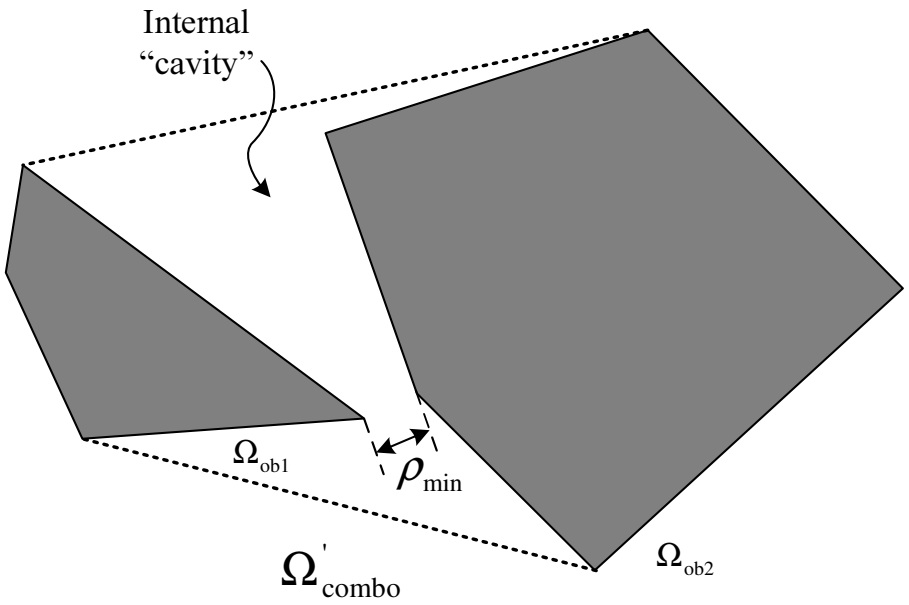

Figure 7.8: Convex obstacles Ω_{ob1} and Ω_{ob2} are located too close to form internal cavity. Again the separation is too narrow for a robot to pass through safely (here dot lines for Ω'_{combo} and shaded area for obstacles Ω_{ob1} and Ω_{ob2} with solid lines for their boundaries). Note that there is a ”cavity” between obstacles Ω_{ob1} and Ω_{ob2} threatening a nearby robot to fall into local minima.

7.4.3 Repulsive Forces with Apparent Obstacle Scheme

Apparent obstacle scheme is very useful and handy for obstacle avoidance purposes. Except the aforementioned advantage of preventing local minima at crevices or cavities, it can simplify the calculation of repulsive force. For robot r_i, the repulsive force generated by apparent obstacle is governed by the following formula:

$$\vec{F}_{i,rep} = -\left(\nabla_x \Phi_{ob}(x)|_{(d^{ob}_{i,ns})}\right) \hat{d}^{ob}_{i,ns}, \tag{7.9}$$

where $\Phi_{ob}(x)$ is a scalar function while $d^{ob}_{i,ns}$ and $\hat{d}^{ob}_{i,ns}$ denote the minimum distance from robot to its nearest point on the apparent obstacle and the unit vector pointing from instantaneous position of r_i to the nearest point $q^{ob}_{i,ns}$ respectively. The minus sign in Equation (7.9) indicates that the force $\vec{F}_{i,rep}$ is repulsive(trying to push the robot away).

Now the problem of finding the nearest point arises again. The good news is that there are no more multiple nearest points issues as revealed by the following proposition.

Proposition 7.4.1 *For any arbitrary apparent obstacle $\Omega_{ob}^{'}$(or $\Omega_{combo}^{'}$) and robot's location denoted by point P_0, if $P_0 \notin \Omega_{ob}^{'}$ (or $\Omega_{combo}^{'}$) and P_0 is not contained in the area Ω' encircled by $\Omega_{ob}^{'}$ (or $\Omega_{combo}^{'}$), then it flows that: (i) the nearest point on the apparent obstacle with respect to robot only dwells at its boundary; (ii) the nearest point is unique.* □

Proof: See Appendix A.17. □

Proposition 7.4.1 proves to be useful as it asserts that the nearest point on apparent obstacle with respect to a robot is unique and consequently it excludes the routine to deal with determining which nearest point to follow and moreover the calculation of repulsive force generated by obstacle avoidance algorithms is greatly simplified. Take the apparent obstacle illustrated in Figure 7.9 for example. Three repulsive force areas I, II and III (depicted in dashed lines) which are facing the robot are highlighted and the other repulsive force areas related to the rest of obstacle's boundary are omitted in this figure. The repulsive force area I and III are rectangle shape denoted by $P_1N_1N_2P_2$ and $P_2N_3N_4P_3$ respectively. The sector-shape repulsive area II $P_2N_2N_3$ exists because once a robot falls into this area, the nearest point on apparent obstacle with respect to robot is fixed at point P_2. Moreover, in area I, the repulsive force is always in the direction perpendicular to P_1P_2 and similarly the repulsive force in area III is perpendicular to P_2P_3. However, a robot in area II will experience a repulsive force pointing from point

P_2 to its instantaneous location. Hence in this case, the direction of repulsive force depends on robot's location and this is different from the cases with area I and III where the direction of corresponding repulsive force is fixed.

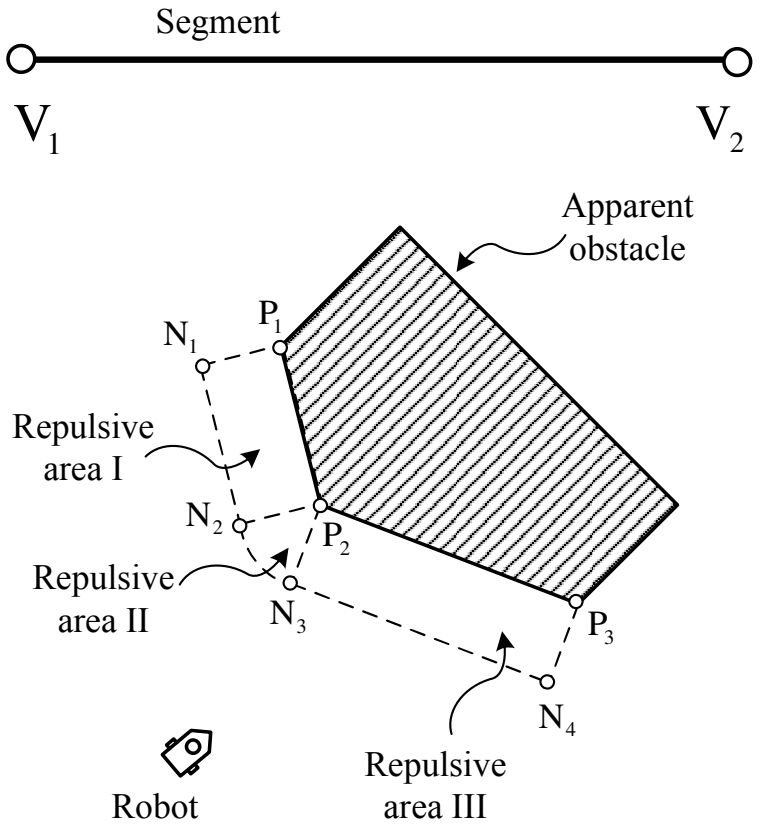

Figure 7.9: Different repulsive force areas related to an apparent obstacle. All the three repulsive force areas are depicted in dashed lines. Note that for illustration purpose, only those areas facing the robot with respect to partial of the boundary (i.e., P_1P_2 and P_2P_3) are highlighted.

7.5 Nearest Points in the Presence of Obstacles

7.5.1 Encroachment of Segment Due to Obstacles

When a single obstacle gets too close to a segment, we are forced to modify the algorithm described by Equation (7.2) when searching for nearest points or determining the

transit points because a portion of the segment may be occupied by the obstacle and therefore this portion cannot accommodate any robots. We refer to this phenomenon as ”encroachment” on segment.

Encroachment on segment is commonly encountered for multiple robot formation and there are several other typical scenarios. For the sake of collision avoidance, a separation threshold denoted by $\rho_{clearance}$ between an obstacle and a robot is usually predefined. When the obstacle-to-robot separation is less than $\rho_{clearance}$, a repulsive force generated by the obstacle will start to be applied on the robot. Based on $\rho_{clearance}$ each obstacle has a repulsive zone which may comprise of several repulsive areas as illustrated in Fig 7.9. Any robot within this repulsive zone will be pushed away by the corresponding repulsive force resulting in virtual ”areas of clearance” prohibiting entry of any robots around the obstacle. Consequently a single obstacle physically not touching any portion of the segment but with its clearance areas covering some part of the segment also leads to encroachment. Those portions of segment which are covered by an obstacle’s repulsive zone are ”encroached” and have to be abandoned by algorithms seeking for nearest points because a robot should not be ushered to these areas. While practically it is admitted that collision may not be inevitable due to possible cancellation between the repulsive force from obstacle and attractive force generated by nearest point, robots may be trapped in local minima in such cases and consequently may fail to reach the desired nearest point on the segment.

As mentioned earlier, a real robot may be regarded as an obstacle. Therefore the followers (robots) to this robot have to consider the encroachment on segment once the robot’s

repulsive zone covers certain part of the segment. The scenario gets more complicated when multiple obstacles, rather than an individual one, together with multiple robots are close to a segment resulting in encroachment. Especially when the obstacles are located within certain crowned area of the segment leading to small separation among each of them, the algorithms seeking for possible nearest points have to take more constraints into account. It is true that if multiple obstacles (including real robots) get too close to impede safely pass-through of robots as illustrated in Figure 7.7, they will be treated as a combined apparent obstacle regardless whether they are close to segment or far away from it. However beneath the above statement lies a simple fact that is worthwhile to point it out. For robot r_i, only its leader robots(i.e., r_1 through r_{i-1}) and all real obstacles are viewed as "obstacles". It means that as far as r_i is concerned, another robot r_j dwelling on the segment with its index $j > i$ has no encroachment on segment and will not be involved in calculating apparent obstacle or combined obstacle, not to mention reckoning on encroachment on segment due to its repulsive zone. This mechanism guarantees that a higher priority on determining nearest point on segment is always assigned to leaders and therefore leader robots will push way any followers in their way to the segment.

A simple illustration of encroachment on a segment is depicted in Figure 7.10, where the obstacles(hatched areas) are deliberately replaced with "apparent obstacle" Ω'_{ob} rather than Ω_{ob}. There are four points $E1$ through $E4$ which are the intersection points between the segment and clearance of the "apparent obstacle". Note that the original segment is encroached and some portions are unavailable for robots to dwell on. We denote the

fragments of segment, which are available to robots as $S_{V_1E_1}$, $S_{E_2E_3}$,$S_{E_4V_2}$ respectively. For each fragment, we can evaluate if there is sufficient room to accommodate at least one robot. Falling that the corresponding fragment should not be employed when seeking or determining the nearest point on obstacles. By ruling out all the fragments with insufficient room for at least one robot to reside, a set of qualified fragments will be screened. For robot r_i, we refer to such a set as "set of qualified fragments" and denote it as $S^{qa}_{fg,i}$. Obviously the set of qualified segments for each robot maybe different.

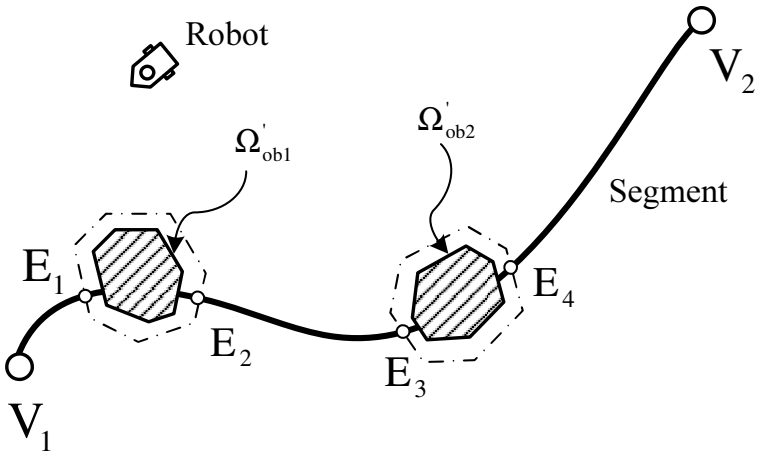

Figure 7.10: Encroachment on segment due to the presence of obstacles. Note that the hatched areas are for "apparent obstacle" Ω'_{ob1} and Ω'_{ob2} respectively while the dashed lines are for the corresponding safety clearance areas.

7.5.2 Seeking Algorithms for Nearest Points

Owing to encroachment incurred by obstacles, for each specific robot we have to identify which portion of the segment is unable to accommodate at least one robot and then calculate the set of qualified fragments. The algorithm seeking for nearest point on segment for a given robot, denoted by r_i, is summarized as follows:

(1) calculate apparent obstacles Ω'_{ob} (or Ω'_{combo}) among those real obstacles and those robots indexed from r_1 through r_{i-1} which are close to the segment;

(2) base on step (1), calculate clearance area for each apparent obstacle and determine which portions of the segment are encroached;

(3) based on step (2), calculate the set of qualified fragments $S^{qa}_{fg,i}$ by discarding all the fragments without sufficient room to accommodate at least one robot;

(4) on $S^{qa}_{fg,i}$, invoke the formula presented in Equation (7.2) to calculate the near point on the segment and check if multiple nearest points exist;

(5) if robot r_{i-1} is not settled on the segment and multiple nearest points found in step (4), disable the attracting force instantaneously;

(6) if robot r_{i-1} is already settled on the segment and multiple nearest points found in step (4), discard those near points which are out of the attractive zone of robot r_{i-1} and if the unique nearest point or none of the multiple nearest points are within the attractive zone then invoke the formula presented in Equation (7.2) only on those fragments which at least partially fall into the attractive zone of r_{i-1};

(7) go to step (1) and repeat the procedures in step (2) through (6) for the next round of seeking.

Remark 7.5.1 *Step (5) is indispensable mainly because of two reasons. First it is reasonable to instruct a robot to stop moving if it is sufficiently close to its nearest point on a segment in practical implementations. Second if the nearest point is out of the attractive zone of r_{i-1}, the highly undesired local minima issues may happen. Therefore we*

need to keep the nearest point within in the attractive zone of r_{i-1}. Obviously since the clearance areas of apparent obstacles are utilized in the calculation of $S^{qa}_{fg,i}$, the nearest point for robot r_i is already excluded from $S^{qa}_{fg,i}$ and hence there is no chance for it to fall into the repulsive zone of robot r_{i-1}. Due to this observation, in step (5) we merely need to deal with these nearest points out of attractive zone of r_{i-1}.

Due to encroachments, following up the procedures described in the seeking algorithm, the minimum distance $d_{min}(x)$ between a robot and the segment based on the set $S^{qa}_{fg,i}$ may be discontinued. However for each qualified fragment of segment, it is very interesting to note that: (1) $d_{min}(x)$ is continuous; (2) $d_{min}(x)$ is locally Lipschitz as guaranteed by previously addressed mathematical properties of $d_{min}(x)$. Also, it can be concluded that transition only exist when multiple nearest points are available no matter whether they belong to the same segment fragment.

7.6 Local Minima and Solutions

It is no surprise that even with "apparent obstacle scheme", local minima may arise under certain circumstances as long as there exists at least one trajectory S_T such that the following condition is met:

$$S_T = \{(x,y) \mid \Sigma\vec{F}_{att} + \Sigma\vec{F}_{rep} = 0\}, \tag{7.10}$$

where $\vec{F}_{att}$ and $\vec{F}_{rep}$ denote the attractive force and repulsive force applied on a given robot respectively. A simplified example is shown in Figure 7.11, where the segment

represented by V_1V_2 is a straight line and P_1P_2 of the apparent obstacle's boundary happens to be also a straight line parallelling with V_1V_2. In this situation, a robot being attracted to the nearest point on the segment is very likely to be captured in a local minimum as the attractive force $\vec{F}_{att}$ seems to cancel out repulsive force $\vec{F}_{rep}$ generated by obstacle avoidance potentials.

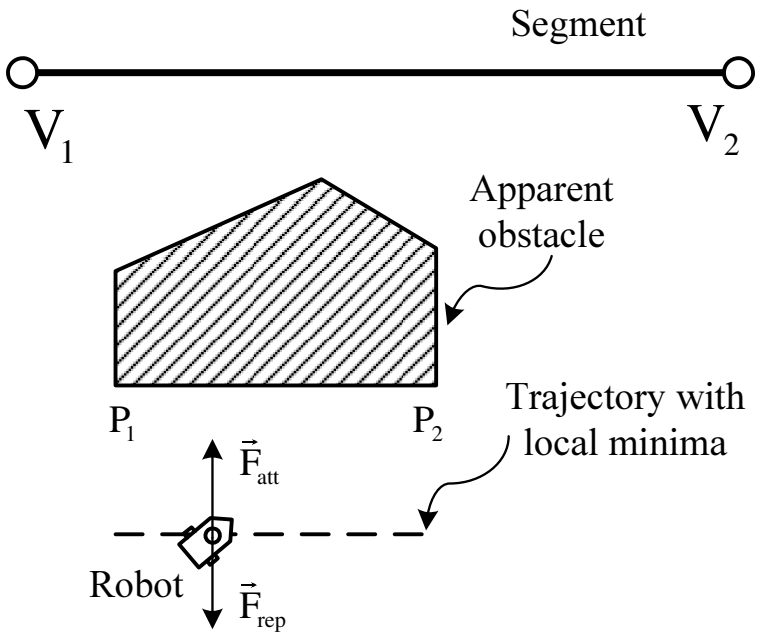

Figure 7.11: Illustration of local minima with the "apparent obstacle scheme". The specific trajectory featuring $\vec{F}_{att}$ cancelling out $\vec{F}_{rep}$ at any point along this line is represented by a dash line, which parallels with the segment V_1V_2 and a portion of the obstacle boundary (i.e., P_1P_2).

Obviously, here the key point is that P_1P_2 of the apparent obstacle parallels with segment V_1V_2. As the segment is known and P_1P_2 is able to be detected by the robot, such a situation is predictable and can be prevented with simple solutions. A straightforward and effective method is to form an auxiliary arc on the part of apparent obstacle to prevent attractive force from cancelling out repulsive force. To this end, Figure 7.12 shows such an effective solution to remove the existing local minima trajectory by forming an artificially created arc centered at point P_0 (on the segment) outside the apparent obstacle.

Each point on the arc $P_1P_3P_2$ has equal distance to P_0. The introduce of arc will not affect the nearest point on the segment. Hence direction of the attractive force $\vec{F}_{att}$ will not be altered. On the other hand, direction on the repulsive force $\vec{F}_{rep}$ is indeed changed due to the arc. For instance, for a robot location as shown in the figure, direction of the repulsive force is no longer opposite to the attractive force. In this way, a robot can pass by the obstacle free of a local minima trajectory as shown in Figure 7.11. The special case when the attractive force is in the direction pointing from P_3 to P_0 and meanwhile the condition $\vec{F}_{att} = -\vec{F}_{rep}$ is met is not a stable local minimum and thus does not affect the conclusions drawn above.

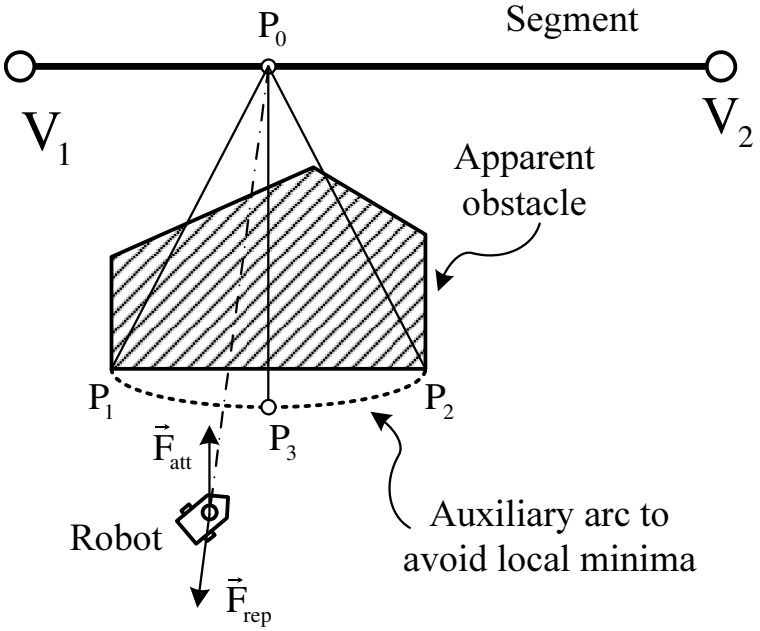

Figure 7.12: An effective elegant solution to overcome the local minima dilemma discussed in Figure 7.11. The auxiliary arc $P_1P_3P_2$ used to prevent local minima is depicted in dot line. The distances from P_0 to P_1, P_3 and P_2 are equal, namely $||P_0P_1||$ = $||P_0P_3||$ =$||P_0P_2||$.

One more example describing another type of local minima is shown in Figure 7.13, where a portion ($P_1P_3P_2$) of the apparent obstacle boundary coincidentally to be an arc centered at point P_0 on the assigned segment. A local minima trajectory exists in this

special case and it turns out to be an arc centered at point P_0 simply because along the trajectory the attractive force $\vec{F}_{att}$ exactly cancels out the repulsive force $\vec{F}_{rep}$ generated by obstacle avoidance potentials. To deal with such an adverse situation, an effective remedy is proposed by constructing two straight lines outside the apparent obstacle. Specifically we can let $P_0P_1 \perp P_1P_4$ and $P_0P_2 \perp P_2P_4$, which is simple and convenient for calculations. The introduce of P_1P_4 and P_2P_4 alters the direction of repulsive force $\vec{F}_{rep}$ and therefore successfully removes the existence of local minima trajectory.

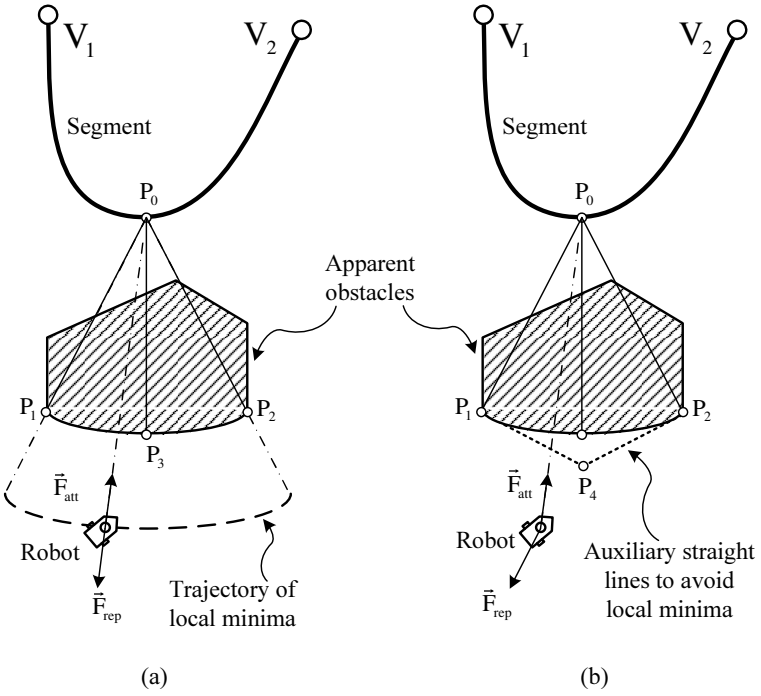

Figure 7.13: One more example of local minima with "apparent obstacle scheme". The left side figure, i.e.(a), illustrates the local minima trajectory (dashed line) due to $\vec{F}_{att}$ cancelling out $\vec{F}_{rep}$ everywhere along this trajectory. The right side figure, i.e.(b), presents a simple solution capable of removing the local minima trajectory by constructing two auxiliary straight lines P_1P_4 and P_2P_4 (doted lines) with $P_0P_1 \perp P_1P_4$ and $P_0P_2 \perp P_2P_4$.

Remark 7.6.1 *It is interesting to note that the area covered by apparent obstacle and the additional arc shown in Figure 7.12 may not necessarily be convex. Whether it is convex or not depends on the shape of the arc and the shape of apparent obstacle.*

However, the area surrounded by auxiliary lines (P_1P_4 and P_2P_4) and apparent obstacle depicted in Figure 7.13 is convex. So to get the combined convex hull of the apparent obstacle and the auxiliary arc or lines may be unnecessary unless it has to do so. Usually we may let the auxiliary arc or lines disappear whenever a robot is not threatened by such kind of local minima trajectory.

7.7 Recovery from Local Minima Caused by Moving Obstacles

In previous sections, several possibilities of local minima associated with apparent obstacle scheme are addressed in detail. It is already shown that local minima trajectory only exists in certain special circumstances and can be handled with simple solutions. For certainty, the proposed solutions in the previous section can prevent local minima on the robot's path approaching the assigned segment if all obstacles are static or if they are separated faraway enough such that the interactions among multiple obstacles do not affect the robot. In other words, the separations among these moving obstacles are always greater than the safety clearance $\rho_{clearance}$ and consequently there is no need to calculate the combined apparent obstacles.

Nevertheless there is another threat that moving obstacles can form a combined apparent obstacle in which a robot is likely to be trapped inside. As a matter of fact one example of such situations is illustrated in Figure 7.14, where Ω_{ob1} is moving towards another obstacle Ω_{ob2} and finally at certain point a combined apparent obstacle has to be formed

and unfortunately the robot is suddenly surrounded within the newly crated apparent obstacle Ω'_{combo}. Now the robot needs a method to recovery from such an adverse situation otherwise local minima may trap the robot. To this end, any robot falling into a combined apparent obstacle will exert the following strategy to escape from local minima. Immediately the attractive force generated by the nearest point (on the segment) has to be suspended temporarily until the robot is fully rescued from apparent obstacles. Meanwhile it will try to approach the nearest point outside Ω'_{combo} at which the repulsive force from the apparent obstacle attenuates to be zero. Take the robot in Figure 7.14 for example, it will start recovery processes once it is sieged by the newly formed Ω'_{combo} and discontinue the attractive force from the nearest point on segment until it reaches a nearest point N_2 outside the apparent obstacle and at this point the repulsive force from Ω'_{combo} reduces to be null.

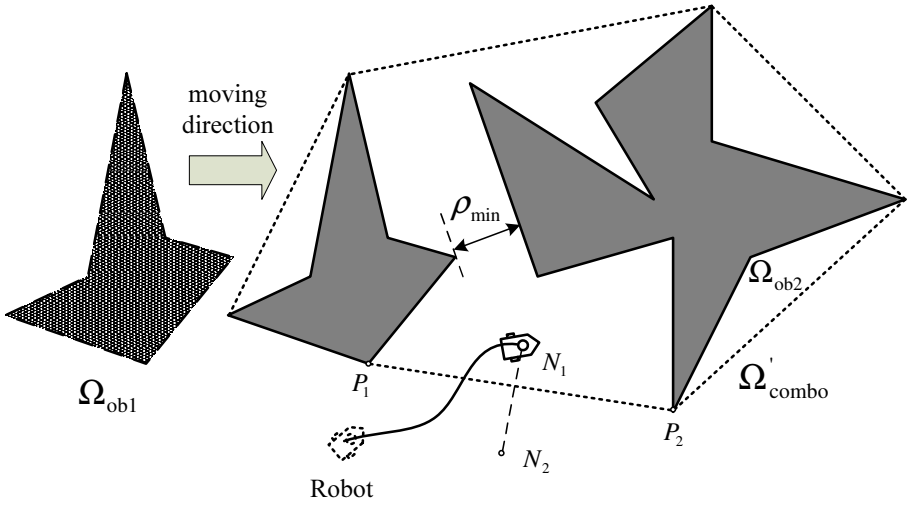

Figure 7.14: Illustration of local minima caused by moving obstacles and the associated recovery method.

7.8 Comparison with Alternative Obstacle Avoidance Methodologies

Since local minima has been a serious inherent problem with many forms of potential field methods from the very beginning, tremendous efforts have been made to overcome it in a great number of ways. It is noted that much of the endeavors has been directed to change the attractive/repulsive potential functions such that the local minima along the desired path will be removed. For example, Ge and Cui [26] proposed a new form of potential function which is constructed by multiplying an commonly used existing potential function with another term to prevent possible local minima. Specially this method aims at improving the conventional potential function which can be given as follows:

$$U_{rep}(q) = \begin{cases} \frac{1}{2}\eta\left(\frac{1}{\rho(q,q_{obs})} - \frac{1}{\rho_o}\right)^2, & \text{if } \rho(q,q_{obs}) \leq \rho_0 \\ 0, & \text{if } \rho(q,q_{obs}) > \rho_0 \end{cases}$$

where η is a positive scalar, $\rho(q,q_{obs})$ denotes the minimal distance from the robot q to the obstacle, q_{obs} represents the point on the obstacle such that the distance between this point and the robot is minimal between the obstacle and the robot, and ρ_0 is a positive constant denoting the distance of influence of the obstacle. To overcome the local minima caused by cancellation of repulsive force and attractive force at somewhere other than the goal point, a new form of repulsive potential function is constructed in

the following way [26]:

$$U_{rep}(q) = \begin{cases} \frac{1}{2}\eta\left(\frac{1}{\rho(q,q_{obs})} - \frac{1}{\rho_o}\right)^2 \rho^n(q,q_{goal}), & \text{if } \rho(q,q_{obs}) \leq \rho_0 \\ 0, & \text{if } \rho(q,q_{obs}) > \rho_0 \end{cases}$$

where $\rho(q,q_{goal})$ is the distance between the robot q and the goal point q_{goal}. The trick in the method is to manipulate the parameters of the whole potential functions (namely the sum of $U_{rep}(q)$ and attractive potential $U_{att}(q)$) after introducing the special term $\rho^n(q,q_{goal})$ such that the goal point will become the unique global minimum. In other words, the previously existing local minimum phenomenon at somewhere other than the goal point is removed if the parameters are properly selected. Consequently the new potential field function usually takes on a sophisticated form and gives rise to computation or analysis complexity on designing suitable potential functions. Moveover, the controller performance become harder to predict with sophisticated potential functions such as the case in Ge and Cui method [26]. There is single obstacle considered and the obstacle is assumed to be convex and interactions among multiple obstacles and the more sophisticated situations with multiple moving obstacles are out of the scope of this method.

Contrast to these traditional methods, apparent obstacle scheme attempts to solve the issue from another perspective. The shapes of obstacles are considered and taken into account during obstacle avoidance while the potential functions do not need to be reconstructed even in the special occasions where local minima is still present with apparent obstacle scheme.

Virtual obstacle method is similar to our work in the sense that it does not need to change the potential field function. Originally the concept of ”virtual obstacle” was proposed in [57] to overcome the local minimum issue associated with potential field method. The main idea is that when a robot approaches or encounters concave or concave-shaped obstacles where a local minimum is most likely to occur, invoke the computation for intermediate via points to be used as temporary path targets, namely the so-called virtual obstacle method. Finally the real line segment (of the obstacle) and virtual lines forms the boundary of a virtual obstacle. Meanwhile if the robot is inside the concave obstacle, then it has to navigate out of the obstacle via a local-minimum recovery scheme. This method is similar to our apparent obstacle scheme. Both virtual obstacle method and apparent obstacle scheme can handle with concave obstacle. Apparent obstacle is derived from the convex hull of the obstacle boundary while virtual obstacle results from combination of real line segment (of the obstacle) and virtual lines. Virtual obstacle method assumes the boundary of obstacles consists of segment while apparent obstacle scheme allow the obstacle to be with arbitrary shapes.

Apparent obstacle scheme can deal with multiple obstacles readily as it provides a mathematical calculation framework and addresses the conditions under which the combined apparent obstacle has to be calculated. But in [57] the explicit mechanism is not stated. Virtual obstacle method may guide a robot to enter dangerous areas, including deep crevices or internal cavities of a single obstacle or crevices formed by multiple obstacles because at these areas the robot is highly likely to be trapped and then has to resort to the associated local minima recovery scheme in order to successfully approach the desired

goal point. However, with apparent scheme, the robot usually is kept from moving into such dangerous areas. Specifically, apparent obstacle are able to get rid of local minima caused by either single static obstacle with crevices (or cavities) or multiple static obstacles as shown in previous analysis and discussion. However there is no such guarantee for the case of virtual obstacle method even for a single static concave obstacle. To some extent, it heavily relies on recovery scheme to make it work. Moreover the scenario of crowded multiple moving obstacles are discussed in our approach and only in such complicated situations the recovery process which is already covered in the previous section will be invoked. It is also worthwhile to point out that virtual obstacle method, like most of other alternatives, is designed to navigate a robot to a predetermined goal point while our method can cope with approaching the nearest point on a segment indicating the goal point is not predetermined and is subject to possible aforementioned transitions.

Furthermore, it should be noted that essentially virtual obstacle method cannot eradicate the issue local minima. For instance in the situation such as the one illustrated in Figure 7.11, a robot navigated by virtual obstacle method is most likely to be trapped in local minima. A formal discussion and possible solutions are missing from the original work [57]. In contrast to virtual obstacle method, apparent obstacle scheme admits such drawbacks and in our case formal solutions are figured out to guarantee a local minima free path.

The Instant Goal (IG) method first proposed in [28] aims to solve the local minima problem where robots are trapped in deep obstacle crevices by giving higher priorities to instant goal than to the actual goal when the path to the actual obstacles obstructed. A

simple vector representation of the local environment is introduced and integrated into behavior-based system, where an instant goal driven behavior is generated to guide the robot. The IG method [28] allows the obstacles to be concave. However in essence it is a behavior-based strategy and no potential field topics are involved. Largely speaking it can be viewed as a special behavior-based recovery scheme coping with local minima on robot navigation for a single robot rather than a multi-robot system.

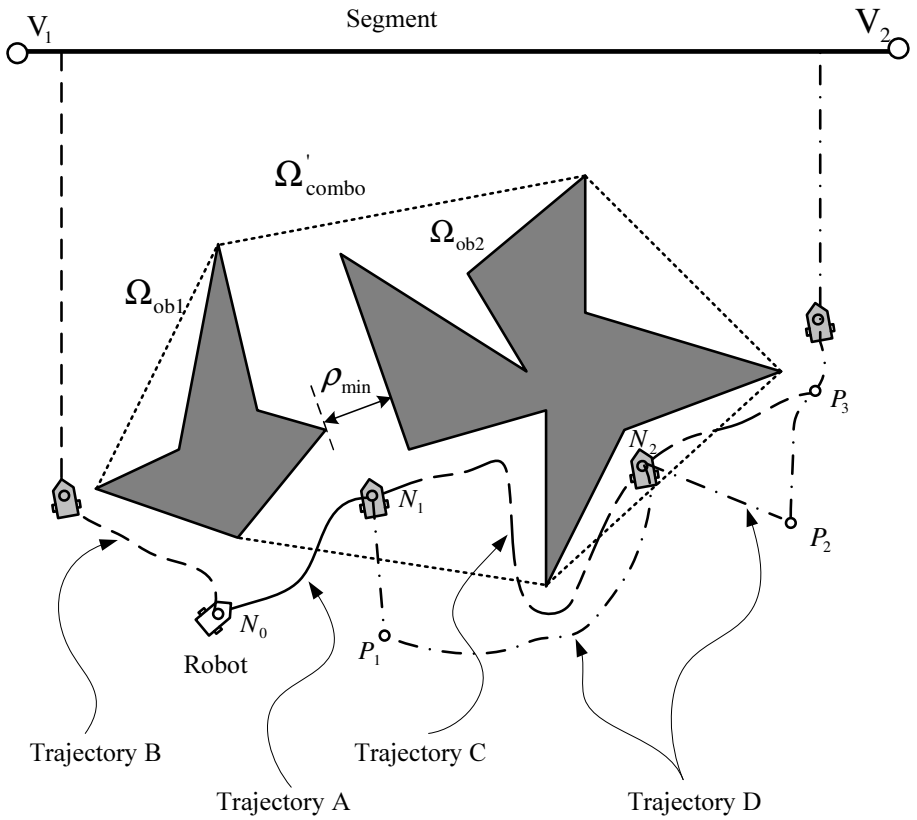

Figure 7.15: Comparison of possible trajectories with different obstacle avoidance algorithms.

To highlight the significant differences among distinct obstacle avoidance methods, Figure 7.15 is depicted for this purpose. In this figure, there is one segment (simplified as a straight line V_1V_2) and a mobile robot which is initially parked at location N_0 and is supposed to approach the nearest point on the segment. The robot at locations other than

its initial place N_0 is depicted in shadows to indicate the possible routines under control of different obstacle avoidance methods. Two static concave obstacles are in the robot's way to the segment and they are deliberately placed so close to form crevices that will threaten the robot under potential field control to be stuck in local minima. Trajectory A (depicted in a solid line) starting from robot's initial location N_0 to point N_1 is expected for most of the conventional potential field methods [50][6] without obstacle avoidance mechanisms because the robot will be trapped at a local minimum point N_1. However if effective obstacle avoidance methods are applied, the robot will be able to reach the segment in different manners. Trajectory B is a possible routine if our Apparent Obstacle Scheme is employed while C may result from Instant Goal(IG) Method [28]. A robot under the control of Virtual Obstacle Method [57] may follow Trajectory D which undergoes a rugged path caused by recovery processes in order to overcome the encountered local minima (namely at location N_1 and N_2). Consequently it results in two straight lines N_1P_1 and N_2P_2 respectively as recovery process has to be invoked twice. It should be noted that a robot under the control by either Instant Goal(IG) Method [28] or Virtual Obstacle Method [57] may pass through Trajectory A during its first stage of approaching to the segment. However, our scheme obviously is the only candidate among the three methods to generate a smooth local-minima-free path even without invoking recovery scheme in this case and the other two methods are likely to follow trajectories passing by local minima locations and have to resort to the associated recovery methods to survive.

7.9 A Coordinated Chain Attracted to a Segment

To control a team (in approaching and being attracted to a given segment) as a coordinated chain, we augment the control as stated in Equation (7.4) with other potential functions solely for the purpose of keeping two robots within a range of each other and avoiding collision with obstacles. The idea is that, as a chain approaches the segment, except the repulsive forces due to obstacles a robot in the chain should normally stay within the neutral zone of its follower. Action must be taken by the follower to enforce this zoning requirement if the leader happens to enter either zone 2 or zone 4 of the follower.

A *zoning potential* is introduced specifically for this purpose. This potential is realized by a function Ψ, which takes on either of two forms, depending on the location of a robot in the zoning scheme of another. A repulsive potential $\hat{\Psi}$ comes into effect when a robot finds its leader in its zone 2, while an attractive potential $\check{\Psi}$ is in effect when a robot finds its leader in its zone 4. Specifically, we can choose

$$\check{\Psi}(d_{i,i-1}) = \begin{cases} \beta/(2\delta_a^m) & \text{if } \rho < d_{i,i-1} < \check{\rho}, \\ c_1/2 & \text{if } \underline{\rho} < d_{i,i-1} \leq \rho, \\ 0 & \text{elsewhere,} \end{cases}$$

$$\hat{\Psi}(d_{i,i-1}) = \begin{cases} \alpha/(2\delta_r^m) & \text{if } \underline{\rho} < d_{i,i-1} < \hat{\rho}, \\ c_2/2 & \text{if } \hat{\rho} \leq d_{i,i-1} < \check{\rho}, \\ 0 & \text{elsewhere,} \end{cases}$$

where

$$d_{i,i-1} \equiv \|\vec{d}_{i,i-1}\| = \|\vec{r}_{i-1} - \vec{r}_i\| = \left((\vec{r}_{i-1} - \vec{r}_i)^T (\vec{r}_{i-1} - \vec{r}_i)\right)^{\frac{1}{2}}, \tag{7.11}$$

$\delta_a = \check{\rho} - d_{i,i-1}$, $\delta_r = d_{i,i-1} - \underline{\rho}$, m (a constant) is either 1 or 2, $c_1 = \beta/(\check{\rho} - \rho)^m$, and $c_2 = \alpha/(\hat{\rho} - \underline{\rho})^m$. Therefore the function for the overall zoning potential, i.e., $\Psi(d_{i,i-1}) = \hat{\Psi}(d_{i,i-1}) + \check{\Psi}(d_{i,i-1})$, is absolutely continuous in the range $\underline{\rho} < d_{i,i-1} < \check{\rho}$. Moreover $\Psi(d_{i,i-1})$ is locally Lipschitz continuous and regular in the same range.

The repulsive potential specified above only ensures no collision between a robot and its leader. To avoid collision between any two robots r_i and r_j in a team (where $j \neq i-1$), the repulsive potentials on r_i is invoked whenever any robot r_m (with $m < i$) enters zone 2 of r_i. Meanwhile, for to avoid collision with real obstacles, repulsive potential on r_i also include these from apparent obstacles. Specifically, the potential

$$\Phi_{i,total} = \Phi_{i,ns}(d_{i,ns}) + \check{\Psi}_{i,i-1}(d_{i,i-1}) + \sum_k \hat{\Psi}^{ob}_{i,k}(d^{ob}_{i,k}) \tag{7.12}$$

is applied on robot r_i, where $d^{ob}_{i,k} \equiv \|\vec{d}^{ob}_{i,k}\| = \|\vec{r}^{ob}_k - \vec{r}_i\| = \left((\vec{r}^{ob}_k - \vec{r}_i)^T (\vec{r}^{ob}_k - \vec{r}_i)\right)^{\frac{1}{2}}$, and $\vec{d}^{ob}_{i,k}$ denotes the vector pointing from the unique nearest point on k-th apparent obstacle to robot r_i, and $\vec{r}^{ob}_k$ is the vector pointing from coordinates origin to the nearest point on k-th apparent obstacle with respect to robot r_i, and $\sum_k \hat{\Psi}_{i,k}(d^{ob}_{i,k})$ denotes sum of all the repulsive forces due to obstacles, including real obstacles and robots r_1 through r_{i-1}. In other words, sum of the potentials due to real robots presented by $\sum_j \hat{\Psi}_{i,j}(d_{i,j})$, where $j = 1, 2, ..., i-1$, is already integrated in $\sum_k \hat{\Psi}^{ob}_{i,k}(d^{ob}_{i,k})$ through the apparent obstacle scheme.

Thus, throughout the process of approaching a segment as a member of a coordinated chain, each robot is subject to the influence of the potential trench function, and possibly additional zoning potentials (attractive or repulsive) depending on its location with respect to all other robots before it (in terms of the rank in the leader-follower pairings) and repulsive potentials from real obstacles.

Theorem 7.9.1 *Consider the following control*

$$\vec{u}_i = \ddot{\vec{r}}_{i,ns} + k_i \dot{\vec{d}}_{i,ns} + \nabla \left(\Phi_{i,total} \right), \tag{7.13}$$

where $\Phi_{i,total}$ is given by Equation (7.12), $\dot{\vec{d}}_{i,ns} = d(\vec{d}_{i,ns})/dt$, and k_i is a positive scalar. In the absence of local minima in the trajectories of the robots, a coordinated chain can be attracted within arbitrary small deviation from the segment by applying Equation (7.4) on the chain leader and Equation (7.13) on all other robots in the chain.

Proof: See Appendix A.18. □

7.10 Simulation

A computer simulation (using MATLAB) has been conducted to demonstrate the effectiveness of the proposed formation and zoning control of a coordinated chain. A group of ten robots, indexed from 1 to 10, were initially randomly placed on a plane with non-zero velocity. The robots were organized in leader-follower pairs. Only the goal point, fixed at $(100, 100)$, of the first robot was specified. Figure 7.16 shows the initial (randomly selected) positions and velocities of each robot, while Table 7.1 lists the radii of the zon-

ing scheme. The segment consists of a straight line connecting $(-5,-5)$ and $(100,100)$. Each robot in the team is attracted the corresponding nearest point on the segment. The repulsive zoning potential $\hat{\Psi}(d_{i,i-1})$ was set to be $5/(d_{i,i-1}-1)^2$ for $1 < d_{i,i-1} < 4$, $5/9$ for $4 \leq d_{i,i-1} < 13$, and 0 elsewhere, while the attractive zoning potential $\check{\Psi}(d_{i,i-1})$ was set to be $5/(13-d_{i,i-1})^2$ for $10 < d_{i,i-1} < 13$, $5/9$ for $1 < d_{i,i-1} \leq 10$, and 0 elsewhere. The potential trench function was set as $\Phi(d_{i,ns}) = 10\left(d_{i,ns}^2+1\right)^{\frac{1}{2}} - 10$.

Table 7.1: Radii of zoning scheme.

$\underline{\rho}$	$\hat{\rho}$	ρ	$\check{\rho}$	$\bar{\rho}$
1	4	10	13	30

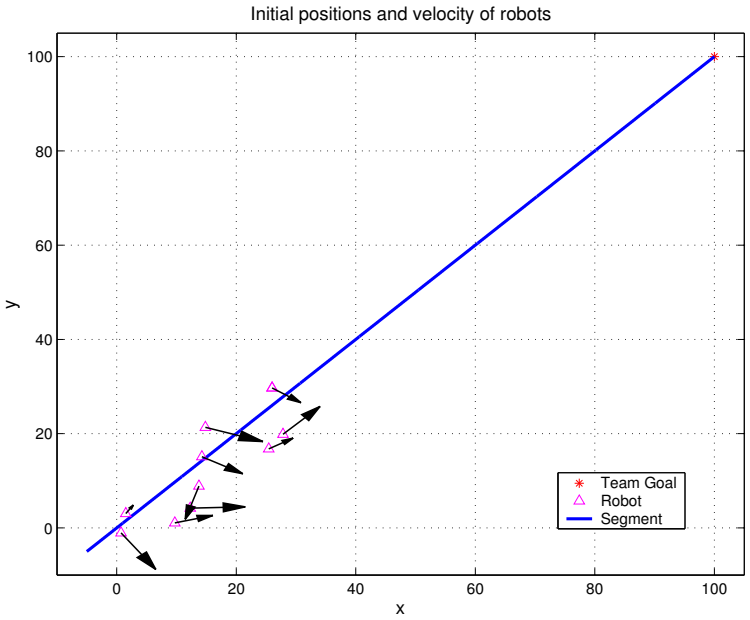

Figure 7.16: The segment, goal point and initial positions/velocities of 10 robots (the arrow denotes initial velocity).

Figure 6.5 illustrates the closed-loop system diagram of an individual robot $\vec{r}_i$, $i > 1$. The simulation was run at a sampling rate of $T_s = 0.01$ second for a period of 200 seconds. For robots r_2 to r_{10}, the positions of their leaders were sampled every 0.01 second. The

trajectories of all robots were recorded every 0.01 second.

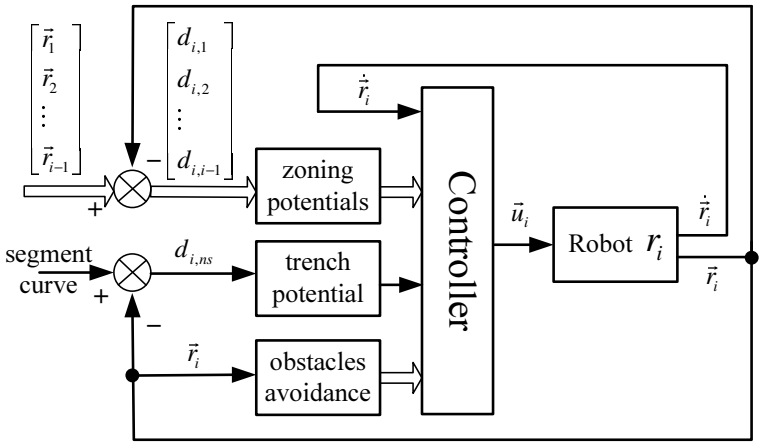

Figure 7.17: Diagram of an individual robot $\vec{r}_i$ for MATLAB simulation.

Figure 7.18 shows the positions of the ten robots at the end of simulations, while Figure 7.19 shows the distance between a robot and its leader. It can be seen from these two figures that, although initially a robot may fall in zone 2 or 4 of its leader, it was eventually steered by the zoning potential and the potential trench to enter and reside in the neutral zone, leading to the final result that the robots approached the segment as a coordinated chain with the team leader r_1 attracted to the specified goal point.

Now we consider the scenario with obstacle avoidance. There are four static cylinder shape obstacles centered at $(30,25)$, $(40,43)$, $(84,86)$, $(92,90)$ respectively while settings for the segment, team goal and robots' initial conditions are the same as previous simulation. Similarly zoning scheme is utilized to prevent robots from collision with $\underline{\rho} = 1$ denoting the size of an obstacle and $\hat{\rho} = 2$, $\rho = 3$ for the edges of repulsive zone. Figure 7.20 shows the positions of the ten robots during the simulations and to highlight the interactive behavior between robots and obstacles, the trajectories of robots r_1 to r_4 are presented in Figure 7.21. From these figures, it is clear that robots reach the segment

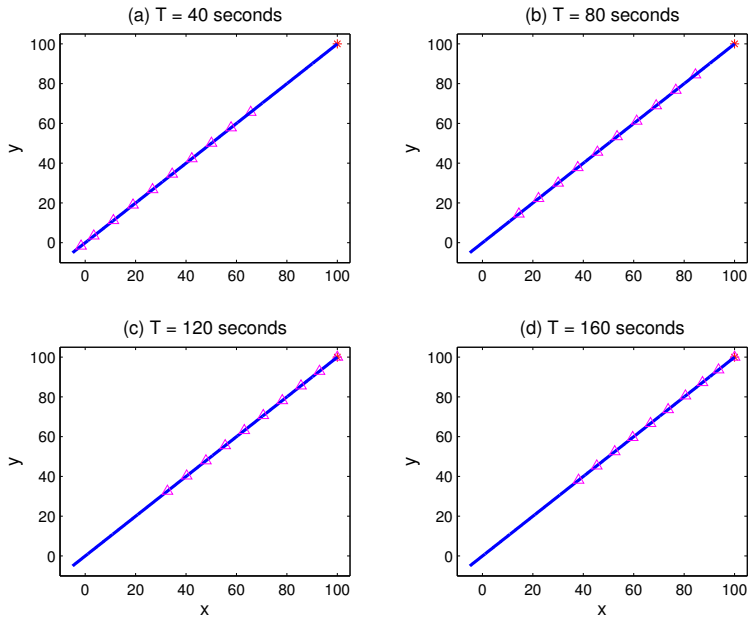

Figure 7.18: Positions of robots during the simulation.

while keep colliding with obstacles. Figure 7.22 shows the distance between a robot and its leader. The same convergent behavior of the ten robots is observed in this case.

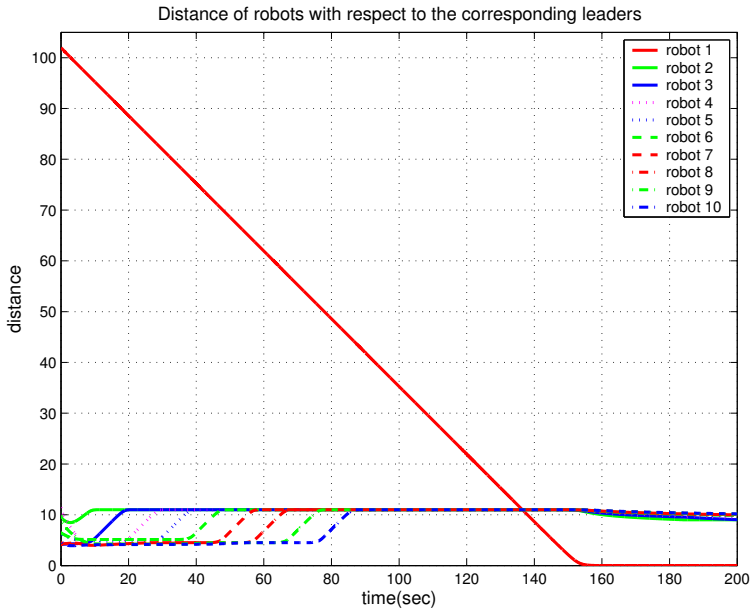

Figure 7.19: Distance between each robot and its leader.

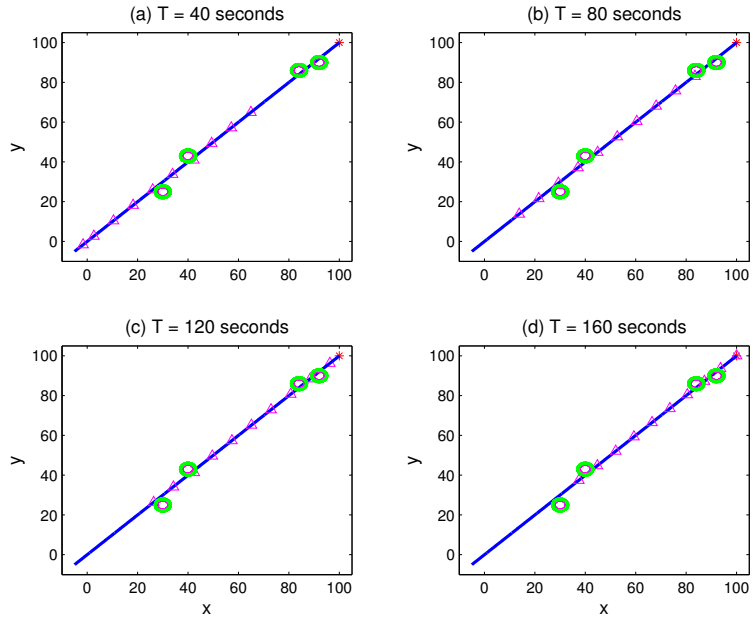

Figure 7.20: Positions of robots during simulation with obstacle avoidance.

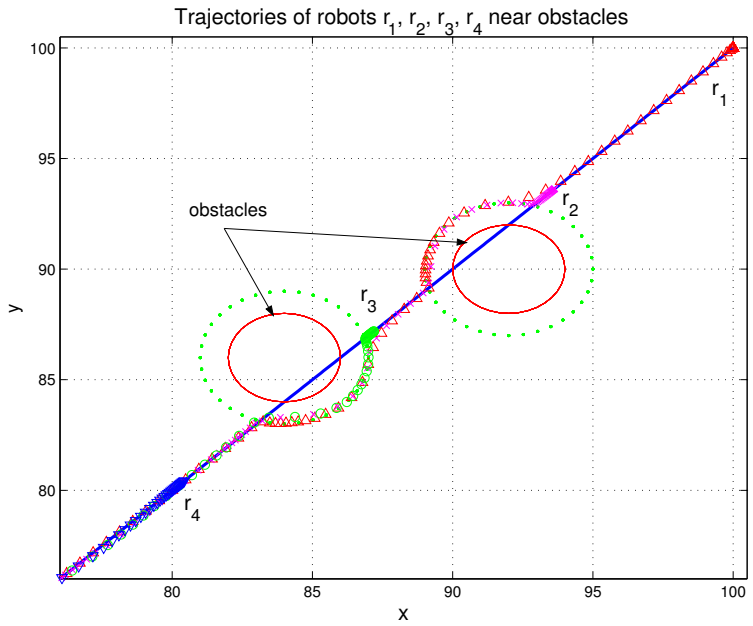

Figure 7.21: Trajectories of robots r_1 to r_4 near obstacles (for obstacles, only $\hat{\rho}$ and ρ depicted).

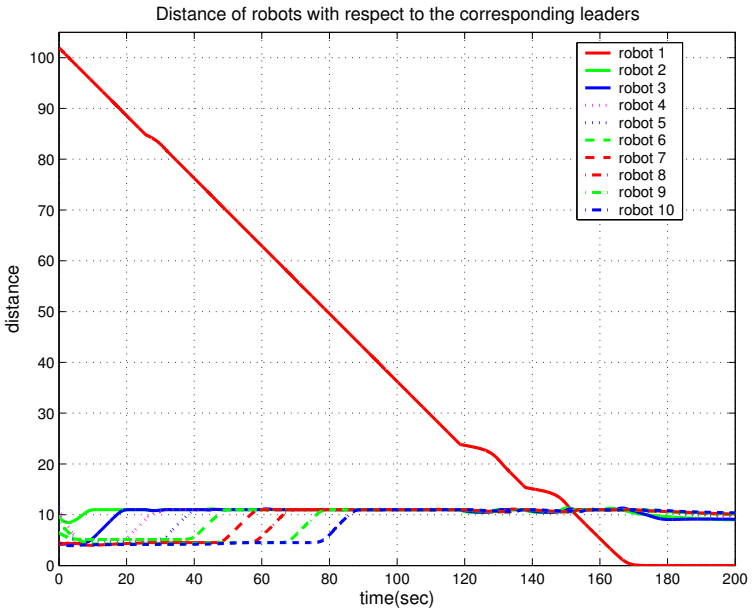

Figure 7.22: Distance between each robot and its leader for the case with obstacle avoidance.

7.11 Conclusions

In this chapter, a framework where a team of robots are attracted to the nearest points on the segment while preventing from collisions with multiple obstacles (static or dynamic) is established. A mathematical framework is developed to analyze the characteristics of motion of the nearest point on the segment. The transition of nearest point is revealed and the incurred discontinuity is well handled by nonsmooth analysis. A novel obstacle avoidance method based on the new concept of apparent obstacle, together with the associated local minima recovery mechanism is proposed to cope with concave obstacles and multiple moving obstacles. Comparison between apparent obstacle scheme and other alternative solutions is discussed in detail and the advantages and benefits of our method is addressed. An elaborated algorithm dedicated to seeking for the nearest point on a segment in the presence of obstacles is presented. The special occasions of local minima are discussed and the corresponding simple solutions are provided. Theoretical analysis and computer simulation have been done to show the effectiveness of this framework.

Chapter 8

Input-to-State Stability

In previous chapters, stability of multi-robot formation control based on the notions of segment and artificial potential trench have been studied extensively. Separations among robots which are managed by zoning potentials and the comprehensive multi-robot formation control by attracting each robot to the nearest point on the segment with obstacles avoidance also have been investigated.

In multi-robot system during formation, it is interesting to study behavior of a single robot's states in response to inputs or external disturbances. Specifically input-to-state stability of formation control is to be addressed.

8.1 Introduction

The notion of input-to-state stability of multi-robot formation control was first proposed in [84] to characterize the internal stability of leader-follower formations. Some results

on formation input-to-state stability are presented in the paper [84]. However, all the results are acquired based on the notion of formation graph. On the basis of segments and queues, input-to-state stability of formation control is to be studied in this chapter.

Definition of input-to-state stability (ISS) already has been reviewed in Chapter 3. To facilitate stability analysis, some key concepts and an important theorem on ISS have to presented. The notions of $\mathscr{K}_\infty$-function and $\mathscr{K}$-function are given below.

Definition 8.1.1 *A function $\gamma : R_{\geq 0} \to R_{\geq 0}$ is a $\mathscr{K}$-function if it is continuous, strictly increasing and $\gamma(0) = 0$; it is a $\mathscr{K}_\infty$-function if it is a $\mathscr{K}$-function and also $\gamma(s) \to \infty$ as $s \to \infty$; and it is positive definite function if $\gamma(s) > 0$ for all $s > 0$, and $\gamma(0) = 0$. A function $\beta : R_{\geq 0} \times R_{\geq 0} \to R_{\geq 0}$ is a $\mathscr{KL}$-function if for each fixed $t \geq 0$ the function $\beta(\cdot, t)$ is a $\mathscr{K}$-function, and for each fixed $s \geq 0$ it is decreasing to zero as $t \to \infty$.*

The following theorem establishes the relationship between the existence of a Lyapunov function and the input-to-state stability.

Theorem 8.1.1 *[79] Let $D = \{x \in R^n \mid \|x\| < r\}$, $D_d = \{d \in R^m \mid \|d\| < r_d\}$, and $f, g : D \times [0, \infty) \to R^n$ be piecewise continuous in t and locally Lipschitz in x. Let $V : D \times [0, \infty) \to R$ be a continuously differentiable function such that*

$$\|x\| \geq \rho(\|d\|) > 0 \quad \Rightarrow \quad \begin{array}{c} \gamma_1(\|x\|) \leq V(t,x) \leq \gamma_2(\|x\|), \\ \dfrac{\partial V}{\partial t} + \dfrac{\partial V}{\partial x} f(x,t) + \dfrac{\partial V}{\partial x} g(x,t) d \leq -\gamma_3(\|x\|), \end{array} \tag{8.1}$$

$\forall (x,t) \in D \times [0, \infty)$ where γ_1, γ_2, γ_3 and ρ are class $\mathscr{K}$ functions. Then, the system given by Equation (3.28) is locally input-to-state stable with $\chi = \gamma_1^{-1} \circ \gamma_2 \circ \rho$, $k_1 = \gamma_2^{-1}(\gamma_1(r))$,

and $k_2 = \rho^{-1}(\min\{k_1, \rho(r_d)\})$. *In addition, if* $D = R^n$, $D_d = R^m$, *and* γ_1 *is a class* $\mathscr{K}_\infty$ *function, then the system is input-to-state stable with* $\chi = \gamma_1^{-1} \circ \gamma_2 \circ \rho$.

8.2 Input-to-State Stability Analysis

Generally speaking, there are two basic control objectives in the formation control. One is to drive the robots to get the desired formation pattern. This is guaranteed to be achieved due to the presence of the potential trench and the force may be calculated as the negative gradient of the potential. The other is to keep desired relative distance between each robot. This could be achieved by the attractive potential and the force can be derived as the negative gradient of the attractive potentials affecting the robots.

Therefore, we can decompose queue formation control into two smaller questions. First, robots are attracted to the corresponding queue by artificial potential trench method, that is ”approaching the queue”. Second, robots in the same queue start formation along the queue curve, while keeping certain distances between each robot in line with formation specifications, i.e. ”keeping desirable distance”.

In Chapter 4, based on kinetic model of mobile robots we have demonstrated that a team of robots can approach the assigned segments and form the desired geometric pattern in pursuit of virtual goal points moving on the segments. As revealed by Theorem 5.4.1, which is based on dynamic model of mobile robot, robots are asymptotically stabilized on the corresponding nearest points on the segment and thus forms the queue under the control of artificial potential trench. Furthermore, Theorem 7.9.1 states that robots are

attractive with respect to the nearest points on the segment in the presence of obstacles. Now we are going to perform input-to-state stability analysis based on a more generic model of mobile robots.

Suppose that there is a group of N_{tot} robots, where N_{tot} is a finite number. The group of robots shall follow a desired trajectory while maintaining certain formation. Let us consider the group of $N_{rob,i}$ robots in queue i. For the j-th robot in queue i, its dynamics can be described by the following Linear-Time-Invariant (LTI) control system as

$$\dot{x}_{i,j} = A_{i,j}x_{i,j} + B_{i,j}u_{i,j}, \tag{8.2}$$

where $x_{i,j} \in R^n$ is the state vector, $u_{i,j} \in R^m$ is the control input, $A_{i,j} \in R^{n\times n}$, $B_{i,j} \in R^{n\times m}$ and $(A_{i,j}, B_{i,j})$ is controllable.

In the potential trench method, each robot belonging to certain queue will be attracted to the nearest point on this queue. In general 3-D space, let $z = g_{vi}(x,y)$ denote the shape of queue i in a formation, where the function $g_{vi}(x,y)$ is continuously differentiable over the range in which the queue exists, and have to pass through all the formation vertices. In addition, every point on the curve must be at a different distance from the origin. This ensures that for any point $q_{i,j}$ in the 3-D (R^3) space, there will be a point $q_{i,jns}$ on $g_{vi}(x,y)$ that is nearest to $q_{i,j}$, while maintaining as close a distance from the origin as possible. The point $q_{i,jns}$ can be found by

$$q_{i,jns} = \arg\min_{q_{s1}\in Q_n}(\|q_{s1}\|), \tag{8.3}$$

where Q_n is the set of points on the queue that satisfies

$$\arg\min_{q_s \in g_i}(l_{Q_i}(q_s)), \tag{8.4}$$

and

$$l_{Q_i}(q_s) = \|q_s - q_{i,j}\|. \tag{8.5}$$

For every pair of $(q_{i,j}, q_{i,jns})$, it associates an error vector that describes the deviation from the desired point in the queue for the robot as

$$e_{i,jns} = x_{i,j} - x_{i,jns}, \tag{8.6}$$

where $x_{i,jns}$ denotes the state vector of the desired point in the queue.

Let the control input be

$$u_{i,j} = -K_{i,j}(x_{i,j} - x_{i,jns}) + \alpha_{i,j}, \tag{8.7}$$

with $B_{i,j}\alpha_{i,j} = -A_{i,j}x_{i,jns}$.

The error dynamics is then given by

$$\dot{e}_{i,jns} = (A_{i,j} - B_{i,j}K_{i,j})e_{i,jns}. \tag{8.8}$$

As $(A_{i,j}, B_{i,j})$ is a pair of controllable matrices, the eigenvalues of the matrix $(A_{i,j} - B_{i,j}K_{i,j})$ can be arbitrarily set. Suppose that all the robots belong to queue *i* has reached

to its desired point $q_{i,jns}$, i.e., the state vector can be described by $x_{i,jns}$. Without loss of generality, let us assume that in i-th queue, the j-th robot is supposed to keep certain distance from the $(j-1)$-th robot and the distance is defined by $d_{i,j} \in R^n$. Accordingly, the error vector that describes the deviation from the specification can be defined by

$$e_{i,j} = x_{i,(j-1)ns} - x_{i,jns} - d_{i,j}. \tag{8.9}$$

Its dynamics is given by

$$\dot{e}_{i,j} = \dot{x}_{i,(j-1)ns} - A_{i,jns}x_{i,jns} - B_{i,jns}u_{i,jns}. \tag{8.10}$$

Consider the following feedback law

$$u_{i,jns} = K_{i,jns}(x_{i,(j-1)ns} - x_{i,jns} - d_{i,j}) + \beta_{i,jns}, \tag{8.11}$$

with $B_{i,jns}\beta_{i,jns} = -A_{i,jns}(x_{i,(j-1)ns} - d_{i,j})$.

Thus, the closed-loop dynamics becomes

$$\dot{e}_{i,j} = (A_{i,jns} - B_{i,jns}K_{i,jns})e_{i,j} + \dot{x}_{i,(j-1)ns}, \tag{8.12}$$

and

$$\dot{x}_{i,jns} = -(A_{i,jns} - B_{i,jns}K_{i,jns})e_{i,j}. \tag{8.13}$$

Suppose that the $(j-1)$-th robot is to follow the $(j-2)$-th robot. Define the error by

$$e_{i,j-1} = x_{i,(j-2)ns} - x_{i,(j-1)ns} - d_{i,j-1}. \tag{8.14}$$

Similarly considering the feedback law

$$u_{i,(j-1)ns} = K_{i,(j-1)ns}(x_{i,(j-2)ns} - x_{i,(j-1)ns} - d_{i,j-1}) + \beta_{i,(j-1)ns}, \tag{8.15}$$

with $B_{i,(j-1)ns}\beta_{i,(j-1)ns} = -A_{i,(j-1)ns}(x_{i,(j-2)ns} - d_{i,j-1})$, we further have

$$\dot{e}_{i,j-1} = (A_{i,(j-1)ns} - B_{i,(j-1)ns}K_{i,(j-1)ns})e_{i,j-1} + \dot{x}_{i,(j-2)ns}, \tag{8.16}$$

and

$$\dot{x}_{i,(j-1)ns} = -(A_{i,(j-1)ns} - B_{i,(j-1)ns}K_{i,(j-1)ns})e_{i,j-1}. \tag{8.17}$$

From Equation (8.17), Equation (8.12) can be re-written as

$$\dot{e}_{i,j} = (A_{i,jns} - B_{i,jns}K_{i,jns})e_{i,j} + \Delta_{i,j}, \tag{8.18}$$

with $\Delta_{i,j} = -(A_{i,(j-1)ns} - B_{i,(j-1)ns}K_{i,(j-1)ns})e_{i,j-1}$, which can be considered as a perturbed system with $\Delta_{i,j}$ being external disturbances. The system described by Equation (8.18) is a nonvanishing perturbation system. And we can treat $\Delta_{i,j}$ as an input for the Equation (8.18).

As $(A_{i,jns}, B_{i,jns})$ is a pair of controllable matrices, the eigenvalue of the matrix $(A_{i,jns} - B_{i,jns}K_{i,jns})$ can be arbitrarily set. For the $(j-1) \leftarrow j$ (target←follower) pair whose dy-

namic is given by Equation (8.18), the stability result is given in the following theorem.

Theorem 8.2.1 *Consider the target-follower system described by Equation (8.18). If* $(A_{i,jns}, B_{i,jns})$ *is a pair of controllable matrices then the system is input-to-state stable with respect to* $\Delta_{i,j}$.

Proof: See Appendix A.19. □

8.3 An Example

Now based on Theorem 8.2.1 which is discussed in the previous section, an example is given to show how the formation error of any robot on the segment can be affect by the team leader, namely the first robot for a given segment. For the first robot in the *i*-th queue, it is supposed to keep a certain distance to a fixed point rather than a robot. Thus, the error dynamics is given by

$$\dot{e}_{i,1} = (A_{i,1ns} - B_{i,1ns}K_{i,1ns})e_{i,1}. \tag{8.19}$$

Consider the Lyapunov function candidate

$$V_{i,1} = e_{i,1}^T P_{i,1} e_{i,1}. \tag{8.20}$$

Its time-derivative along Equation (8.19) is

$$\dot{V}_{i,1} = -e_{i,1}^T Q_{i,1} e_{i,1} \leq -\lambda_{\min}(Q_{i,1})\|e_{i,1}\|^2. \tag{8.21}$$

Following the similar analysis, we can obtain

$$\|e_{i,1}(t)\| \leq \sqrt{\frac{\lambda_{\max}(P_{i,1})}{\lambda_{\min}(P_{i,1})}}\|e_{i,1}(t_0)\|e^{-\frac{\lambda_{\min}(Q_{i,1})}{2\lambda_{\max}(P_{i,1})}(t-t_0)}. \tag{8.22}$$

Thus,

$$\|e_{i,1}(t)\| \leq \sqrt{\frac{\lambda_{\max}(P_{i,1})}{\lambda_{\min}(P_{i,1})}}\|e_{i,1}(t_0)\|. \tag{8.23}$$

Therefore, we can conclude that $e_{i,1}(t)$ is uniformly bounded given any finite initial condition $e_{i,1}(t_0)$.

For the second robot in the i-th queue, from Equation (74), we can conclude that

$$\begin{aligned}\|e_{i,2}(t)\| \quad \leq \quad & \sqrt{\frac{\lambda_{\max}(P_{i,2})}{\lambda_{\min}(P_{i,2})}}\|e_{i,2}(t_0)\|e^{-\frac{\lambda_{\min}(Q_{i,2})}{2\lambda_{\max}(P_{i,2})}(1-\theta_{i,2})(t-t_0)} \\ & +2\frac{\lambda_{\max}^{\frac{3}{2}}(P_{i,2})\mu_{i,(j-1)}}{\theta_{i,2}\lambda_{\min}(Q_{i,2})\lambda_{\min}^{\frac{1}{2}}(P_{i,2})}\sup_{\tau\geq t_0}\|e_{i,1}(\tau)\|,\end{aligned} \tag{8.24}$$

i.e.,

$$\begin{aligned}\|e_{i,2}(t)\| \quad \leq \quad & \sqrt{\frac{\lambda_{\max}(P_{i,2})}{\lambda_{\min}(P_{i,2})}}\|e_{i,2}(t_0)\| \\ & +2\frac{\lambda_{\max}^{\frac{3}{2}}(P_{i,2})\mu_{i,(j-1)}}{\theta_{i,2}\lambda_{\min}(Q_{i,2})\lambda_{\min}^{\frac{1}{2}}(P_{i,2})}\sqrt{\frac{\lambda_{\max}(P_{i,1})}{\lambda_{\min}(P_{i,1})}}\|e_{i,1}(t_0)\|,\end{aligned} \tag{8.25}$$

and

$$\begin{aligned}\|e_{i,j}(t)\| \leq\ & \sqrt{\frac{\lambda_{\max}(P_{i,j})}{\lambda_{\min}(P_{i,j})}}\|e_{i,j}(t_0)\|e^{-\frac{\lambda_{\min}(Q_{i,j})}{2\lambda_{\max}(P_{i,j})}(1-\theta_{i,j})(t-t_0)} \\ & +2\frac{\lambda_{\max}^{\frac{3}{2}}(P_{i,j})\mu_{i,1}}{\theta_{i,j}\lambda_{\min}(Q_{i,j})\lambda_{\min}^{\frac{1}{2}}(P_{i,j})}\sqrt{\frac{\lambda_{\max}(P_{i,j-1})}{\lambda_{\min}(P_{i,j-1})}}\|e_{i,j-1}(t_0)\| \\ & +\prod_{k=j}^{j-1}\Big[2\frac{\lambda_{\max}^{\frac{3}{2}}(P_{i,k})\mu_{i,(k-1)}}{\theta_{i,k}\lambda_{\min}(Q_{i,k})\lambda_{\min}^{\frac{1}{2}}(P_{i,k})}\Big]\sqrt{\frac{\lambda_{\max}(P_{i,j-2})}{\lambda_{\min}(P_{i,j-2})}}\|e_{i,j-2}(t_0)\|+\ldots \\ & +\prod_{k=j}^{2}\Big[2\frac{\lambda_{\max}^{\frac{3}{2}}(P_{i,k})\mu_{i,(k-1)}}{\theta_{i,k}\lambda_{\min}(Q_{i,k})\lambda_{\min}^{\frac{1}{2}}(P_{i,k})}\Big]\sqrt{\frac{\lambda_{\max}(P_{i,1})}{\lambda_{\min}(P_{i,1})}}\|e_{i,1}(t_0)\|. \qquad (8.26)\end{aligned}$$

8.4 Additional Results

In fact, based on Theorem 8.2.1, additional results can be obtained. Boundness of formation error is revealed by the following proposition.

Proposition 8.4.1 *Queue formation error for any robot in a queue with finite length is bounded if the initial formation errors of all the robots ahead and that of itself are bounded.* □

Proof: See Appendix A.20. □

Formation stability of each queue is worth investigating. Here, we treat each queue formation as an independent interconnected system. Suppose a team of *m* robots for the *i*th queue are all attracted to respective nearest points on the queue curve, and is to form

a specified pattern. This interconnected system can be represented as follows.

$$\begin{aligned}
\dot{e}_{i,1} &= (A_{i,1ns} - B_{i,1ns}K_{i,1ns})e_{i,1}, \\
\dot{e}_{i,2} &= (A_{i,2ns} - B_{i,2ns}K_{i,2ns})e_{i,2} - (A_{i,1ns} - B_{i,1ns}K_{i,1ns})e_{i,1}, \\
&\ldots \\
\dot{e}_{i,m} &= (A_{i,mns} - B_{i,mns}K_{i,mns})e_{i,m} - (A_{i,(m-1)ns} - B_{i,(m-1)ns}K_{i,(m-1)ns})e_{i,(m-1)},
\end{aligned} \tag{8.27}$$

where m denotes the length of the ith queue, i.e., the maximum number of robots of the queue. For convenience of expression, let e_1 denote $e_{i,1}$ and so on for the rest in Equation (8.27). Then Equation (8.27) can be rewritten into the following form.

$$\begin{aligned}
\dot{e}_1 &= (A_1 - B_1K_1)e_1, \\
\dot{e}_2 &= (A_2 - B_2K_2)e_2 - (A_1 - B_1K_1)e_1, \\
&\ldots \\
\dot{e}_m &= (A_m - B_mK_m)e_m - (A_{(m-1)} - B_{(m-1)}K_{(m-1)})e_{(m-1)}.
\end{aligned} \tag{8.28}$$

Theorem 8.4.1 *Consider the interconnected system of a queue formation described by Equation (8.28), the queue formation is globally uniformly asymptotically stable.*

Proof: See Appendix A.21. □

In real implementation of formation control, each robot is subject to malfunction or

damaged due to internal failure or external forces. Therefore for such cases, the whole team may lose some robot members.

Proposition 8.4.2 *A Queue formation with finite length given by (8.28) remains globally uniformly asymptotically stable under structure changes, i.e., when any one or more than one robots in queue quit or external robots join in.* □

Proof: See Appendix A.22. □

Remark 8.4.1 *Proposition 8.4.2 indicates that queue formation remains globally uniformly asymptotically stable when communication links among robots in the same queue intermittently break down.*

If the communication links among the robots in the same queue intermittently break down, the follower robot on the side of the broken communication link will lose the information of its leader, the one before it. Thus, all the robots behind this one will be affected. All those robots losing information of their leaders can always be identified by their own sensors.

A simple way to solve this trouble is to set the target of the whole queue to those robots behind the broken communication links until the communication links resume. When the communication links recover, the whole queue formation can be viewed as combination of discrete robot teams on the same queue and it is globally uniformly asymptotically stable as shown in the above proposition.

8.5 Conclusions

In this chapter, the stability of the formation control of multiple robots using artificial potential trench method and queue formation method is investigated. It is shown in this chapter that the closed-loop system of each robot to its leader's initial formation error be Input-to-State stable and each queue formation is global uniformly asymptotically stable. Furthermore, queue formation is robust when subject to structure changes or intermittently communication link breakdown.

Chapter 9

Conclusions

The focus of this dissertation is on the design of formation control for multi-robot systems based on the framework of queue and artificial potential trench method. Emphases are placed on multiple robot formation control laws, separation management during formation, collision prevention and obstacle avoidance, and stability analysis for the synthesized formation controls.

9.1 Contributions of this Dissertation

Generally speaking, this thesis addresses the following topics: (1) comparative investigation of two existing nonlinear feedback controls and analysis on a novel improved robust control for mobile robots; (2) real implementation and formation control experiments for a multi-robot system; (3) extracting explicit control laws and performing stability analysis which are missing from the original framework of queue and artificial potential trench method; (4) zoning potentials for distance maintaining; (5) stability

analysis on attracting robots to the nearest points on a segment and the proposal of an advanced obstacle avoidance scheme; (6) input-to-state stability.

First, we review the stability issues of nonlinear feedback control for differential mobile robots. A novel perspective on how a family of nonlinear feedback controls can be derived from Lyapunov function is presented. Then we extract the qualitative similar characteristics of two continuous nonlinear feedback controls. More importantly, for the first time, we reveal the robust control problem for a simple nonlinear tracking control and solve it through stability analysis. Stable zone for a given gain set is identified and guidelines for designing proper parameters are discussed. Due to the fruitful research, an improved robust controller is proposed. Apart from robustness, the proposed new method is capable of better performance such as faster response. This is revealed by theoretical analysis and verified through computer simulation.

Second, real implementation and formation control experiments for a multi-robot system are conducted. We integrate a series of hardware such as CCD color camera, frame grabber, radio transmission modules, other subsystems and dedicated application programmes into a setup, which provides the platform for multiple robots formation control. Noise analysis on the vision subsystem is accomplished. Finally three-robot triangle and four-robot square pattern formations of MRKIT robots are successfully demonstrated to show the effectiveness of theoretical analysis.

Third, based on the framework [29] of queue and artificial potential trench, we extract explicit multi-robot formation control laws and accomplish stability analysis which are not addressed in the original work [29]. Benefits and advantages of trench potentials

(or speed-nulling potentials) are summarized. A refined concept of artificial potential trench, which allows admissible potential functions to be nonsmooth, is defined for the first time. Various ways of constructing admissible potential trench functions are proposed. Stability of formation control based on the method of artificial potential trench is investigated through a solid mathematical nonsmooth analysis. We impose constraints on artificial potential trench to synthesize a control law that stabilizes a team of robots on a given formation. It is done without considering specific requirements on the distance between any two robots.

Fourth, we presented a complete stability of formation control for a team of robots operating as a coordinated chain, namely a group of robots organized in leader-follower pairs. Maximum and minimum separation constraints are imposed on a robot with respect to its leader. New stable controls are synthesized based on the notions of artificial potential trench. The introduction of the concept of zoning scheme, together with the associated zoning potentials, ensures that a robot maintains a certain separation from its leader while forming a formation. Computer simulation is conducted to demonstrate the effectiveness of this approach on stable formation and zoning control. These results provide a novel framework, which can analyze the stability of multi-robot formation based on the notion of artificial potential trench. While the notion of artificial potential trench provides scalability in multi-robot formation, the controls presented in this thesis ensure that such scalable formations are stable even under the constraint of coordination.

Fifth, we investigate a more generic formation control, which attracts a team of robots to the corresponding nearest points on a segment with obstacle avoidance taken into

account. A framework is developed to analyze mathematical characteristics of the motions of the nearest point on a segment. Phenomenon of nearest points' transition is revealed and the incurred discontinuity is well handled by nonsmooth analysis. We propose a novel obstacle avoidance framework based on the new concept of apparent obstacle scheme and the associated local minima recovery scheme. This new method can cope with concave obstacles and multiple moving obstacles. Comparison between the apparent obstacle avoidance method and other alternative solutions is presented and the advantages of our method are summarized. A detailed algorithm searching for the nearest point on a segment with the presence of obstacles is presented. The inherent local minima problem of potential fields has been almost avoided effectively in our work. The special cases of local minima and the corresponding simple solutions are discussed in detail. Theoretical analysis and computer simulation are carried out to show the effectiveness of this framework.

Finally, stability of the formation control of multiple robots using artificial potential trench method and queue formation method is investigated in a more generic form. It is shown that the closed-loop system of each robot is input-to-state stable to its leader's initial formation error and each queue formation is globally uniformly asymptotical stable. Furthermore, queue formation is robust when subject to structural changes or intermittent communication link breakdown.

9.2 Directions of Future Work

From a novel perspective, we present a quick review on the stability issues of nonlinear feedback control for differential mobile robots through Lyapunov function in Chapter 4. One interesting point worth noting is that a family of nonlinear control laws can be derived from a generic Lyapunov function. Another worthwhile standpoint is that these control laws may essentially have similar characteristics in common as we have demonstrated on two similar nonlinear controls. More comparative quantitative analysis on such nonlinear controls seems promising to provide interest for further research work, which may facilitate real implementations and evaluation of controller performance.

The notion of direction of attraction proposed in this thesis makes it possible for a robot to approach the segment without a pre-assigned goal point. Furthermore this new idea can usher a team of robots to reach a segment in a coordinated manner without the help of other methods such as virtual structure or virtual leaders. Directions of attraction for each robot can be varied if necessary to enhance the flexibilities or for the purpose of overcoming possible local minima. However, we do not address in detail the consolidated framework for obstacle avoidance, which takes into account obstacles and separations among robots. The extend, to which this method can cope with complicated situations of obstacle avoidance, remains unknown. Investigation on this aspect may lead to fruitful results of more flexible formation control scheme.

In obstacle avoidance and separation management via zoning potentials, the overall potentials applied on a single robot do not consider the robot's locomotion constraints,

such as maximum acceleration capabilities or maximum allowable velocity. As typical for other potential field methods, study on such constraints and its impact on performance of the formation control remains challenging. We also note that for practical implementations, the issue of boundedness of the potential functions used in the proposed controls still needs to be resolved.

Most of the works presented in this thesis focus on the stability and zoning control of the formation-forming process with or without obstacles. A logical extension is to investigate the stability and robustness of a formation when it is in pursuit of a moving goal point in complicated dynamic environments. This includes studying the ability of the team to maintain formation while avoiding obstacles (static or dynamic) and to reject disturbance experienced by the individual robots. For further research along this direction, concepts and techniques associated with the subject of vehicle-platooning may prove to be useful.

Based on the new concept of apparent obstacle scheme, and the associated local minima recovery scheme, a novel obstacle avoidance framework is proposed, which can effectively cope with concave obstacles and multiple moving obstacles without collisions. However, there is a prerequisite; the boundary of an obstacle has to be identified before the apparent obstacle scheme can be performed. This condition may seem to be too strict in the complicated unconstructed dynamic environments, even though acquisition of the obstacle's boundary information through team-wide sensor network or coordination is promising and feasible. Sometimes global information on obstacles' boundary seems unnecessary as far as sensor's detection capabilities and local obstacle avoidance

are concerned. Discussion on this issue has been addressed in Chapter 7. Moreover, another problem may arise when the apparent obstacle avoidance scheme is applied to constrained environments where global information of obstacles' boundary is unavailable or difficult to obtain. One example is shown in Figure 9.1 where a long narrow corridor is formed by two walls; the boundary information of such obstacles may be inaccessible to robots' on-board sensors. The failure of the apparent obstacle scheme

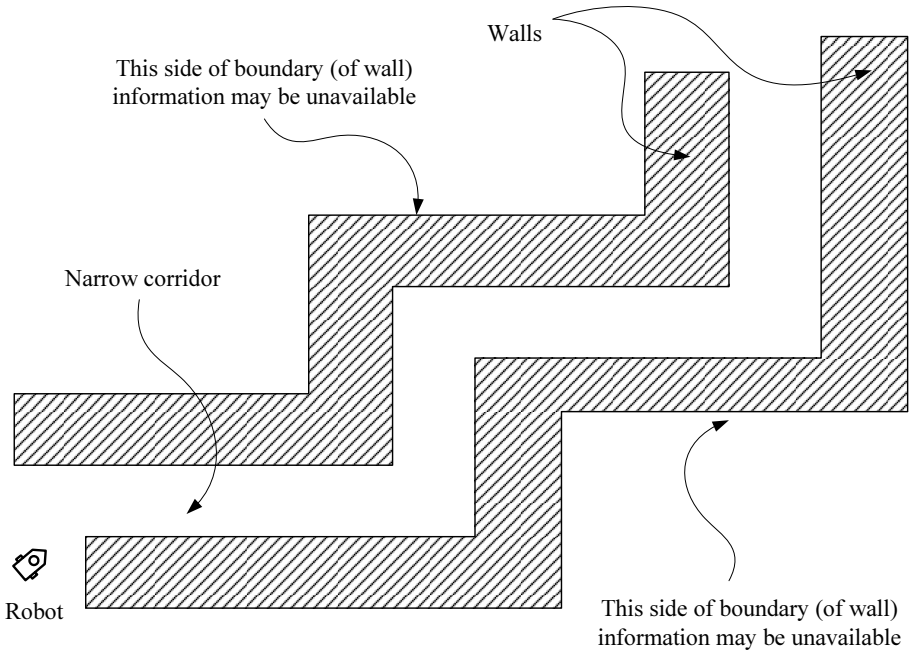

Figure 9.1: Long narrow corridors: an example of typical indoors environment.

to obtain obstacles' boundary information should not impede the robot in Figure 9.1 to pass through the narrow corridor if the separation of walls is wide enough. An important question has to be answered. What kind of improvements can be made to make the apparent obstacle scheme to work properly even with partial walls' boundary information? An improvement of apparent obstacle scheme by relaxing the prerequisite on obstacles' boundary information seems appealing. It may lessen the requirements on detecting obstacles' boundary and separations, not to mention the obvious benefits of

passing through a narrow corridor and easing the demands for computation capabilities.

Bibliography

[1] T. Arai, E. Pagello, and L. Parker. Editorial: advances in multi-robot systems. *IEEE Transactions on Robotics and Automation*, 18(5):655–661, 2002.

[2] R. C. Arkin. Motor schema based mobile robot navigation. *International Journal of Robotics Research*, 8(4):92–112, 1989.

[3] T. Balch and R. Arkin. Behavior-based formation control for multi-robot teams. *IEEE Transactions on Robotics and Automation*, 14(6):926–939, 1998.

[4] T. Balch and R. C. Arkin. Behavior-based formation control for multirobot teams. *IEEE Trans. Robot. Automat.*, 14(6):926–939, 1998.

[5] D. C. Benson. Comparison and oscillation theory for lienard's equation with positive damping. *SIAM Journal on Applied Mathematics*, 24(2):251–271, Mar. 1973.

[6] J. Borenstein and Y. Koren. The vector field histogram-fast obstacle avoidance for mobile robots. *IEEE Trans. on Robotics and Automation*, 7(3), 1991.

[7] R. W. Brockett. Control theory and singular riemannian geometry. In *New directions in applied mathematics*. Springer-Verlag, NY, 1981.

[8] R. W. Brockett. *Asymptotic stability and feedback stabilization*, pages 181–191. Birkhauser, Boston, U.S., 1983.

[9] D. C. Brogan and J. K. Hodgins. Group behaviors for systems with significant dynamics. *Autonomous Robots*, 4(1):137–153, Mar. 1997.

[10] J. Brraquand and J. C. Latombe. On nonholonomic mobile robots and optimal maneuvering. In *Proc. IEEE Conf. Intelligent Control*, pages 340–347, Albany, NY, Sep. 1989.

[11] S. Carpin and L. E. Parker. Cooperative leader following in a distributed multi-robot system. In *Proceedings. ICRA '02. IEEE International Conference on Robotics and Automation*, 2002.

[12] E. Carvalho, M. P. Silva, and C. Cardeira. Decentralized formation control of autonomous mobile robots. In *Industrial Electronics, IECON'09, 35th Anual Conference of IEEE*, pages 1504–1509, Nov. 2009.

[13] F. Clarke. *Optimization and Nonsmooth Analysis*. Classics in applied mathematics; 5. SIAM, Philadelphia, 1990.

[14] F. Clarke, Y. L. R. Stern, and P. Wolenski. *Nonsmooth Analysis and Control Theory*. Graduate Texts in Mathematics; 178. Springer, 1998.

[15] C. C. de Wit and B. Siciliano. *Theory of robot control*. Springer, 1996.

[16] C. C. de Wit and O. J. Sordalen. Exponential stabilization of mobile robots with nonholonomic constraints. *IEEE Transcations on Automatic Control*, 37(11):1791–1797, Nov. 1992.

[17] J. P. Desai, J. Ostrowski, and V. Kumar. Controlling formations of multiple mobile robots. In *Proc. IEEE Conf. Robotics and Automation*, volume 4, pages 2864–2869, Leuven, Belgium, 1998.

[18] J. P. Desai, J. P. Ostrowski, and V. Kumar. Modeling and control of formations of nonholonomic mobile robots. *IEEE Trans. Robot. Automat.*, 17(6):905–908, 2001.

[19] G. N. DeSouza and A. C. Kak. Vision for mobile robot navigation: A survey. *IEEE Transactions on Pattern Analysis and Machine Intelligence*, 24(2):237–267, 2002.

[20] W. E. Dixon, D. M. Dawson, E. Zergeroglu, and A. Behal. *Nonlinear control of wheeled mobile robots*. Springer, 2001.

[21] D. D. Dudenhoeffer and M. P. Jones. A formation behavior for large-scale micro-robot force deployment. In *Simulation Conference Proc*, pages 972–982, Dec. 2000.

[22] M. Egerstedt and X. Hu. Formation constrained multi-agent control. *IEEE Trans. Robot. Automat.*, 17(6):947–951, 2001.

[23] H. R. Everett. *Sensor for Mobile Robots, Theory and Application*. A. K. Peters, Ltd., New York, Ntick, MA, 1995.

[24] J. A. Fax and R. M. Murray. Information flow and cooperative control of vehicle formations. *IEEE Transactions on Automatic Control*, 49(9):1465–1476, Sept. 2004.

[25] R. Fierro, A. Das, V. Kumar, and J. P. Ostrowski. Hybrid control of formations

of robots. In *Proc. IEEE Conf. Robotics and Automation*, pages 157–162, Seoul, Korea, 2001.

[26] S. S. Ge and Y. J. Cui. New potential functions for mobile robot path planning. *IEEE Trans. Robot. Automat.*, 16(5):615 – 620, Oct. 2000.

[27] S. S. Ge and Y. J. Cui. Dynamic motion planning for mobile robots using potential field method. *Autonomous Robots*, 13:207–222, 2002.

[28] S. S. Ge, Y. J. Cui, and C. Zhang. Instant-goal-driven methods for behavior-based mobile robot navigation. In *Proc. IEEE International Symposium on Intelligent Control*, pages 269–275, 2003.

[29] S. S. Ge and C.-H. Fua. Queues and artificial potential trenches for multi-robot formations. *IEEE Transactions on Robotics*, 21(4):646–656, Aug. 2005.

[30] J. Godhavn and O. Egeland. A lyapunov approach to exponentially stabilization of nonholonomic systems in power form. *IEEE Transcations on Automatic Control*, 42(7):1028–1032, 1997.

[31] C. Godsil and G. Royle. *Algebraic Graph Theory*. Springer-Verlag, New York, 2nd edition, 2000.

[32] J. Gross and J. Yellen. *Graph theory and its applications*. CRC Press, Boca Raton, Fl., 1998.

[33] H. Hashimoto, F. Harashima, V. I. Utkin, S. A. Krasnova, and I. M. Kaliko. Sliding mode control and potential fields in obstacle avoidance. In *Proc. European Cont. Conf.*, pages 859–862, 1993.

[34] N. Hogan. Impedance control: an approach to manipulation: parts i-iii. *ASME J. Dynamic Syst. Measure. Contr.*, 107:1–24, 1985.

[35] L. Iocchi, D. Nardi, and M. Salerno. *Reactivity and deliberation: a survey on multi-robot systems*. Balancing Reactivity and Social Deliberation in Multi-Agent Systems: From RoboCup to Real-World Applications. Springer-Verlag, lecture notes in computer science edition, 2001.

[36] J.Baillieul. *The Geometry of Sensor Information Utilization in Nonlinear Feedback Control of Vehicle Formations*. Lecture Notes in Control and Information Sciences 309: Cooperative Control. Springer-Verlag, Berlin Heidelberg, 2005.

[37] N. Jennings, K. Sycara, and M. Wooldridge. A roadmap of agent research and development. In *Autonomous Agents and Multi-Agent Systems*, pages 7–38. Springer Verlag, July 1998.

[38] Y. Kanayama, Y. Kimura, F. Miyazaki, and T. Noguchi. A stable tracking control method for an autonomous mobile robot. In *Proc. IEEE Conf. Robotics Automation*, pages 384–389, 1990.

[39] H. K. Khalil. *Nonlinear Systems*. Prentice Hall, 3rd edition, 2002.

[40] O. Khatib. Real time obstacle avoidance for manipulators and mobile robots. *Int. J. Robot. Res.*, 5(1):90–98, 1986.

[41] J.-O. Kim and P. Khosla. Real-time obstacle avoidance using harmonic potential functions. In *Proc. IEEE Conf. Robotics and Automation*, pages 790–796, 1991.

[42] D. E. Koditschek. Exact robot navigation by means of potential functions: some topological considerations. In *Proc. IEEE Conf. Robotics and Automation*, pages 1–6, 1987.

[43] I. Kolmanovsky and N. H. McClamroch. Developments in nonholonomic control problems. *IEEE Control Systems Magazine*, 15:20–36, 1995.

[44] T. J. Koo and S. M. Shahruz. Formation of a group of unmanned aerial vehicles (uavs). In *Proc. of the American Control Conference*, 2001.

[45] Y. Koren and J. Borenstein. Potential field methods and their inherent limitations for mobile robot navigation. In *Proc. IEEE Conference on Robotics and Automation*, pages 1398–1404, Sacramento, CA, Apr. 1991.

[46] W. Kowalczyk. Target assignment strategy for scattered robots building formation. ro-moco '02. In *Proceedings of the Third International Workshop on Robot Motion and Control*, 2002.

[47] B. H. Krogh. A generalized potential field approach to obstacle avoidance control. In *Proc. SME Conf. Robot. Res.*, 1984.

[48] G. Lafferiere and H. J. Sussmann. Motion planning for controllable system without drift. In *Proc. IEEE Conf. Robotics and Automation*, pages 1148–1153, Sacramento, CA, Apr. 1991.

[49] G. Lafferriere, J. Caughman, and A. Williams. Graph theoretic methods in the stability of vehicle formations. In *Proc. of the American Control Conference*, pages 3729–3734, Boston, Massachusetts, June 2004.

[50] J.-C. Latombe. *Robot Motion Planning*. Kluwer Academic Publishers, Boston, 1991.

[51] D. J. Lee. *Passivity-based switching control for stabilization of wheeled mobile robots*. Robotics: Science and Systems III. The MIT Press, Ceorgia Institute of Technology, Atlanta, Geogia, USA, June 2007.

[52] D. J. Lee and P. Y. Li. Passive decomposition approach to formation and maneuver control of multiple agents with inertias. *Journal of Dynamical Systems, Measurement and Control*, 129:662–677, 2007.

[53] S. O. Lee, Y. J. Cho, M. H. B., B. J. You, and S. R. Oh. A stable target-tracking control for unicycle mobile robots. In *Proc. IEEE/RSJ Conf. Intelligent Robots and Systems*, pages 1822–1827, Takamatsu, Japan, 2000.

[54] N. E. Leonard and E. Fiorelli. Virtual leaders, artificial potentials and coordinated control of groups. In *Proc. 40th IEEE Conf. Decision and Control*, pages 2968–2973, Orlando, FL, 2001.

[55] M. A. Lewis and K.-H. Tan. High precision formation control of mobile robots using virtual structuresirtual structures. *Autonomous Robots*, 4(4):387–403, 1997.

[56] Z. Lin, B. Francis, and M. Maggiore. Feasibility for formation stabilizaiton of multiple unicycles. In *Proc. of the IEEE International Conference on Decision and Control*, pages 1796–1801, Atlantis, Paradise Island, Bahamas, Dec. 2004.

[57] C. Q. Liu, M. H. A. Jr., H. Krishnan, and L. S. Yong. Virtual ostacle concept for local-minimum-recovery in potential-field based navigation. In *Proc. of the*

2000 IEEE Internal Conference on Robotics and Automation, pages 983–988, San Francisco, CA, Apr. 2000.

[58] J. Liu and J. Wu. *Multi-agent robotic systems*. CRC Press, London, 2001.

[59] A. D. Luca, G. Oriolo, and M. Vendittelli. *Control of Wheeled Mobile Robots: An Experimental Overview*. Lecture Notes in Control and Information Sciences 270: RAMSETE. Springer-Verlag, Berlin Heidelberg, 2001.

[60] J. A. Marshall, M. E. Broucke, and B. A. Francis. Unicycles in cyclic pursuit. In *Proc. of the 2004 American Control conference*, pages 5344–5349, Boston, Massachusetts, June 2004.

[61] D. Q. Mayne. Control of constrained dynamic systems. *European Journal of Control*, 7:87–99, 2001.

[62] D. Q. Mayne, J. B. Rawlings, C. V. Rao, and P. O. M. Scokaert. Contrained model predictive control: Stability and optimality. *Automatica*, 36:789–814, 2000.

[63] R. M'Closkey and R. Murray. Exponentially stabilization of driftless nonlinear control systems using homogeneous feedback. *IEEE Transactions on Automatic Control*, 42(5):614–628, May 1997.

[64] M. B. Milam, K. Mushambi, and R. M. Murray. A new computational approach to real-time trajectory generation for constrained mechanical systems. In *Proc. of the Conference on Decision and Control*, 2000.

[65] S. Monteiro and E. Bicho. A dynamical systems approach to behaviorbased for-

mation control. In *Proc. of the IEEE International Conference on Robotics and Automation*, pages 2606–2611, May 2002.

[66] R. M. Murray and S. S. Sastry. Steering nonholonomic systems using sinusoids. In *Proc. IEEE Conf. Decision and Control*, pages 2097–2101, Honolulu, HI., Dec. 1990.

[67] P. Ogren, M. Egerstedt, and X. Hu. A control lyapunov function approach to multi-agent coordination. *IEEE Transactions on Robotics and Automation*, 18(5):847–851, Oct. 2002.

[68] M. Okutomi and M. Mori. Decision of robot movement by means of a potential field. *Advanced Robot*, 1(2):131–141, 1986.

[69] M. E. P. Ogren and X. Hu. A control lyapunov function approach to multiagent coordination. *IEEE Trans. Robot. Automat.*, 18(5):847–851, 2002.

[70] B. E. Paden and S. S. Sastry. Calculus for computing filipov's differential inclusion with application to the variable structure control of robot manipulators. *IEEE Transactions on Circuits and Systems*, CAS-34:73–82, 1987.

[71] J. H. Reif and H. Wang. Social potential fields: a distributed behavioral control for autonomous robots. *Robotics and Autonomous Systems*, 27:171–194, 1999.

[72] W. Ren and R. W. Beard. A decentralized scheme for spacecraft formation flying via the virtual structure approach. In *Proc. American Control Conf.*, volume 2, pages 1746–1751, Denver, Colorado, 2003.

[73] C. Reynolds. Flocks, herds and schools: a distributed behavioral model. *Computer Graphics*, 21(4):25–34, 1987.

[74] E. Rimon and D. E. Koditschek. Exact robot navigation using cost functions: the case of distinct spherical bounddaries. In *Proc. IEEE Conf. Robotics and Automation*, pages 1791–1796, 1988.

[75] E. Rimon and D. E. Koditschek. Exact robot navigation using artificial potential functions. *IEEE Trans. Robot. Automat.*, 8(5):501–518, 1992.

[76] J. Rosenblatt. Damn: a distributed architecture for mobile navigation. In *Working Notes AAAI 1995 Spring Symposium: Lessons Learned for Implemented Software Architectures for Physical Agents*, Palo Alto, CA,, Mar. 1995.

[77] D. Shevitz and B. Paden. Lyapunov stability theory of nonsmooth systems. *IEEE Transactions on Automatic Control*, 39(9):1910–1914, 1994.

[78] R. Siegwart and I. Nourbakhsh. *Introduction to Autonomous Mobile Robots*, chapter 2, pages 13–46. MIT Press, March 2004.

[79] E. D. Sontag and Y. Wang. On characterizations of input-to-state stability property. *Systems & Control Letters*, 24:351–359, 1995.

[80] S. Spry and J. K. Hedrick. Formation control using generalized coordinates,. In *Proc. of IEEE International Conference on Decision and Control*, pages 2441–2446, Atlantis, Paradise Island, Bahamas, Dec. 2004.

[81] H. Takahashi, H. Nishi, and K. Ohnishi. Autonomous decentralized control for for-

mation of multiple mobile robots considering ability of robot. *IEEE Transactions on Industrial Electronics*, 51(6):1272–1279, Dec. 2004.

[82] H. G. Tanner. On the controllability of nearest neighbor interconnections. In *Proc. of the IEEE Conference on Decision and Control*, pages 2467–2472., Atlantis, Paradise Island, Bahamas, Dec. 2004.

[83] H. G. Tanner, A. Jadbabaie, and G. J. Pappas. Stable flocking of mobile agents – part ii: dynamic topology. In *Proc. of the 42nd IEEE Conference on Decision and Control*, pages 2016–2021, Maui, Hawali, USA, Dec. 2003.

[84] H. G. Tanner and G. J. Pappas. Formation input-to-state stability. In *Proc. IFAC 15th World Congress*, Barcelona, Spain, 2002.

[85] T.Blach and M.Hybinette. Social potentials for scalable multi-robot formations. In *Proc. IEEE Conf. Robotics and Automation*, volume 1, pages 73–81, San Francisco, CA, April 2000.

[86] A. Teel, R. Murray, and C. Walsh. Nonholonomic control systems: from steering to stabilization with sinusoids. *Int. Journal Control*, 62(4):849–870, 1995.

[87] X. Tu and D. Terzopoulos. Artificial fishes: physics, locomotion, perception, behavior. In *Proc. SIGGRAPH 94 Conference*, pages 43–50, Orlando, FL, July 1994.

[88] V. I. Utkin, S. Drakunov, H. Hashimoto, and F. Harashima. Robot path obstacle avoidance control via sliding mode approach. In *Proc. IEEE/RSJ Int. Workshop on Intell. Robots and Syst.*, pages 1287–1290, 1991.

[89] M. Van Fosson. Role of robotics in ground combat of the future. In *Proceedings of the SPIE Conference on Unmanned Ground Vehicle Technology III*, pages 16–17, Orlando, U.S.A., April 2001.

[90] S. L. Veherencamp. Individual, kin, and group selection. In P. Marler and J. G. Vandenbergh, editors, *Handbook of Behavioral Neurobiology, Volume 3: Social Behavior and Communication*, pages 354–382. New York, 1987.

[91] R. Volpe and P. Khosla. Artificial potentials with elliptical isopotential contours for obstacle avoidance. In *Proc. IEEE Conf. Decision and Control*, pages 180–185, 1987.

[92] P. Wang. Navigation strategies for multiple autonomous mobile robots moving in formation. *J. Robotic Systems*, 8(2):177–195, 1991.

[93] P. Wang and F. Hadaegh. Self-organizing control of multiple free-flying miniature spacecraft in formation. In *AIAA Guidance, Navigation, and Control Conference*, 2000.

[94] R. L. Wernli. Low cost uuv's for military applications: Is the technology ready? In *Pacific Congress on Marine Science and Technology 2001*, San Francisco, CA, July 8-11 2001.

[95] M. Yamakita and M. Saito. Formation control of smc with multiple coordinate systems. In *Proc. of the International Conference on Intelligent Robots and Systems*, pages 1023–1028, Sendai, Japan, Sept. 2004.

[96] J. Yan and R. R. Bitmead. Coordinated control and information architecture. In

Proc. of the 42nd IEEE Conference on Decision and Control, pages 3919–3923, Dec. 2003.

[97] X. Yun, G. Alptekin, and O. Albayrak. Line and circle formation of distributed physical mobile robots. *Journal of Robotic Systems*, 14(2):63–76, 1997.

[98] X. Yun and Y. Yamamoto. Internal dynamics of a wheeled mobile robot. In *Proceedings of the 1993 IEEE/RSJ International Conference on Intelligent Robots and Systems*, pages 1288–1294, Yokohama, Japan, July 26-30 1993.

[99] M. G. Zhang and P. S. Krishnaprasad. Control of small formaiton using shape coordinates. In *Proc. of the International conference on Robotics and Automation*, pages 2510–2446, Taipei, Taiwan, Sept. 2003.

Author's Publications

Journal Papers

1. Peter C. Y. Chen, Jie Wan, Aun N. Poo, and Shuzhi S. Ge. Formation and zoning control of multi-robot systems. *International Journal of Robotics and Automation*, Issue 1, Volume 26, 2011

Book Chapters

1. Jie Wan and Peter C. Y. Chen. A Robust Nonlinear Control for Differential Mobile Robots and Implementation on Formation Control. *Multi-Robot Systems, Trends and Development*. pages 71 - 94, ISBN: 978-953-307-425-2, InTech, January, 2011

Conference Papers

1. Jie Wan and Peter C. Y. Chen. Analysis on nonlinear feedback controls for differential mobile robots and its application to multi-robot formation control-part one. In

Proceedings of the 10th International Conference on Control, Automation, Robotics and Vision(ICARCV), pages 1224 - 1229, Hanoi, Vietnam, Dec. 2008.

2. Jie Wan and Peter C. Y. Chen. Analysis on nonlinear feedback controls for differential mobile robots and its application to multi-robot formation control-part two. In *Proceedings of the 10th International Conference on Control, Automation, Robotics and Vision(ICARCV)*, pages 1987 - 1992, Hanoi, Vietnam, Dec. 2008.

3. Peter C. Y. Chen, Jie Wan, Aun N. Poo, and Shuzhi S. Ge. Tracking control of mobile robots and its application to formation control. In *Proceedings IEEE International Conference on System, Man and Cybernetics*, pages 3132 - 3137, Singapore, Oct. 2008.

Appendix

A.1 Proof of Proposition 4.1.1

The proof for this proposition is straightforward by constructing a Lyapunov function candidate as

$$V = \frac{1}{2}r^2 + \frac{1}{2}\phi^2. \tag{1}$$

Simplifying Equation (4.2) leads to

$$\begin{aligned}
\begin{bmatrix} \dot{r} \\ \dot{\phi} \end{bmatrix} &= \begin{bmatrix} -g_1(r,\phi)\cos(\phi) \\ \frac{1}{r}g_1(r,\phi) + g_2(r,\phi) \end{bmatrix} \begin{bmatrix} r \\ \phi \end{bmatrix} + \begin{bmatrix} 0 \\ -g_1(r,\phi)\sin(\phi) \end{bmatrix} \\
&= \begin{bmatrix} -rg_1(r,\phi)\cos(\phi) \\ g_1(r,\phi)\sin(\phi) + \phi g_2(r,\phi) \end{bmatrix} + \begin{bmatrix} 0 \\ -g_1(r,\phi)\sin(\phi) \end{bmatrix} \\
&= \begin{bmatrix} -rg_1(r,\phi)\cos(\phi) \\ \phi g_2(r,\phi) \end{bmatrix}.
\end{aligned} \tag{2}$$

From Equations (2) and (4.3), the first time derivative of V can be calculated readily as

$$\begin{aligned}\dot{V} &= r\dot{r} + \phi\dot{\phi} \\ &= -r^2 g_1(r,\phi)\cos(\phi) + \phi^2 g_2(r,\phi) \\ &= -K_1\phi^{2q} r^{n+2}(\cos(\phi))^{2p+2} - K_2\phi^{2s+2} \leq 0, \end{aligned} \tag{3}$$

thus completes the proof.

A.2 Proof of Proposition 4.1.2

Obviously, if we let $n = p = q = s = 0$, then Equation (4.4) can be reduced into the simplest form as shown below:

$$\begin{aligned} v &= K_1 r\cos(\phi), \\ \omega &= -K_1\sin(\phi)\cos(\phi) - K_2\phi, \end{aligned}$$

which turns out to be Equation (3.10) that is first proposed in [53].

However, it is noted that control in Equation (3.10) is actually not the "simplest". We can adopt another family of possible functions $g_1(r,\phi)$ and $g_2(r,\phi)$ as: $g_1(r,\phi) = K_1 r^n \phi^{2q}$, and $g_2(r,\phi) = -K_2\phi^{2s}$, where $n = 0,1,2,\cdots$, $p = 0,1,2,\cdots$ and $s = 0,1,2,\cdots$. There-

fore a more simplified control law can be found as follows:

$$\begin{aligned} v &= K_1 r, \\ \omega &= -K_1 \sin(\phi) - K_2 \phi, \end{aligned}$$

which is identical to the control law presented in Equation (3.9) by simply letting $n = q = s = 0$.

A.3 Proof of Proposition 4.2.2

To complete the proof of this proposition, we need to transform the solution $r(t)$ of the closed-loop system into the following form:

$$\begin{aligned} r(t) &= r_0 e^{-K_1 \int_0^t \cos^2(\phi_0 e^{-K_2 s}) ds} \\ &= r_0 e^{-K_1 \int_0^t \frac{1+\cos(2\phi_0 e^{-K_2 s})}{2} ds} \\ &= r_0 e^{-\frac{K_1}{2} t} e^{-K_1 \int_0^t \frac{\cos(2\phi_0 e^{-K_2 s})}{2} ds} \\ &= r_0 e^{-\frac{K_1}{2} t + \frac{K_1}{2K_2} \int_{2\phi_0}^{2\phi(t)} \frac{\cos(u)}{u} du}. \end{aligned} \tag{4}$$

We assume that there are two different sets of nonzero gains (K_1, K_2) and (J_1, J_2) that meets $\lambda = \frac{K_1}{K_2} = \frac{J_1}{J_2}$. Based on the results in Equation (4), the trajectory generated by the gain set (K_1, K_2) will be solely determined by $r_1(t)$ and $\phi_1(t)$, namely the solutions of

the closed-loop system, as shown below:

$$\begin{aligned} r_1(t) &= r_0 e^{-\frac{K_1}{2}t+\frac{\lambda}{2}\int_{2\phi_0}^{2\phi_1(t)}\frac{\cos(u)}{u}du}, \\ \phi_1(t) &= \phi_0 e^{-K_2 t}. \end{aligned}$$

Similarly, the solutions $r_2(t)$ and $\phi_2(t)$ of the same closed-loop system corresponding to another gain set (J_1, J_2) can be derived as

$$\begin{aligned} r_2(\tau) &= r_0 e^{-\frac{J_1}{2}\tau+\frac{\lambda}{2}\int_{2\phi_0}^{2\phi_2(\tau)}\frac{\cos(u)}{u}du}, \\ \phi_2(\tau) &= \phi_0 e^{-J_2\tau}, \end{aligned}$$

where τ denotes time in domain $[0,+\infty)$. For $\forall t \in [0,+\infty)$, we can always find a $\tau \in [0,+\infty)$ by taking $\tau = \frac{K_2}{J_2}t$. Then it follows that $\phi_2(\tau) = \phi_0 e^{-J_2\tau} = \phi_0 e^{-K_2 t} = \phi_1(t)$.

On the other hand, since we have

$$\frac{J_1}{2}\tau = \frac{J_1}{2}\cdot\frac{K_2}{J_2}t = \frac{K_1}{2}\cdot\frac{K_2}{K_2}t = \frac{K_1}{2}t,$$

then we arrive at the conclusion that $r_2(\tau) = r_1(t)$. Thus the proof is completed.

A.4 Proof of Proposition 4.3.2

It is noted that the equation

$$\dot{\phi} = -K_2\phi - K_4\sin(2\phi)$$

has a unique solution on time interval $[0,t_1)$ for any $t_1 > 0$ because $f(\phi) = -K_2\phi - K_4\sin(2\phi)$ is locally Lipschitz. Let $p(t) = \phi^2(t)$, then

$$\begin{aligned}
\dot{p}(t) &= 2\phi\dot{\phi} \\
&= -2K_2\phi^2 - 2K_4\phi\sin(2\phi) \\
&\leq -2K_2\phi^2 \\
&= -2K_2 p(t).
\end{aligned}$$

Let $q(t)$ be the solution of $\dot{q}(t) = -2K_2 q(t)$ with $q(0) = \phi(0)$, given by $q(t) = \phi^2(0)e^{-2K_2 t}$. According to the comparison principle, the solution $\phi(t)$ is defined for all $t \geq 0$ and satisfies

$$|\phi(t)| = \sqrt{p(t)} \leq |\phi(0)|e^{-K_2 t}, \forall t \geq 0,$$

thus the proof is completed.

A.5 Proof of Proposition 5.2.1

Since $\ddot{\vec{r}}_i = \vec{u}_i$ and $\vec{d}_{i,g} = \vec{r}_{i,g} - \vec{r}_i$, we have $\ddot{\vec{d}}_{i,g} = -k_i\dot{\vec{d}}_{i,g} - \Phi'_{i,g}\hat{d}_{i,g}$, which can be expressed as

$$\frac{d}{dt}\begin{bmatrix} \vec{d}_{i,g} \\ \dot{\vec{d}}_{i,g} \end{bmatrix} = \begin{bmatrix} \dot{\vec{d}}_{i,g} \\ -k_i\dot{\vec{d}}_{i,g} - \Phi'_{i,g}\hat{d}_{i,g} \end{bmatrix} = f(\vec{d}_{i,g}, \dot{\vec{d}}_{i,g}). \tag{5}$$

Equation (40) is time-invariant, with the origin $\vec{d}_{i,g} = 0$ being the equilibrium point since for an admissible $\Phi_{i,g}$, $0 \in \partial\Phi(0)$.

We choose the following Lyapunov function candidate (which is time-independent, Lipschitz and regular)

$$V_i = V_i(\vec{d}_{i,g}, \dot{\vec{d}}_{i,g}) = \frac{1}{2}\dot{\vec{d}}_{i,g}^T\dot{\vec{d}}_{i,g} + \Phi(d_{i,g})\,. \tag{6}$$

By the Generalized Gradient Formula [14], the generalized gradient of $\Phi(d_{i,g})$ with respect to $\vec{d}_{i,g}$ is

$$\partial\Phi(\vec{d}_{i,g}) = \overline{co}\{\lim\nabla\Phi(\vec{d}) \mid \vec{d} \to \vec{d}_{i,g}, \vec{d} \notin \Omega_f\}, \tag{7}$$

with Ω_f being the set of Lebesgue measure zero where the gradient of $\Phi(\vec{d}_{i,g})$ is not defined. Furthermore the relationship

$$\frac{d\Phi(\vec{d}_{i,g})}{d(\vec{d}_{i,g})} = \frac{d\Phi(d_{i,g})}{d(d_{i,g})} \cdot \frac{d(d_{i,g})}{d(\vec{d}_{i,g})} = \Phi'_{i,g}\hat{d}_{i,g},$$

reduces Equation (42) to $\partial\Phi(\vec{d}_{i,g}) = \partial\Phi\hat{d}_{i,g}$. By the Chain Rule Theorem [77], we have

$$\frac{d}{dt}V_i(\vec{d}_{i,g},\dot{\vec{d}}_{i,g}) \in^{a.e.} \dot{\tilde{V}}_i(\vec{d}_{i,g},\dot{\vec{d}}_{i,g}), \tag{8}$$

where $\dot{\tilde{V}}_i(\vec{d}_{i,g},\dot{\vec{d}}_{i,g}) = \bigcap_{\xi\in\partial V_i(\vec{d}_{i,g},\dot{\vec{d}}_{i,g})} \xi^T K[f](\vec{d}_{i,g},\dot{\vec{d}}_{i,g})$, with K being a map (as defined and discussed in detail in [70]) having, for this case, the specific form

$$K[f](\vec{d}_{i,g},\dot{\vec{d}}_{i,g}) = \begin{bmatrix} \dot{\vec{d}}_{i,g} \\ -k_i\dot{\vec{d}}_{i,g} - \partial\Phi(d_{i,g})\hat{d}_{i,g} \end{bmatrix}. \tag{9}$$

For brevity, we write $\dot{\tilde{V}}_i(\vec{d}_{i,g},\dot{\vec{d}}_{i,g})$ simply as $\dot{\tilde{V}}_i$ in the sequel. From Equation (13), we have

$$\partial V_i(\vec{d}_{i,g},\dot{\vec{d}}_{i,g}) = \begin{bmatrix} \partial\Phi(d_{i,g})\hat{d}_{i,g} \\ \dot{\vec{d}}_{i,g} \end{bmatrix}. \tag{10}$$

Substituting Equations (45) and (44) into Equation (43) yields $\dot{\tilde{V}}_i = -k_i\left\|\dot{\vec{d}}_{i,g}\right\|^2$, which is negative semidefinite. By the nonsmooth version of LaSalle's Theorem [77], the largest invariant set is $E = cl\left(\{(\vec{d}_{i,g},\dot{\vec{d}}_{i,g})|0\in\dot{\tilde{V}}_i\}\right) = (\vec{0},\vec{0})$, which implies that the origin is asymptotically stable.

A.6 Proof of Lemma 5.2.1

1) Since $f(x)$ is essentially bounded, we can assume that there exists a positive constant M such that $|f(x)| \leq M$ for any $x \notin \Omega_f$, where Ω_f denotes any set of measure zero on

which $f(x)$ is unbounded. For any two points x and y in the domain R, we obtain $F(y) - F(x) = \int_x^y f(s)ds \leq M|y-x|$. It means that F is Lipschitzian on the whole domain.

By definition, we can calculate the generalized directional derivative (represented by symbol $F^o(x;v)$) and the usual one-sided directional derivative (represented by symbol $F'(x;v)$) of F at x in the direction of v as

$$\begin{aligned} F^o(x;v) &= \lim_{\substack{y \to x \\ t \downarrow 0}} \sup \frac{F(y+tv) - F(y)}{t} \\ &= \lim_{t \downarrow 0} \frac{\int_0^{tv} f(s)ds}{t}, \end{aligned}$$

and

$$\begin{aligned} F'(x;v) &= \lim_{t \downarrow 0} \frac{F(x+tv) - F(x)}{t} \\ &= \lim_{t \downarrow 0} \frac{\int_0^{tv} f(s)ds}{t} \end{aligned}$$

respectively. It is shown above that $F^o(x;v) = F'(x;v)$ holds at any point x in the domain. Thus we can draw the conclusion that F is regular.

2) A convenient way to complete the proof is to invoke the Generalized Gradient Formula Theorem [14]. For δ -neighborhood of point x, by this theorem, we can calculate the gradient of $F(x)$ as

$$\partial F(x) = \overline{co}\{lim \nabla F(x_i) \mid x_i \to x, x_i \in B_r, \text{ and } x_i \notin \Omega_f\},$$

where $B_r = [x-\delta, x+\delta]$ and Ω_f denotes set of measure zero where the gradient of $F(x)$ is not defined. As $f^-(x)$ and $f^+(x)$ are the essential supremum and essential infimum of f at x, then we have

$$\partial F(x) = [f^-(x), f^+(x)].$$

If F is strictly differentiable at point x, it means that $f^-(x) = f^+(x) = f(x)$. Therefore $\partial F(x)$ is reduced to $\partial F(x) = \{f(x)\}$.

A.7 Proof of Lemma 5.2.2

1) It is obvious that $F(0) = \int_0^0 f(s)ds = 0$. For an arbitrary small positive scalar ε, we investigate the integral of $f(x)$ on the interval $[0, \varepsilon]$. If there are no points in this interval such that the condition $xf(x) > 0$ fails, then we reach the conclusion that the integral $F(\varepsilon) = \int_0^\varepsilon f(s)ds > 0$. If the interval contains points where the condition $xf(x) > 0$ does not hold, then without loss of generality, we can assume that there are N points denoted by $0 < x_1 < x_2 < \cdots < x_{N-1} < x_N < \varepsilon$ where the condition $xf(x) > 0$ is not met. The whole interval $[0, \varepsilon]$ is separated into $N+1$ smaller intervals as $[0, x_1)$,(x_1, x_2),$\cdots$,(x_{N-1}, x_N),(x_N, ε). Then on each interval, the integral of $f(x)$ exists and is positive. Consequently the sum of all the integral of these $N+1$ intervals, namely, $F(\varepsilon)$ is greater than zero. In the case when $\varepsilon < 0$, through a similar method, the same conclusion holds. Moreover, we can prove that $F(x)$ is monotonically increasing on domain $[0, +\infty)$ and monotonically decreasing on domain $(-\infty, 0]$. Let us investigate the interval $[x, x+\varepsilon]$, where $x \geq 0$ and ε is an arbitrary small positive scalar. Through

similar procedures, we have $F(x+\varepsilon) > F(x)$ thus $F(x)$ is monotonically increasing on domain $[0,+\infty)$. Similarly, we can prove that $F(x)$ is monotonically decreasing on domain $(-\infty,0]$. To sum up, F is positive definite.

2) From the proof procedures of Lemma 5.2.1, it is shown that at the origin, we have $\partial F(0) = [f^-(0), f^+(0)]$. Since we have $f(x) > 0$ for $x > 0$ and $f(x) < 0$ for $x < 0$ from the given condition $xf(x) > 0$ for $x \neq 0$, then there must exist $f^-(0) \leq 0$ and $f^+(0) \geq 0$. Hence zero is contained in the set $\partial F(0)$.

A.8 Proof of Lemma 5.2.3

Here, we will apply a property of convex functions as follows:

Proposition A.8.1 *A differentiable function of one variable is convex on an interval if and only if its derivative is monotonically non-decreasing on that interval.*

Suppose that $f(0) < 0$, then there must exist an non-trivial interval $[0,\varepsilon]$ such that on this interval condition $f(x) < 0$ strictly holds due to continuity of f (from given condition that $F(x)$ is continuously differentiable.). So the integral of f on this interval is less than zero. Since the integral of f on this interval can be represented by $\int_0^\varepsilon f(s)ds = F(\varepsilon) - F(0) = F(\varepsilon)$ because $F(0) = 0$. Therefore, we have $F(\varepsilon) < 0$ which contradicts the given condition that F is positive definite. Similarly, we can prove that $f(0) > 0$ will contradicts the positive definite condition too. Finally, we have $f(0) = 0$. Thus the proof is completed .

A.9 More Examples of Potential Trench Functions

Since we can decompose vector $\vec{r}$ into scalar components in Cartesian coordinates, then we can simplify the error dynamics into a differential equation which is commonly referred to as Lienard's Equation:

$$\ddot{x} + k(x)\dot{x} + \phi(x) = 0, \tag{11}$$

which has been investigated for many years. In 1973, D. C. Benson published some fundamental results [5] on the solution of this equation in the case of positive damping. Some of these results can be used in this thesis. Two concepts have to be addressed before presenting the relevant material. Both of the concepts and Corollary A.9.1 are from Benson's paper [5]. Regarding the Lienard's Equation, we define two potential functions as

$$K(x) = \int_0^x k(\xi)d\xi$$
$$\Phi(x) = \int_0^x \phi(\xi)d\xi$$

Definition A.9.1 *(Oscillation at $+\infty$:) A solution of Equation (11) is said to oscillate at $+\infty$ if it has a sequence of zeros tending to $+\infty$ and if it is not identically zero on any interval.* □

Definition A.9.2 *(Critical Damping:) The Equation (11) is said to has critical damping at $+\infty$ if*

(i) there exists a nonoscillatory (at $+\infty$) solution to Equation (11), and
(ii) all solutions oscillate at $+\infty$ provided that exist $\eta > 1$ and $\varepsilon > 0$ such that

$$\frac{\Phi_1(x)}{K_1^2(x)} \geq \eta \frac{\Phi(x)}{K^2(x)}$$

for all x such that $0 < |x| < \varepsilon$. □

Corollary A.9.1 *For Equation(11), let $k(x) > 0$ and $x\phi(x) > 0$* for $x \neq 0$, then the zero solution will be critically damped at $+\infty$ if $\int_0^1 \frac{1}{K(x)} dx = \infty$ and $\Phi(x) = \frac{1}{8}K^2(x)$.

The above corollary is useful because it reveals the information on the solutions of Equation (11) and also presents a hint to construct potential trench functions.

Example A.9.1 *Let $k(x) = C$, where C is a positive scalar. Obviously we can obtain the following results:*

$$K(x) = \int_0^x k(\xi) d\xi = Cx,$$

$$\int_{0+}^1 \frac{1}{K(x)} = \frac{1}{C} \ln x \Big|_{0+}^1 = \infty.$$

Accordingly the trench potential function which leads to critical damping can be calculated as

$$\Phi(x) = \frac{1}{8}K^2(x) = \frac{C^2}{8}x^2,$$

$$\phi(x) = \frac{C^2}{4}x.$$

In fact, this example is the simplest case because the corresponding differential equation can be solved readily and is very common in control engineering. It is observed that $\Phi(x) = \frac{\alpha}{2}x^2$ is a commonly used attractive potential [26], where α is a positive scalar.

□

Example A.9.2 *If let* $k(x) = \frac{\alpha|x|}{\sqrt{x^2+a^2}}$*,where* $\alpha > 0$*,* $a > 0$ *are all positive scalars and it means* $K(x) = \int_0^x k(\xi)d\xi = \alpha \cdot sgn(x)(\sqrt{x^2+a^2} - a)$*. It is easy to check that* $\int_{0+}^{1} \frac{1}{K(x)} = \infty$ *as shown by the following equation.*

$$\int_{0+}^{1} \frac{1}{K(x)}dx = \left[\frac{1}{\alpha}\ln|x+\sqrt{x^2+a^2}| - \frac{\sqrt{x^2+a^2}+a}{\alpha x}\right]_{0+}^{1} = \infty.$$

According we can invoke the Corollary A.9.1, and derive the potential trench function as

$$\Phi(x) = \frac{1}{8}K^2(x) = \frac{\alpha^2}{8}(\sqrt{x^2+a^2} - a)^2.$$

And the corresponding ϕ *can be derived as*

$$\phi(x) = \frac{1}{4}K(x)k(x) = \frac{\alpha^2 x^3}{4(x^2+a^2+a\sqrt{x^2+a^2})}.$$

□

Example A.9.3 *Let us consider the saturated potential trench functions taking the same form as given by Example A.9.2. Without loss of generality, we assume that* $k(x)$ *becomes saturated when* $|x| > 1$ *as shown below:*

$$k(x) = \begin{cases} \frac{\alpha|x|}{\sqrt{x^2+a^2}} & |x| \le 1 \\ \frac{\alpha}{\sqrt{a^2+1}} & |x| > 1 \end{cases}$$

Readily we can calculate the expression of $K(x)$ as

$$K(x) = \begin{cases} \frac{\alpha(x+a^2)}{\sqrt{a^2+1}} - a\alpha & x > 1 \\ \alpha(\sqrt{x^2+a^2} - a) & |x| \leq 1 \\ \frac{\alpha(x-a^2)}{\sqrt{a^2+1}} + a\alpha & x < -1 \end{cases}$$

According to the relationship that $\phi(x) = \frac{1}{4}K(x)k(x)$, we obtain the expression of $\phi(x)$ which leads to critical damping as shown be the following equation.

$$\phi(x) = \begin{cases} \frac{1}{4}[\frac{\alpha^2(x+a^2)}{a^2+1} - \frac{a\alpha^2}{\sqrt{a^2+1}}] & x > 1 \\ \frac{\alpha^2 x^3}{4(x^2+a^2+a\sqrt{x^2+a^2})} & |x| \leq 1 \\ \frac{1}{4}[\frac{\alpha^2(x-a^2)}{a^2+1} + \frac{a\alpha^2}{\sqrt{a^2+1}}] & x < -1 \end{cases}$$

□

The concept of critical damping and Corollary A.9.1 is important in the sense that for given trench potential function, the response is of practical implications. For some cases overshooting (under-damping) is preferred and in some applications over-damping is required. For the look-ahead control of mobile robots, overshooting is not preferred. To cope with it, we can adjust the damping term to be critical damping or under-damping. Take the damping term in Example A.9.2 for example, if we let

$$\phi_1(x) = \frac{\beta^2 x^3}{4(x^2+a^2+a\sqrt{x^2+a^2})},$$

where $\beta > \alpha$, obviously it will lead the zero solution to be over-damping.

A.10 Proof of Theorem 5.3.1

In order to derive the error dynamics of $\vec{r}_i$, combining the double integrator dynamics for $\vec{r}_i$ and control law in Equation (5.2) with the knowledge $\vec{d}_{i,g} = \vec{r}_{i,g} - \vec{r}_i$ yields,

$$\begin{aligned} \ddot{\vec{r}}_i &= \ddot{\vec{r}}_{i,g} + K'_{i,g}\dot{\vec{d}}_{i,g} + \Phi'_{i,g}\hat{d}_{i,g}, \\ \ddot{\vec{d}}_{i,g} &= -K'_{i,g}\dot{\vec{d}}_{i,g} - \Phi'_{i,g}\hat{d}_{i,g}. \end{aligned} \tag{12}$$

Note that the error dynamics described by Equation (12) is time-invariant, which implies that LaSalle's Theorem is applicable. Also it should be noted that the origin $\vec{d}_{i,g} = 0$ is the equilibrium of the error dynamics equation in that $\Phi'_{i,g} = 0$ according to the definition of potential trench function.

First, we investigate the smooth case when $\Phi(d_{i,g})$ is continuously differentiable. For this dynamics equation, we can construct the Lyapunov function candidate as

$$V_i = V_i(\vec{d}_{i,g}, \dot{\vec{d}}_{i,g}) = \frac{1}{2}\dot{\vec{d}}^T_{i,g}\dot{\vec{d}}_{i,g} + \Phi(d_{i,g}). \tag{13}$$

One can obtain the derivative of the scalar $d_{i,g}$ with respect to time through the following steps:

$$\begin{aligned} \frac{d}{dt}d^2_{i,g} &= \frac{d}{dt}\vec{d}^T_{i,g}\vec{d}_{i,g}, \\ 2d_{i,g}\dot{d}_{i,g} &= \dot{\vec{d}}^T_{i,g}\vec{d}_{i,g} + \vec{d}^T_{i,g}\dot{\vec{d}}_{i,g}, \\ \dot{d}_{i,g} &= \dot{\vec{d}}^T_{i,g}\hat{d}_{i,g}, \end{aligned} \tag{14}$$

recalling that the transpose of a scalar is equal to itself. Therefore, the time derivative of the Lyapunov function can be calculated as

$$\begin{aligned} \dot{V}_i &= \dot{\vec{d}}_{i,g}^T \ddot{\vec{d}}_{i,g} + \Phi'_{i,g} \dot{d}_{i,g} \\ &= \dot{\vec{d}}_{i,g}^T \left(\ddot{\vec{d}}_{i,g} + \Phi'_{i,g} \hat{d}_{i,g} \right). \end{aligned} \tag{15}$$

Now substituting Equation (12) into Equation (15) yields

$$\dot{V}_i = -K'_{i,g} \dot{\vec{d}}_{i,g}^T \dot{\vec{d}}_{i,g} = -K'_{i,g} \left\| \dot{\vec{d}}_{i,g} \right\|^2 \leq 0, \tag{16}$$

which shows that $\dot{V}_i$ is negative semidefinite and is zero on the set where $\dot{\vec{d}} = \vec{0}$. By Equation (12) and conclusions from Lemma 5.2.2 or 5.2.3, the system cannot remain in this set except at $\vec{d} = \vec{0}$. Therefore, by LaSalle's Theorem, $\vec{d}$ tends to zero and the system is asymptotically stable.

Second, we deal with the nonsmooth case; namely $\Phi(d_{i,g})$ is not continuously differentiable. It is known that $\Phi(d_{i,g})$ is differentiable almost everywhere. We rewrite Equation (12) into the following form.

$$\frac{d}{dt} \begin{bmatrix} \vec{d}_{i,g} \\ \dot{\vec{d}}_{i,g} \end{bmatrix} = \begin{bmatrix} \dot{\vec{d}}_{i,g} \\ -K'_{i,g} \dot{\vec{d}}_{i,g} - \Phi'_{i,g} \hat{d}_{i,g} \end{bmatrix} = f(\vec{d}_{i,g}, \dot{\vec{d}}_{i,g}). \tag{17}$$

Again we construct the Lyapunov function candidate V_i given by Equation (13) and it is

noted that V_i is time-independent, Lipschitz and regular as $\Phi(d_{i,g})$ is regular.

Note that $d_{i,g} = d_{i,g}(\hat{d}_{i,g}\hat{d}_{i,g}^T) = \vec{d}_{i,g}\hat{d}_{i,g}^T$; hence $\Phi(d_{i,g})$ is in fact a function of $\vec{d}_{i,g}$ and for brevity of notation we regard that $\Phi(d_{i,g})$ and $\Phi(\vec{d}_{i,g})$ are exchangeable in this thesis. Moreover, by Generalized Gradient Formula [14], we are able to calculate the generalized gradient of $\Phi(d_{i,g})$ with respect to $\vec{d}_{i,g}$ as,

$$\partial\Phi(\vec{d}_{i,g}) = \overline{co}\{lim\nabla\Phi(\vec{d}) \mid \vec{d} \to \vec{d}_{i,g}, \vec{d} \notin \Omega_f\}, \tag{18}$$

where Ω_f is the set of measure zero where the gradient of $\Phi(\vec{d}_{i,g})$ fails to be defined.

Furthermore we have the following relationship

$$\frac{d\Phi(\vec{d}_{i,g})}{d(\vec{d}_{i,g})} = \frac{d\Phi(d_{i,g})}{d(d_{i,g})} \cdot \frac{d(d_{i,g})}{d(\vec{d}_{i,g})} = \Phi'_{i,g}\hat{d}_{i,g},$$

which leads Equation (42) to being simplified as

$$\partial\Phi(\vec{d}_{i,g}) = \partial\Phi\hat{d}_{i,g}. \tag{19}$$

According to Chain Rule Theorem [77], for the above time-independent Lyapunov function candidate $V_i(\vec{d}_{i,g}, \dot{\vec{d}}_{i,g})$, its derivative with respect to time, i.e., $(d/dt)V_i(\vec{d}_{i,g}, \dot{\vec{d}}_{i,g})$ exists almost everywhere and

$$\frac{d}{dt}V_i(\vec{d}_{i,g}, \dot{\vec{d}}_{i,g}) \in^{a.e.} \dot{\tilde{V}}_i(\vec{d}_{i,g}, \dot{\vec{d}}_{i,g}), \tag{20}$$

where

$$\dot{\tilde{V}}_i(\vec{d}_{i,g},\dot{\vec{d}}_{i,g}) = \bigcap_{\xi \in \partial V_i(\vec{d}_{i,g},\dot{\vec{d}}_{i,g})} \xi^T K[f](\vec{d}_{i,g},\dot{\vec{d}}_{i,g}).$$

One obtains $\partial V_i(\vec{d}_{i,g},\dot{\vec{d}}_{i,g})$ from Equation (13) as

$$\partial V_i(\vec{d}_{i,g},\dot{\vec{d}}_{i,g}) = \begin{bmatrix} \partial\Phi(d_{i,g})\hat{d}_{i,g} \\ \dot{\vec{d}}_{i,g} \end{bmatrix}. \tag{21}$$

On the other hand, one can calculate $K[f](\vec{d}_{i,g},\dot{\vec{d}}_{i,g})$ as

$$\begin{aligned} K[f](\vec{d}_{i,g},\dot{\vec{d}}_{i,g}) &= K \begin{bmatrix} \dot{\vec{d}}_{i,g} \\ -K'_{i,g}\dot{\vec{d}}_{i,g} - \Phi'_{i,g}\hat{d}_{i,g} \end{bmatrix} \\ &= \begin{bmatrix} \dot{\vec{d}}_{i,g} \\ -\partial K(d_{i,g})\dot{\vec{d}}_{i,g} - \partial\Phi(d_{i,g})\hat{d}_{i,g} \end{bmatrix}. \end{aligned} \tag{22}$$

For the sake of brevity let $\dot{\tilde{V}}_i$ denote $\dot{\tilde{V}}_i(\vec{d}_{i,g},\dot{\vec{d}}_{i,g})$. Then Substituting Equation (45, 44)

into Equation (43) yields,

$$\begin{aligned}\dot{\tilde{V}}_i \subset & \begin{bmatrix} \partial\Phi(d_{i,g})\hat{d}_{i,g} \\ \dot{\vec{d}}_{i,g} \end{bmatrix}^T \cdot \\ & \begin{bmatrix} \dot{\vec{d}}_{i,g} \\ -\partial K(d_{i,g})\dot{\vec{d}}_{i,g}\dot{\vec{d}}_{i,g} - \partial\Phi(d_{i,g})\hat{d}_{i,g} \end{bmatrix} \\ = & \partial\Phi(d_{i,g})\hat{d}_{i,g}^T\dot{\vec{d}}_{i,g} - \partial K(d_{i,g})\dot{\vec{d}}_{i,g}^T\dot{\vec{d}}_{i,g} \\ & -\partial\Phi(d_{i,g})\dot{\vec{d}}_{i,g}^T\hat{d}_{i,g}. \end{aligned} \tag{23}$$

As shown in Equation (14), it is obvious that the scalar term $\hat{d}_{i,g}^T\dot{\vec{d}}_{i,g} = \dot{\vec{d}}_{i,g}^T\hat{d}_{i,g} = \dot{d}_{i,g}$. Therefore Equation (23) can be further simplified as

$$\dot{\tilde{V}}_i = -\partial K(d_{i,g}) \left\| \dot{\vec{d}}_{i,g} \right\|^2 .$$

Obviously, $\dot{\tilde{V}}_i$ is negative semidefinite. By the nonsmooth version of LaSalle's Theorem [77], we can determine the largest invariant set E as

$$E = cl\left(\{ (\vec{d}_{i,g}, \dot{\vec{d}}_{i,g}) | 0 \in \dot{\tilde{V}}_i \} \right) = (\vec{0}, \vec{0}),$$

which implies that the origin is asymptotically stable.

A.11 Proof of Theorem 5.4.1

Construct the Lyapunov function candidate according to Equation (13) for each robot in the chain. Define the Lyapunov function candidate for the chain as $V = \sum_{j=1}^{N} V_j(\vec{d}_{j,g}, \dot{\vec{d}}_{j,g})$. Then

$$\dot{\tilde{V}} = \sum_{j=1}^{N} \dot{\tilde{V}}_j(\vec{d}_{j,g}, \dot{\vec{d}}_{j,g}) = -\sum_{j=1}^{N} k_j \|\dot{\vec{r}}_j - \dot{\vec{r}}_{j,g}\|^2 \leq 0$$

is negative semidefinite. And because equation $\dot{\tilde{V}} = \sum_{j=1}^{N} \dot{\tilde{V}}_j(\vec{d}_{j,g}, \dot{\vec{d}}_{j,g}) = 0$ holds if and only if $\dot{\vec{r}}_j = \dot{\vec{r}}_{j,g}$ for all $j \in \{1, 2, ..., N\}$, by the nonsmooth version of LaSalle's Theorem, the chain is asymptotically stable on the segment.

A.12 Proof of Proposition 6.4.1

We first note that, regardless of the motion trajectory of its direct leader, a follower robot r_i in a coordinated chain under the control law given by Equation (6.1) can never exit the region consisting of zones 2, 3, and 4 of its leader. This is because (i) the energy required for r_i to do so is infinite, i.e., $\int_{d_\circ}^{\check{\rho}} \check{\Psi}'(d_{i,i-1})\, d(d_{i,i-1}) = \infty$ or $\int_{d_\circ}^{\rho} \hat{\Psi}'(d_{i,i-1})\, d(d_{i,i-1}) = \infty$, and (ii) the contribution of $\Phi_{i,p}$ to the motion of the robot in terms of energy will be finite due to the initial condition of finite instantaneous distance $d_{i,p}$.

We outline the proof for Theorem 6.4.1 before presenting the detailed steps. From Proposition 5.3.1, the team leader r_1 in a coordinated chain can be asymptotically stabilized on the segment. For practical purpose, we can stop r_1 when it is within an

arbitrarily small deviation ε to the segment after a finite period of time T_1^*. For robot r_2 (whose leader is r_1), we can construct a Lyapunov function V_2 and show that, under the control given by Equation (6.1), $\dot{V}_2|_{t>T_1^*} \leq 0$ as $t \to \infty$. We thus conclude that r_2 will also asymptotically stabilize on the segment, and so can be made to stop within an arbitrarily small deviation to the segment after a finite period of time T_2^*. This reasoning concerning r_2 can be similarly applied to all other robots, leading to the final conclusion that the whole team can be controlled by Equation (6.1) to approach and stabilize on the segment as a coordinated chain.

We now present the detailed proof. Let $\Delta_{px} = r_{px} - r_{ix}$, $\Delta_{py} = r_{py} - r_{iy}$, $\Delta_{ix} = r_{(i-1)x} - r_{ix}$, $\Delta_{iy} = r_{(i-1)y} - r_{iy}$, $\Delta_{(i,j)x} = r_{jx} - r_{ix}$, and $\Delta_{(i,j)y} = r_{jy} - r_{iy}$. Now $\|\dot{\vec{r}}_i\|^2 = \dot{r}_{ix}^2 + \dot{r}_{iy}^2$, and $\cos\gamma_p = \Delta_{px}/d_{i,p}$, $\sin\gamma_p = \Delta_{py}/d_{i,p}$, $\cos\gamma_i = \Delta_{ix}/d_{i,i-1}$ and $\sin\gamma_i = \Delta_{iy}/d_{i,i-1}$, and $\cos\gamma_{(i,j)} = \Delta_{(i,j)x}/d_{i,j}$ and $\sin\gamma_{(i,j)} = \Delta_{(i,j)y}/d_{i,j}$. Since $d_{i,i-1} \equiv \|\vec{d}_{i,i-1}\| = \left(\Delta_{ix}^2 + \Delta_{iy}^2\right)^{\frac{1}{2}}$, $d_{i,p} \equiv \|\vec{d}_{i,p}\| = \left(\Delta_{px}^2 + \Delta_{py}^2\right)^{\frac{1}{2}}$, $d_{i,j} \equiv \|\vec{d}_{i,j}\| = \left(\Delta_{(i,j)x}^2 + \Delta_{(i,j)y}^2\right)^{\frac{1}{2}}$, we have $\dot{d}_{i,i-1} = (\Delta_{ix}\dot{\Delta}_{ix} + \Delta_{iy}\dot{\Delta}_{iy})/d_{i,i-1}$, and $\dot{d}_{i,p} = (\Delta_{px}\dot{\Delta}_{px} + \Delta_{py}\dot{\Delta}_{py})/d_{i,p}$, and $\dot{d}_{i,j} = (\Delta_{(i,j)x}\dot{\Delta}_{(i,j)x} + \Delta_{(i,j)y}\dot{\Delta}_{(i,j)y})/d_{i,j}$.

For a robot r_i with $i > 1$, we construct a Lyapunov function candidate V_i

$$V_i = \frac{1}{2}\|\dot{\vec{r}}_i\|^2 + \Phi_{i,p}(d_{i,p}) + \Psi_{i,j}^{\Sigma}, \tag{24}$$

where $\Psi_{i,j}^{\Sigma} = \Psi_{i,i-1}(d_{i,i-1}) + \sum_j \hat{\Psi}_{i,j}(d_{i,j})$, and augment the state with variables $d_{i,p}$ and

$d_{i,i-1}$ as

$$\begin{aligned} & \frac{d}{dt}\begin{bmatrix} \dot{r}_{ix} & \dot{r}_{iy} & d_{i,p} & d_{i,i-1} & d_{i,i-2} & \dots & d_{i,1} \end{bmatrix}^T \\ = & \begin{bmatrix} \zeta & \xi & \dot{d}_{i,p} & \dot{d}_{i,i-1} & \dot{d}_{i,i-2} & \dots & \dot{d}_{i,1} \end{bmatrix}^T \\ = & f(\dot{r}_{ix}, \dot{r}_{iy}, d_{i,p}, d_{i,i-1}, d_{i,i-2}, \cdots, d_{i,1}), \end{aligned} \tag{25}$$

which is invariant. Since V_i as defined in Equation (47) is time-independent, locally Lipschitz and regular (because Φ and Ψ are admissible), its generalized gradient is

$$\partial V_i = \left[\dot{r}_{ix}\ \dot{r}_{iy}\ \partial\Phi_{i,p}(d_{i,p})\ \partial\Psi_{i,i-1}(d_{i,i-1})\ \dots\ \partial\hat{\Psi}_{i,1}(d_{i,1})\right]^T$$

while $K[f](\dot{r}_{ix}, \dot{r}_{iy}, d_{i,p}, d_{i,i-1}, d_{i,i-2}, \cdots, d_{i,1})$ can be expressed as:

$$\begin{aligned} & K[f](\dot{r}_{ix}, \dot{r}_{iy}, d_{i,p}, d_{i,i-1}, d_{i,i-2}, \cdots, d_{i,1}) \\ = & \left[K[f](\zeta)\ K[f](\xi)\ \dot{d}_{i,p}\ \dot{d}_{i,i-1}\ \dot{d}_{i,i-2}\ \dots\ \dot{d}_{i,1}\right]^T . \end{aligned}$$

Now $K[f](\zeta)$ and $K[f](\xi)$ can be expressed as follows:

$$\begin{aligned}
K[f](\zeta) &= -k_i\dot{r}_{ix} + \partial\Psi_{i,i-1}(d_{i,i-1})\cos\gamma_i \\
&\quad + \partial\Phi_{i,p}(d_{i,p})\cos\gamma_p + K[f](\delta_1) \\
&\quad + \sum_j \partial\hat{\Psi}_{i,j}(d_{i,j})\cos\gamma_{i,j}, \\
K[f](\xi) &= -k_i\dot{r}_{iy} + \partial\Psi_{i,i-1}(d_{i,i-1})\sin\gamma_i \\
&\quad + \partial\Phi_{i,p}(d_{i,p})\sin\gamma_p + K[f](\delta_2) \\
&\quad + \sum_j \partial\hat{\Psi}_{i,j}(d_{i,j})\sin\gamma_{i,j}.
\end{aligned}$$

Invoking the Chain Rule Theorem yields

$$\begin{aligned}
\dot{\hat{V}}_i^* &\subset \partial V_i^T K[f](\dot{r}_{ix}, \dot{r}_{iy}, d_{i,p}, d_{i,i-1}, d_{i,i-2}, \cdots, d_{i,1}) \\
&= -k_i\dot{r}_{ix}^2 + \dot{r}_{ix}\partial\Psi_{i,i-1}(d_{i,i-1})\cos\gamma_i + \dot{r}_{ix}K[f](\delta_1) \\
&\quad + \dot{r}_{ix}\partial\Phi_{i,p}(d_{i,p})\cos\gamma_p + \dot{r}_{ix}\sum_j \partial\hat{\Psi}_{i,j}(d_{i,j})\cos\gamma_{i,j} \\
&\quad - k_i\dot{r}_{iy}^2 + \dot{r}_{iy}\partial\Psi_{i,i-1}(d_{i,i-1})\sin\gamma_i + \dot{r}_{iy}K[f](\delta_2) \\
&\quad + \dot{r}_{iy}\partial\Phi_{i,p}(d_{i,p})\sin\gamma_p + \dot{r}_{iy}\sum_j \partial\hat{\Psi}_{i,j}(d_{i,j})\sin\gamma_{i,j} \\
&\quad + \partial\Phi_{i,p}(d_{i,p})\dot{d}_{i,p} + \partial\Psi_{i,i-1}(d_{i,i-1})\dot{d}_{i,i-1}. \qquad (26)
\end{aligned}$$

Now,

$$\begin{aligned} & \dot{r}_{ix}\partial\Phi_{i,p}(d_{i,p})\cos\gamma_p + \dot{r}_{iy}\partial\Phi_{i,p}(d_{i,p})\sin\gamma_p \\ = \;& \|\dot{\vec{r}}_i\|\partial\Phi_{i,p}(d_{i,p})\cos(\gamma_p-\theta_i)\,, \end{aligned} \tag{27}$$

and

$$\begin{aligned} & \dot{r}_{ix}\partial\Psi_{i,i-1}(d_{i,i-1})\cos\gamma_i + \dot{r}_{iy}\partial\Psi_{i,i-1}(d_{i,i-1})\sin\gamma_i \\ = \;& \|\dot{\vec{r}}_i\|\partial\Psi_{i,i-1}(d_{i,i-1})\cos(\gamma_i-\theta_i). \end{aligned} \tag{28}$$

For $\|\dot{\vec{r}}_i\| \neq 0$ we have $K[f](\delta_1) = \lambda_i\partial\Phi_{i,p}(d_{i,p})\cos\phi$ and $K[f](\delta_2) = \lambda_i\partial\Phi_{i,p}(d_{i,p})\sin\phi$.

Hence,

$$\begin{aligned} & \dot{r}_{ix}K[f](\delta_1) + \dot{r}_{iy}K[f](\delta_2) \\ = \;& -\|\dot{\vec{r}}_{i,p}\|\partial\Phi_{i,p}(d_{i,p})\cos(\gamma_p-\varphi_p). \end{aligned} \tag{29}$$

Furthermore we note that

$$\begin{aligned} \partial\Phi_{i,p}(d_{i,p})\dot{d}_{i,p} &= \partial\Phi_{i,p}(d_{i,p})[\Delta_{px}\dot{\Delta}_{px} + \Delta_{py}\dot{\Delta}_{py}]/d_{i,p} \\ &= \|\dot{\vec{r}}_{i,p}\|\partial\Phi_{i,p}(d_{i,p})\cos(\gamma_p-\varphi_p) - \\ &\quad \|\dot{\vec{r}}_i\|\partial\Psi_{i,i-1}(d_{i,i-1})\cos(\gamma_p-\theta_i), \end{aligned} \tag{30}$$

and

$$\begin{aligned} & \partial\Psi_{i,i-1}(d_{i,i-1})\dot{d}_{i,i-1} \\ = \; & \partial\Psi_{i,i-1}(d_{i,i-1})[\Delta_{ix}\dot{\Delta}_{ix}+\Delta_{iy}\dot{\Delta}_{iy}]/d_{i,i-1} \\ = \; & -\|\dot{\vec{r}}_i\|\partial\Psi_{i,i-1}(d_{i,i-1})\cos(\gamma_i-\theta_i)\,. \end{aligned} \tag{31}$$

Since $\dot{d}_{i,j}=(\Delta_{(i,j)x}\dot{\Delta}_{(i,j)x}+\Delta_{(i,j)y}\dot{\Delta}_{(i,j)y})/d_{i,j}$, one obtains $\dot{d}_{i,j}=-\dot{r}_{ix}\cos\gamma_{i,j}-\dot{r}_{iy}\sin\gamma_{i,j}$, which means

$$\partial\hat{\Psi}_{i,j}(d_{i,j})\dot{d}_{i,j}=-\dot{r}_{ix}\partial\hat{\Psi}_{i,j}(d_{i,j})\cos\gamma_{i,j}-\dot{r}_{iy}\partial\hat{\Psi}_{i,j}(d_{i,j})\sin\gamma_{i,j}.$$

Readily we reach the following equation:

$$\begin{aligned} & \sum_j \partial\hat{\Psi}_{i,j}(d_{i,j})\cos\gamma_{i,j}\dot{d}_{i,j} \\ = \; & -\dot{r}_{ix}\sum_j \partial\hat{\Psi}_{i,j}(d_{i,j})\cos\gamma_{i,j} \\ & -\dot{r}_{iy}\sum_j \partial\hat{\Psi}_{i,j}(d_{i,j})\sin\gamma_{i,j}. \end{aligned} \tag{32}$$

Substituting Equations (27-32) into Equation (49) yields $\dot{\tilde{V}}_i^* = -k_i\|\dot{\vec{r}}_i\|^2$.

It is shown that all terms except $(-k_i\dot{r}_{ix}^2-k_i\dot{r}_{iy}^2)$ on the right-hand-side of Equation (49) cancel out, leading to $\dot{\tilde{V}}_i^* = -k_i\|\dot{\vec{r}}_i\|^2$, which is negative semidefinite. The largest invariant set M is $\{\dot{r}_{ix},\dot{r}_{iy},d_{i,p},d_{i,i-1},d_{i,i-2},\cdots,d_{i,1}\}=\{0,0,0,0,0,\cdots,0\}$. Therefore, the

system is asymptotically stable.

A.13 Proof of Proposition 7.2.1

For the sake of simplicity, we define a function $D = D(x, x_s)$ as follows:

$$D(x, x_s) = \sqrt{(x - x_s)^2 + \big(g(x) - f(x_s)\big)^2}.$$

Then we can rewrite $d_{min}(x)$ as

$$d_{min}(x) = \min_{x_s \in [a_s, b_s]} \big\{ D(x, x_s) \big\}.$$

Similarly, $d_{min}(x + \Delta x)$ can be expressed in the following form:

$$\begin{aligned}
& d_{min}(x + \Delta x) \\
= & \min_{x_s \in [a_s, b_s]} \left\{ \sqrt{(x + \Delta x - x_s)^2 + \big(g(x + \Delta x) - f(x_s)\big)^2} \right\} \\
= & \min_{x_s \in [a_s, b_s]} \left\{ \sqrt{(x + \Delta x - x_s)^2 + \big(g(x) + \Delta g(x) - f(x_s)\big)^2} \right\} \\
= & \min_{x_s \in [a_s, b_s]} \left\{ \sqrt{D^2(x, x_s) + 2\Delta x(x - x_s) + (\Delta x)^2 + 2\Delta g(x)\big(g(x) - f(x_s)\big) + \big(\Delta g(x)\big)^2} \right\}
\end{aligned}$$

Using the simple fact that

$$\sqrt{x + \Delta x} \leq \sqrt{x} + \sqrt{|\Delta x|},$$

we obtain

$$d_{min}(x+\Delta x) \leq \min_{x_s \in [a_s,b_s]} \left\{ D(x,x_s) + \sqrt{|2\Delta x(x-x_s) + (\Delta x)^2 + 2\Delta g(x)\big(g(x) - f(x_s)\big) + \big(\Delta g(x)\big)^2|} \right\}.$$

Moreover, we can calculate the limit of $d_{min}(x+\Delta x)$ as

$$\begin{aligned}
& \lim_{\Delta x \to 0} d_{min}(x+\Delta x) \\
\leq\ & \lim_{\Delta x \to 0} \min_{x_s \in [a_s,b_s]} \left\{ D(x,x_s) + \sqrt{|2\Delta x(x-x_s) + (\Delta x)^2 + 2\Delta g(x)\big(g(x) - f(x_s)\big) + \big(\Delta g(x)\big)^2|} \right\} \\
=\ & \min_{x_s \in [a_s,b_s]} \left\{ \lim_{\Delta x \to 0} \left(D(x,x_s) + \sqrt{|2\Delta x(x-x_s) + (\Delta x)^2 + 2\Delta g(x)\big(g(x) - f(x_s)\big) + \big(\Delta g(x)\big)^2|} \right) \right\} \\
=\ & \min_{x_s \in [a_s,b_s]} \{D(x,x_s)\} \\
=\ & d_{min}(x) \qquad (33)
\end{aligned}$$

Similarly, we can deduce that

$$d_{min}(x+\Delta x) \geq \min_{x_s \in [a_s,b_s]} \left\{ D(x,x_s) - \sqrt{|2\Delta x(x-x_s) + (\Delta x)^2 + 2\Delta g(x)\big(g(x) - f(x_s)\big) + \big(\Delta g(x)\big)^2|} \right\},$$

because $\sqrt{x+\Delta x} \geq \sqrt{x} - \sqrt{|\Delta x|}$.

Therefore, we have the following relationship:

$$\begin{aligned}
& \lim_{\Delta x\to 0} d_{min}(x+\Delta x) \\
\geq\ & \lim_{\Delta x\to 0} \min_{x_s\in[a_s,b_s]} \left\{ D(x,x_s) - \sqrt{|2\Delta x(x-x_s)+(\Delta x)^2+2\Delta g(x)\big(g(x)-f(x_s)\big)+\big(\Delta g(x)\big)^2|} \right\} \\
=\ & \min_{x_s\in[a_s,b_s]} \left\{ \lim_{\Delta x\to 0} \left(D(x,x_s) - \sqrt{|2\Delta x(x-x_s)+(\Delta x)^2+2\Delta g(x)\big(g(x)-f(x_s)\big)+\big(\Delta g(x)\big)^2|} \right) \right\} \\
=\ & \min_{x_s\in[a_s,b_s]} \{D(x,x_s)\} \\
=\ & d_{min}(x) \qquad (34)
\end{aligned}$$

Obviously,

$$d_{min}(x) \leq \lim_{\Delta x\to 0} d_{min}(x+\Delta x) \leq d_{min}(x),$$

which means that

$$\lim_{\Delta x\to 0} d_{min}(x+\Delta x) = d_{min}(x).$$

Hence we conclude that d_{min} is continuous.

A.14 Proof of Proposition 7.2.2

First, we check the simple case where $d_{min}(x) = 0$. With the condition that

$$d_{min}(x) = \min_{x_s\in[a_s,b_s]} \left\{ \sqrt{(x-x_s)^2+\big(g(x)-f(x_s)\big)^2} \right\} = 0, \qquad (35)$$

we know that there exists at least one value of x_s within interval $[a_s, b_s]$ that leads to $x = x_s$ and $g(x) = f(x_s)$. Since $d_{min}(x)$ is nonnegative, $d_{min}(x+\Delta x)$ is not less than $d_{min}(x)$. The upper bound of $d_{min}(x+\Delta x)$ can be determined through the following steps:

$$
\begin{aligned}
& d_{min}(x+\Delta x) \\
= & \min_{x_s \in [a_s, b_s]} \left\{ \sqrt{D^2(x,x_s) + 2\Delta x(x-x_s) + (\Delta x)^2 + 2\Delta g(x)\big(g(x) - f(x_s)\big) + \big(\Delta g(x)\big)^2} \right\} \\
\leq & \min_{x_s \in [a_s, b_s]} \left\{ D(x,x_s) + \sqrt{|2\Delta x(x-x_s) + (\Delta x)^2 + 2\Delta g(x)\big(g(x) - f(x_s)\big) + \big(\Delta g(x)\big)^2|} \right\} \\
\leq & \min_{x_s \in [a_s, b_s]} \left\{ D(x,x_s) + \sqrt{|2\Delta x(x-x_s) + 2\Delta g(x)\big(g(x) - f(x_s)\big)|} + \sqrt{\big(\Delta g(x)\big)^2 + (\Delta x)^2} \right\} \\
\leq & \min_{x_s \in [a_s, b_s]} \left\{ D(x,x_s) + \sqrt{|2\Delta x(x-x_s) + 2\Delta g(x)\big(g(x) - f(x_s)\big)|} \right\} \\
& + \sqrt{\big(\Delta g(x)\big)^2 + (\Delta x)^2}. \qquad (36)
\end{aligned}
$$

According to Equation (35), we have

$$
\min_{x_s \in [a_s, b_s]} \left\{ D(x,x_s) + \sqrt{|2\Delta x(x-x_s) + 2\Delta g(x)\big(g(x) - f(x_s)\big)|} \right\} = 0. \qquad (37)
$$

Then it follows that Equation (36) can be further simplified as

$$
d_{min}(x+\Delta x) \leq \sqrt{\big(\Delta g(x)\big)^2 + (\Delta x)^2}.
$$

From the above equation, it is easy to check that the ratio

$$\frac{d_{min}(x+\Delta x)-d_{min}(x)}{|\Delta x|} \leq \frac{d_{min}(x+\Delta x)}{|\Delta x|} \leq \sqrt{L^2+1},$$

is bounded.

Second, we consider the nontrivial case where $d_{min}(x) \neq 0$. Note that inequality $\sqrt{Z+\Delta Z} \leq \sqrt{Z}+\frac{\Delta Z}{2\sqrt{Z}}$ always holds as long as $Z>0$ and $Z+\Delta Z>0$. We can employe this fact to determine the maximum value of $d_{min}(x+\Delta x)$.

$$\begin{aligned}
& d_{min}(x+\Delta x) \\
= & \min_{x_s\in[a_s,b_s]} \left\{ \sqrt{D^2(x,x_s)+2\Delta x(x-x_s)+(\Delta x)^2+2\Delta g(x)\big(g(x)-f(x_s)\big)+\big(\Delta g(x)\big)^2} \right\} \\
\leq & \min_{x_s\in[a_s,b_s]} \left\{ D(x,x_s)+\frac{2\Delta x(x-x_s)+(\Delta x)^2+2\Delta g(x)\big(g(x)-f(x_s)\big)+\big(\Delta g(x)\big)^2}{2D(x,x_s)} \right\} \\
\leq & \min_{x_s\in[a_s,b_s]} \left\{ D(x,x_s)+\frac{\Delta Z(x,x_s,\Delta x)}{2D(x,x_s)} \right\},
\end{aligned}$$

where $\Delta Z(x,x_s,\Delta x)=2\Delta x(x-x_s)+(\Delta x)^2+2\Delta g(x)\big(g(x)-f(x_s)\big)+\big(\Delta g(x)\big)^2$ as $\Delta g(x)$ can be viewed as certain unknown function of Δx. This result helps us to calculate and

estimate the ratio

$$
\begin{aligned}
& \frac{d_{min}(x+\Delta x)-d_{min}(x)}{|\Delta x|} \\
= & \left(\min_{x_s\in[a_s,b_s]}\left\{\sqrt{D^2(x,x_s)+\Delta Z(x,x_s,\Delta x)}\right\}-\min_{x_s\in[a_s,b_s]}\{D(x,x_s)\}\right)/|\Delta x| \\
\leq & \left(\min_{x_s\in[a_s,b_s]}\left\{D(x,x_s)+\frac{\Delta Z(x,x_s,\Delta x)}{2D(x,x_s)}\right\}-\min_{x_s\in[a_s,b_s]}\{D(x,x_s)\}\right)/|\Delta x| \\
\leq & \left(\min_{x_s\in[a_s,b_s]}\left\{D(x,x_s)+\frac{|\Delta Z(x,x_s,\Delta x)|}{2D(x,x_s)}\right\}-\min_{x_s\in[a_s,b_s]}\{D(x,x_s)\}\right)/|\Delta x| \\
\leq & \max_{x_s\in[a_s,b_s]}\left\{\frac{|\Delta Z(x,x_s,\Delta x)|}{2D(x,x_s)}\right\}/|\Delta x| \\
= & \max_{x_s\in[a_s,b_s]}\left\{\frac{\left|2(x-x_s)+\Delta x+2\Delta g(x)\big(g(x)-f(x_s)\big)/\Delta x+\big(\Delta g(x)\big)^2/\Delta x\right|}{2D(x,x_s)}\right\} \\
< & \infty. \qquad (38)
\end{aligned}
$$

Since we are able to choose sufficient small Δx to assure that $|\Delta Z(x,x_s,\Delta x)|/D(x,x_s) = |2\Delta x(x-x_s)+(\Delta x)^2+2\Delta g(x)\big(g(x)-f(x_s)\big)+\big(\Delta g(x)\big)^2|/D(x,x_s)<1$. Inequality $\sqrt{Z+\Delta Z}\geq\sqrt{Z-|\Delta Z|}\geq\sqrt{Z}-\frac{\Delta Z}{\sqrt{Z}}$ always holds as long as $Z>0$ and $|\Delta Z|<1$. We can link this fact to the value of $d_{min}(x+\Delta x)$ as follows:

$$
\begin{aligned}
& d_{min}(x+\Delta x) \\
= & \min_{x_s\in[a_s,b_s]}\left\{\sqrt{D^2(x,x_s)+\Delta Z(x,x_s,\Delta x)}\right\} \\
\geq & \min_{x_s\in[a_s,b_s]}\left\{\sqrt{D^2(x,x_s)-|\Delta Z(x,x_s,\Delta x)|}\right\} \\
\geq & \min_{x_s\in[a_s,b_s]}\left\{D(x,x_s)-\frac{|\Delta Z(x,x_s,\Delta x)|}{D(x,x_s)}\right\}.
\end{aligned}
$$

Again, we use the results obtained from above equation to show that

$$\begin{aligned}
& \frac{d_{min}(x+\Delta x)-d_{min}(x)}{|\Delta x|} \\
= & \left(\min_{x_s\in[a_s,b_s]}\left\{\sqrt{D^2(x,x_s)+\Delta Z(x,x_s,\Delta x)}\right\}-\min_{x_s\in[a_s,b_s]}\{D(x,x_s)\}\right)/|\Delta x| \\
\geq & \left(\min_{x_s\in[a_s,b_s]}\left\{D(x,x_s)-\frac{|\Delta Z(x,x_s,\Delta x)|}{D(x,x_s)}\right\}-\min_{x_s\in[a_s,b_s]}\{D(x,x_s)\}\right)/|\Delta x| \\
\geq & -\max_{x_s\in[a_s,b_s]}\left\{\frac{|\Delta Z(x,x_s,\Delta x)|}{D(x,x_s)}\right\}/|\Delta x| \\
= & -\max_{x_s\in[a_s,b_s]}\left\{\frac{\left|2(x-x_s)+\Delta x+2\Delta g(x)\big(g(x)-f(x_s)\big)/\Delta x+\big(\Delta g(x)\big)^2/\Delta x\right|}{D(x,x_s)}\right\},
\end{aligned} \tag{39}$$

is also bounded.

To sum up, we can compare the two bounds from Equation (38) and (39) and assert that the following condition:

$$\begin{aligned}
& \frac{|d_{min}(x+\Delta x)-d_{min}(x)|}{|\Delta x|} \\
\leq & \max_{x_s\in[a_s,b_s]}\left\{\frac{\left|2(x-x_s)+\Delta x+2\Delta g(x)\big(g(x)-f(x_s)\big)/\Delta x+\big(\Delta g(x)\big)^2/\Delta x\right|}{D(x,x_s)}\right\}
\end{aligned}$$

holds for sufficient small Δx such that $|\Delta Z(x,x_s,\Delta x)|/D(x,x_s) = |2\Delta x(x-x_s)+(\Delta x)^2 + 2\Delta g(x)\big(g(x)-f(x_s)\big)+\big(\Delta g(x)\big)^2|/D(x,x_s) < 1$.

A.15 Proof of Proposition 7.2.3

It is straightforward to use contradiction to prove the above proposition. Suppose that motion of the nearest points is discontinuous somewhere, say at non-adjacent points N_1 and N_2, for a robot located near position P and meanwhile q_{ns} remains unique. Immediately it follows that $||PN_1|| \neq ||PN_2||$, which obviously contradicts the conclusion that d_{min} is continuous.

A.16 Proof of Theorem 7.3.2

Since $\ddot{\vec{r}}_i = \vec{u}_i$ and $\vec{d}_{i,ns} = \vec{r}_{i,ns} - \vec{r}_i$, we have $\ddot{\vec{d}}_{i,ns} = -k_i \dot{\vec{d}}_{i,ns} - \Phi'_{i,ns} \hat{d}_{i,ns}$, which can be expressed as

$$\frac{d}{dt} \begin{bmatrix} \vec{d}_{i,ns} \\ \dot{\vec{d}}_{i,ns} \end{bmatrix} = \begin{bmatrix} \dot{\vec{d}}_{i,ns} \\ -k_i \dot{\vec{d}}_{i,ns} - \Phi'_{i,ns} \hat{d}_{i,ns} \end{bmatrix} = f(\vec{d}_{i,ns}, \dot{\vec{d}}_{i,ns}). \tag{40}$$

Equation (40) is time-invariant, with the origin $\vec{d}_{i,ns} = 0$ being the equilibrium point since for an admissible $\Phi_{i,ns}$, $0 \in \partial\Phi(0)$.

We choose the following Lyapunov function candidate (which is time-independent, Lipschitz and regular)

$$V_i = V_i(\vec{d}_{i,ns}, \dot{\vec{d}}_{i,ns}) = \frac{1}{2} \dot{\vec{d}}^T_{i,ns} \dot{\vec{d}}_{i,ns} + \Phi(d_{i,ns}). \tag{41}$$

By the Generalized Gradient Formula [14], the generalized gradient of $\Phi(d_{i,ns})$ with

respect to $\vec{d}_{i,ns}$ is

$$\partial\Phi(\vec{d}_{i,ns}) = \overline{co}\{\lim \nabla\Phi(\vec{d}) \mid \vec{d} \to \vec{d}_{i,ns}, \vec{d} \notin \Omega_f\}, \tag{42}$$

with Ω_f being the set of Lebesgue measure zero where the gradient of $\Phi(\vec{d}_{i,ns})$ is not defined. Furthermore the relationship

$$\frac{d\Phi(\vec{d}_{i,ns})}{d(\vec{d}_{i,ns})} = \frac{d\Phi(d_{i,ns})}{d(d_{i,ns})} \cdot \frac{d(d_{i,ns})}{d(\vec{d}_{i,ns})} = \Phi'_{i,ns}\hat{d}_{i,ns},$$

reduces Equation (42) to $\partial\Phi(\vec{d}_{i,ns}) = \partial\Phi\hat{d}_{i,ns}$. By the Chain Rule Theorem [77], we have

$$\frac{d}{dt}V_i(\vec{d}_{i,ns}, \dot{\vec{d}}_{i,ns}) \in^{a.e.} \dot{\tilde{V}}_i(\vec{d}_{i,ns}, \dot{\vec{d}}_{i,ns}), \tag{43}$$

where $\dot{\tilde{V}}_i(\vec{d}_{i,ns}, \dot{\vec{d}}_{i,ns}) = \bigcap_{\xi \in \partial V_i(\vec{d}_{i,ns}, \dot{\vec{d}}_{i,ns})} \xi^T K[f](\vec{d}_{i,ns}, \dot{\vec{d}}_{i,ns})$, with K being a map (as defined and discussed in detail in [70]) having, for this case, the specific form

$$K[f](\vec{d}_{i,ns}, \dot{\vec{d}}_{i,ns}) = \begin{bmatrix} \dot{\vec{d}}_{i,ns} \\ -k_i\dot{\vec{d}}_{i,ns} - \partial\Phi(d_{i,ns})\hat{d}_{i,ns} \end{bmatrix}. \tag{44}$$

For the sake of brevity, we write $\dot{\tilde{V}}_i(\vec{d}_{i,ns}, \dot{\vec{d}}_{i,ns})$ simply as $\dot{\tilde{V}}_i$ in the sequel. From Equation (41), we have

$$\partial V_i(\vec{d}_{i,ns}, \dot{\vec{d}}_{i,ns}) = \begin{bmatrix} \partial\Phi(d_{i,ns})\hat{d}_{i,ns} \\ \dot{\vec{d}}_{i,ns} \end{bmatrix}. \tag{45}$$

Substituting Equations (45) and (44) into Equation (43) yields $\dot{\tilde{V}}_i = -k_i \left\| \dot{\vec{d}}_{i,ns} \right\|^2$, which is negative semidefinite. By the nonsmooth version of LaSalle's Theorem [77], the largest invariant set is $E = cl\left(\{(\vec{d}_{i,ns}, \dot{\vec{d}}_{i,ns}) | 0 \in \dot{\tilde{V}}_i\}\right) = (\vec{0}, \vec{0})$, which implies that the origin is asymptotically stable.

A.17 Proof of Proposition 7.4.1

The proof by contradiction is straightforward. We assume that there exists a nearest point P_{ns} that is not on the apparent obstacle boundary. Thus we have $P_{ns} \notin \Omega_{ob}^{'}$(or $\Omega_{combo}^{'}$) and $P_{ns} \in \Omega'$. Then a straight line linking P_0 and P_{ns} will intersect with $\Omega_{ob}^{'}$(or $\Omega_{combo}^{'}$) at some point, which is denoted as $P_{ns}^{'}$. It is obvious that

$$||P_0 P_{ns}^{'}|| < ||P_0 P_{ns}||,$$

which contradicts the previous assumption that P_{ns} is the nearest point. To complete the proof, by contradiction, we refer to Figure 2. Without loss of generality, we assume that there exist two points P_1 and P_2 on apparent obstacle $\Omega_{ob}^{'}$ such that

$$||P_0 P_1|| = ||P_0 P_2||$$

and

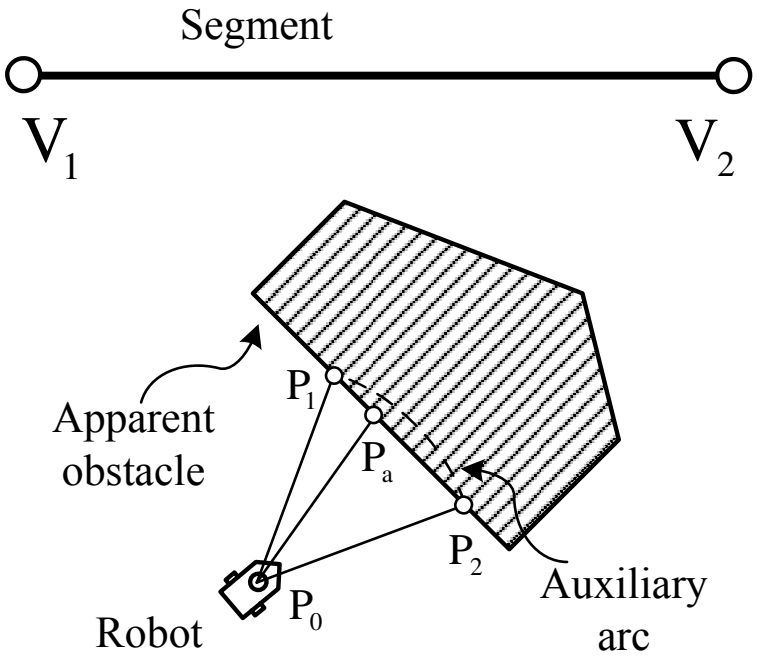

Figure 2: Illustration a robot and the nearest point on an apparent obstacle (i.e., convex hull) depicted in hatched area. The auxiliary arc is represented by dash line.

$$\{P_1, P_2\} = \arg \min_{(x_{ob}, y_{ob}) \in \Omega'_{ob}} \left\{ \sqrt{(x_r - x_{ob})^2 + \left(y_r - y_{ob}\right)^2} \right\}, \tag{46}$$

where $(x_r, y_r) \in R^2$ is the coordinates of point P_0. Then we can construct an auxiliary arc connecting P_1 and P_2 with its center at P_0. An arbitrary point P_a on the straight line P_1P_2 excluding P_1 and P_2 is picked up for study. Since Ω' is convex, $P_1 \in \Omega'$ and $P_1 \in \Omega'$, readily it follows from geometry that

$$P_a \in \Omega',$$

and

$$||P_0P_a|| < ||P_0P_1||.$$

However this conclusion contradicts the assumption that P_1 and P_2 are the nearest point. Thus the proof is completed.

A.18 Proof of Theorem 7.9.1

We first note that, regardless of the motion trajectory of its direct leader, a follower robot r_i in a coordinated chain under the control law given by Equation (7.13) can never exit the region consisting of zones 2, 3, and 4 of its leader. This is because (i) the energy required for r_i to do so is infinite, i.e., $\int_{d_\circ}^{\check{\rho}} \check{\Psi}'(d_{i,i-1})\, d(d_{i,i-1}) = \infty$ or $\int_{d_\circ}^{\rho} \hat{\Psi}'(d_{i,i-1})\, d(d_{i,i-1}) = \infty$, and (ii) the contribution of $\Phi_{i,ns}$ to the motion of the robot in terms of energy will be finite due to the initial condition of finite instantaneous distance $d_{i,ns}$ and (iii) there are no other repulsive potentials cancelling out zoning potentials due to r_{i-1} in the absence of local minima.

We outline the proof for Theorem 7.9.1 before presenting the detailed steps. From Theorem 7.3.2 obviously the team leader r_1 in a coordinated chain can be asymptotically stabilized at a nearest point on the segment without considering the presence of obstacles. For practical purpose, we can stop r_1 when it is within an arbitrarily small deviation ε to the segment after a finite period of time T_1^*. For robot r_2 (whose leader is r_1), we can construct a Lyapunov function V_2 and show that, under the control given by Equation

(7.13), $\dot{V}_2|_{t>T_1^*} \leq 0$ as $t \to \infty$. We thus conclude that r_2 will be attracted on the segment, and so can be made to stop within an arbitrarily small deviation to the segment after a finite period of time T_2^*. This reasoning concerning r_2 can be similarly applied to all other robots, leading to the final conclusion that the whole team can be controlled by Equation (7.13) to approach the segment as a coordinated chain.

We now present the detailed proof. Without loss of generality and for the sake of completeness, it is convenient to define $d_{i,0} = 0$ and $\check{\Psi}_{i,0}(d_{i,0}) = 0$, namely the special case with $i = 1$ for $\check{\Psi}_{i,i-1}(d_{i,i-1})$ where there may have no actual leader assigned to robot r_1. Thus, for a robot r_i with $i \geq 1$, we construct a Lyapunov function candidate

$$V_i = \frac{1}{2}\|\dot{\vec{d}}_{i,ns}\|^2 + \Phi_{i,total}.$$

With Equation (7.12), V_i can rewritten as

$$V_i = \frac{1}{2}\|\dot{\vec{d}}_{i,ns}\|^2 + \Phi_{i,ns}(d_{i,ns}) + \check{\Psi}_{i,i-1}(d_{i,i-1}) + \sum_k \hat{\Psi}^{ob}_{i,k}(d^{ob}_{i,k}), \tag{47}$$

and augment the state with variables $\vec{d}_{i,ns}$, $\vec{d}_{i,i-1}$ and $\vec{d}^{ob}_{i,k}$as

$$\begin{aligned} & \frac{d}{dt}\begin{bmatrix} \vec{d}_{i,ns} & \dot{\vec{d}}_{i,ns} & \vec{d}_{i,i-1} & \vec{d}^{ob}_{i,k} & \vec{d}^{ob}_{i,k-1} & \dots & \vec{d}^{ob}_{i,1} \end{bmatrix}^T \\ = & \begin{bmatrix} \dot{\vec{d}}_{i,ns} & \ddot{\vec{d}}_{i,ns} & \dot{\vec{d}}_{i,i-1} & \dot{\vec{d}}^{ob}_{i,k} & \dot{\vec{d}}^{ob}_{i,k-1} & \dots & \dot{\vec{d}}^{ob}_{i,1} \end{bmatrix}^T \\ = & f(\vec{d}_{i,ns}, \dot{\vec{d}}_{i,ns}, \vec{d}_{i,i-1}, \vec{d}^{ob}_{i,k}, \vec{d}^{ob}_{i,k-1}, \vec{d}^{ob}_{i,1}), \end{aligned} \tag{48}$$

which is invariant. Similar to the procedures shown in the proof of Theorem 7.3.2, V_i is

actually a multi-variable function $V_i = V_i(\vec{d}_{i,ns}, \dot{\vec{d}}_{i,ns}, \vec{d}_{i,i-1}, \vec{d}^{ob}_{i,k}, \vec{d}^{ob}_{i,k-1}, \vec{d}^{ob}_{i,1})$. Since V_i as defined in Equation (47) is time-independent, locally Lipschitz and regular (because Φ and Ψ are admissible), its generalized gradient is

$$\partial V_i = \left[\partial\Phi(d_{i,ns})\hat{d}_{i,ns}\ \dot{\vec{d}}_{i,ns}\ \partial\check{\Phi}(d_{i,i-1})\hat{d}_{i,i-1}\ \partial\hat{\Psi}(d^{ob}_{i,k})\hat{d}^{ob}_{i,k}\ \ldots\ \partial\partial\hat{\Psi}(d^{ob}_{i,1})\hat{d}^{ob}_{i,1}\right]^T$$

while $K[f](\vec{d}_{i,ns}, \dot{\vec{d}}_{i,ns}, \vec{d}_{i,i-1}, \vec{d}^{ob}_{i,k}, \vec{d}^{ob}_{i,k-1}, \vec{d}^{ob}_{i,1})$ can be expressed as:

$$\begin{aligned} & K[f](\vec{d}_{i,ns}, \dot{\vec{d}}_{i,ns}, \vec{d}_{i,i-1}, \vec{d}^{ob}_{i,k}, \vec{d}^{ob}_{i,k-1}, \vec{d}^{ob}_{i,1}) \\ = & \left[\dot{\vec{d}}_{i,ns}\ K[f](\dot{\vec{d}}_{i,ns})\ \dot{\vec{d}}_{i,i-1}\ \dot{\vec{d}}^{ob}_{i,k}\ \dot{\vec{d}}^{ob}_{i,k-1}\ \ldots\ \dot{\vec{d}}^{ob}_{i,1}\right]^T . \end{aligned}$$

Since $\ddot{\vec{r}}_i = \vec{u}_i$ and $\vec{d}_{i,ns} = \vec{r}_{i,ns} - \vec{r}_i$, it flows that $\ddot{\vec{d}}_{i,ns} = -k_i\dot{\vec{d}}_{i,ns} - \nabla\left(\Phi_{i,total}\right)$. Therefore $K[f](\dot{\vec{d}}_{i,ns})$ can be expressed as follows:

$$\begin{aligned} K[f](\dot{\vec{d}}_{i,ns}) \ = \ & -k_i\dot{\vec{d}}_{i,ns} - \partial\check{\Psi}(d_{i,ns})\hat{d}_{i,ns} \\ & -\partial\Psi(d_{i,i-1})\hat{d}_{i,i-1} - \partial\hat{\Psi}(d^{ob}_{i,k})\hat{d}^{ob}_{i,k} \\ & -\partial\hat{\Psi}(d^{ob}_{i,k-1})\hat{d}^{ob}_{i,k-1} - \ldots - \partial\partial\hat{\Psi}(d^{ob}_{i,1})\hat{d}^{ob}_{i,1}. \end{aligned}$$

Invoking the Chain Rule Theorem yields

$$\begin{aligned} \dot{\hat{V}}^*_i \ & \subset \ \partial V_i^T K[f](\vec{d}_{i,ns}, \dot{\vec{d}}_{i,ns}, \vec{d}_{i,i-1}, \vec{d}^{ob}_{i,k}, \vec{d}^{ob}_{i,k-1}, \ldots, \vec{d}^{ob}_{i,1}) \\ & = \ -k_i\ ||\dot{\vec{d}}_{i,ns}||^2. \end{aligned} \tag{49}$$

It can be shown that all terms except $||\dot{\vec{d}}_{i,ns}||^2$ on the right-hand-side of Equation (49) cancel out, leading to $\dot{\tilde{V}}_i^* = -k_i\|\dot{\vec{d}}_{i,ns}\|^2$, which is negative semidefinite.

A.19 Proof of Theorem 8.2.1

Choose the Lyapunov function candidate as

$$V_{i,j} = e_{i,j}^T P_{i,j} e_{i,j}. \tag{50}$$

Since $(A_{i,jns}, B_{i,jns})$ is controllable, $K_{i,jns}$ can be chosen so that $(A_{i,jns} - B_{i,jns}K_{i,jns})$ is Hurwitz. Letting $Q_{i,j} = Q_{i,j}^T > 0$, there exists $P_{i,j}^T = P_{i,j} > 0$ (symmetric and positive-definite) such that

$$P_{i,j}(A_{i,jns} - B_{i,jns}K_{i,jns}) + (A_{i,jns} - B_{i,jns}K_{i,jns})^T P_{i,j} = -Q_{i,j}. \tag{51}$$

In particular, the Lyapunov function candidate $V_{i,j}$ satisfies the following properties

$$\lambda_{\min}(P_{i,j})\|e_{i,j}\|^2 \leq V_{i,j} \leq \lambda_{\max}(P_{i,j})\|e_{i,j}\|^2, \tag{52}$$

$$\frac{\partial V_{i,j}}{\partial e_{i,j}}(A_{i,jns} - B_{i,jns}K_{i,jns})e_{i,j} = -e_{i,j}^T Q_{i,j} e_{i,j} \leq -\lambda_{\min}(Q_{i,j})\|e_{i,j}\|^2, \tag{53}$$

$$\left\|\frac{\partial V_{i,j}}{\partial e_{i,j}}\right\| = \|2e_{i,j}^T P_{i,j}\| \leq 2\|P_{i,j}\|\|e_{i,j}\| = 2\lambda_{\max}(P_{i,j})\|e_{i,j}\|. \tag{54}$$

The time derivative of $V_{i,j}$ along the trajectories of the perturbed system satisfies

$$\begin{aligned}
\dot{V}_{i,j} &= e_{i,j}^T[P_{i,j}^T(A_{i,jns}-B_{i,jns}K_{i,jns})+(A_{i,jns}-B_{i,jns}K_{i,jns})^T P_{i,j}]e_{i,j} \\
&\quad -2e_{i,j}^T P_{i,j}(A_{i,(j-1)ns}-B_{i,(j-1)ns}K_{i,(j-1)ns})e_{i,j-1} \\
&= -e_{i,j}^T Q_{i,j} e_{i,j} - 2e_{i,j}^T P_{i,j}(A_{i,(j-1)ns}-B_{i,(j-1)ns}K_{i,(j-1)ns})e_{i,j-1} \\
&\leq -\lambda_{\min}(Q_{i,j})\|e_{i,j}\|^2 + 2r\lambda_{\max}(P_{i,j})\mu_{i,(j-1)}\|e_{i,j}\|^2,
\end{aligned}$$

where $\mu_{i,(j-1)}$ is the norm of matrix $(A_{i,(j-1)ns}-B_{i,(j-1)ns}K_{i,(j-1)ns})$ described by,

$$\begin{aligned}
\mu_{i,(j-1)} &= \|(A_{i,(j-1)ns}-B_{i,(j-1)ns}K_{i,(j-1)ns})\| \\
&= \lambda_{\max}^{\frac{1}{2}}[(A_{i,(j-1)ns}-B_{i,(j-1)ns}K_{i,(j-1)ns})^T(A_{i,(j-1)ns}-B_{i,(j-1)ns}K_{i,(j-1)ns})].
\end{aligned}$$

Since

$$\|e_{i,j-1}\| \leq r\|e_{i,j}\|, \tag{55}$$

And we can choose $r < \lambda_{\min}(Q_{i,j})/[2\lambda_{\max}(P_{i,j})\mu_{i,(j-1)}]$. Thus

$$\dot{V}_{i,j} \leq -\left[\lambda_{\min}(Q_{i,j}) - 2r\lambda_{\max}(P_{i,j})\mu_{i,(j-1)}\right]\|e_{i,j}\|^2 \leq 0. \tag{56}$$

Let $r = \theta_{i,j}\lambda_{\min}(Q_{i,j})/[2\lambda_{\max}(P_{i,j})\mu_{i,(j-1)}]$ with $0 < \theta_{i,j} < 1$, then

$$\dot{V}_{i,j} \leq -\lambda_{\min}(Q_{i,j})(1-\theta_{i,j})\|e_{i,j}\|^2 \leq 0. \tag{57}$$

Note that in Equation (57) $\dot{V}_{i,j} = 0$ if and only if $\|e_{i,j}\| = 0$. In addition, according to Theorem (8.1.1), the solution $e_{i,j}$ exists and satisfies

$$\|e_{i,j}\| \leq \beta(\|e_{i,j}(t_0)\|, t - t_0) + \chi\Big(\sup_{\tau \geq t_0} \|\Delta_{i,j}(\tau)\|\Big), \tag{58}$$

where $\chi = \gamma_1^{-1} \circ \gamma_2 \circ \rho$ with

$$\begin{aligned}
&\gamma_1(\|x\|) = \lambda_{\min}(P_{i,j})\|x\|^2,\\
&\gamma_2(\|x\|) = \lambda_{\max}(P_{i,j})\|x\|^2,\\
&\gamma_3(\|x\|) = \lambda_{\min}(Q_{i,j})(1-\theta_{i,j})\|x\|^2,\\
&\rho(\|d\|) = \frac{1}{r}\|d\|.
\end{aligned} \tag{59}$$

Accordingly, we have

$$\begin{aligned}
\rho\Big(\sup_{\tau \geq t_0} \|\Delta_{i,j}(\tau)\|\Big) &= \frac{1}{r}\sup_{\tau \geq t_0} \|\Delta_{i,j}(\tau)\|,\\
(\gamma_2 \circ \rho)\Big(\sup_{\tau \geq t_0} \|\Delta_{i,j}(\tau)\|\Big) &= \gamma_2\Big(\rho\Big(\sup_{\tau \geq t_0} \|\Delta_{i,j}(\tau)\|\Big)\Big) = \lambda_{\max}(P_{i,j})\Big(\frac{1}{r}\sup_{\tau \geq t_0} \|\Delta_{i,j}(\tau)\|\Big)^2,\\
(\gamma_1^{-1} \circ \gamma_2 \circ \rho)\Big(\sup_{\tau \geq t_0} \|\Delta_{i,j}(\tau)\|\Big) &= \gamma_1^{-1}\Big[(\gamma_2 \circ \rho)\Big(\sup_{\tau \geq t_0} \|\Delta_{i,j}(\tau)\|\Big)\Big],\\
&= 2\frac{\lambda_{\max}^{\frac{3}{2}}(P_{i,j})\mu_{i,(j-1)}}{\theta_{i,j}\lambda_{\min}(Q_{i,j}\lambda_{\min}^{\frac{1}{2}}(P_{i,j})}\sup_{\tau \geq t_0} \|\Delta_{i,j}(\tau)\|.
\end{aligned} \tag{60}$$

Thus,

$$\chi\Big(\sup_{\tau\geq t_0}\|\Delta_{i,j}(\tau)\|\Big)=2\frac{\lambda_{\max}^{\frac{3}{2}}(P_{i,j})\mu_{i,(j-1)}}{\theta_{i,j}\lambda_{\min}(Q_{i,j}\lambda_{\min}^{\frac{1}{2}}(P_{i,j})}\sup_{\tau\geq t_0}\|\Delta_{i,j}(\tau)\|. \tag{61}$$

For ease of discussion, let us define the following two sets

$$\begin{aligned}\Omega_I&=\Big\{\ e_{i,j}\in R^n\ \Big|\ \|e_{i,j}\|\leq\rho\big(\sup_{\tau\geq t_0}\|\Delta_{i,j}(\tau)\|\big)\ \Big\},\\ \Omega_O&=\Big\{\ e_{i,j}\in R^n\ \Big|\ \|e_{i,j}\|\geq\rho\big(\|\Delta_{i,j}(t)\|\big)\ \}.\end{aligned} \tag{62}$$

Note that $\Omega_I\cup\Omega_O=R^n$.

Let us discuss the following two cases: (i) the state $e_{i,j}(t)\in\Omega_I$; and (ii) $e_{i,j}(t)\in\Omega_O$.

Case (i): If $e_{i,j}(t_0)\in\Omega_I$, then $e_{i,j}$ will satisfy

$$\|e_{i,j}(t)\|\leq\gamma_1^{-1}\circ\gamma_2\circ\rho\big(\sup_{\tau\geq t_0}\|\Delta_{i,j}(\tau)\|\big),\ \ \forall t\geq t_0 \tag{63}$$

as $\gamma_1^{-1}\circ\gamma_2(\|x\|)\geq\|x\|$.

Case (ii): If $e_{i,j}(t_0)\in\Omega_O$, we have Equation (57). Noting Equation (50), we further have

$$\dot{V}_{i,j}\leq-\frac{\lambda_{\min}(Q_{i,j})}{\lambda_{\max}(P_{i,j})}(1-\theta_{i,j})V_{i,j}, \tag{64}$$

i.e.,

$$\dot{V}_{i,j}\leq-\gamma_3\circ\gamma_2^{-1}(V_{i,j}). \tag{65}$$

Integrating Equation (64) over $[t_0, t]$ yields

$$V_{i,j}(t) \leq V_{i,j}(t_0) e^{-\frac{\lambda_{\min}(Q_{i,j})}{\lambda_{\max}(P_{i,j})}(1-\theta_{i,j})(t-t_0)}, \tag{66}$$

Noting Equation (52), we have

$$\lambda_{\min}(P_{i,j})\|e_{i,j}\|^2 \leq V_{i,j}(t) \leq V_{i,j}(t_0) e^{-\frac{\lambda_{\min}(Q_{i,j})}{\lambda_{\max}(P_{i,j})}(1-\theta_{i,j})(t-t_0)}, \tag{67}$$

i.e.,

$$\|e_{i,j}\|^2 \leq \frac{V_{i,j}(t_0)}{\lambda_{\min}(P_{i,j})} e^{-\frac{\lambda_{\min}(Q_{i,j})}{\lambda_{\max}(P_{i,j})}(1-\theta_{i,j})(t-t_0)}. \tag{68}$$

Since

$$V_{i,j}(t_0) = e_{i,j}^T(t_0) P_{i,j} e_{i,j}(t_0) \leq \lambda_{\max}(P_{i,j})\|e_{i,j}(t_0)\|^2, \tag{69}$$

we further have

$$\|e_{i,j}(t)\|^2 \leq \frac{\lambda_{\max}(P_{i,j})}{\lambda_{\min}(P_{i,j})}\|e_{i,j}(t_0)\|^2 e^{-\frac{\lambda_{\min}(Q_{i,j})}{\lambda_{\max}(P_{i,j})}(1-\theta_{i,j})(t-t_0)}, \tag{70}$$

i.e.,

$$\|e_{i,j}(t)\| \leq \sqrt{\frac{\lambda_{\max}(P_{i,j})}{\lambda_{\min}(P_{i,j})}}\|e_{i,j}(t_0)\| e^{-\frac{\lambda_{\min}(Q_{i,j})}{2\lambda_{\max}(P_{i,j})}(1-\theta_{i,j})(t-t_0)}. \tag{71}$$

By defining

$$\beta_V(x(t_0),t-t_0) \triangleq x(t_0)e^{-\frac{\lambda_{\min}(Q_{i,j})}{\lambda_{\max}(P_{i,j})}(1-\theta_{i,j})(t-t_0)}.$$

$$\beta(x(t_0),t-t_0) \triangleq \gamma_1^{-1}(\beta_V(\gamma_2(x(t_0),t-t_0))), \tag{72}$$

then Equation (71) can be expressed as

$$\|e_{i,j}(t)\| \leq \beta(\|e_{i,j}(t_0)\|,t-t_0). \tag{73}$$

Thus, from Equations (63) and (73),

$$\|e_{i,j}(t)\| \leq \beta(\|e_{i,j}(t_0)\|,t-t_0)+\chi\Big(\sup_{\tau\geq t_0}\|\Delta_{i,j}(\tau)\|\Big),\ \ \forall t \geq t_0 \geq 0 \tag{74}$$

which completes the proof.

A.20 Proof of Proposition 8.4.1

As Equation (8.26) shows, if formation errors of all the robots ahead are bounded, then each term multiplied by $\|e_{i,(j-1)}\|$, $\|e_{i,(j-2)}\|$, $\cdots$, $\|e_{i,1}\|$ is bounded. In other words, the queue formation error of jth robot with respect to initial formation errors of all those robot ahead is bounded. Obviously if the initial formation error of itself is bounded, then the first term in Equation(8.26) is bounded. Given a queue formation has finite length, according the above statement, $\|e_{i,j}\|$ is bounded.

A.21 Proof of Theorem 8.4.1

Choose the Lyapunov function candidate for each robot in any queue of the whole formation as

$$V_k = e_k^T P_k e_k. \tag{75}$$

where k=1,2,...m. And m denotes the length of the corresponding queue. Since (A_k, B_k) in controllable, K_j can be properly chosen such that $(A_k, B_k K_k)$ is Hurwitz. Letting Q_k=$Q_k^T > 0$, there exists P_k^T=P_k> 0 such that

$$P_k(A_k - B_k K_k) + (A_k - B_k K_k)^T P_k = -Q_k. \tag{76}$$

For each Lyapunov function in Equation (75), we have,

$$\left\| \frac{\partial V_k}{\partial e_k} \right\| \leq 2\lambda_{max}(P_k)\|e_k)\|. \tag{77}$$

Define a function $\partial hi_j(e_k) = \|e_k\|$. Then Equation (77) can be rewritten as

$$\begin{aligned} &\left\| \frac{\partial V_k}{\partial e_k} \right\| \leq \beta_k(e_k), \\ &\beta_k = 2\lambda_{max}(P_k). \end{aligned} \tag{78}$$

And V_k satisfies

$$\frac{\partial V_k}{\partial e_k}(A_k - B_k K_k)e_j \leq -\lambda_{min} Q_k \|e_k\|^2 = -\alpha_k \partial hi_k^2(e_k),$$
$$\alpha_k = \lambda_{min}(Q_k). \tag{79}$$

We decompose the equations given by Equation (8.28) into 2 parts, one is the dynamic of its own, and the other is the disturbance imposed on. The basic form is as below.

$$\begin{aligned} \dot{e}_k &= (A_k - B_k K_k)e_k + g_k(e), \\ g_k(e) &= -(A_{k-1} - B_{k-1} K_{k-1})e_{i,k-1}. \end{aligned} \tag{80}$$

where $k = 1, 2, \ldots, m$ and $e = [e_1\ e_2\ \cdots\ e_m]$. And for the disturbance term of each robot,

we have

$$
\begin{aligned}
\|g_1(e)\| &= 0 \leq \gamma_{11}\partial hi_1(e_1), \\
\gamma_{11} &= 1, \\
\|g_2(e)\| &= \|-(A_1 - B_1K_1)e_1\| \leq \mu_1\|e_1\| = \gamma_{21}\partial hi_1(e_1), \\
\gamma_{21} &= \mu_1 = \lambda_{max}^{\frac{1}{2}}[(A_1 - B_1K_1)^T(A_1 - B_1K_1)], \\
&\vdots, \\
\|g_m(e)\| &= \|-(A_{m-1} - B_{m-1}K_{m-1})e_{m-1}\|, \\
&\leq \mu_{m-1}\|e_{m-1}\|, \\
&= \gamma_{m(m-1)}\partial hi_{m-1}(e_{m-1}), \\
\gamma_{m(m-1)} &= \mu_{m-1} = \lambda_{max}^{\frac{1}{2}}[(A_{m-1} - B_{m-1}K_{m-1})^T(A_{m-1} - B_{m-1}K_{m-1})]. \qquad (81)
\end{aligned}
$$

S is an $m \times m$ matrix whose elements are defined by

$$
s_{ij} = \begin{cases} \alpha_i - \beta_i\gamma_{ii} & i = j, \\ -\beta_i\gamma_{ii} & i \neq j. \end{cases}
$$

Then matrix S can be explicitly represented as below.

$$S = \begin{bmatrix} s_{11} & 0 & 0 & \dots & 0 \\ s_{21} & s_{22} & 0 & \dots & 0 \\ 0 & s_{32} & s_{33} & \ddots & \vdots \\ \vdots & \ddots & \ddots & \ddots & 0 \\ 0 & \dots & 0 & s_{m(m-1)} & s_{mm} \end{bmatrix}. \tag{82}$$

where

$$\begin{cases} s_{ii} = \lambda_{min}(Q_i) - 2\lambda_{max}(P_i) \\ s_{i(i-1)} = -2\lambda_{max}(P_{i-1})\mu_{i-1} \leq 0 \\ s_{ij} = 0 \qquad\qquad j \neq i \text{ or } j \neq i-1 \end{cases} \tag{83}$$

D is an $m \times m$ unit matrix. Namely $D = diag(d_1\ d_2\ \cdots\ d_m) = I$. It is obvious that $det(S) > 0$ if properly choose P_k and Q_k such that

$$\lambda_{min}(Q_k) - 2\lambda_{max}(P_k) > 0, \tag{84}$$

And the Lyapunov function $V(t,e)$ of the whole queue meets the followings,

$$\begin{aligned} V(t,e) &= \sum_{k=1}^{m} d_k V_k(t,e_k). \\ \dot{V}(t,e) &\leq -\frac{1}{2}\partial hi^T (DS + S^T D)\partial hi. \end{aligned} \tag{85}$$

According to Lemma 9.7 and Theorem 9.2 of Nonlinear Systems by Khalil, the queue

formation is globally uniformly asymptotically stable, thus completing the proof.

A.22 Proof of Proposition 8.4.2

When robots quit or join in the queue, we can establish a new interconnected system after treating the following two cases:

case 1 The queue formation is free of sequence, i.e., a robot can takes any assigned place of sequence in the queue no matter what kind of the robot it is or what identity it has. No further action needs at this stage.

case 2 Each robot has its own sequence in the queue according to specification.

case 2.1 When robots quit and no further adjustment of previous assignment after this event, then no further action needs at this stage.

case 2.2 When there is a new adjustment of sequence or there are new comers joining in the queue, then a sorting of the robots needs. By properly choosing those robots to move among the queue to form the desired sequence of the queue while the rest remains static in the queue. Since the length of the queue is finite, this sorting can be finished within finite times of sequence adjustment.

After this treatment, robots in the queue form the desired sequence. Then for those group of robots in the queue, we can establish a new interconnected system as we did in proof of Theorem 8.4.1. For this new interconnected system, following similar procedures and applying Lemma 9.7 and Theorem 9.2 of *Nonlinear System* by Khalil, the conclusion

holds.